EXPERIMENTAL ANALYSIS OF UNREINFORCED AND REINFORCED PILED EMBANKMENT SUBJECTED TO CYCLIC LOADS

K. M. A. AQOUB

PHD

2018

EXPERIMENTAL ANALYSIS OF UNREINFORCED AND REINFORCED PILED EMBANKMENT SUBJECTED TO CYCLIC LOADS

KHALED M. A. AQOUB

Submitted for the Degree of

Doctor of Philosophy

Faculty of Engineering and Informatics

University of Bradford

2018

ABSTRACT

KHALED M. A. AQOUB

EXPERIMENTAL ANALYSIS OF UNREINFORCED AND REINFORCED PILED EMBANKMENT SUBJECTED TO CYCLIC LOADS

Keywords: Geosynthetics, reinforced piled embankment, cyclic loadings, soil reinforcement, arching, membrane effects.

Reinforced piled embankment technique is becoming increasingly utilised for the construction over soft grounds. Most of the studies focused on studying the behaviour of piled embankments that are loaded with static surcharge load. However, less attention has been given to the behaviour of piled embankments under cyclic loading conditions.

In this study, an experimental programme has been undertaken to improve our understanding for the behaviour of unreinforced and reinforced shallow piled embankments subject to cyclic loadings that are applied over a specific area of the embankment. The results showed that arching of the soil was adversely affected during the initial stages of cyclic loading regardless of the embankment height. However, regain of strength and recovery of the arching effect was observable during further stages of cyclic loadings. Inclusion of reinforcement layers was found to enhance the performance of load transfer mechanisms. The surface settlement increased with raising the embankment height and reduced with increasing the number of reinforcement layers.

Two preliminary experimental studies have been carried out in order to be able to understand and design the main experiment. The results showed that with increasing number of reinforcement layers, enormous cycles of loading could be applied without experiencing excessive deformation or loss of

bearing resistance. Furthermore, it was observed that alternating the direction of movement significantly affected the formation of arching during the initial cycles irrespective of the embankment height.

LIST OF PUBLICATIONS

Conference Papers

- Aqoub, K., Mohamed, M., Sheehan, T. (2017). Strength and Deformation of Reinforced Soils Subject to Repeated loads. *International Conference on Advances in Structural and Geotechnical Engineering (ICASGE, 17), Hurghada, Egypt,*1-10.

Journal Papers

- Aqoub, K., Mohamed, M. and Sheehan, T. (2018). Analysis of sequential active and passive arching in granular soils. *International Journal of Geotechnical Engineering*, 1-10. (published).
- Aqoub, K., Mohamed, M. and Sheehan, T.(2018). Analysis of unreinforced and reinforced shallow piled embankments subject to cyclic loading. *Geosynthetics International*, (published).
- Aqoub, K., Mohamed, M. and Sheehan, T.(2018). Quantitative analysis of shallow unreinforced and reinforced piled embankments with different heights subject to cyclic loads: Experimental Study. *Geotextiles and Geomembranes* , ((under review).
- Aqoub, K., Mohamed, M. and Zidan, A. (2019). Numerical and experimental modelling of reinforced shallow piled embankments subject to cyclic loading, (Under preparation).

ACKNOWLEDGEMENTS

Initially, I would like to thank my God for giving me the ability to finish this research. Secondly, I would like to acknowledge my gratitude to my principal supervisor, **Dr. Mostafa Mohamed,** for his continuous support, encouragement and guidance throughout my research. Without his excellent advice and constant attention on my work, this thesis would not have been completed. I am considerably thankful to him for being so patient with me. Also, I am heartily grateful to my second supervisor, **Dr. Therese Sheehan** for her continuous support and her guidance from the initial to the end of this work.

I would like to extend my thanks to my Colleague **Ahmed Elshesheny** for his help during this work especially during the laboratory time. My heartfelt gratitude also goes to all **technicians** who helped me during this work.

Very warm and deep thanks go to **my parents** for their continuous encouragement and support. A special thanks to **my wife**, for her daily encouragement throughout the whole process. Many thanks to all **my friends** who supported and encouraged me in order to finish this work.

Finally, I am greatly appreciate the financial support provided by **the Higher Education Institute** of the Libyan Government.

.

TABLE OF CONTENT

LIST OF FIGURES

CHAPTER TWO

CHAPTER THREE

CHAPTER FOUR

CHAPTER FIVE

CHAPTER SIX

LIST OF TABLES

CHAPTER TWO

CHAPTER THREE

CHAPTER FOUR

NOTATION

σ_v	Vertical stress (kN/m^2)
σ_h	Horizontal stress (kN/m^2)
σ_s	Vertical stress applied on the sub soil (kN/m^2)
σ_i	Vertical stress acting immediately beneath the crown of the arch (kN/m^2)
σ_c	Vertical stress on the pile cap (kN/m^2)
σ_n	Normal stress at the interface between embankment and soft soil (kN/m^2)
σ_p	Stress under the plunger (MPa)
p_o	Average vertical stress applied on trapdoor or geosynthetics reinforcement (kN/m^2)
τ	Shear strength in (kN/m^2)
w_s	Uniformly distributed surcharge loading (kN/m^2)
q	Uniform surcharge load applied on the embankment fill surface (kN/m^2)
W_T	Distributed load acting on the reinforcement layer between two adjacent piles (kN/m)
γ	Unit weight of the soil (kN/m^3)
G_s	Specific gravity (-)
Φ	Angle of internal friction of the soil mass (degree)
Φ_s	Friction angle of embankment fill (degree)
Φc	Friction angle of soft soil (degree)

δ'	Angle of friction between soil and geosynthetics reinforcement layer surface (degree)
c	Soil cohesion (kN/m^2)
T	Axial tensile load in the reinforcement layer (kN/m)
ε	Axial strain in the geosynthetic reinforcement layer (-)
K_g	Tensile stiffness of geosynthetic reinforcement (kN/m)
E	Elastic modulus (kN/m^2)
E_0	Stiffness of soft soil (kN/m^2)
E_c	Elastic modulus of soft soil (kN/m^2)
E_g	Elastic modulus of geosynthetics reinforcement layer (kN/m^2)
E_s	Elastic modulus of sand soil (kN/m^2)
E_{equ}	Equivalent modulus (Mpa)
F^*	Stress on the underground structure to overburden pressure (-)
F	Stress on roof of underground structure (kN/m^2)
F_0	overburden pressure (kN/m^2)
k	Coefficient of lateral earth pressure (-)
k_a	Coefficient of active earth pressure (-)
k_p	Coefficient of passive earth pressure (-)
k_0	Coefficient of earth pressure at rest (-)
δ^*	Underground structure displacement to the width of the underground structure (-)
δ	Underground structure displacement (m)
d	Depth of reinforcement layer from the interface (m)
S	Piles center to center spacing (m)
a	Size of the pile cap (m)
H	Height of the embankment (m)
Z	the thickness of the soil overlying the element (m)

w	Width of reinforcement layer in (m)
t	deflection in geosynthetics reinforcement layer at mid-point (m)
h_s	Depth of soft soil layer in (m)
L	Trapdoor length (m)
S’	Cap beams clear spacing (m)
B	Width of underground structure (m)
d	Settlement of the underground structure (m)
d_{50}	Average of particle size (mm)
H_C	Critical height of arching (m)
d_c	Column dimeter (m)
S’	Columns clear spacing (m)
t_0	Settlement in the soft ground when the reinforcement was not used (m)
K^*	Factor of arching reduction ratio (-)
d_{50}	Average particle size of the soil (mm)
u	Measured elastic deformation (mm)
D	Plunger dimeter (mm)
n	Number of reinforcement layers (-)
E	Efficiency (%)
E_{min}	Lower efficiency (%)
E_{crown}	Efficiency at the crown (%)
E_{pile}	Efficiency at the pile (%)
ρ	Soil Arching Ratio or Stress Reduction Ratio (-)
SRR	Stress Reduction Ratio (-)
SCR	Stress concentration ratio (-)
s^*	Settlement ratio (-)

λ factor ranged from 0.7 to 0.9 (-)

λ' Loading recovery index (-)

M_A Modulus of initial arching (-)

M_B Secant Modulus of arching (-)

ν Poisson's ratio

CHAPTER ONE

INTRODUCTION

1.1 General view

Due to increasing world urbanisation, a high demand for the construction of infrastructures such as highway road, bridges, railway, buildings and underground structures has been noted in recent decades. However, the existence of soft soil layers in several regions around the world may hinder and/or delay the construction of such engineering projects. Soft soil layers pose a high risk of excessive settlement and ground instability due to bearing capacity failure and potential slope movement if care is not undertaken. Preventative ground improvement techniques such as preloading, vertical drains, grouting and soil replacement can be used to minimise and/or eliminate the adverse effects on infrastructures but they are costly and time consuming. Geosynthetics reinforcement along with granular soil replacement have successfully been used to enhance the stability of subsurface weak soils (see for example, Duncan-Williams and Attoh-Okine 2008 and Naeini and Mirzakhanlari 2008). The use of high tensile strength reinforcing layers improves the bearing capacity and reduces settlement (Ashs and Latha, 2010). Recently, the reinforced pile embankment technique has proven to be an efficient and cost-effective solution for the construction on soft clay layers in comparison to other techniques (Mitchell 1981; Magnan 1994; Shen et al. 2005; Oh and Shin 2007). Coupling geosynthetics reinforcement with piles underneath soil embankment significantly enhanced the bearing capacity, reduced total and differential settlement and saved time. However, a deeper understanding for the precise type and contribution of different load transfer

mechanisms is still required under different conditions of loading, embankment heights and reinforcement.

1.2 Reinforced piled embankment

The main idea behind the construction of the piled embankment is to use a grid of piles or columns to support the embankment fill with the supposition that the load of embankment will be transmitted through the piles down to a competent stratum such as firm soil or bedrock. As a consequence, the soft ground is not directly relevant to the performance of the embankment itself. Although, it is assumed that the natural arches created over the soft soil between foundations reduce the settlement on soft soil surface, geosynthetics reinforcement which acts in tension at the base of the embankment can enhance transferring of loads to the foundations. Geosynthetics reinforcement such as geogrid or geotextile also is used to increase the spacing between the piles and to reduce the height of embankment (Satibi et al. 2007; Zhuang 2009).

1.3 Soil arching and geosynthetics membrane

Loads are transferred on reinforced pile embankments through a combination of arching mechanisms in the embankment fill material and membrane effect by geosynthetics reinforcement layers (Villard and Giraud 1998; Villard et al. 2004). Due to the greater stiffness of the piles, shear resistance is mobilised along the soil columns above the pile caps leading to partial transfer of loads to pile caps by an arching mechanism alongside decreased pressure on the soft soil. The arching mechanism is well recognised since Terzaghi (1943). Inclusion of layers of geosynthetic reinforcement above the pile caps offer a substantial contribution to transferring load to piles through a membrane effect

(see for example, Stewart and Filz 2005; Van Eekelen et al. 2012 a and b; Zhuang and Wang 2018).

1.4 Significance of research

Firstly, cyclic triaxial test is the best technique to study the strength of reinforced weak soils under cyclic loading condition. However, practically it is very expensive and not straight forward to be conducted in several developing countries. Thus, California Bearing Ratio (CBR) and Repeated Load California Bearing Ratio (RL-CBR) are practical alternatives to gain insight of the behaviour of reinforced soil under repeating loading conditions. To the best of the author's knowledge, no experimental studies have been undertaken using CBR to assess and optimise the location and number of reinforcement layers under repeated and cyclic loading conditions.

Secondly, although a lot of studies have been conducted to study the behaviour of soil arching, the focus has been on investigating distinctive modes of arching e.g. either active or passive mode separately in isolation of external environmental influences. For example, underground inclusions or structures may undergo cycles of upward and downward movement due to swelling and shrinking of expansive soil layers. Expansive soil layers that exist beneath the underground inclusions are prone to cycles of swelling and shrinking upon slight change in moisture content. This may in turn change the arching mechanism from active to passive mode or vice versa and deviate the stresses from those that were determined based on one of the two recognised arching mechanisms. The additional loads due to passive mode may lead to damage of the buried structures if care is not undertaken (Clark 1971). In this

study therefore, the effect of repeated sequential active and passive arching on the distribution of stresses within the granular soil mass is assessed.

Finally, several studies have been carried out to study the behaviour of reinforced piled embankments under different types of loads. Most of previous studies focused on the behaviour of unreinforced soil and reinforced soils under static loading conditions. However, the behaviour of reinforced piled embankment under cyclic loading conditions is not yet fully understood and still needs to be studied further. Also, these methods assume that the external surcharge load is distributed on the whole embankment surface. However, it is worth noting that applying surcharge load over the whole area of the embankment is only valid where the embankment is of adequate height to ensure uniform distribution of load at the level of piles and soft soil. This is not applicable in the case of shallow embankment in which surcharge loads are applied and transferred through a relatively small zone of the embankment resulting in propagation of high stresses on the region below the loaded area. Therefore, the load in this study was applied over part of the embankment to show potential differential settlement which has never been assessed in previous research studies or considered in design equation since uniform loads were always applied. In addition, most experimental studies that are available used artificial soft material. These artificial materials would not represent the real behaviour of soft soil under static nor cyclic loadings. Moreover, during the life time of the structure the capacity of traffic load might be needed to increase. Therefore, it is beneficial to investigate the effect of increasing live loads on the behaviour of reinforced piled embankment.

1.5 Aims and objectives

The main aim of this research is to study, through a reduced scale experimental modelling, the effect of different stages of cyclic loading applied over a predetermined area on unreinforced and reinforced shallow piled embankment. Also, in order to understand the main mechanism that are responsible to transfer the loads through the embankment to piles, two preliminary tests were carried out to investigate i. the effect of repeated loading conditions on unreinforced and reinforced soil, ii. the effect of sequentially alternating active and passive arching on behaviour of granular soil. These preliminary tests also can provide ample data for the design of the main experimental test.

The primary objectives are as follows

- To investigate the effect of thickness of granular layer overlying soft subbase under repeated loading condition.
- To optimise the location of reinforcement layers within the granular layer under repeated loading condition.
- To assess whether increasing the number of reinforcement layers has a remarkable effect on long term stability behaviour under repeated loading conditions.
- To quantify the beneficial effect of reinforcement layers in reducing the settlement of soft soil subject to the same level of loading under repeated loading conditions.
- To evaluate the effect of reinforcement layers on the stiffness of unreinforced samples under repeated loading conditions.

- To investigate the influence of displacement and soil height on the resulting stresses during sequentially alternating active and passive arching.
- To explore potential impacts for the number of alternating cycles of active and passive arching on stress reduction.
- To investigate the effects of embankment fill height on load transfer mechanisms, surface settlement and soft soil deformation under static and different stages of cyclic loading conditions.
- To investigate the effects of increasing the number of reinforcement layers on load transfer mechanisms, surface settlement and soft soil deformation under static and different stages of cyclic loading conditions.
- To investigate the effect of number of cycles on load transfer mechanisms.
- To measure the tension and vertical deformation in reinforcement layers.

1.6 Methodology

These aims and objectives are fulfilled experimentally by using, i. repeated loading California Bearing Ratio technique ii. a well-developed trapdoor set-up and, iii. a fully instrumented testing rig which was designed, manufactured and commissioned, through reduced-scale physical modelling, that is capable of providing measurements for pile load, load on soft soil, deformation measurements and tension in reinforcement layers.

1.7 Thesis organization

This thesis consists of seven chapters.

Chapter one: A brief insight into the research topic is presented in this chapter.

Chapter two: A comprehensive literature review is provided in this chapter. This contains a critical review of some existing design methods and research related to reinforced piled embankments, previous studies in the areas of reinforced piled embankments under cyclic loading conditions and some of previous studies focused on the behaviour of reinforced soil and the mechanism of arching in granular soils under static and cyclic loading conditions.

Chapter three: this chapter provides description in details of the design and manufacture of the preliminarily experimental work and the main experimental work. Preparation of materials used, the experimental procedure and the tests programme are justified.

Chapter four: In this chapter the results of the effect of static and repeating loading conditions on the behaviour of unreinforced and reinforced soil (preliminarily experimental test 1) are presented. Deeper discussion and analysis are provided in this chapter.

Chapter five: Chapter 5 presents the results of the developed classic trap door experimental test (preliminarily test 2). The effect of repeated sequential active and passive arching on the behaviour of granular soil is investigated and analysed.

Chapter six: Chapter 6 contains the interpretation and analysis of the main test results, All the tests results are presented and discussed deeply in order

to find the effect of embankment height and number of reinforcement layers on the behaviour of reinforced embankment under static, monotonic and three stages of cyclic loading.

Chapter seven: chapter 7 provides a summary of work accomplished, a summary of conclusions, and recommendations for further research.

CHAPTER TWO

LITERATURE REVIEW

2.1 Introduction

This chapter contains a review of the literature and the gaps in knowledge are identified. The phenomenon of arching in granular soils, the load transfer mechanism in reinforced piled embankment, previous design methods, the shape of arching and the factors affecting the arching mechanism and the strength of reinforced soil are presented and discussed in detail. Finally, previous studies that focused on the behavior of load transfer mechanism under cyclic loading conditions are presented and discussed.

2.2 Load transfer mechanism

According to Han and Gabr (2002) the transfer of loads onto geosynthetics piled supported embankment can be categorized into three different mechanisms: soil arching effect, tensioned membrane or stiffened platform effect and stress concentration effect, as shown in Figure 2.1. Arching of soil occurs as the column of soil above the sub soil (w2) tends to move downward more than the column of soil above the piles (w1) (Figure 2.1). Tensioned membrane effect is generated due to the deformation in geosynthetic reinforcement and the settlement in the sub soil as shown in Figure 2.1. When multi layers of geosynthetic reinforcement are used, the layer of embankment with reinforcement layers will act as stiffened platform as shown in Figure 2.2. However, when there is no soil arching effect and tensioned membrane effect, the load is transferred by the stress concentration mechanism. Due to the difference in the stiffness between the pile caps and surrounding sub soil, the

stresses are transferred from sub soil (σ_s) to the pile caps (σ_c) as shown in Figure 2.1. The behavior of each mechanism is dependent on many factors such as properties of embankment materials, properties and number of geosynthetic reinforcement layers and properties of piles and sub soil.

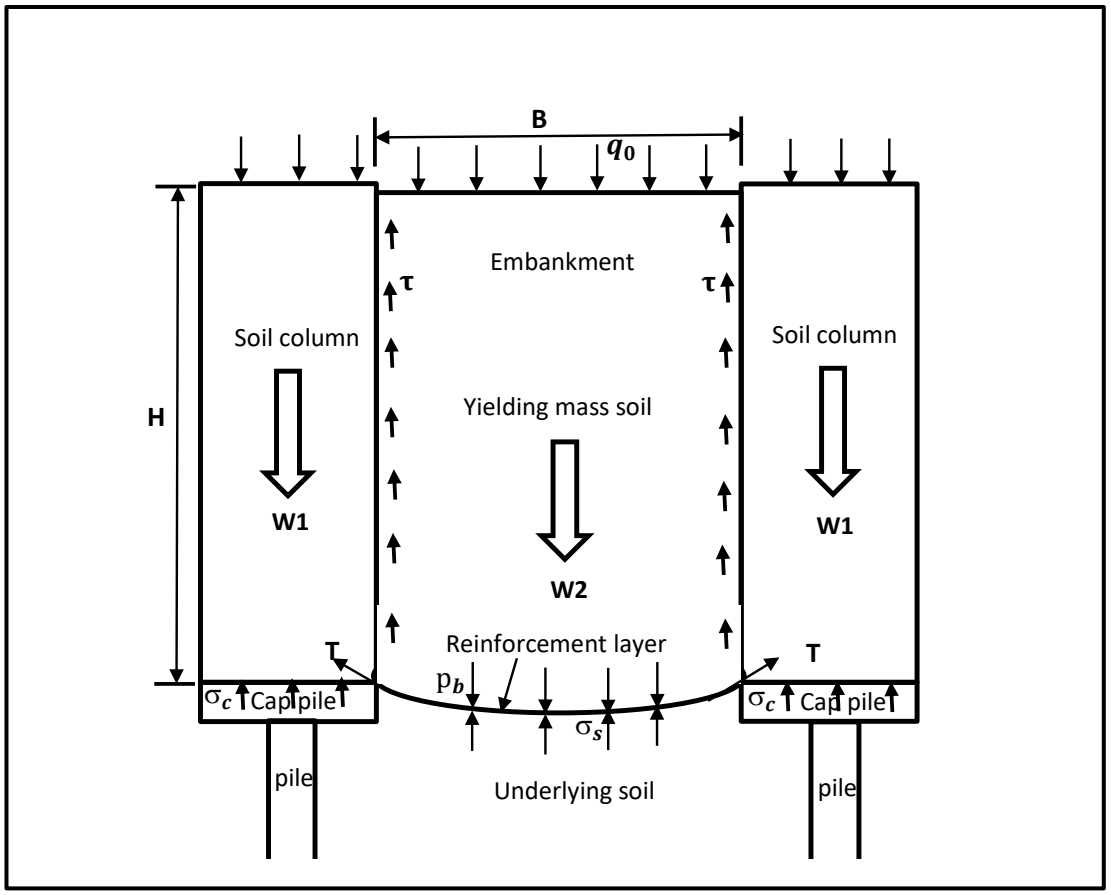

Figure 2.1. Load transfer mechanism (Han and Gabr 2002).

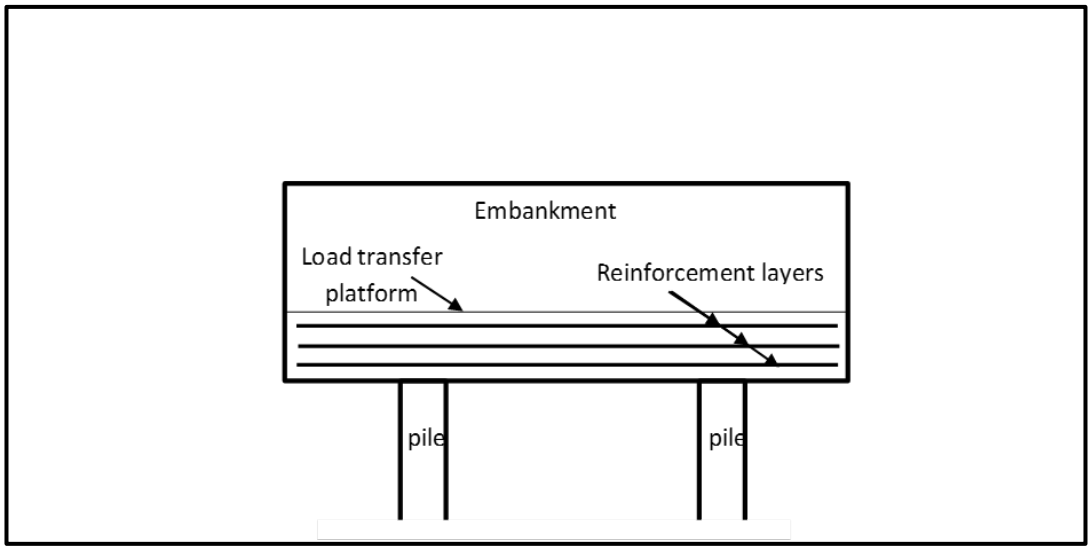

Figure 2.2. Load transfer mechanism - stiff reinforced soil mass (Collin et al. 2005).

2.2.1 Concept and application of soil arching

Underground structures such as buried conduits, tunnels, piled embankments, shelters and vertical anchors are increasingly built and utilised for prosperity of societies all over the world. It is paramount that such an underground structure is designed sustainably, efficiently and effectively. One of the major uncertainties in the design is the interaction between underground structure and surrounding soils which is dependent on the type and shape of structure, type of surrounding soils and free field stresses. Arching mechanisms play a pivotal role in the interaction between surrounding soils and underground structures/inclusions (e.g., Lee et al. 2006; Meguid et al. 2008; Costa et al. 2009; Van Eekelen 2015; Fattah et al. 2016). Depending upon the relative displacement between the underground structure/inclusion and adjacent soils, redistribution of stresses would occur as a result of the formation of either active or passive arching. For instance, if an underground inclusion subsides, a reduction in vertical stress occurs on the yielding area or the region of the

underground inclusion in comparison with the anticipated undisturbed overburden pressure in the free field due to active arching. The relative movement between the yielding region and the adjacent less deformable regions of the ground mobilises shear stresses. The evolving shear stress tends to minimise and/or prevent the settlement of the yielding part by reducing the pressure on this yielding region of the inclusion as well as increasing the pressure on the relatively stationary soil regions (Terzaghi 1943). In contrast, if an underground inclusion is stiffer than the adjacent soil regions, an increase in the loads/vertical stress occurs on the underground inclusion alongside a reduction in the stresses on the adjacent soil regions (passive arching) (Iglesia et al. 2013). Several experimental, analytical and numerical investigations were conducted with different perspectives including developing analytical equations (see for example, Terzaghi 1943; Iglesia et al.1999; Pirapakaran and Sivakugan 2007a and b; Cui et al. 2018), studying the shape of soil arching (see for example, Handy 1985; Iglesia et al. 1999 and 2013; Chevalier et al. 2008, 2009 and 2012; Moradi et al. 2015), quantifying the effect of soil type (see for example, Stone and Muir Wood 1992; Iglesia et al., 2013; Pardo and Saez, 2014; Wang et al., 2018) and studying the mode of arching (see for example, Vardoulakis et al 1981; Koutsabeloulis and Griffith 1989; Costa et al. 2009; Dalvi and Pise 2012).

2.2.2 Tensioned membrane effect

Le Hello and Villard (2009) defined the membrane effect as the ability of a geosynthetic reinforcement layer to adjust to the forces by tensile stresses that initially act perpendicular to its plane. Large deformation in the reinforcement sheet and large settlement in the sub soil is required to create the membrane

effect (Le Hello and Villard 2009). Due to the applications of the loads the sub soil is deformed downward, as a result the geosynthetic reinforcement layer is deformed as well. When the deformation in the reinforcement layer reaches the maximum value the tension membrane is generated. Based on the stiffness of the geosynthetic sheet the deformed reinforcement layer creates upward reaction forces to support the applied loads. Therefore, the stress underneath the reinforcement layer or on the sub soil layer will be reduced.

2.3 Design methods of reinforced piled Embankments

There are several design approaches to assess the performance of reinforced piled embankments such as Terzaghi (1943), Carlsson (1987) Guido (1987), Hewlett and Randolph (1988), Low et al. (1994), BS 8006 (1995), Russell and Pierpoint (1997), Kempton et al. 1998 Love and Milligan (2003), Russell et al. (2003), Kempfert et al. (2004), Abusharar et al. (2009), BS 8006-1 (2010), EBGEO (2010), Van Eekelen et al. (2011) and (2013) and Zhuang et al. (2014). A number of these methods will be presented and discussed in this section.

2.3.1 Terzaghi solution (1943)

Arching effect in granular soils was studied experimentally by Terzaghi using a trapdoor test (Terzaghi 1936). Terzaghi then proposed an analytical solution based on his trapdoor experimental results. It was found that lowering of strip plate under soil will cause the soil above the trap door to yield. It was noted that the yielding materials above trap door tends to settle and this movement was opposed by shear stresses created along the planes between moving part and fixed parts resulting in decreasing pressure on trap door and increasing pressure on the fixed sides.

Terzaghi analysed the forces acting on a rectangular element of soil with thickness of dz and weight of dW as shown in Figure 2.3. Due to the soil materials and surcharge (q) applied above this element, the vertical stress (σ_v) applied on the upper surface is:

$$\sigma_v = \gamma H + q \quad (2.1)$$

where;

σ_v = the vertical stress (kN/m^2)

γ = the unit weight of the soil in (kN/m^3)

q = the surcharge load applied on the surface of soil in (kN/m^2)

The corresponding normal stress on the vertical sliding (σ_h) is given by:

$$\sigma_h = k\sigma_v \quad (2.2)$$

where;

σ_h = the horizontal stress in (kN/m^2)

k = the earth pressure coefficient (dimensionless parameter)

The shear strength of the soil at failure according to Mohr-Coulomb failure criterion can be determined:

$$\tau = c + \sigma_h \tan\Phi \quad (2.3)$$

where;

τ = the shear strength in (kN/m^2)

Φ = the angle of internal friction of the soil in (degrees)

c = soil cohesion in (kN/m^2)

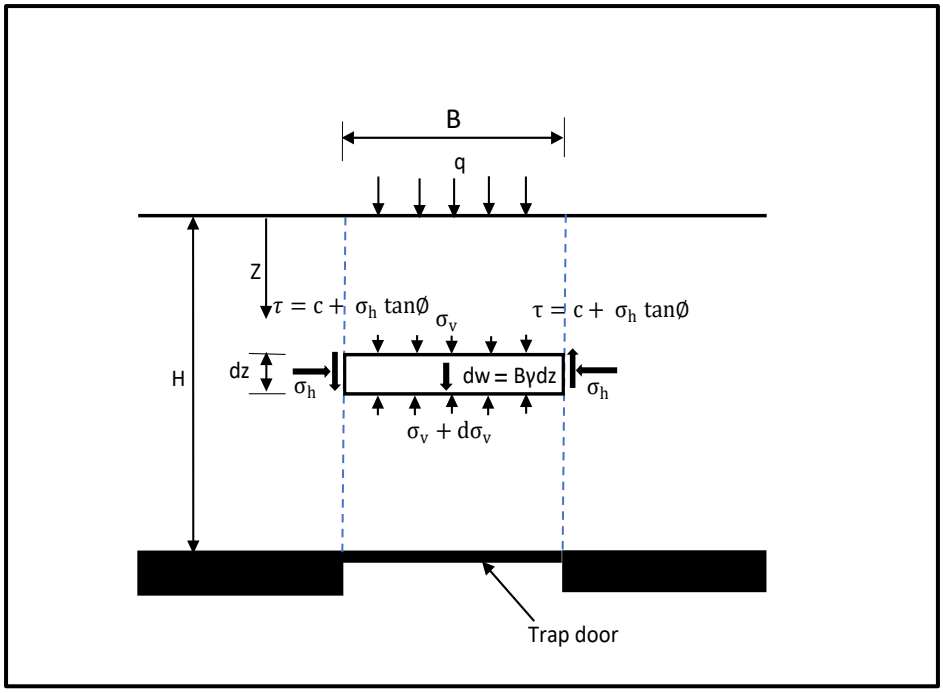

Figure 2.3. Load transfer mechanism (Terzaghi 1943).

When this rectangular element is in equilibrium, the summation of the vertical forces applied on this soil element must be equal to zero. Therefore, the vertical equilibrium can be expressed as

$$\frac{d\sigma_v}{dz} = \gamma - \frac{2c}{B} - k\sigma_v \frac{2\tan\Phi}{B} \qquad (2.4)$$

where;

B = the width of the trapdoor in (m)

Z = the thickness of the soil overlying the element in (m)

With boundary condition σ_v= q at z = 0 and solving this equation we obtain

$$\sigma_v = \frac{B\left(\gamma - \frac{c}{B}\right)}{2k\tan\Phi}\left(1 - e^{-\frac{2k\tan\Phi z}{B}}\right) + \left(qe^{-\frac{2k\tan\Phi z}{B}}\right) \qquad (2.5)$$

When, $c = 0$ and $q > 0$ the equation tends to be

$$\sigma_v = \frac{\gamma B}{2k\tan\Phi}\left(1 - e^{-\frac{2k\tan\Phi z}{B}}\right) + \left(qe^{-\frac{2k\tan\Phi z}{B}}\right) \quad (2.6)$$

When, $c = 0$ and $q = 0$ the equation tends to be

$$\sigma_v = \frac{\gamma B}{2k\tan\Phi}\left(1 - e^{-\frac{2k\tan\Phi z}{B}}\right) \quad (2.7)$$

Later on Pirapakaran and Sivakugan (2007a and b) extended Terzaghi's solution to a 3-D situation where the vertical load was placed on a rectangular trapdoor of finite length and width (L x B). Although Equation 2.5 has been widely used in calculating the stresses on yielding inclusions, it requires an accurate value for the earth pressure coefficient (k) which proves to be an issue to most engineers. Terzaghi (1943) assumed that an empirical value of k equals to 1.0 for practical applications whereas Krynine (1945) assumed a k value higher than the value of active earth pressure based on an inclined shearing surface. Russell and Pierpoint (1997) extended Terzaghi's solution by using a square arrangement of square columns supporting the embankment and recommended the use of a k value equals to 1.0 as proposed by Terzaghi (1943). Russell et al. (2003) suggested that the k value is to be taken 0.50. Recently, Potts and Zdravkovic (2008) showed that a coefficient of lateral pressure equal to unity gave comparable results to those obtained from a plane strain numerical analysis to arching over a void. Vardoulakis et al. (1981) proposed expressions for the distributions of the soil loads on the trapdoor in active and passive modes based on shear bands. The expression for active arching is consistent with Terzaghi's (1943) equation when k=1.0. However, the proposed equation for passive arching involves a

correction factor which was proposed to be 1~1.5. Handy (1985) found that the shape of arching is catenary and the (k) value can be determined by the following equation.

$$k = 1.06(\cos^2 \Theta + k_a \sin^2 \Theta) \quad (2.8)$$

where:

$$\theta = 45^o + \frac{\Phi}{2}$$

$$k_a = \frac{(1 - \sin \Phi)}{(1 + \sin \Phi)},$$

Where, k_a = the coefficient of active earth pressure

Krynine (1945) used the following equation to calculate the earth pressure coefficient (k)

$$k = \frac{(1 - \sin^2 \Phi)}{(1 + \sin^2 \Phi)} \quad (2.9)$$

When compares these different values of the earth pressure coefficient(k) by using the Terzaghi equation (equation 2.7). It can be noted that the vertical stress (σ_v) on the trap door is decreased with increasing the value of (k). This means that the value of vertical stress (σ_v) is very sensitive to the (k) value and is very important to choose an appropriate value.

2.3.2 Hewlett and Randolph solution (1988)

Hewlett and Randolph (1988) developed analytical solution from experimental tests based on the results of arching effect on the granular free draining soil. From their analysis, they presumed that three distinctive actions support the piled embankment. Firstly, the piles can reinforce and stiffen the underlying soft soil. Secondly, the piles can support the embankment soil by the arching effect and finally, the membrane action created by geosynthetic reinforcement

materials which were laid over the piles caps can transfer the loads to the piles caps. However, only unreinforced models were investigated in this study. The method of Hewlett and Randolph (1988) considers actual arches in the soil fill instead of vertical boundaries as considered by Terzaghi as shown in Figure 2.3. These arches transfer most of the embankment loads to the piles caps. The weight of embankment underneath the arches is supported by underlying soil. This method assumed that the arches are semi-circular in 2D with uniform thicknesses and no overlapping can be occurred between these arches. Also, the pressure applied on the sub soil is assumed to be uniform. In each arch, for analysis of equilibrium of an element on the crown of the arch, the major stress is in the horizontal (tangential) direction while the minor stress in the vertical (radial) direction which means that the yielding is occurred in the passive mode and is related to the passive coefficient of earth pressure (k_p). The vertical stress (σ_s) acting on the surface of the sub soil is presented as follows:

$$\sigma_s = \sigma_i + \frac{\gamma(S-a)}{2}, \tag{2.10}$$

$$\text{where, } \sigma_i = \gamma\left(H - \frac{S}{2}\right)\left(\frac{S-a}{S}\right)^{(k_p-1)} \tag{2.11}$$

$$\sigma_s = \gamma\left(H - \frac{S}{2}\right)\left(\frac{S-a}{S}\right)^{(k_p-1)} + \frac{\gamma(S-a)}{2} \tag{2.12}$$

where;

σ_i = the vertical stress acting immediately beneath the crown of the arch in (kN/m^2)

γ = the unit weight of the embankment soil in (kN/m^3)

H = the height of the embankment in (m)

k_p = the coefficient of passive earth pressure defined as

$$k_p = \frac{(1 + \sin \Phi)}{(1 - \sin \Phi)} \qquad (2.13)$$

S = the piles centre to centre spacing in (m)

a = the size of the pile cap in (m)

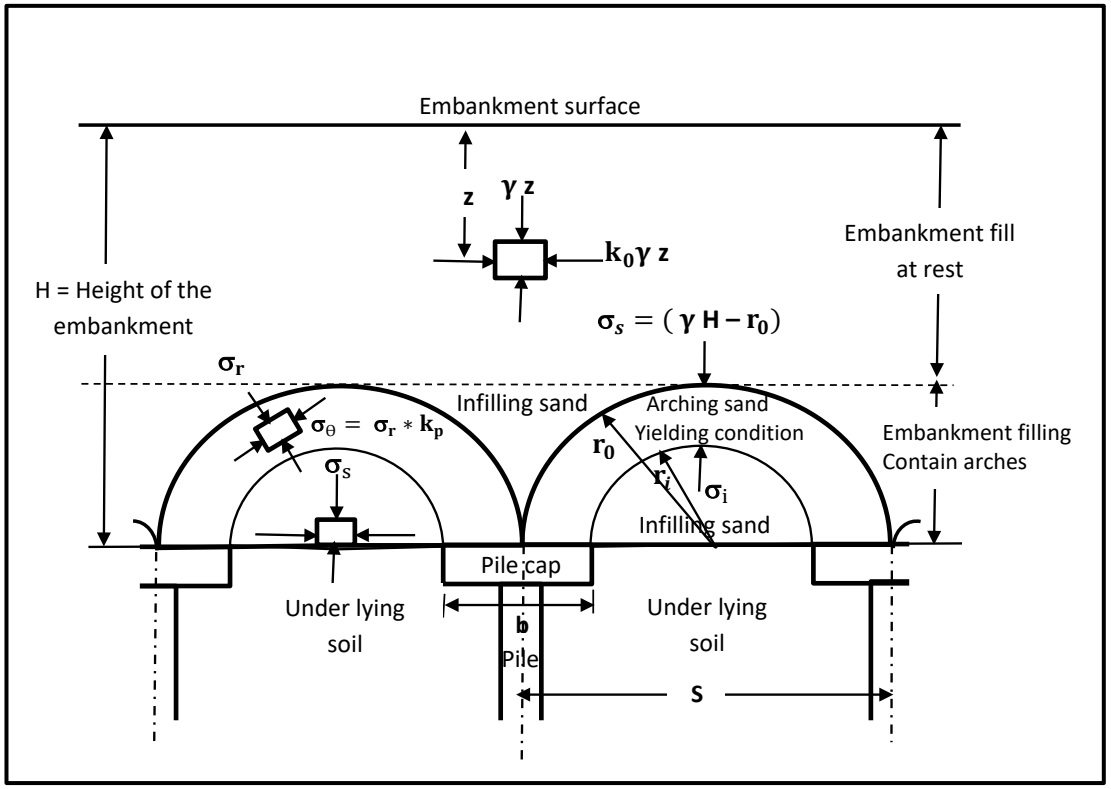

Figure 2.4. Section through piled embankment (Hewlett and Randolph 1988).

At the pile cap the major stress is in the vertical (radial) direction while the minor stress is in the horizontal (tangential) direction which means that the yielding is occurred in the active mode. However, the results of 2D case showed that the critical point is always on the crown of the arch and the stress ratio at anywhere else on the arch is less than the value of (k_p). Hewlett and Randolph (1988) also derived 3D solution which is more relevant to the arching above grid of piles. In this solution the analysis of arching is assumed as domes of hemispherical shape supported by the pile caps as shown in Figure 2.5-A. For 3D case, they proved that the critical point of the arches, where the

value of vertical stress (σ_s) resulting from the failure arch, is not only on the crown of the arch, it can also occur on the pile cap due the limited area of piles cap which may lead to bearing failure as shown in Figure 2.5-B. Moreover, it was noted that the critical point of the arch is located on the crown of arch when the embankment height is shallow. With increasing the embankment height, the critical point is transferred to the pile cap. Hewlett and Randolph (1988) developed two equations to calculate the efficiency, which represents the ratio between the loads carried by the piles to the total load of embankment, for both critical cases.

(a) Failure at the crown of the arch

The efficiency at the crown is presented as follows

$$E_{crown} = 1 - \left[1 - \left(\frac{a}{S}\right)^2\right]\left[\left(1 - \frac{a}{S}\right)^{2(k_P - 1)}\left(1 - \frac{(S-a)}{\sqrt{2}H}\frac{2(k_P-1)}{(2k_P-3)}\right) + \left(\frac{(S-a)}{\sqrt{2}H}\frac{2(k_P-1)}{(2k_P-3)}\right)\right] \quad (2.14)$$

(b) Failure at the pile

The efficiency at the pile is presented as the following

$$E_{pile} = \frac{\beta}{\beta + 1} \quad (2.15)$$

where,

$$\beta = \left(\frac{2k_P}{k_P + 1}\right)\left(\frac{1}{1 + \frac{a}{S}}\right)\left[\left(1 - \frac{a}{S}\right)^{(-k_P)} - \left(1 + \frac{a}{S}k_P\right)\right] \quad (2.16)$$

It is necessary for design purpose to consider that the value of efficiency is resulting of the failure of arch at the crown or at the pile cap and the lower efficiency (E_{min}) from both equations (2.14) and (2.15) will be the critical.

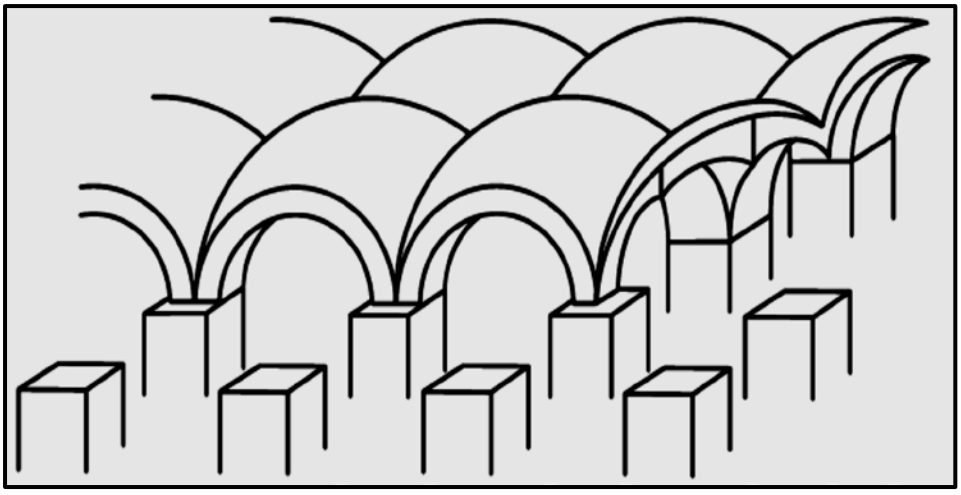

(A)

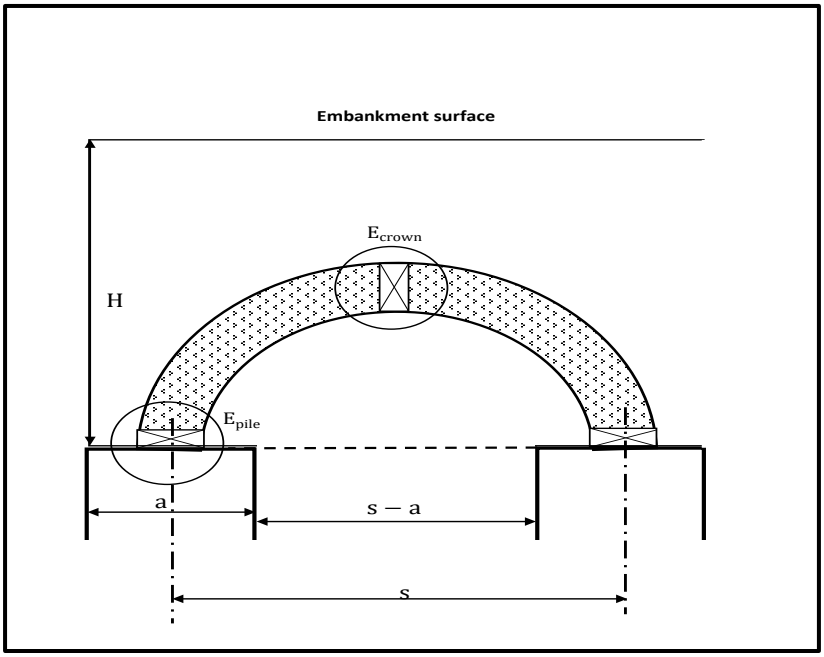

(B)

Figure 2.5. Arching theory according to Hewlett & Randolph (A) arching of soil development in 3D case (B) critical regions of failure on the arch (BS 8006 2010).

2.3.3 BS8006, 2010

The method used in British Standard code of practice for the design of strengthened/reinforced soils and fills has been initially developed by Jones et al. (1990) based on 2-dimensional geometry. The first version of the design code of this method was published in 1995 and later on it was updated in 2010.

BS8006 uses the Marston's formula for positively projecting conduits to obtain the amount of loads carried by the piles as following

$$\frac{\sigma_c}{\sigma_s} = (\frac{C_c a}{H})^2 \qquad (2.17)$$

Where;

σ_s = the vertical stress at the base of embankment in (kN/m^2) = $(\gamma H + w_s)$

γ = the unit weight of the embankment fill in (kN/m^3)

w_s = the uniformly distributed surcharge loading in (kN/m^2)

σ_c = the vertical stress on the pile cap in (kN/m^2)

a = the size of the pile cap in (m)

H = the height of the embankment in (m)

C_c = the arching coefficient defined as,

$c_c = 1.95\frac{H}{a} - 1.80$; for end − bearing piles and

$c_c = 1.50\frac{H}{a} - 0.07$; for friction and other piles

From this equation it can be noted that the strength of embankment fill is not taken into account which may affect the calculated stresses on the piles and sub soil. Eq. (2.17) is suitable for the 3D case; for the 2D situation the stress on cap beam can be determined as following

$$\frac{\sigma_c}{\sigma_s} = \frac{C_c a}{H} \qquad (2.18)$$

Depending on the critical height which is equal 1.4(s – a) according to this method, two situations of arching can be considered in the design of reinforced piled embankment. The distributed load (W_T) acting on the reinforcement

layer between two adjacent piles can be determined from the following two equations.

(a) for $H > 1.4(S - a)$ (full arching)

$$W_T = \frac{1.4S\gamma(S-a)}{S^2 - a^2}\left[S^2 - a^2\left(\frac{\sigma_c}{\sigma_s}\right)\right] \qquad \text{3D case} \qquad (2.19)$$

$$W_T = \frac{1.4s\gamma(S-a)}{S-a}\left[S - a\left(\frac{\sigma_c}{\sigma_s}\right)\right] \qquad \text{2D case} \qquad (2.20)$$

(b) for $0.7(S - a) \leq H \leq 1.4(S - a)$ (partial arching)

$$W_T = \frac{S(\gamma H + w_s)}{S^2 - a^2}\left[S^2 - a^2\left(\frac{\sigma_c}{\sigma_s}\right)\right] \qquad \text{3D case} \qquad (2.21)$$

$$W_T = \frac{S(\gamma H + w_s)}{S-a}\left[S - a\left(\frac{\sigma_c}{\sigma_s}\right)\right] \qquad \text{2D case} \qquad (2.22)$$

Also in this method an equation was developed to calculate the tension per meter (T) in the geosynthetics reinforcement layer.

$$T = \frac{W_T(S-a)}{2a}\sqrt{1 + \frac{1}{6\varepsilon}} \qquad (2.23)$$

where;

T = the axial tensile load in the reinforcement layer in (kN/m)

ε = the axial strain in the reinforcement layer

S = the piles centre to centre spacing in (m)

2.3.4 Low method (1994)

Low et al. (1994) derived an analytical solution to study the arching effect in the piled embankment with a layer of geotextile and caps beams based on the results from small scale model tests. The assumption in this method is based on the arching effect in piled embankment presented by Hewlett and Randolph

(1988). In this method the critical point always occurs on the crown of arch due to the area of cap beam is large enough to prevent occurring of the bearing failure. Therefore, the efficiency on the pile being always higher than the efficiency on the crown of the arch. Also, in this method the introduction of a factor (α) which was used in this method can allow the nonuniform vertical stress on the soft soil. The vertical stress acting on the underlying soil at midpoint between cap beams (σ_s) is given by Equation 2.24.

$$\sigma_s = \frac{\gamma\,(S-a)(k_p-1)}{2(k_p-2)} + \left(\frac{(S-a)}{S}\right)^{k_p-1}\left[\gamma H - \frac{\gamma S}{2}\,(1+\frac{1}{k_p-2})\right] \qquad (2.24)$$

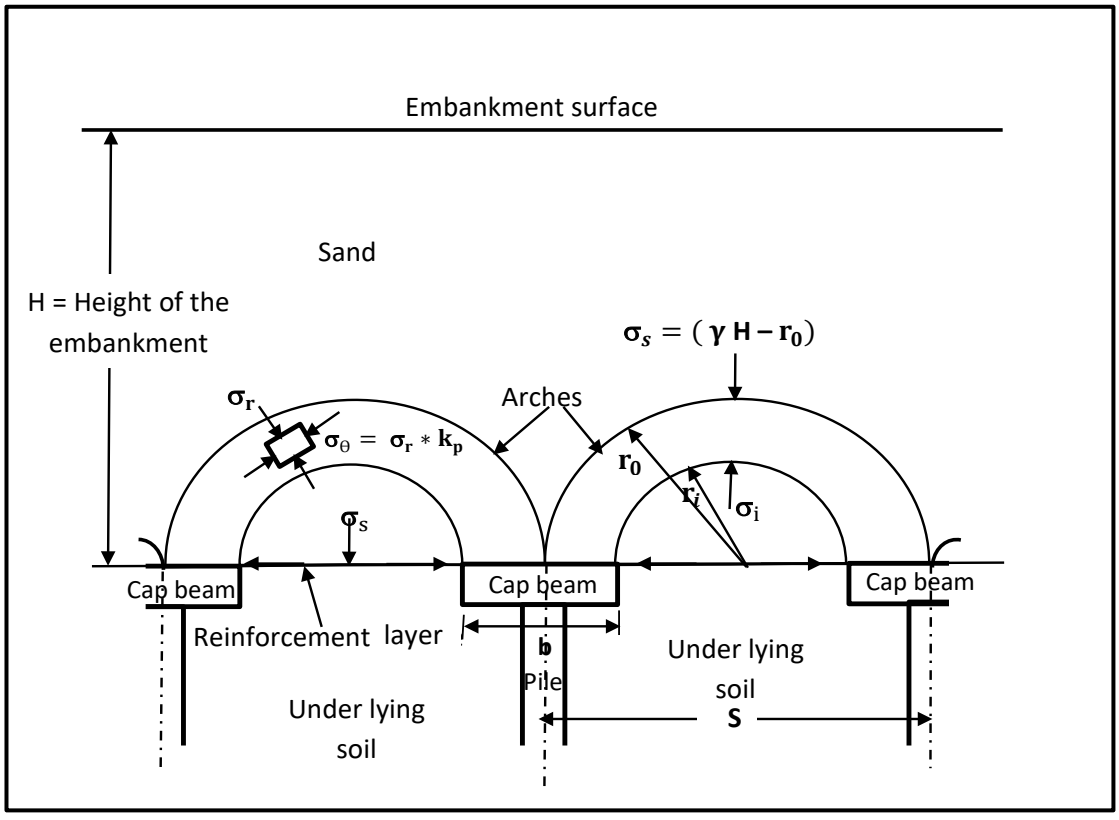

Figure 2.6. Section through piled embankment (Low et al.1994).

According to Low et al. (1994) the tension in reinforcement layer can be approximated as:

$$T = k_g \varepsilon \quad (2.25)$$

where;

T = the axial tensile load in the geosynthetic layer in (kN/m)

ε = the axial strain in the geosynthetic layer

k_g = the tensile stiffness of geosynthetic in (kN/m),

Low et al. (1994) also illustrated that the shape of deformation of the reinforcement layer is a circular arc with radius of (R) as shown in the Figure 2.7 and from this geometry the axial tension can be found from the following relation:

$$\frac{T}{R} = p_o = S'\left(\sigma_s - \frac{tE_c}{D}\right) \quad (2.26)$$

Based on the formation in reinforcement layer the axial strain can be determined by:

$$\varepsilon = \frac{\theta - \sin\theta}{\sin\theta} \quad (2.27)$$

And θ can be calculated as following:

$$\theta = \sin^{-1}\left[\frac{4\left(\frac{t}{S'}\right)}{1 + 4\left(\frac{t}{S'}\right)^2}\right] \quad (2.28)$$

where;

p_o = the pressure applied on the geosynthetics reinforcement layer in (KN/m^2)

σ_s = the pressure applied on soft ground in (KN/m^2)

E_c = the elastic modulus of soft soil in (KN/m^2)

t = the deflection in geosynthetics reinforcement layer at mid-point in (m)

D = the depth of soft soil layer in (m)

S' = the cap beams clear spacing in (m)

In order to determine the deflection in the geosynthetics reinforcement layer (t), Low et al. (1994) used trial values of (t) until the value of soil reaction force is satisfied with the vertical force equilibrium. If the maximum deflection in the reinforcement layer is known, (θ) can be directly calculated and then the axil strain (ε) and axil stress (T) in the geosynthetic reinforcement layer can be determined.

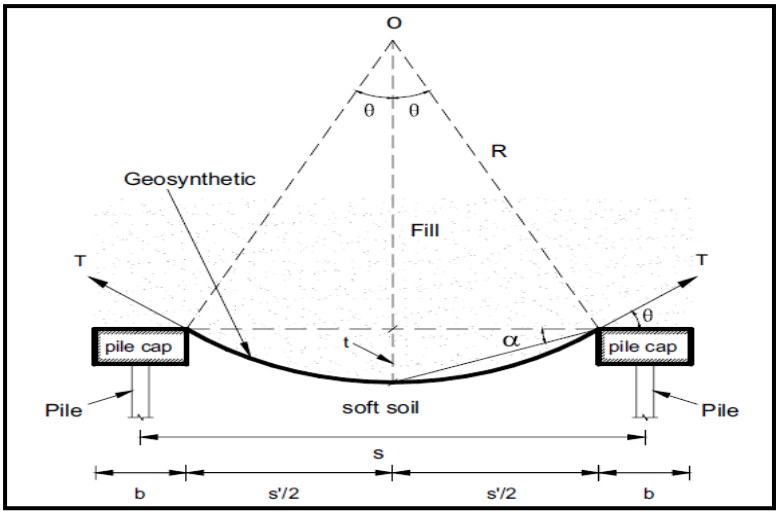

Figure 2.7. Geosynthetics overlying pile caps and soft soil ground (Low et al. 1994; Abusharar et al. 2009).

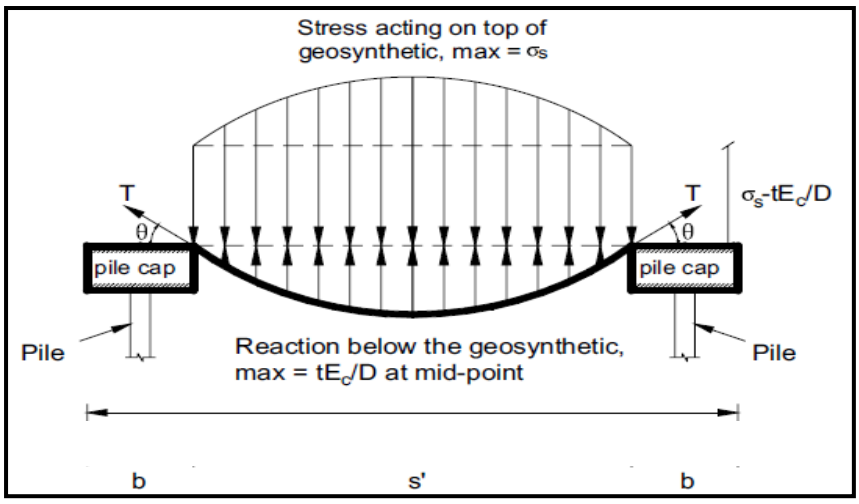

Figure 2.8. Stress distribution in reinforcement layer (Low et al. 1994; Abusharar et al. 2009).

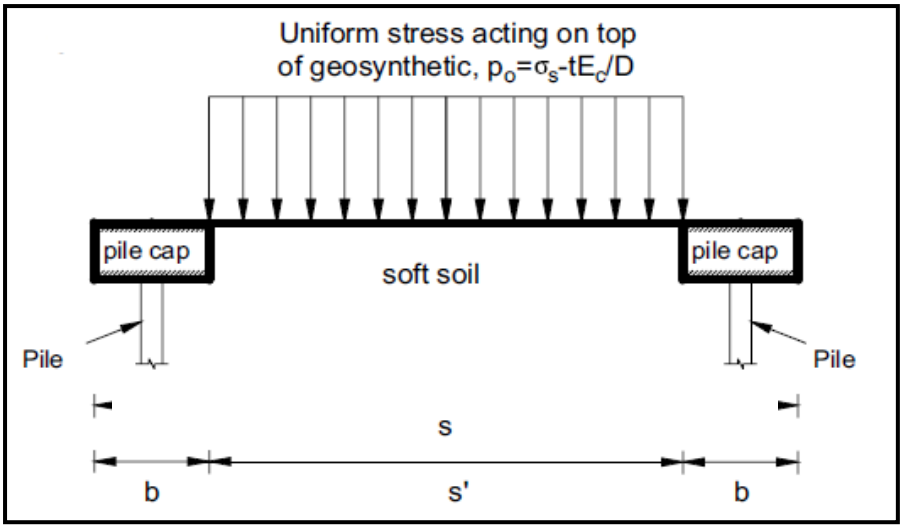

Figure 2.9. Net stress distribution in reinforcement layer (Low et al. 1994; Abusharar et al. 2009).

2.3.5 Abusharar method (2009)

The pervious solution (Low et al.1994) was carried out only under the overburden pressure (weight of the embankment). However, Abusharar et al. (2009) studied analytically the arching of embankment with layer of geotextile place at the base of embankment. The assumption of this method is the same with Low et al. (1994) with some modifications. These modifications in this method are inclusion of uniform surcharge (q), Individual square caps are arranged in a square grid pattern and skin friction mechanism at soil-geosynthetics interface is considered. The vertical stress on the soft soil ($\boldsymbol{\sigma_s}$) at the midpoint between any two piles is:

$$\sigma_s = \frac{\gamma\,(S-a)(k_p-1)}{2(k_p-2)} + \left(\frac{(S-a)}{S}\right)^{k_p-1}\left[q+\gamma H-\frac{\gamma S}{2}\,(1+\frac{1}{k_p-2})\right] \qquad (2.29)$$

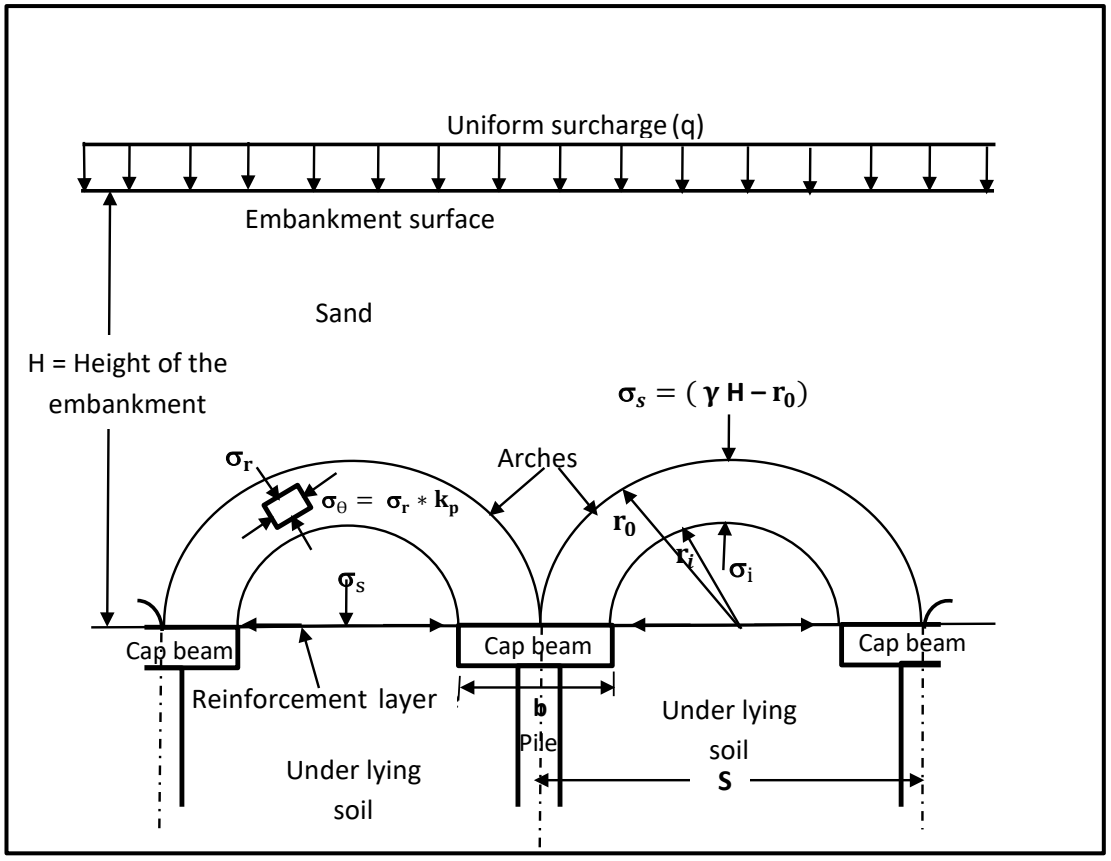

Figure 2.10. Section through piled embankment (Abusharar et al. 2009).

In the previous method the tension in reinforcement layer was estimated based on trial and error. However, Abusharar et al. (2009) improved Low et al. (1994) method by deriving a new equation to calculate the deflection in the reinforcement layer. As it was mentioned above skin friction mechanism is a new modification in this method which can enhance soil-reinforcement interface resistance as shown in the Figure 2.11. According to Figures 2.7 – 2.9, the axial strain (ε_a) can be found from the following equations.

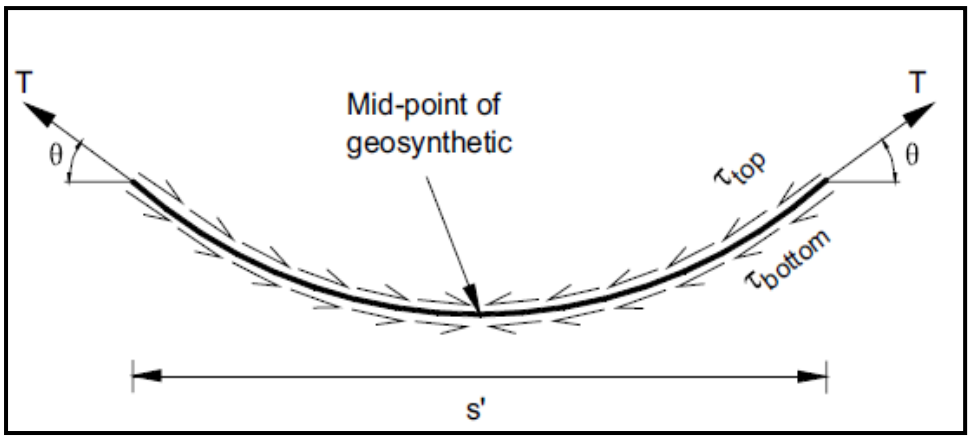

Figure 2.11. Deformation of reinforcement layer (Abusharar et al. 2009).

$$\sin\theta = \frac{4\left(\frac{t}{S'}\right)}{1+4\left(\frac{t}{S'}\right)^2} = \frac{4\beta}{1+4\beta^2} \quad ,\text{where, } \beta(\text{sag ratio}) = \frac{t}{S'} \text{ , } \theta = 2\alpha \ = 2(2\beta)$$

$$= \ 4\,\beta$$

The axial strain(ε) in reinforcement layer is calculated by the following equation:

$$\varepsilon_G = \frac{\Delta l}{S'} = \frac{\theta - \sin\theta}{\sin\theta} = 4\beta^2 \qquad (2.30)$$

And the axial tension (T) in reinforcement layer is calculated by the following equation:

$$2T\sin\theta = p_o\, S' = \ S'\left(\sigma_s - \frac{tE_c}{D}\right) \qquad (2.31)$$

Soil-geosynthetics interface shear stress (τ) can calculated as following:

$$\tau = \tau_{top} + \tau_{bottom} \ = \sigma_n \tan\delta' \ = \lambda\left(\sigma_s \tan\phi_s + \frac{tE_c}{D}\tan\phi_c\right) \qquad (2.32)$$

where; (σ_n) is normal stress at the interface in (kN/m^2), (δ) is angle of friction between soil and reinforcement $(\tan\delta \ = \lambda\tan\phi)$, (λ) is a factor ranged from 0.7 to 0.9 depending on the type of reinforcement.

From the equilibrium of the horizontal forces in Figure 2.11 can get the following equation

$$\Delta l = \frac{4T\,S' - \tau\,S'^2}{4(E_g * w)} \qquad (2.33)$$

where, (E_g) is the elastic modulus of reinforcement layer in (kN/m^2) and (w) is the width of reinforcement layer in (m).

$k_g = E_g\,w$

From the equations (2.31), (2.32) and (2.33) can get the following equation

$$a\beta^3 + b\beta^2 + c\beta + d = 0 \qquad (2.34)$$

where; $a = 32Dk_g + 4\,S'^2E_c$, $b = 2S'^2\,\lambda E_c \tan\phi_c - 4\,S'\,D\,\sigma_s$,

$c = 2S'\,\lambda D\sigma_s \tan\phi_s + S'^2E_c$, $d = -S'\,D\,\sigma_s$

By solving this equation one can find the value of (β) which can be used directly to find the values of settlement in the reinforcement layer and the axial tension in the reinforcement layer. These values can be used to find the vertical stress applied on the reinforcement layer. The value of (β) depends on the properties of embankment fill, properties of the reinforcement layer, properties of soft ground soil and the geometry of structure.

2.3.6 Zhuang method (2014)

Zhuang et al. (2014) developed new method to study the arching effect in reinforced piled embankment which is simple compared with other methods. The assumption in this method is based on the arching effect presented by Hewlett and Randolph (1988) (including the effect of geosynthetic reinforcement layer and subsoil support). In this method the stress acting on the sub soil (σ_s) at the midpoint between any two piles and the magnitude of tensile stress generated in reinforcement layer can be determined. The vertical

stress acting on the sub soil (σ_s) and the deflection in the middle of geosynthetic reinforcement layer (t) are defined from the equations (2.35), (2.36) and (1.37) as follows:

(a) Equilibrium analysis at the crown of the arch

$$\sigma_s = \gamma \frac{(S-a)}{\sqrt{2}}\left(\frac{2K_P-2}{2K_P-3}\right)+\left\{\gamma H - \frac{\gamma S}{\sqrt{2}}\left(\frac{2K_P-2}{2K_P-3}\right)\right\}\left(1-\frac{a}{S}\right)^{(2K_P-2)} \quad (2.35)$$

(b) Equilibrium analysis at the pile

$$\sigma_s = \frac{\gamma H}{\left\{\left(1-\frac{a^2}{S^2}\right)+\left(\frac{2K_P}{(K_P+1)}\right)\left[\left(1-\frac{a}{S}\right)^{(1-K_P)}-\left(1-\frac{a}{S}\right)\left(1+\frac{K_P a}{S}\right)\right]\right\}} \quad (2.36)$$

$$\frac{64k_g}{3S'^4}t^3+E_0\frac{t}{D}-\sigma_s=0 \quad (2.37)$$

where; (t) is the deflection at the midpoint in the base of embankment and geosynthetic reinforcement layer in (m), (K_g) is the stiffness of reinforcement layer in (kN/m), (E_0) is the stiffness of soft soil in (kN/m^2), (D) is thickness of soft soil in (m), (S') is the clear spacing between pile caps in (m).

2.3.7 Other arching methods

Guido et al. (1987) derived an empirical method according to the results from plate loading tests. He assumed that the load spreads through the fill layer by an angle of 45^o with the horizontal as shown in Figures 2.12 and 2.13. Also, he suggested that the weight of soil under the pyramid shape which is not transferred to the piles is supported by layers of geogrid reinforcement.

According to this method the stress acting on sub soil in two dimensional case can be estimated as following

$$\sigma_s = \frac{\gamma(S - a)}{4} \qquad (2.38)$$

While in three dimensional case it can be estimated as

$$\sigma_s = \frac{\gamma(S - a)}{3\sqrt{2}} \qquad (2.39)$$

where;

σ_s = the stress on sub soil in (KN/m^2)

γ = the unit weight of embankment soil in (KN/m^3)

S = centre to centre distance of pile caps in (m)

a = the pile cap width in (m)

From equations 2.38 and 2.39 it can be seen that the height and shear strength of embankment fill is not considered in this method. However, this method assumes that load spreads through compacted fill soil with multiple layers of geogrid.

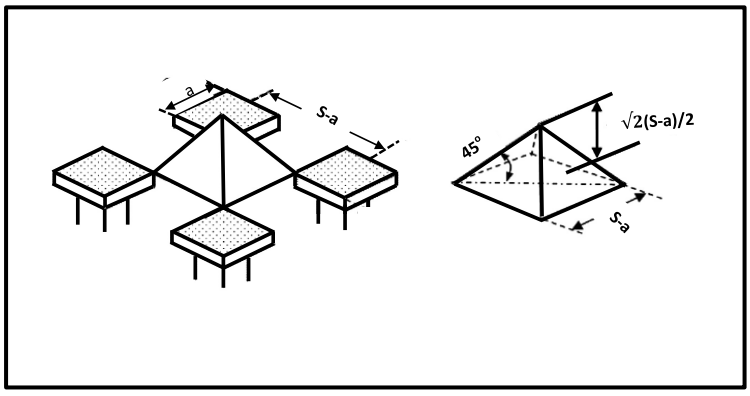

Figure 2.12. The shape of arching in 3 dimensions based on Guido et al. (1987), method

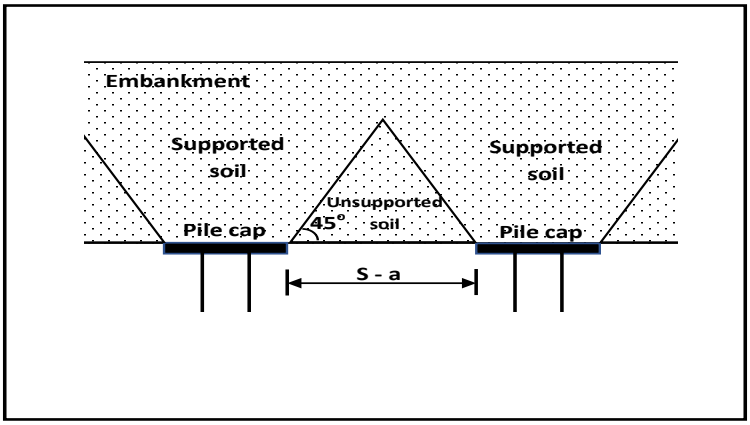

Figure 2.13. The shape of arching in 2 dimensions based on Guido et al. (1987), method

Carlsson (1987) suggested that the arching shape can be approximated by two wedges with an internal angle at the apex equal to 30°. Kempfert et al. (2004) verified a new method in three-dimensional case based on equilibrium of dome shaped arches and the measurements from his experimental models which were carried out in the lab in a scale of 1:3. In this method for unreinforced case, the sub soil foundation is allowed to support a part of loads which are not supported by the piles. Also, in this method the tension and strain in geosynthetics reinforcement are estimated according to the theory of elastically embedded membranes.

2.4 Ground Reaction Curve (GRC)

The previous methods considered one shape of the formed arching, however, Iglesia et al. (1999 and 2013) found that the formed arch shape went through many stages between circular, triangular and prismatic stages as shown in Figure 2.14. Iglesia et al. (1999) used ground reaction curve (GRC) to describe the stages of formed arch. GRC described the relation between the shape of formed arch and related sub soil displacement. Iglesia et al. (1999) was the

first who described the ground reaction curve for tunnelling applications by the combination of the arching theories and the experimental data form centrifuge test. They illustrated that the development of arching went through five characteristic features of stages during the underground structure displacement, at rest stage (no arching developed), the initial arching stage, the maximum arching stage (minimum loading stage), recovery loading stage and the ultimate state stage (final stage). The Ground reaction curve represents the normalized stress (F^*) (the stress on the underground structure to overburden pressure) to the normalized displacement (δ^*) (the underground structure displacement to the width of the underground structure).

$$F^* = \left(\frac{F}{\gamma H}\right) \qquad (2.40)$$

$$\delta^* = \left(\frac{\delta}{B}\right) \qquad (2.41)$$

Where;

F = the stress on the roof of underground structure in (kN/m^2)

γ = the unit weight of soil mass above the underground structure in (kN/m^3)

H = the height of soil mass above the underground structure in (m)

B = the width of the underground structure in (m)

δ = the settlement of the underground structure in (m)

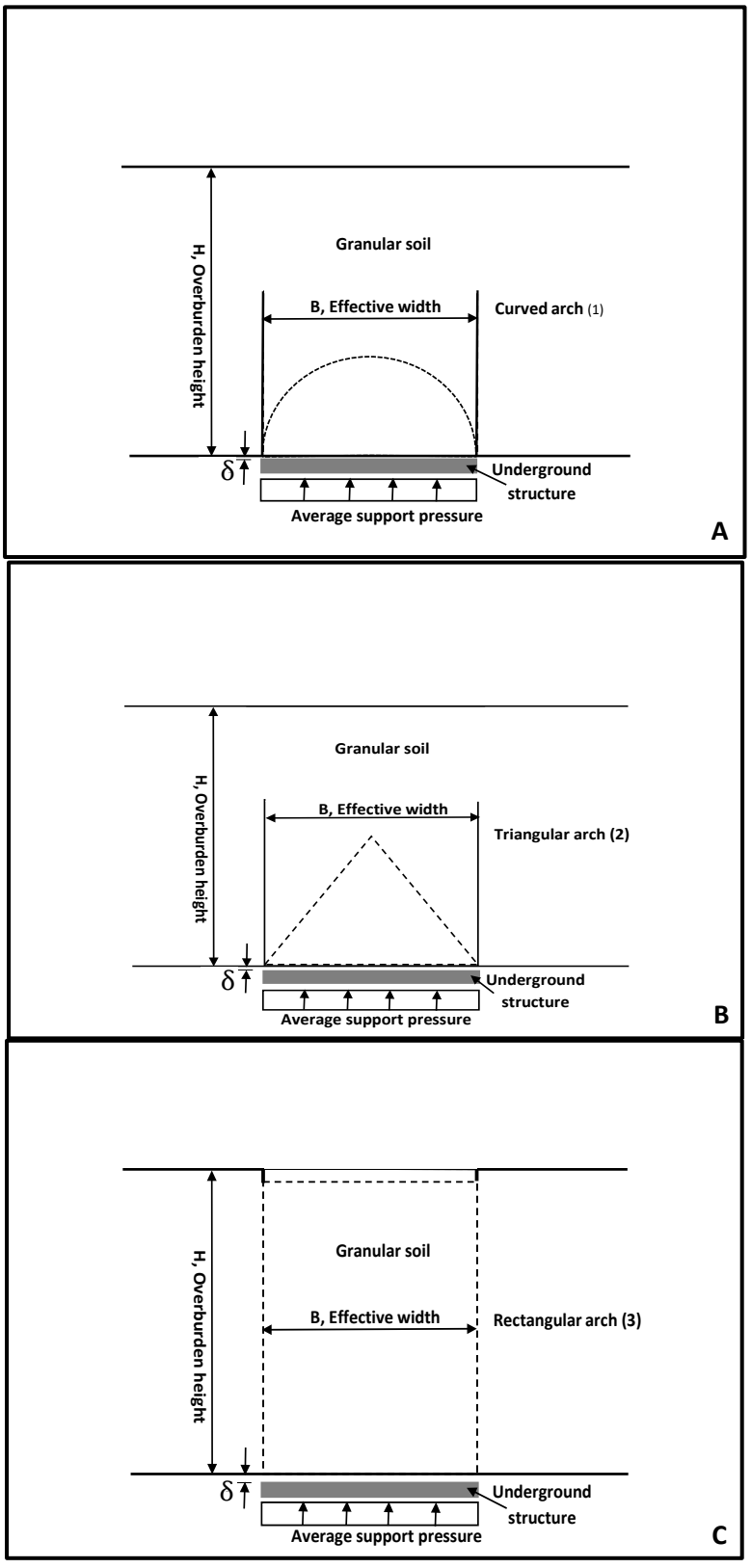

Figure 2.14. Arching evolution, (A) maximum arching (B) transition stage and (C) ultimate stage (Iglesia et al. 1999).

As shown in Figure 2.15 the Ground reaction curve (GRC) starts from geostatic condition where the pressure on the underground structure is equal to overburden pressure (γH) and during this stage no arching effect is developed. The initial response causes a significant reduction in the vertical stress on the underground structure with small relative structure displacement. Iglesia et al. (1999) assumed that the semi-curved arching starts to form over the trap door during this stage. Iglesia et al. (1999) represented the rate of stress decrease during this stage by arching modulus parameter (M_A) and they found that the arching modulus was about 125 based on experimental results of centrifuge trapdoor with granular media. Also, Iglesia et al. (1999) observed that when the shape of ground reaction curve appearance started to change from linear line to curve, the breakpoint can be occurred. The breakpoint seems to be accrued at displacement of around 1% of trapdoor width. The straight line fit from the starting point to the breakpoint produces a slope of ~63. This slope represents the secant modulus (M_B) of active arching. When the vertical load on the structure reaches minimum value, the maximum arching is occurred and semi curved arching is developed as shown in Figure 2.14-A (Iglesia et al.1999). With further underground structure displacement, the surrounding soil starts to follow the structure which causes to increase the vertical load on it. The ground reaction curve changes from maximum arching stage (minimum load) to the loading recovery stage. Iglesia et al. (1999) illustrated that the loading recovery curve might be straight line and can be characterised by loading recovery index (λ') and according to test results it was found that the load recovery index increased with increasing B/d_{50} (d_{50} is the average of particle size) and decreasing H/B. Also, Iglesia et al. (1999)

suggests that the triangular arch is formed during this stage as shown in Figure 2.14-B. With further underground structure displacement the convergence of surrounding soil to underground structure continues to increase and the arch will eventually collapse. Also, Iglesia et al. (1999) suggests that the configuration of the arch is changed from triangular shape to rectangular shape and the mass of soil on the trapdoor is bounded by two vertical shear planes during this stage as shown in Figure 2.14-C. Iglesia et al. (1999) used the solution of Terzaghi to determine the ultimate stress on the structure. Further details about the ground reaction curve (GRC) can be found in Iglesia et al. (1999 and 2013).

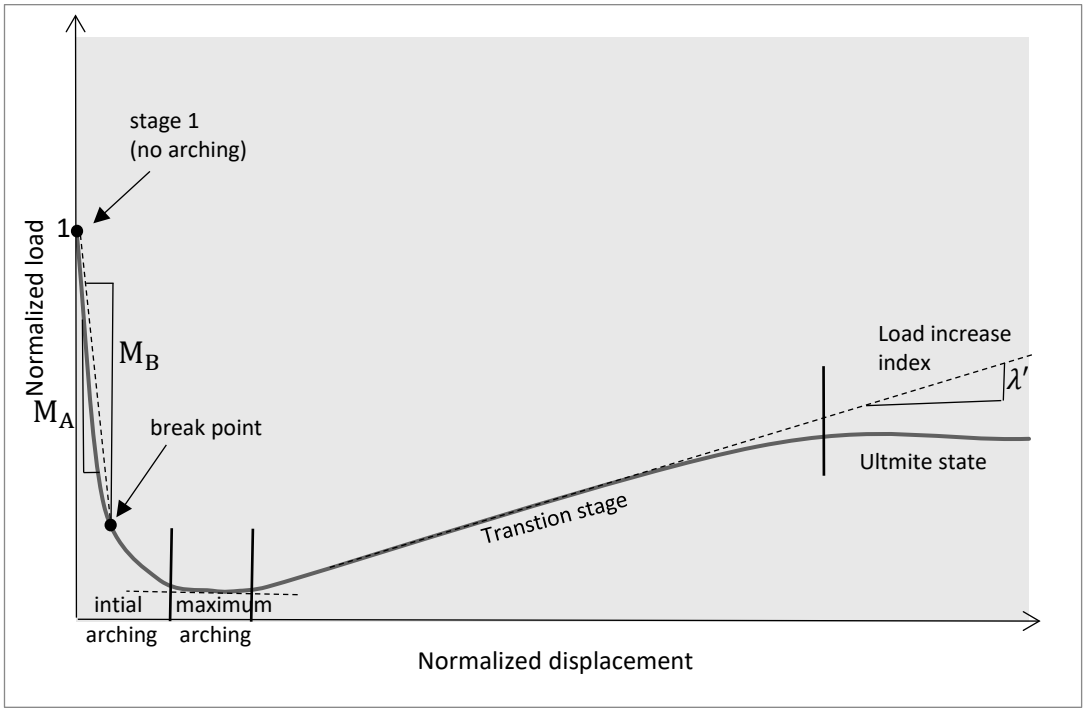

Figure 2.15. Ground reaction curve (GRC) (Iglesia et al 1999).

Also, Chevalier et al. (2008), found experimentally and numerically that different shapes of arching were formed along the trap door settlement which is consistent with finding by Iglesia et al. (1999) as shown in Figure 2.16. It

was resulted that three distinctive phases of arching were developed during the trapdoor displacement i. Initial phase where the maximum arching was developed ii. transition phase where the vertical stress on the trap door starts gradually to increase and iii. final phase where the increase of the vertical stress on the trapdoor nearly becomes constant and during this stage two vertical slipping planes occur at the edges of the trap door. Cui et al. (2018) found that the shape of arching depends on the height of the embankment and the pile spacing. When the height of the embankment and piles spacing was small, the development of arching shape goes between triangular to parabolic and finally became hyperbolic while when the embankment height and piles spacing was large the arching expended to the embankment surface in parabolic shape and finally formed in rectangular shape. Costa et al. (2009) used a centrifuge facility to investigate failure mechanisms in sand over a deep active trapdoor. It was found a significant difference in the failure mechanism that developed under active trapdoor conditions between shallow embankments and deep embankments.

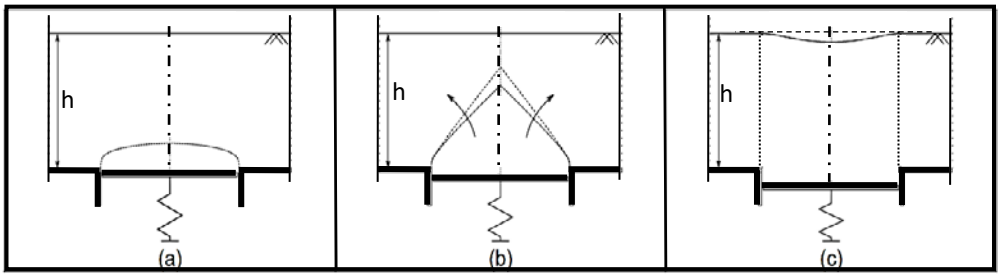

Figure 2.16. Arching development during trapdoor displacement (a) first stage (b) transition stage and (c) final stage (Chevalier et al. 2008).

2.5 Critical height of arching (H_C)

The critical height (H_C) is defined by McKelvey (1994) and Chevalier et al. (2007) as the point where the differential settlement between soil element and adjacent soil is equal to zero as shown in Figure 2.17. In piled embankment the height of the region where the arching mechanism is working effectively is called the critical height. The soil particles under this region tend to move downwards to the sub soil while the soil particles above this region stay in the original position without movement. The previous methods such as (Terzaghi 1943; Carlsson 1987; Hewlett and Randolph 1988; Low et al. 1994; BS 8006 1995; Kempfert et al. 2004) used the critical height to estimate the magnitude of the arching. A number of these methods linked the effective region with the width of the yielding part of soil or the piles spacing. Terzaghi (1943) reported that on his trapdoor experimental investigation, the shearing resistance in the sand soil is still active up to the height of 2.5 times the width of the trapdoor from the trapdoor surface. Also, Hewlett and Randolph (1988), Low et al. (1994), BS 8006 (1995 and 2010) and Abusharar et al. (2009) suggested that in the piled embankment analysis the complete arching is occurred when the height of the embankment is equal or more than 1.4 of piles spacing. However, Kempfert et al. (2004) derived a new design method based on experimental and numerical models. According to his assumption the critical height is equal to the half of the clear spacing. In addition, Horgan and Sarby (2002) conducted an experimental plane strain model test by using a trapdoor system for two types of granular materials and found the critical height for both soils to be located between 1.545 and 1.92 times the width between the supports. Naughton (2007) proposed a method for estimating of the magnitude of the

arching based on the critical height. He concluded that the critical height is strongly dependent on the angle of shearing resistance of soil. Naughton (2007) calculated the variation in critical height with different values angle of shearing resistance ranging between 30^{o} and 45^{o}.The critical height varies between 1.24 and 2.4 times the piles clear spacing. McGuire (2011) proposed an equation to calculate the critical height using bench-scale laboratory tests. It was found that the critical height ($\mathrm{H_c}$) is dependent on the columns dimeter ($\mathrm{d_c}$) and the columns clear spacing (S') and is given by the following equation for 3 dimensional case.

$$\mathrm{H_c} = 1.15S' + 1.44\mathrm{d_c} \qquad (2.42)$$

For 2 dimensional case the critical height can be estimated as follows

$$\mathrm{H_c} = 1.725S' + 1.44\mathrm{d_c} \qquad (2.43)$$

Ellis and Aslam (2009 a and b) found from the results of centrifuge tests that for unreinforced embankments no differential settlement is occurred at the surface when the height of the embankment is equal to or greater than twice the clear spacing between pile caps, (S - a). Recently Cui et al. (2018) presented a new mothed to determine the stress acting on the sub soil based on the experimental tests of studying the behaviour of piled embankment. According to their calculation the height of embankment required to prevent any differential settlement in the embankment surface is equal to or more than four times the pile caps clear spacing. A summary of the critical heights for the existing design methods is presented in Table1. However, all these methods studied the critical height under static loading conditions only. Applying repeating or cyclic loads might change the location of the critical height.

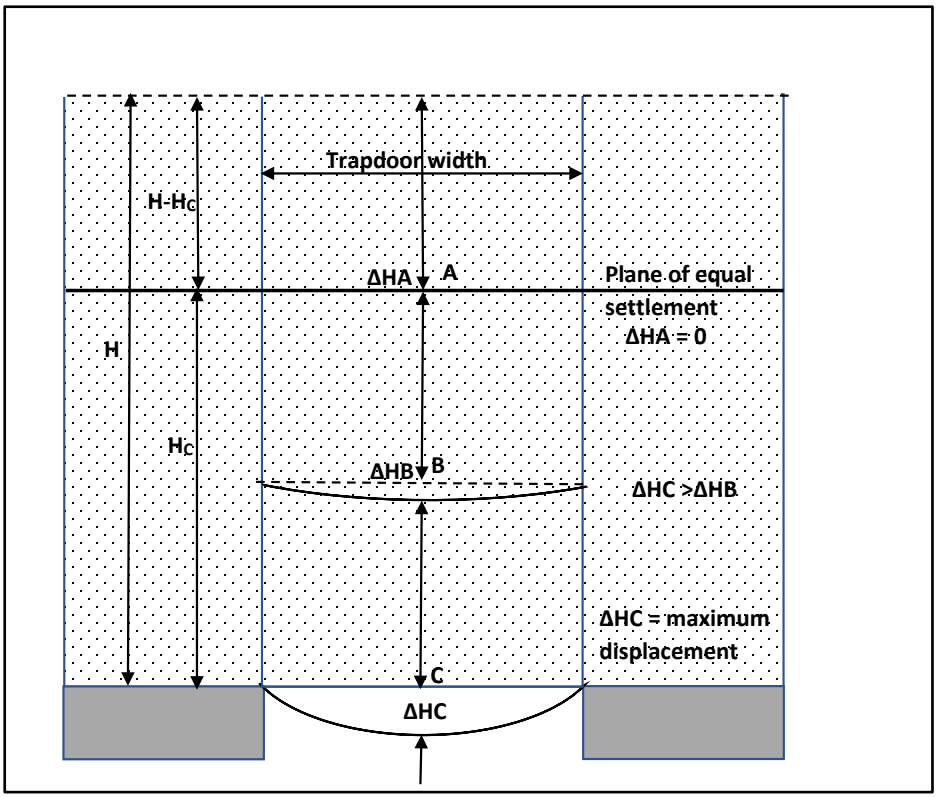

Figure 2.17. Plane of equal settlement (McKelvey 1994).

Table 2.1. Summary of critical height in different methods.

Design method	Critical arch height
Terzaghi (1936)	2.5 (S-a)
Carlsson et al. (1987)	1.87 (S-a)
Hewlett and Randolph(1988)	1.4 (S-a)
Low et al. (1994)	1.4 (S-a)
BS8006 (1995 and 2010)	1.4 (S-a)
Horgan and Sarsby (2002)	(1.545-1.92) (S-a)
Kempfert et al. (2004)	S/2
Naughton (2007)	(1.25-2.40) (S-a)
Abusharar et al. (2008)	1.4 (S-a)
Yun-min et al. (2008)	1.4 -1.6 (S-a)
Ellis and Aslam (2009a,b)	2.0 (S-a)

Note: H, embankment height; S, pile caps spacing; and a, pile cap width

2.6 Assessment of load transfer mechanism

There are many parameters which are widely used to assess the degree of load transfer mechanism such as efficiency, stress concentration ratio, settlement ratio and tension and axial strain in geosynthetic reinforcement.

2.6.1 Efficiency (E)

One of the most important of these parameters is efficiency (E) which represents the ratio between the loads carried by the piles to the total load of embankment and surcharge load (Abusharar et al. 2009). The efficiency can be defined as

(a) Without reinforcement layer and without uniform surcharge

$$E = 1 - \frac{S'\sigma_s}{S\gamma H} \qquad (2.44)$$

(b) Without reinforcement layer and with uniform surcharge

$$E = 1 - \frac{S'\sigma_s}{S(\gamma H + q)} \qquad (2.45)$$

(c) With reinforcement layer and with surcharge

$$E = 1 - \frac{S'p_o}{S(\gamma H + q)} \qquad (2.46)$$

where; (σ_s) is the load applied on soft ground in (kN/m^2), (p_o) is the stress applied on the reinforcement layer in (kN/m^2), (γ) is unit weight of the embankment fill in (kN/m^3), (H) is height of embankment in (m) and (S) is piles

centerline spacing in (m), (S') is pile clear spacing in (m) and (q) is uniform surcharge load applied on the embankment fill surface in (kN/m^2).

2.6.2 Soil Arching ratio or stress reduction ratio $(\boldsymbol{\rho})$

The effect of arching within embankment fill can be measured by the soil arching ratio or stress reduction ratio (ρ) which is defined as follows (as proposed by McNulty (1965)

$$\rho = \frac{p_o}{(H\gamma + q)} \qquad (2.47)$$

where; (p_o) is the average vertical stress applied on the trapdoor (for Terzaghi, (1943) or McNulty, (1965) studies) or geosynthetics (for Han and Gabr, (2002) and Borges and Marques, (2011) studies) in (kN/m^2), (γ) the unit weight of the embankment fill in (kN/m^3), (H) is the height of embankment in (m) and (q) is uniform surcharge on the embankment in (kN/m^2).

When $\rho = 0$ that means the complete arching is occurred and the complete load of the fill on the soft soil is transferred to the pile. When $\rho = 1$ which indicates no arching occurring and no load of the fill on the soft soil is transferred to the pile (Han and Gabr 2002; Borges and Marques 2011).

2.6.3 Stress concentration ratio (SCR)

The stress concentration ratio (SCR) is a factor that is used to measure the degree of load transfer to the piles head. According to Abusharar et al. (2009) the stress concentration ratio can be defined by dividing the stress on the pile caps to the stress on the sub soil. This factor can be used for both unreinforced and reinforced piled embankment.

$$SCR = \frac{\sigma_p}{\sigma_s} \tag{2.48}$$

$$SCR = \frac{S(\gamma H + q) - S'\,\sigma_s}{b\sigma_s} \qquad \text{without reinforcement} \tag{2.49}$$

$$SCR = \frac{S(\gamma H + q) - S' p_0}{a p_0} \qquad \text{with reinforcement} \tag{2.50}$$

where; (SCR) is stress concentration ratio, (σ_p) is the vertical stress on the pile caps in (kN/m^2), (σ_s) is the vertical stress on the soil in (kN/m^2), (p_o) represents the vertical stress applied on the geosynthetics reinforcement layer in (kN/m^2), (H) is the embankment height in (m), (S) is the pile caps center to center distance in (m), (q) is uniform surcharge pressure applied on the embankment fill surface in (kN/m^2), (γ) the unit weight of the embankment fill in (kN/m^3) and (a) is the pile caps width in (m).

2.6.4 Settlement ratio (s)

Settlement ratio (s) represents the ratio between the settlements in the reinforced case to the settlement in the unreinforced case (Abusharar et al., 2008).

$$s^* = \frac{t}{t_0} \tag{2.51}$$

where; (s^*) is settlement ratio, (t_0) is the settlement in the soft ground when the reinforcement was not used ($t_0 = \sigma_s \frac{D}{E_c}$) in (m) and (t) is the settlements in soft ground when the reinforcement layer was used in (m).

2.7 Influencing factors in arching mechanism

A number of studies reported that the behaviour and degree of soil arching is strongly dependent on many factors such as embankment height, properties of embankment soil, pile cap width, spacing between piles and tensile strength of reinforcement layers.

2.7.1 Influence of embankment height and piles spacing

Several experimental, analytical and numerical investigations were conducted to study the behaviour and load transfer mechanisms in piled embankments with and without reinforcement layers. A number of studies have reported that height of embankment has a crucial impact on load transfer mechanism. Examples are Han and Gabr (2002), Ganggakhedar (2004) and Truc et al. (2018) with numerical analysis of geosynthetic-reinforced piled embankment, Abusharar et al. (2009), Deb and Mohapatra (2013) and Zhao et al. (2017) with analytical calculations and Yun-min et al. (2008) with 2D experiments with and without geosynthetics reinforcement. All these studies showed that, the stress concentration ratio increased with increasing the embankment height. This is due to the fact that increasing embankment height increases the accumulation of shear resistance which results in increasing of the load transfer to the piles cap and enhancing the arching development. Also, Abusharar et al. (2009), Deb and Mohapatra (2012) and Van Eekelen et al. (2013) with analytical methods, Jenck et al. (2007), Hello and Villard (2009) and Borges and Marques (2011) with numerical analysis, Ellis and Aslam (2009), Blanc et al. (2014), Fagundes et al. (2015) and (2017) with centrifuge models with and without geosynthetics reinforcement and Jenck et al. (2009) with 2D experimental tests and numerical models without geosynthetics

reinforcement reported that, efficiency of arching increases with increasing embankment height and it seemed to be stabilized with the thicker embankments. Borges and Marques (2011) showed that the efficiency was increased with increasing the embankment height except the embankments with heights more than 3 m where the efficiency was nearly remined constant. However, the settlement ratio was decreased with increasing the embankment height. In addition, Hello and Villard (2009) resulted that the deformation in reinforcement layer was not increased a lot with increasing the embankment height. This means that it does not need a lot of reinforcement deformation to carry the overload which it was not transferred by arching effect. Also, the results by Jenck et al. (2007) showed that the surface settlement decreases with increasing embankment height and becomes negligible with the thicker platforms.

On the other hand, the improvement of load transfer mechanism was decreased with increasing the spacing between piles or reducing the capping ratio (pile cap width/clear spacing) irrespective of the embankment height. Jenck et al. (2007) reported that the efficiency was decreased from 58 % to 49 % by reducing the cap ratio from 31 % to 22 % when the embankment height was 0.5 m (Figure 2.18). Also, Abusharar et al. (2009) found that for the unreinforced case increase the ratio of pile caps width to the clear spacing decreased the efficiency significantly and decreased stress concentration ratio slightly as shown in Figure 2.19. For reinforced case it was noted that using large spacing between pile caps decreased the load transfer to the pile caps with increasing embankment height. Also tension in reinforcement layer was increased with increasing the embankment height and decreased with

increasing the capping ratio. Hello and Villard (2009) studied the effect of pile caps area to the total area. Six different area ratios ranging between 4% and 44% were tested in this investigation. It was concluded that the recorded efficiency increased with increasing the area ratio. The efficiency of load transfer varied between 32.5 and 86.2 % for area ratio varying between 4 and 44 %. In similar research which was carried out experimentally, 15 models with and without reinforcement were tested to investigate the behaviour of reinforced pile supported embankments. Different area ratios were investigated in this experimental study. It was found that the stress concentration ratio was 2.81, 3.57 and 4.51 for the capping ratios 1/4, 1/3.2 and 1/2 respectively. Also, it was resulted that the maximum settlement and the maximum differential settlement decreased with increasing the capping ratio. The settlement was reduced from 37 mm to 35 mm and differential settlement was reduced from 26 mm to 22 mm with increasing the capping ratio from 1/4 to 1/2 which means that the arch of soil transformed to completed form with reduction in the differential settlement (Yun-min et al. 2008). Huang and Han (2010) reported that the settlement was increased more than double when the spacing increased from 2 m to 3 m. Borges and Marques (2011) found that the maximum settlement at the embankment base was increased with increasing the piles spacing. It was found that at spacing of 7.6 m the maximum settlement on the underlying soil was about 31.6 cm which is nearly the same as the one without reinforcement. This means that the effect of adding layers of reinforcement is not adequate when spacing between piles is very large. A field study was carried out by Almeida et al. (2007) to monitor the behaviour of reinforced piled embankment. It was noted that increase in the

piles spacing leads to increase in the settlement at the base of the embankment. Fagundes et al. (2015) found that the efficiency was increased with increasing capping area ratio. For embankment height of 2.0 m, the efficiency was increased by about 30 % by increasing the pile cap size from 0.5 m to 1.0 m.

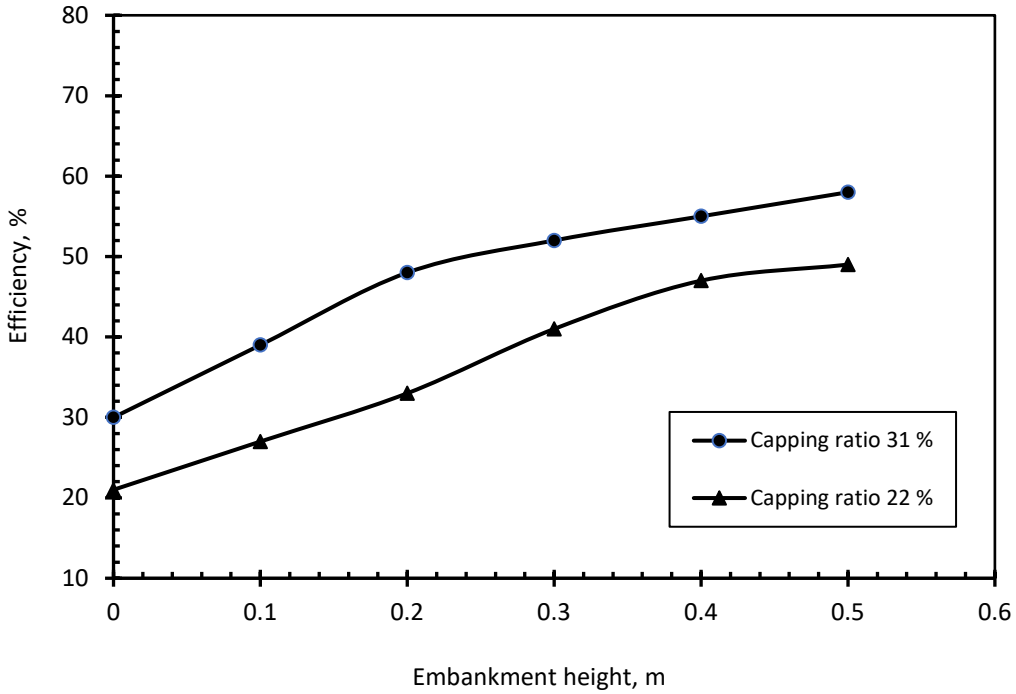

Figure 2.18. Variations of Efficiency with different unreinforced embankment heights for two capping ratios area (Jenck et al. 2007).

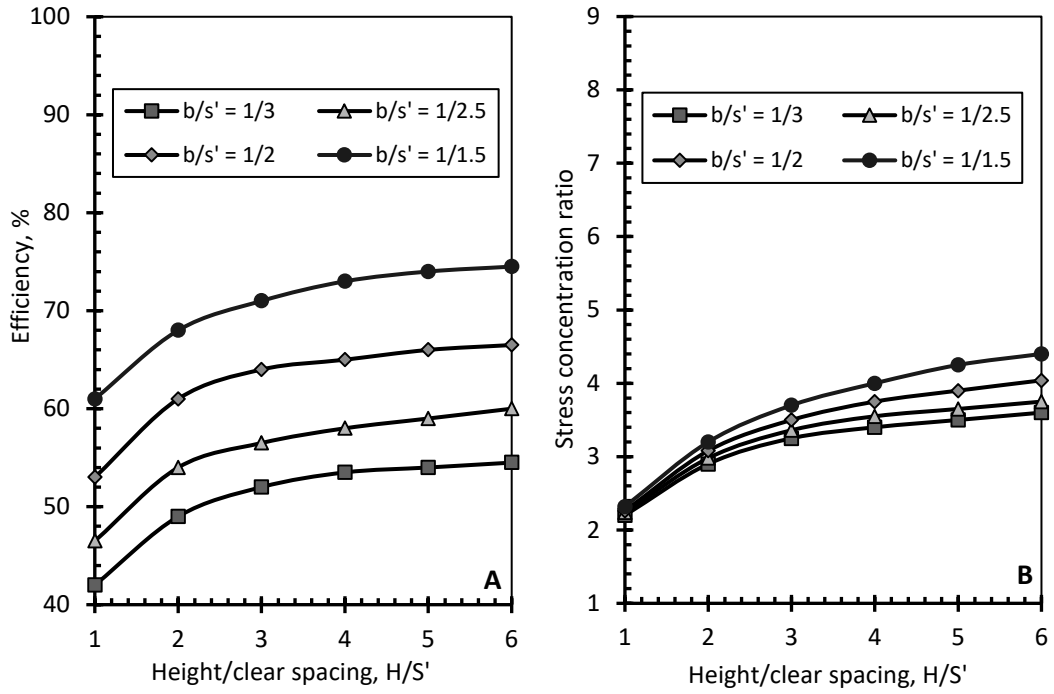

Figure 2.19. (A) Efficiency and (B) stress concentration ratio for unreinforced piled embankment for different heights and capping ratios (Abusharar et al. 2009).

2.7.2 Influence of fill materials properties

Many studies have reported that the properties of fill materials have a significant effect on the behaviour of piled embankment. Chevalier et al. (2007) studied numerically the effect of friction angle on the load transfer mechanism. It was noted that about 69% of embankment load was transferred to the piles for embankment with height of 2.0 m and peak angle friction of 27^{o} while about 89% of the fill load was transferred to the piles when the peak angle of friction was 39^{o} for the same height of the fill. Jenck et al. (2007) studied numerically the behaviour of load transfer mechanism in a granular platform supported by a group of piles. It was found that the shear strength of platform materials had a crucial influence on transfer the loads to the piles and reductions in the surface settlement. Van Eekelen et al. (2012) and Ariyarathne (2014) examined experimentally the effect of embankment materials on the behaviour

of piled embankment. Two different types of fill materials were selected and tested in this study. It was found that the arching increases with increasing the friction angle of embankment fill materials. Deb (2010) found that increasing ultimate shear resistance of embankment materials enhances the transfer of loads to the column due to the improvement of arching. On the other hand, Potts and Zdravkovic (2010) argued that under static loading condition, the effect of friction angle on the soil arching is negligible. Also, Zhuang and Li (2015) studied numerically the arching of soil in unreinforced piled embankment under traffic loading condition. They reported that the effect of friction angle in the soil arching under traffic loading condition is negligible. In this study they used embankment fill materials with friction angle ranging between 30^{o} and 40^{o}. Yapage and Liyanapathirana (2014) found numerically that the angle of friction of embankment fill materials has a significant effect on the load transfer mechanism and surface settlement of embankment. Also, Okyay and Dias (2010) observed numerically that the stress efficacy of the system increased with an increase in cohesion of the embankment fill.

2.7.3 Influence of properties and number of layers of geosynthetics reinforcement

Several studies have been performed to evaluate the effects of properties, type and number of geosynthetics reinforcement layers on the behaviour of reinforced piled supported embankment. Han and Gabr (2002) found numerically that the stress concentration ratio and maximum tension in geosynthetic reinforcement decrease with increasing the stiffness of geosynthetic reinforcement due to the reduction in soft soil deformation. The distribution of tension in geosynthetic reinforcement layer showed that the

maximum tension occurs near the edge of the pile. Van Eekelen et al. (2012) found experimentally that the effect of reinforcement type on the behaviour of piled embankment, geogrid or geotextile with same mechanical characteristics is negligible. Hello and Villard (2009) studied the effect of geotextile stiffness on the load transfer mechanism and found that the transfer of load was not effected with increasing the stiffness of geotextile. However, the reinforcement deformation was decreased significantly with increasing the reinforcement stiffness. Roy and Bhasi (2018) reported numerically the transfer of loads to the piles decreases with increasing tensile stiffness of geosynthetics reinforcement. Nunez et al. (2013) presented a comparison between the existing design methods with real experimental results of full scale reinforced piled embankment. It was reported that inclusion of two layers of geogrid with tensile stiffness of 520 kN/m increased the efficiency compared with the embankment with one layer of geotextile with tensile stiffness of 750 kN/m. Potts and Zdravkovic (2010) studied numerically the effect of geosynthetic stiffness on the formation of soil arching. It was found that the higher the reinforcement stiffness, the smaller deformation created on the soil column above the void and therefore the distribution of fill load by the arching mechanism is also smaller and the major stresses stay in vertical direction. Yan et al. (2006) preformed a numerical study to investigate the deformation behaviour of geosynthetics reinforcement and found that the maximum and differential settlement is decreased when the number of geosynthetics reinforcement increases especially in the embankments with large piles spacing. Gebreselassie et al. (2010) studied the effect of geogrid reinforcement type and number on the load transfer mechanism of reinforced

piled embankment. It was observed that the lower layer is most effective in carrying the applied loads. However, with increasing the embankment height the influence of geosynthetics reinforcement membrane reduces. It was also noted that the surface settlement decreases with increasing the number of reinforcement layers. Deb (2010) and Yapage and Liyanapathirana (2014) and Fonseca et al. (2018) noted that the load transfer to the piles increases while the load transfer to the geosynthetics reinforcement layer and soft soil decreases with increasing the tensile stiffness of geosynthetics reinforcement. Also, the results showed that the settlement in the crest of embankment is effected more than the settlement in the base of the embankment. Deb et al. (2008) suggested that multilayer reinforcement is more effective when no columns are incorporated. Ariyarathne and Liyanapathirana (2014) based on numerical analysis found that multilayer reinforced piled embankment works as stiffened platform while single-layered reinforced piled embankment works as tensioned membrane system. However, due to the similarity between using a single layer of high tensile stiffness and multi layers with low tensile stiffness, it was preferred to use single layer of geosynthetic reinforcement. It was argued that using multi layers of geosynthetic reinforcement is complex due to it has more influence factors such as number and spacing of reinforcement layers compared with using single layer of geosynthetic reinforcement.

2.7.4 Influence of sub soil properties

Another important factor that can affect the load transfer mechanism is sub-soil properties. Van Eekelen et al. (2012) reported that the increase the consolidation of sub soil enhances the load transfer by arching and the load transfer by geosynthetics reinforcement. On the other hand, EBGEO (2010)

reported that consolidation of soft soil results in no increase in the load transfer to the piles by soil arching effect. Yan et al. (2006) and Abusharar et al. (2009) found that the higher of sub soil elastic modulus the less settlement on the surface of the embankment. Yapage and Liyanapathirana (2014) found numerically that settlement at surface of the embankment and sub soil decreases with increasing the elastic modulus of sub soil. Another numerical study found that the efficiency and the maximum vertical displacement of the reinforcement sheet was decreased with increase in the underlying compressible soil settlement. This is because increasing the underlying compressible soil reduces the deformation of underlying soil leading to decrease the soil arching and displacement of reinforcement layer. However, Hello and Villard (2009) reported that no influence on the efficiency of load transfer was observed by increasing the underlying compressible soil. Zhuang et al. (2014) reported that the soft subsoil can support between 3% and 53% of the applied loads with increasing the compression modulus of subsoil.

2.8 Strength of reinforced soil

Several testing techniques with varying degrees of simplicity and reliability could be used to assess the degree of improvement in the strength of soils. Among there California Bearing Ratio (CBR) test has been developed and used to examine the strength of subbase soils (see for example, Chegenizadeh and Nikraz 2012; Asmani et al. 2013). Results from CBR tests on samples of granular soils have been reported examining the effect of introducing various reinforcements such as geotextile, geogrid and geonet (see for example, Duncan-Williams and Attoh-Okine 2008; Naeini and

Mirzakhanlari 2008; Kumar and Rajkumar 2012; Ashs and Latha 2011; Elshakankery et al. 2013). Kamel et al. (2004) examined the effect of geogrid layer position on the strength of subgrade soil using CBR and traixial tests. It was concluded that the highest increase in the bearing capacity can be attained when a geogrid layer is placed at depth between 72% and 76% from the surface. Also, it was found that resilient modulus of reinforced soil is lower than that recorded for unreinforced soil due to the fact that reinforced soils result in higher elastic deformation. A number of reinforcement layers was also tested using CBR to quantify their impact on the strength of granular soil. It was found that the bearing capacity of soil increases with increasing the number of geotextile layers (Hossain et al. 2015). Furthermore, You-Chang et al. (2009) conducted CBR tests to study the effect of spacing between geotextile layers on the improved soil strength. It was found that the strength of granular soil improves with the addition of a reinforcement layer at particular location. The aforementioned studies highlighted the effectiveness of CBR tests in examining the degree of improvement in the strength of soils as a function of various parameters. However, the effect of cyclic and repeated loading conditions was not considered.

Ashs and Latha (2012) conducted a number of California Bearing Ratio (CBR) tests to investigate the effects of cyclic and repeated loading on the strength of soil-aggregate and reinforced soil-aggregate. The study highlighted the fact that the bearing capacity of unreinforced soil samples was nearly similar to the bearing capacity of soil sample reinforced by one layer of reinforcement under repeated loading conditions. This is due to the fact that the properties of granular materials were very high and only one layer of reinforcement was

used. Their results showed no improvement on the resilient modulus with the addition of one reinforcement layer whereas secant modulus showed a degree of improvement. However, the effect of number and position of reinforcement layers was not examined. Araya et al. (2011) investigated experimentally and numerically the stiffness of granular soil under repeated loading conditions using Repeated Loading California Bearing Ratio (RL-CBR) and large scale triaxial tests. It was suggested that results of RL-CBR can be utilised with reasonable confidence. Only one type of soil was used in their study and without reinforcement materials. Mekkawy et al. (2011) investigated used CBR tests to investigate the performance of nine samples of granular layers on soft subgrade with a reinforcement layer at the interface under cyclic loading. Based on the results of CBR tests, a correlation between rut depth and number of load cycles was developed. Nevertheless, no accounts for the location or number of reinforcement layers were given.

2.9 Reinforced piled embankment under cyclic loading conditions

Limited studies have been carried out to study the behaviour of piled embankments under cyclic loading conditions. Most of these studies are based on numerical analysis. Van Eekelen et al. (2010a) carried out a field investigation to monitor the behaviour of reinforced piled embankment in the Kyoto road under heavy traffic passages. It was reported that arching of soil reduced temporarily under the initial passages. Then during the rest of the day arching was recovered although other passages were occurred. Jenck et al. (2014) studied experimentally the effect of monotonic and cyclic loading on the arching behaviour of a granular soil. The study highlighted the fact that the arching of soil was affected significantly and the basal displacement increased

slightly during unloading cycles. Heitz et al. (2008) studied experimentally and numerically the effect of static and cyclic loading on the behaviour of reinforced piled embankment. Different heights of embankment, different loading frequency and different number of reinforcement layers were investigated. The results showed that arching of the soil was significantly affected under cyclic loading conditions as shown in Figure 2.20. It was also concluded that the effect of vibrations was decreased significantly by inclusion of layers of reinforcement and/or increasing the embankment height. However, cyclic loads were applied over the whole area of the embankment which is not representative of the loading condition. Also, the pressure and deformation of the soft soil were not investigated. Heitz et al. (2008) based on their experimental results and analytical solution by soil arching reduction factor (k^*) was derived. The soil arching reduction factor (k^*) is equal to the efficiency under static loading condition divided by the efficiency under cyclic loading condition. If the factor of arching reduction (k^*) is calculated the stress on soft soil under cyclic loading condition can be estimated. However, this factor is dependent to many factors such as embankment geometry, magnitude of loading and loading frequency.

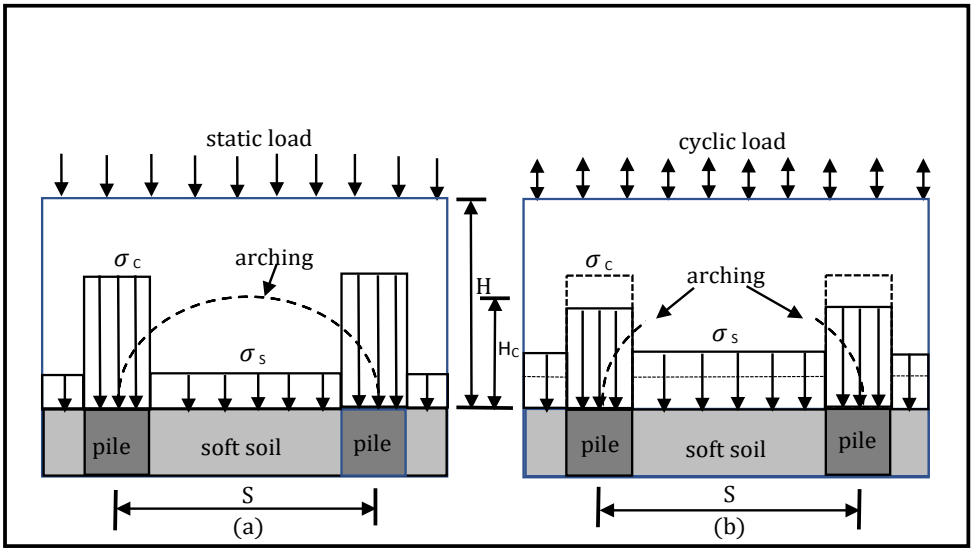

Figure 2.20. Behaviour of the arching under (a) static loading condition and (b) cyclic loading condition (Heitz et al., 2008).

The experimental study conducted by Houda et al. (2016) on an unreinforced piled embankment suggested that the efficiency of the system increases under monotonic loads and decreases under higher cyclic loads. Despite the fact that real soil was not used in Houda et al. (2016), it was observed that about 50% of the surface settlement occurred during the first 10 cycles of loading. Notably, cyclic loads were applied over the whole area of the embankment which is not typically the case in most engineering projects e.g. highways and railway. Also, pressure and deformation on the soft soil were not investigated. In addition, the effect of embankment height and reinforcement numbers was not studied. Han et al. (2015), based on experimental and numerical analysis, found that the height of the embankment has a significant effect on the soil arching under dynamics loading. It was suggested that arching in unreinforced embankments collapses if the ratio of embankment height to pile clear spacing is less than 3. This ratio dropped to 1.4 when a layer of reinforcement was added to the embankment which indicated that inclusion of a reinforcement

layer enhanced the stability of the embankment under dynamic loads. However, the effect of the number of reinforcement layers was not investigated.

Zhuang and Li (2015) found numerically that traffic loads had a significant effect on unreinforced piled embankment behaviour whilst the effect of the fill friction angle was very limited. Wang et al. (2018) investigated numerically the soil arching in highway piled embankments under moving shakedown limit loads and found that although the soil arching effect was reduced under cyclic loading conditions, it still existed in highway piled embankments. Zhuang and Wang (2018) used 3D numerical models with layer of geosynthetics reinforcement to study the effect of type and magnitude of dynamic loads on the behaviour of the piled embankment. It was resulted that although the arching of the soil was significantly affected by the application of dynamic loads, it was still remain existing. The influence was increased with increasing the magnitude of dynamic load. Moreover, according to Zhuang and Wang (2018), it should be noted that a long period of time is required for a considerable degree of soft soil consolidation to occur which means that a large number of load cycles are needed to be applied in the numerical model. Zhuang and Wang (2018) validated their numerical results with experimental data, but the effects of number of reinforcement layers and the embankment height were not studied. Lehn et al. (2016) carried out 3D numerical parametric study with real dimensions in order to get a good understanding of the behaviour of reinforced piled embankment under cyclic loading condition. It was found that the shape of arching is not stable during the initial cycles and then after about 50 cycles the stable arch is developed. However, only

embankments with one height and one layer of reinforcement were studied. Han and Bhandari (2009) found numerically that the settlement of unreinforced piled embankment was reduced by about 25 % when a layer of geogrid was incorporated under cyclic loading conditions. Also, the stress concentration ratio of reinforced piled embankment was higher than unreinforced one. Another 3D numerical study focused on the effect embankment height and number of geogrid reinforcement layers on load transfer mechanism, settlement in sub soil and embankment and the tension in the geogrid layers under cyclic loading conditions (Pham et al. 2018). The results showed that increase the embankment height and presence a layer of reinforcement seems to enhance the arching effect under cyclic loading. Also, increase the height of embankment increases the accumulated surface embankment settlement and decreases the sub soil accumulated settlement. In addition, increase the number of the geosynthetic reinforcement layers did not have a significant effect on arching of soil and accumulated settlements (Pham et al. 2018). Gaoxiao et al. (2011) proved numerically that the arching of soil transfer the stresses created by the dynamic loads. However, the magnitude of dynamic load and the thickness of embankment fill have influence on the arching of soil. With increasing the thickness of soil, the time required to reach the failure of the arch increases significantly. With increasing the magnitude of dynamic load the possibility of arching failure increases significantly.

2.10 Summary

Arching mechanisms in the infill materials and membrane effects by geosynthetics reinforcement layers which are responsible for transferring loads onto reinforced piled embankments. There are several design

approaches to assess the performance of reinforced piled embankments. These methods reported that the behaviour and degree of soil arching is strongly dependent on many factors such as embankment height, properties of embankment soil, pile cap width, spacing between piles and tensile strength of reinforcement layers. A general consensus was reached that soil arching improves with increasing the height of embankment, pile cap width and shear strength parameters of the embankment soil. It was also noted that soil arching deteriorates with increasing the spacing between piles and the tensile stiffness of the reinforcement. The results suggested that increasing the embankment height and pile spacing and reducing the pile cap width lead to higher tensile stresses in the reinforcement layers. It is worth noting that the most of aforementioned studies focused on the analysis of reinforced piled embankments under static loads only, which might not be representative of cases where reinforced pile embankments are subject to cyclic loading. Finally, California Bearing Ratio (CBR) is simple and reliable technique to assess the strength of unreinforced and reinforced soil under repeated and cyclic loading conditions.

CHAPTER THREE

EXPERIMENTAL METHODS AND MATERAILS USED

3.1 Introduction

In this study, three experimental investigations were carried out, two preliminary experimental studies which assisted the conduction of the main experimental investigation and the main experimental test. The first preliminary test was conducted by using Repeated Loading California Bearing Ratio (RL-CBR). The setup of this test was nearly the same as normal CBR. However, in order to investigate the effect of repeated loads on the strength of unreinforced and reinforced soil, the loading machine was modified to allow applying monotonic and repeated loads on the samples. The second preliminary experimental investigation was carried out by using classic trapdoor test which was designed and manufactured to aid the study. The setup was nearly the same as the classical trapdoor test used by Terzaghi (1936). However, one of main aims in this study was to investigate the effect of repeated sequential of active and passive arching on the distribution of stresses within the granular soil. Therefore, the trapdoor test equipment was designed and manufactured to allow the trapdoor to go up (passive arching) or down (active arching) at specific times. The main experimental rig was also designed and manufactured in order to present the real model of reinforced piled embankment under cyclic loading conditions.

3.2 Preliminary Test 1

This preliminary experimental test aims to i) investigate the effect of thickness of granular layer overlying soft subbase, ii) optimise the location of reinforcement layers within the granular layer, iii) assess whether increasing the number of reinforcement layers has a remarkable effect on long term stability under repeated loading conditions, iv) effect the number of cycles, and v) evaluate the effect of reinforcement layers on the overall stiffness of samples.

3.2.1 Repeated Load California Bearing Ratio test (RL - CBR)

The principles and procedure of repeated load CBR (RL-CBR) test is similar to the standard CBR test (British Standards Institution part 4 1990) but repeated loads are applied upon completion of the first loading stage. This means that RL-CBR test is performed until a penetration of 2.50 mm is achieved at a strain rate of 1.00 mm/min. The load at this designated deformation is recorded and then the sample is unloaded gradually at the same rate until the load approaches nearly zero. The maximum load level for the first cycle is therefore recorded and kept constant in all subsequent loading cycles. Repeated cycles of loading are then performed until the elastic deformation reaches nearly a constant value and the permanent deformation due to the last 5 loading cycles is less than 2 % of the total permanent deformation at that point. The elastic deformation for each cycle during RL-CBR testing is measured as the difference between the LVDT readings at maximum loading and minimum after unloading (Araya et al. 2011; Sas et al. 2012).

3.2.2 Materials used

In this experimental work two different types of soil including clay and sand were utilised in addition to layers of geotextile reinforcement

3.2.2.1 Clay soil

The cohesive soil used in this study was in the form of dry clay powder. The important index properties of the clay were determined according to British Standards Institution part 2 and part 4 (1990). Liquid and plastic limits were found to be 39.8 % and 25.6 % respectively. As a result, the cohesive soil was classified as clay soil with medium plasticity (CI) based on classification guidance British Standards Institution (1999) and (2002). Proctor tests indicated that maximum dry unit weight was 17.10 kN/m^3 achieved at an optimum water content of 17.70 % as shown in Figure 3.1.

3.2.2.2 Sand soil

The second soil utilised in this experimental study was a sand material with a range of sand particles sized between 410 and 710 µm. The important index properties of the sandy soil are summarized in the Table 3.1. According to British Standards Institution (2004), the sand soil was classified as uniformly-graded medium sand.

Table 3.1. Properties of sand soil used in this study.

property	Measured value
d_{10} (mm)	0.570
d_{30} (mm)	0.630
d_{50} (mm)	0.690
d_{60} (mm)	0.710
Uniformity coefficient (C_u)	1.250
Coefficient of curvature (C_c)	0.980
Maximum dry unit weight (kN/m^3)	16.80
Optimum water content (%)	8.00
Specific gravity (G_s)	2.64
Angle of friction (ϕ)	33^o

3.2.2.3 Reinforcement

Layers of geotextile with dimensions 149.0 mm in diameter were selected as reinforcement. These layers were placed at the interface between clay and sand and also within the sand layer. The important index properties of the geotextile are summarized in the Table 3.2.

Table 3.2. Properties of geotextile reinforcement used in this study.

property	value
Thickness (mm)	1.35
Maximum Tensile strength (KN/m)	9.0
Maximum axial strain (%)	14

3.2.3 Preparation of samples

Fifteen samples were prepared and tested in order for a deeper understanding of the behaviour and deformation characteristics of unreinforced and reinforced soil under repeated loading cycles. A soft clay subgrade was prepared by mixing clay soil with higher amount of water than OMC to produce softer samples. All samples were prepared with water content of 24%. As a result, the attained unit weight of clay was found to be 15.70 KN/m^3 which is

90% of the maximum dry unit weight as shown in Figure 3.2. In all experiments, the CBR mould was filled with clay in three layers. Then, sand soil was mixed with 8.0 % water content (optimum water content) and compacted in one layer using a manually operated compaction rammer in order to reduce the effect of the hummer drops on the interface surface between clay layer and sand layer as shown in Figures 3.2, 3.3 and 3.4. This increase in the thickness of sand layer under the plunger which affected the strength of the combined samples as shown in Figure 3.5. Therefore, the height of hummer drop was decreased to a half (from 300 mm to 150 mm) and the number of blows was increased doubled (from 62 blows to 124 blows) in order to conserve the same compaction energy during the test. The mould was then placed at the base of the CBR machine, with the plunger placed into the hole of the weights. In case of samples with layers of reinforcements, the same process was followed but with layers of reinforcement placed at the required depths.

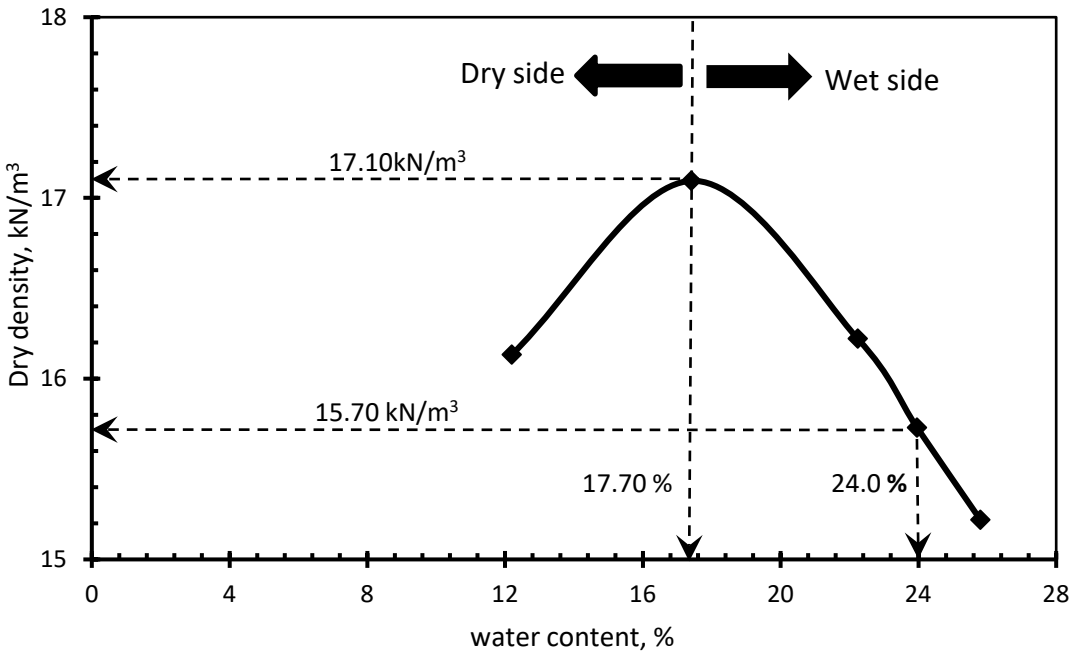

Figure 3.1. Maximum dry density and water content of clay soil.

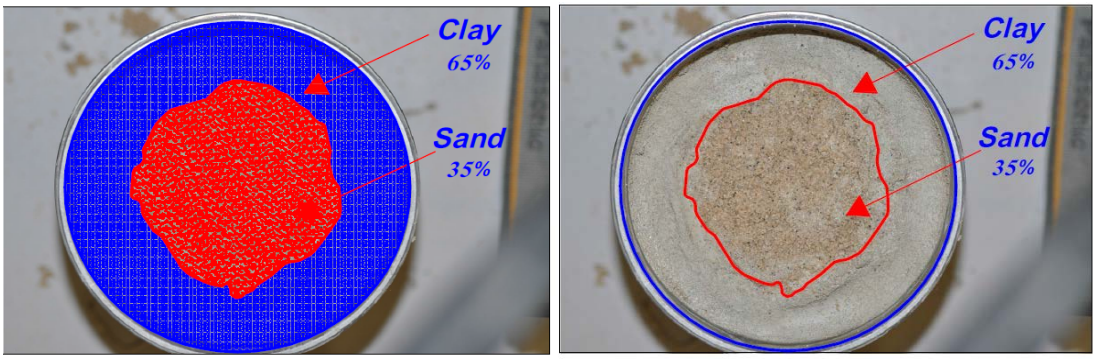

Figure 3.2. The surface of combined sample after the compaction at the interface (at height of hammer of 300 mm under 62 blows).

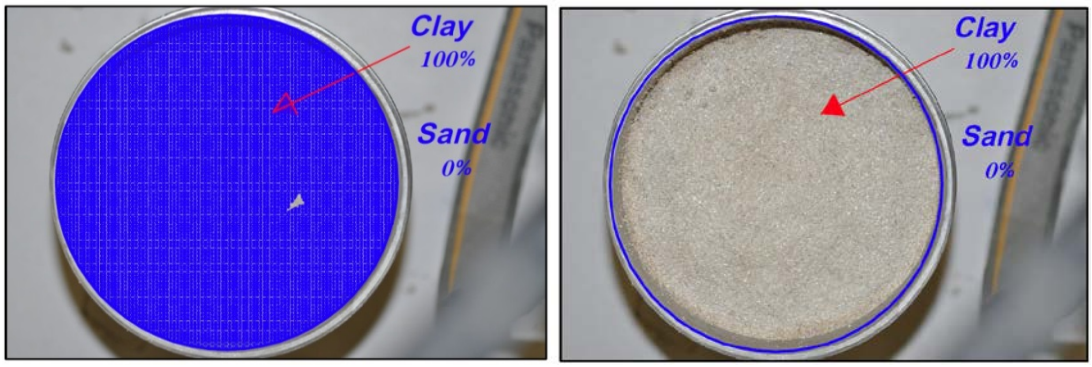

Figure 3.3. The surface of combined sample after the compaction at the interface (at height of hammer of 150 mm under 126 blows).

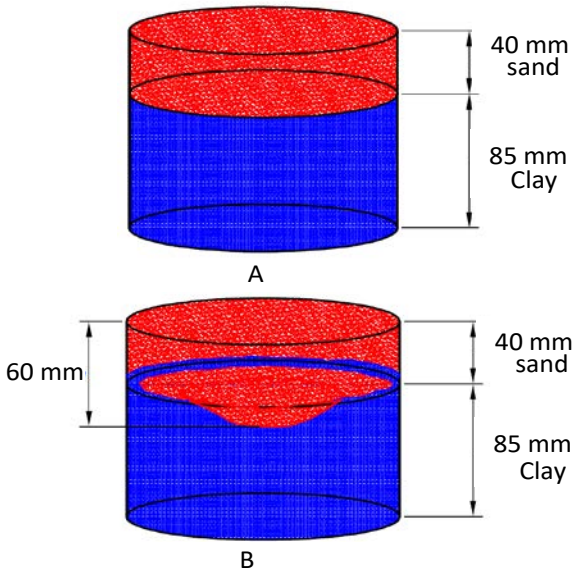

Figure 3.4. (A) The surface of combined sample before the compaction (B) the surface of combined sample after the compaction.

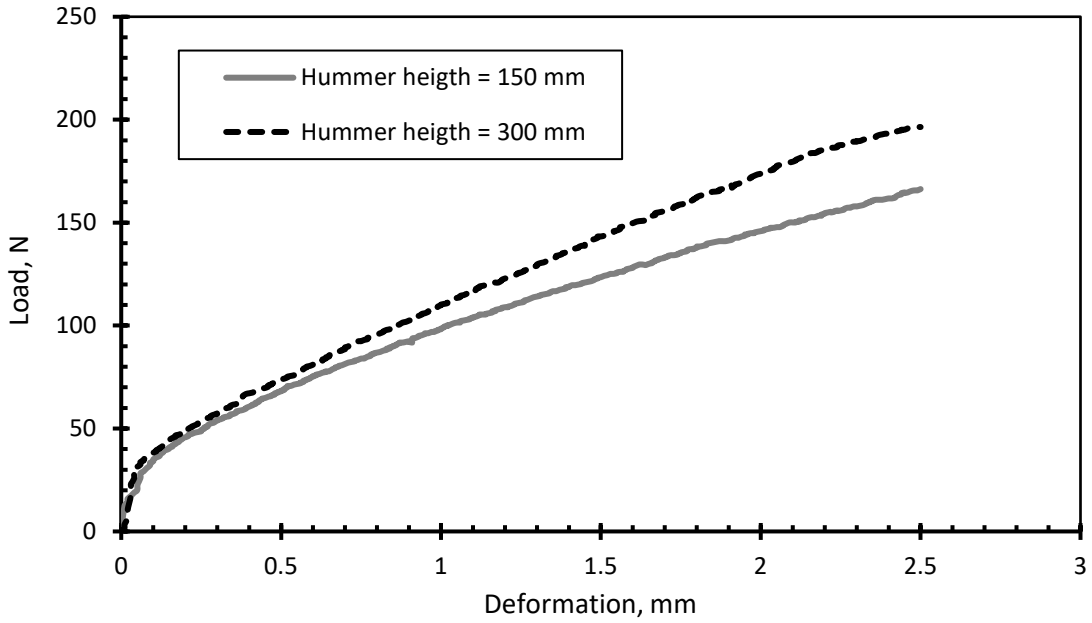

Figure 3.5. Effect of hammer height on strength of unreinforced sample.

Four series of tests were carried out during this experimental programme. The first series of tests was performed on four unreinforced samples with different thicknesses of sand layers to investigate the influence of sand layer thickness on the behaviour of the clay subgrade bed. Figure 3.6 and Table 3.3 illustrates all fixed and variable parameters of series I on unreinforced clay/sand samples. The layer of sand was placed with different thicknesse of 0, 15, 25 and 40 mm above the clay bed subgrade as shown in Figure 3.6-A and Table 3.3. The results of the test on clay with zero mm of sand are used as a control for unreinforced and reinforced clay/sand samples. The second experimental series is on four samples of clay bed overlaid with a reinforced sand layer of 40 mm. The reinforcement layer was placed at different locations e.g. at the interface between clay and sand, and 10, 20 and 30 mm above the interface (see, Table 3.3 and Figure 3.6-B). Results from the second series of tests were compared with those of the clay subgrade with the 40 mm layer of overlying sand. The third series was undertaken on clay/sand samples whilst the

thickness of the sand layer was kept at 40 mm but the number of reinforcement layers was varied. The reinforcement layers were placed at a vertical spacing of 10 mm (see, Table 3.3 and Figure 3.6-C). The last series was the same as the third series but all of the samples were tested under the same applied load (see, Table 3.3 and Figure 3.6-D)

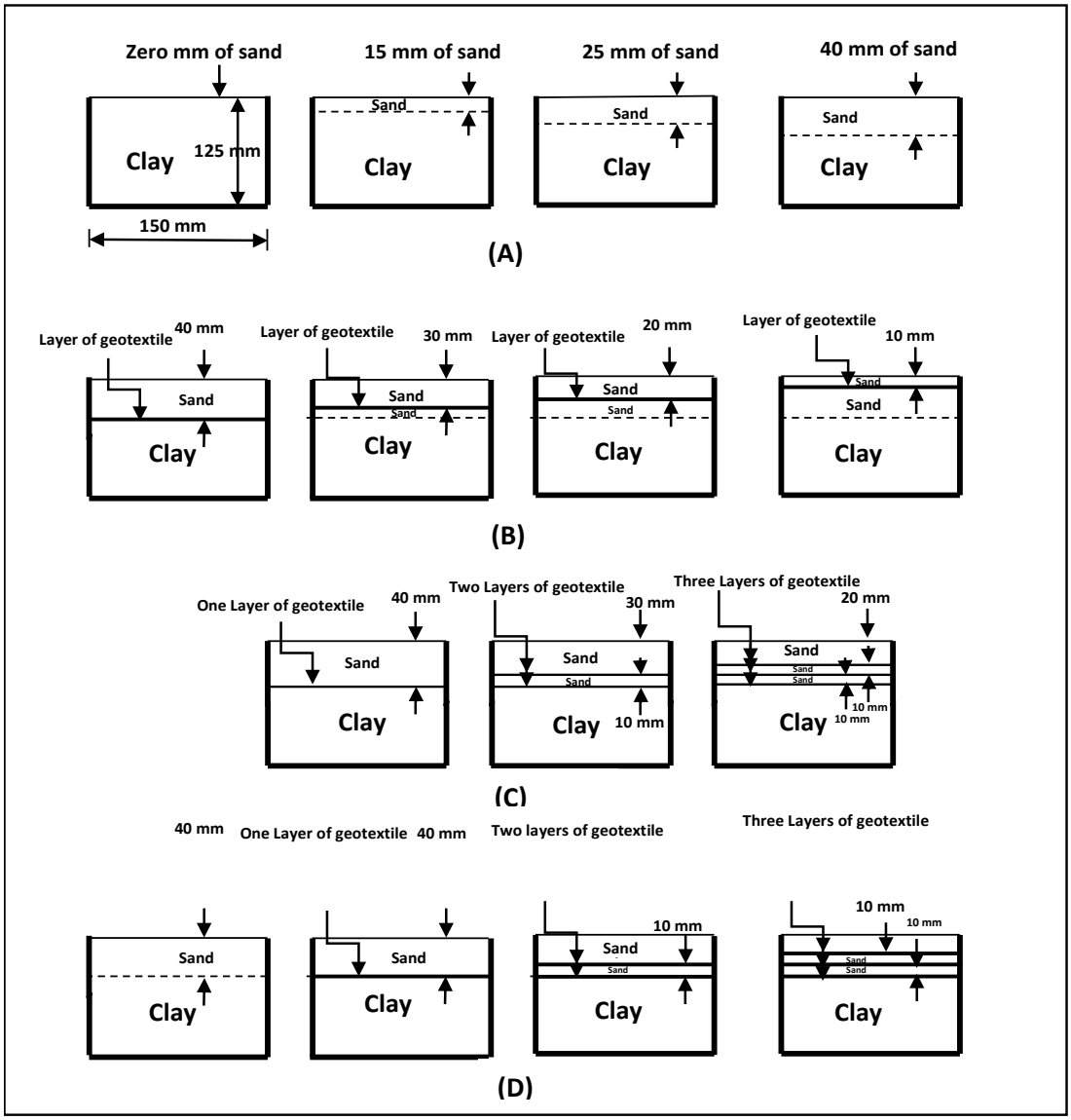

Figure 3.6. CBR mould with (A) clay and three different layers of coarse sand (B) clay soil and 40 mm of sand soil with a layer of geotextile at three different positions (C) clay, 40 mm sand and different numbers of geotextile layers (D) clay, 40 mm sand and different numbers of geotextile layers (at the same magnitude of load**).**

Table 3.3. Summary of experimental programme.

Series	Number of tests	Variable	Investigated parameters	Fixed parameters
I	4	Thickness of granular layer	H = 0 , 15, 25 and 40 mm	----------
II	4	Location of reinforcement layer	d = 10 , 20, 30 and 40 mm	H = 40 mm
III	3	Number of reinforcement layers	One, two and three layers	H= 40 mm
IV	4	Number of reinforcement layers	Zero, One, two and three layers	H = 40 mm

H = Thickness of granular layer, d = Height of reinforcement layer above interface,

3.2.4 Test procedure

After preparation of samples, the sample were placed in CBR machine as shown in Figure 3.7. The test was continued until a penetration of 2.50 mm was reached. The test was then stopped and the load at this penetration was recorded using data acquisition system (Geodatalog series 6000) with computer software. Subsequently the unloading stage was initiated by pulling the plunger upwards until the magnitude of load was close to zero. The sample underwent 30 cycles of loading and unloading to the recorded CBR load while recording the deformations (plastic and elastic deformations) characteristics at each cycle. This process was repeated using the same samples with layers of sand which was placed above clay soil in different thicknesses. Also, it was done on samples with layers of geotextile placed in different levels and numbers between sand and clay as well as between sand layers.

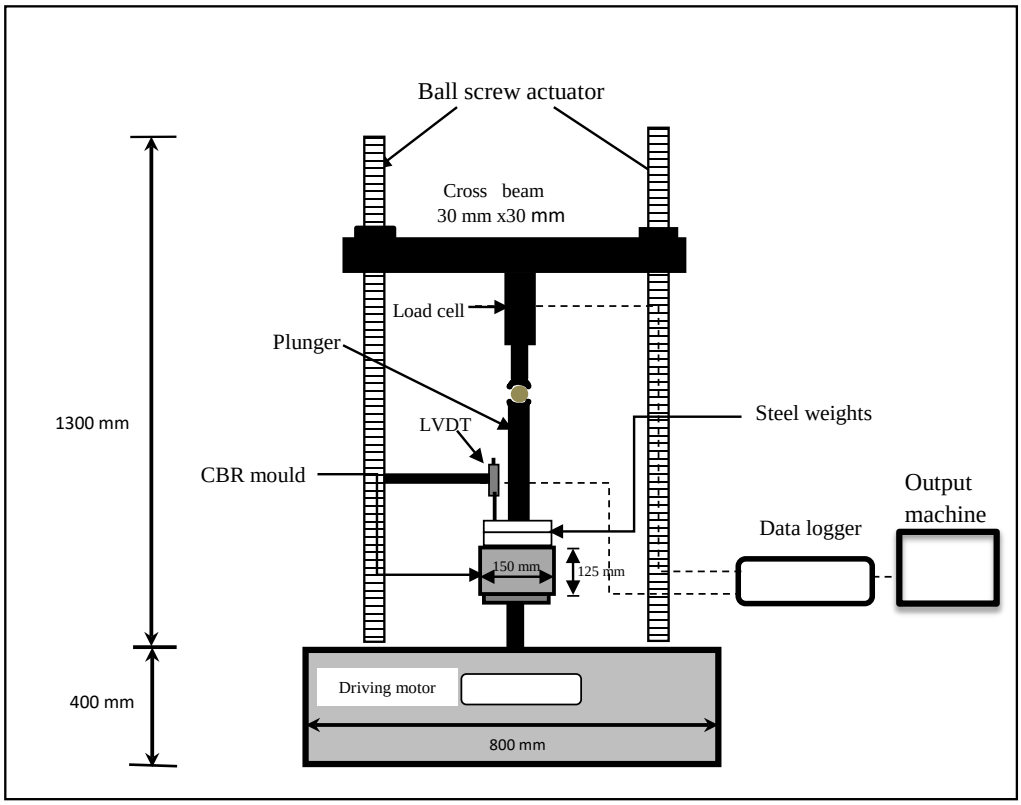

Figure 3.7. Loading machine with CBR mould.

3.3 Preliminary Test 2

The aims of this preliminary work are to i) quantify the effect of a sequentially alternating arching mode on redistribution of loads exerted on underground inclusions, ii) investigate the influence of displacement and soil height on the resulting stresses during sequentially alternating active and passive arching, and iii) explore potential impact of the number of alternating cycles of active and passive arching on stress reduction.

3.3.1 Testing Approach

The testing setup used in this section is fundamentally similar to the trapdoor setup used in previous experimental studies (see for example, Terzaghi 1936; Evans 1983; Stone 1988; Dewoolkar et al. 2007; Chevalier et al. 2008; Costa et al. 2009; Iglesia et al. 2013). Figure 3.8 shows a schematic drawing of the testing set-up. The test setup consisted of a wooden tank with the front wall made of thick Plexiglass in order to enable visual observation and measurement of the soil deformation. The utilised testing tank had a length of 700 mm, a width of 250 mm and a height of 600 mm as shown in Figures 3.8 and 3.9. The trapdoor with a width of 100 mm was centred and located at the base of the testing tank. The trapdoor itself was designed to move downward or upward at a constant rate of 1.0 mm/min by a ball screw actuator in order to release or induce pressure on the trapdoor as a result of active and passive arching mechanisms respectively. A load cell was mounted to the base of the trapdoor to measure the applied load on the trapdoor as shown in Figures 3.8 and 3.9. In order to avoid or minimise frictional resistance and to prevent ingress of fine sand particles between the trapdoor edges and the opening side walls a fibre seal that covered all four edges of the trapdoor was used.

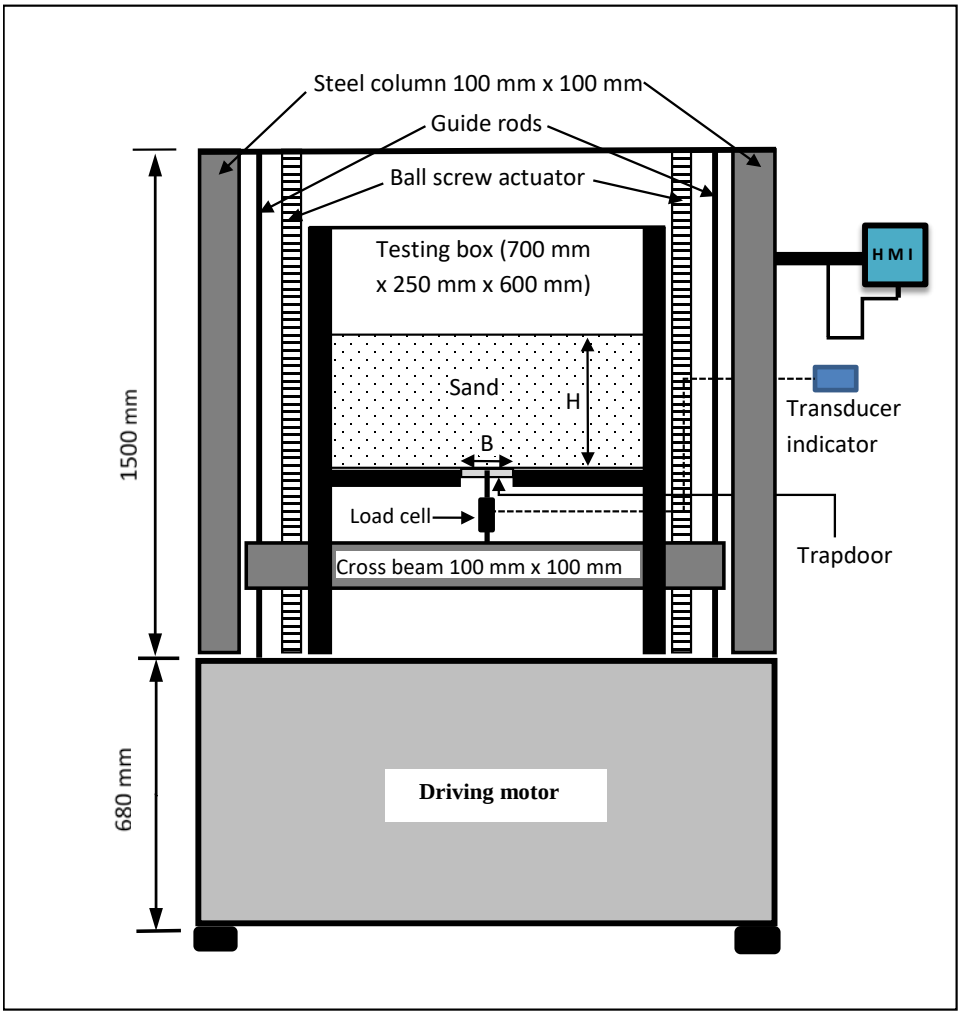

Figure 3.8. Schematic drawing of the experimental set-up.

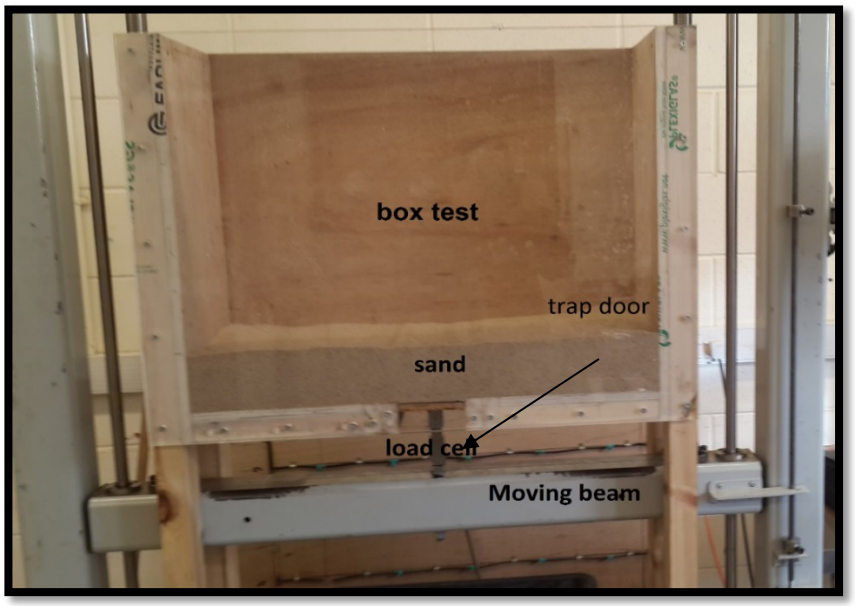

Figure 3.9. Test box with loading machine.

3.3.2 Load cell calibration

The load cell used on the trap door test was calibrated by using dead weights in order to simulate the expected weight of soil overburden. Different known loads (2, 5, 10, 14, 18 and 22 kg) which are equivalent to the weight of soil (overburden pressure) during every test were placed on the trap door. The difference between the actual loads and the measured loads was less than 2.0 % of the measured load.

3.3.3 Materials used

Sand was used as a testing material in this experimental investigation. The sand utilised in this experimental study had a range of particle sizes between 410 µm and 710 µm. The important index properties of the sand are summarized in the Table 3.4. According to British Standards Institution (2004), the sand was classified as uniformly-graded medium sand. Standard Proctor compaction tests revealed that the optimum moisture content and maximum dry unit weight of the sand were 8.0 % and 16.50 kN/m^3 respectively. In order to prepare samples with uniform dry unit weight, a sand raining technique was utilised by which dry sand was dropped from a predetermined height at a constant rate. The rate of sand raining was controlled by changing the aperture size of the holes in the sand raining box base whilst the dropping height was kept constant by gradually lifting the raining box upward. The unit weight of the formed sand beds was measured at different heights to ensure its uniformity across the whole tank. Measurements were taken at three different points at each level. Table 3.5 illustrates values of measured dry unit weight taken from five preliminary tests. Data in Table 3.5 shows an average dry unit weight of 16.37 ± 0.02 kN/m^3 which was considered acceptable. The measured dry unit

weight values indicate that adopting the sand raining technique resulted in preparation of dense sand beds with dry unit weight comparable to the maximum achieved dry unit weight from the Standard Procter Compaction test.

Table 3.4. Properties of sand used in this study.

property	Measured value
d_{10} (mm)	0.570 mm
d_{30} (mm)	0.630 mm
d_{50} (mm)	0.690 mm
d_{60} (mm)	0.710 mm
Uniformity coefficient (c_u)	1.250
Coefficient of curvature (c_c)	0.980
Maximum dry unit weight (kN/ m^3)	16.50
Optimum water content (%)	8.0
Angle of friction (ϕ)	33^o

Table 3.5. Measured dry unit weight at different heights.

Thickness of sand bed (mm)	Measurement level (mm)					Average dry unit weight (kN/m^3)
	0	100	200	300	400	
50	16.36					16.36
100	16.36					16.36
200	16.38	16.36				16.37
300	16.40	16.41	16.35			16.38
400	16.42	16.41	16.38	16.33		16.39
500	16.42	16.41	16.40	16.36	16.32	16.39

3.3.4 Testing procedure and programme

A sand bed was created by pouring sand particles into the testing tank through the raining box until reaching the required height. Then the surface of the sand bed was levelled off in order to avoid any discrepancy in the overburden pressure. Typically, each test was initiated by moving the trapdoor at a rate of 1.0 mm/min until reaching a predetermined displacement e.g. 10.0 mm. The

test was then temporarily stopped and movement of the trapdoor was reversed to perform the opposite stage of arching. Loads on the trapdoor were recorded every 10 seconds. Each test was conducted to simulate 10 cycles of alternating active and passive arching.

Thirteen experiments were performed as illustrated in Table 3.6 in order for a deeper understanding of the behaviour of granular soil arching in sequentially alternating active and passive modes to be acquired. The first series of tests was performed on a sand bed with a thickness of 100 mm to investigate the formation of monotonic active and passive arching in granular soil, the results of which were used as a control. The second series included testing of two samples with a fixed sand bed thickness of 100 mm to study the effect of the first arching mode on the load transfer onto the inclusion as a function of sequential changes of arching mode. The third series of tests was conducted to investigate the sequential active and passive arching under different trapdoor displacements of 2, 10 and 20 mm respectively. The last series of experiments was devoted to the effect of burial depth/sand bed thickness on the behaviour of soil arching in sequentially alternating active and passive modes. Six samples of sand beds with different thicknesses were prepared and then tested at the same displacement of 10 mm.

Table 3.6. Summary of experimental programme.

Series	Number of tests	Variable parameters	Fixed parameters
I	2	monotonic active and passive arching	H = 100 mm B = 100 mm d = 10 mm
II	2	initial active mode and initial passive mode	H = 100 mm B = 100 mm d = 10 mm n=5
III	3	Normalised displacement 2, 10, 20 %	H = 100 mm B = 100 mm active & passive n=10
IV	6	H = 0.5B, 1B, 2B, 3B, 4B, 5B	d = 10 mm B = 100 mm active & passive n=5

H = Thickness of sand bed, d = Trapdoor displacement, B = Trapdoor width and n = number of cycles

3.4 Main Experiments

A comprehensive experimental investigation was conducted to provide quantitative analysis for unreinforced and reinforced piled embankments with different heights which are subject to cyclic loading. A testing rig was designed and manufactured to provide accurate measurements for the loads on the piles and soft soil, the deformation of the embankment and bottom reinforcement layer and the induced tension force in the reinforcement layers. Three stages of cyclic loading were applied in order to represent the increase in the capacity of the cyclic loads after the embankment was built.

3.4.1 Scaling of testing rig

The dimensions of the testing rig were decided based on the scaling rules that were proposed and applied in earlier studies by Kempfert et al. (1999 and 2004), Zaeske (2001), Heitz (2006) and Van Eekelen et al. (2015) as shown

in Table 3.7. According to Van Eekelen (2016), piles are installed at a centre-to-centre spacing less than or equal to 2.50 m and pile caps have a width greater than or equal to 15 % of the centre-to-centre pile spacing. In addition, the embankment height is at least 0.5 of the centre-to-centre pile spacing (Van Eekelen et al. 2010; Van Eekelen 2016). In this study, the testing tank was scaled by a factor of 4.0 in comparison with field applications (the prototype) based on Van Eekelen (2015) who used a scale factor between 1.6 and 4.50. Table 3.8 illustrate all scaled values in this study. Of note, the stresses in this study were selected to be the same as those in reality in order to avoid difficulties due to stress-dependent behaviour of the embankment fill material as suggested by Van Eekelen and Bezuijen (2012) and Van Eekelen (2015). However, this may lead to overestimating the results from the model tests which should be taken into account in any further analytical and numerical evaluations. Careful inspection of all design methods indicated that a uniformly distributed surcharge load is used to simulate the effect of traffic load. Of note, in previous studies loads were applied over the whole embankment which is appropriate for deep embankments. However, when the embankment height is shallow the applied surcharge loads might be transferred through a relatively small portion of the embankment resulting in non-uniform pressure at the level of piles and soft soil. Therefore, high stresses are concentrated in the region under the loading area. Van Eekelen and Bezuijen (2012) suggested that traffic loads can result in a pressure between 43.0 and 79.0 kPa on shallow embankments with height ≤ 3 m. In addition, the average maximum applied traffic load is 62.11 kPa for 2.5 m centre-to-centre pile spacing and an embankment height of 1.0 m (Van Eekelen 2016). Traffic loads are transferred

to the embankment fill through the pavement layer which can be considered as a flexible foundation or a reinforced slab depending on the materials used. The flexible foundation undergoes differential settlement while the rigid foundation undergoes uniform settlement. Due to difficulties to run tests under uniform pressure, this study was performed by applying loads on a rigid plate. A similar experimental study by Heitz et al. (2008) was carried out using a rigid loading plate. In order to appropriately explore the load transfer mechanisms of traffic loads over shallow embankment, cyclic loads are applied over a specific area of 900 mm X 1000 mm on the surface of the embankment. The cyclic loading was applied on three consecutive stages to produce mean surface pressures of 31.1, 42.2 and 53.3 kPa with pressure amplitudes of 22.2, 33.3 and 44.4 kPa respectively. In each stage of loading, 1000 cycles were simulated with a frequency of 0.5 Hz.

Table 3.7. Scaling rules for experiment against prototype.

Parameter	Dimension	Scale ratio
Length	m	1: x
Area	m^2	1: x^2
Stress	kPa	1:1
Force	kN	1: x^2
Tensile strength of reinforcement	kN/m	1: x
Deformation and distances	m/m	1:1

Table 3.8. Scaling applied in this study.

Parameters	Laboratory	prototype
Testing tank dimensions, m	1.5 x 1.0	6.0 x 4.0
Centre-to-centre pile spacing, m'	0.5	2.0
Pile cap width, m	0.1	0.40
Embankment height, m	0.2, 0.4, 0.6	0.80,1.60, 2.4
Tensile stiffness of reinforcement, kN/m'	9.0	36.0
Surface average pressure due to traffic load, kPa	53.2 - 97.8	53.2 - 97.8
Pressure due to self-weight of embankment, kPa	3.36, 6.72, 10.07	13.44, 26.88, 40.28

3.4.2 Testing rig

A fully instrumented 2-D testing rig was designed, manufactured and commissioned to investigate the behaviour of unreinforced and reinforced pile supported embankment, although the 3-D model is more realistic. However, due to the complexity of the test, the model test was carried out in 2-D situation. Ariyarathne et al. (2014) has experimented the behaviour of 2D and 3D embankments numerically and found that the difference between two-dimensional model results and three-model results was within 30%.

The testing tank has internal dimensions of 1500 mm length, 1000 mm width and 1000 mm height, the rig was manufactured out of wooden frames and marine plywood sheets. In order to make the preparation of the test samples easier, the test box was divided into two parts (bottom part and upper part) with height of 500 mm per part which can be separated and connected by about 30 strong bolts. Figure 3.10 shows a schematic drawing of the testing rig with details of measurement devices. The testing tank was placed on the top of and fastened onto four steel I-beams to ensure stability and rigidity during the application of external loads. The vertical walls of the testing tank

were also stiffened by three steel square box sections as shown in Figure 3.10. Very smooth plastic sheet was glued to all internal surfaces of the testing tank to minimise frictional effect between soils and walls and to minimise/eliminate the loss of moisture from the sub-grade soft soil.

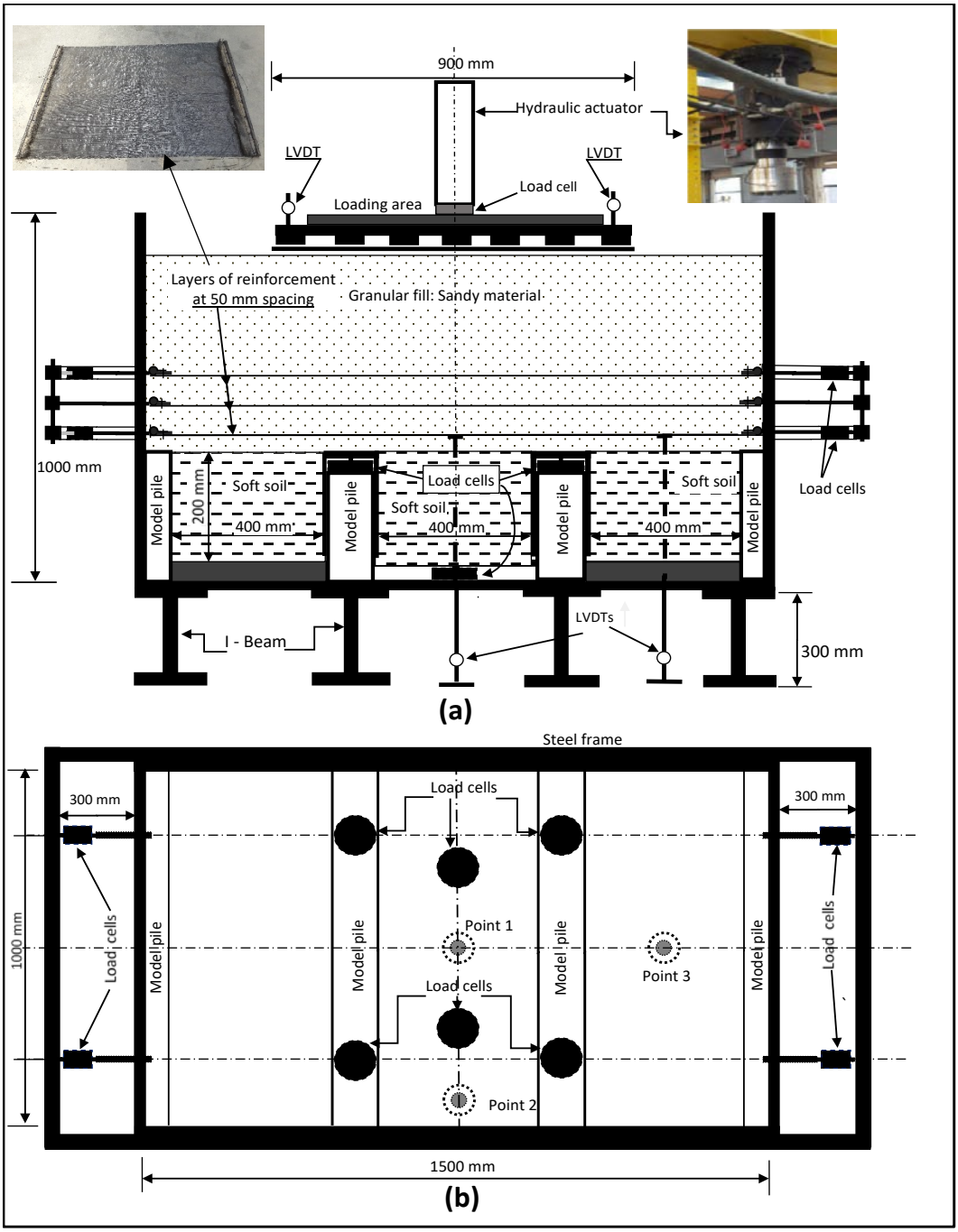

Figure 3.10. (a) Vertical cross section (b) Plan view.

Figure 3.11. Test box with sample and model loading area.

3.4.2.1 Model piles

Four model piles were constructed over the base of the testing tank to create three panels of soft soil with a clear width of 400 mm and a height of 200 mm. The rigid model piles were manufactured out of steel box section with dimensions of 200 mm x 100 mm as shown in Figures 3.10 and 3.12. It should be noted that the two intermediate model piles have a width of 100 mm whereas the two side model piles have a width of 50 mm for symmetry reasons. All model piles have a length of 1000 mm to cover the whole width of the testing tank simulating 2-D conditions as shown in Figures 3.10 and 3.12. All model piles were fastened securely onto the I-beams underneath to prevent any potential movement during the application of surface loads. The finished top level of all four model piles was kept the same. To minimise friction with soft soils and protect against rusting, all model piles were painted by a layer of epoxy coating.

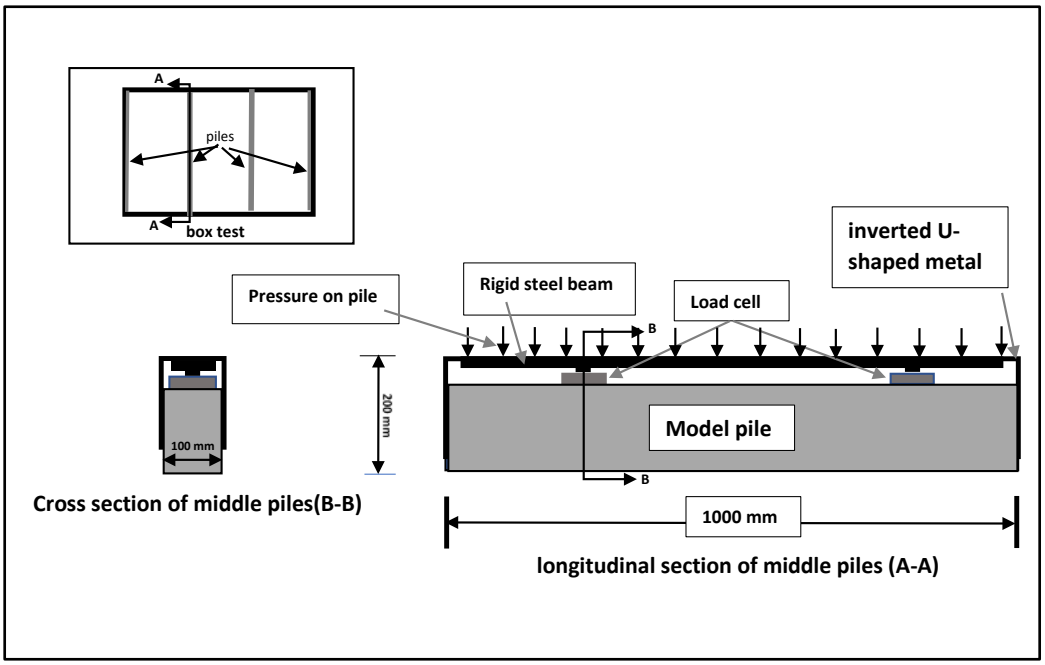

Figure 3.12. Model pile.

3.4.2.2 Model loading area

As measuring embankment settlement is one of the main objectives in this study, it is extremely important to produce uniform settlement underneath the loading plate. Therefore, cyclic loads were applied over an area of 900 mm x 1000 mm through a rigid plate system which was positioned at the centre of the embankment surface as shown in Figures 3.10 and 3.11. Servo Hydraulic Actuator system installed by ServoCon Ltd was used to apply the external loads on the embankment. The actuator is controlled via computer software and can perform any loading conditions including monotonic and cyclic loads. The actuator is capable of performing controlled displacement or load tests. In this study, all tests were carried out whilst applied loads were controlled and set at predetermined values.

3.4.2.3 Instrumentation

In order to measure the loads on piles, two load cells were fixed on top of each intermediate model pile and placed below a thick metal plate as shown in Figures 3.10 and 3.12. The model piles and load measurement equipment were then enclosed by inverted U-shaped metal sheets to protect the load cells, prevent the ingress of soil into the area around the load cells and minimise the friction between soft soil and piles. Data from the load cells were utilised to determine the pressure on pile caps at different stages of testing.

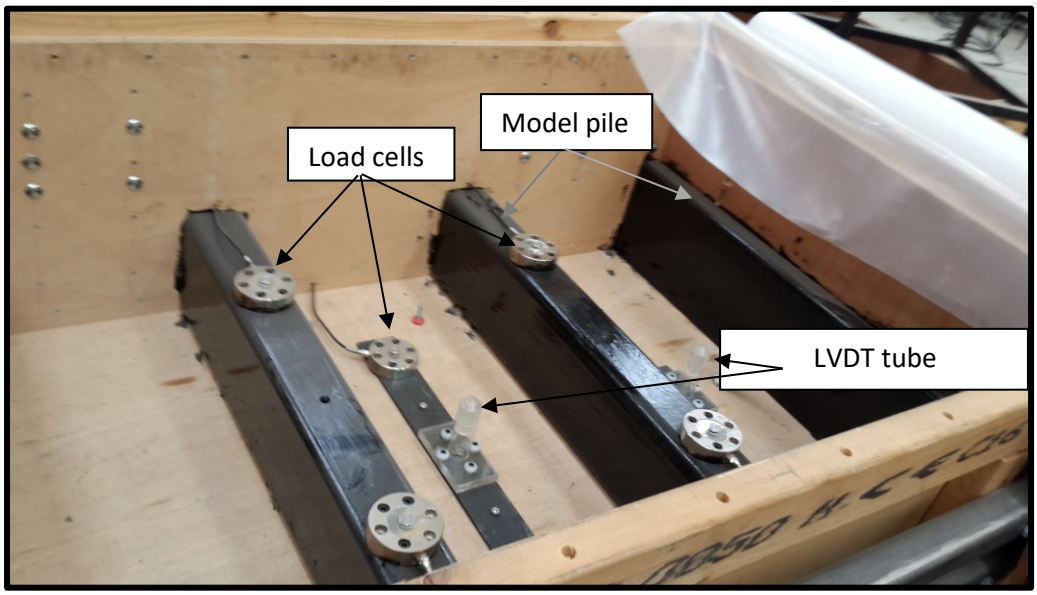

Figure 3.13. Load cells and LVDTs tube before placing the steel covers.

An additional two load cells were placed, as shown in Figure 3.10, at the base of the tank underneath the soft soil in the middle panel to measure the increase in pressure on soft soil due to monotonic and cyclic loadings. The two load cells were covered with a rigid steel plate and a flexible seal was applied on the boundary to prevent ingress of soil particles into the load cells area and to assist with prevention of moisture loss as shown in Figure 3.10.

The results of Han and Gabr (2002) indicated that maximum tension occurs near the edge of the pile. Therefore, it was crucial in this study that an attempt was made to capture the tension forces in the reinforcement layers, in particular the bottom one. To enable this, a complex system was manufactured and assembled to hold the reinforcement layer from each side and to transfer the load to the external load cells using a coupling mechanism. Load cells were mounted on the stiffening steel square box sections that were used to strengthen the walls of the testing tank as shown in Figure 3.10. Two steel bars were fastened to each end of reinforcement layer and can move freely with the reinforcement layer in the vertical direction. The external connection was designed to be able to rotate in order to always measure tangential tension forces as shown in Figure 3.14. The utilisation of a coupling mechanism was important to ensure that tangential forces were always measured. In total, eight load cells were used, two load cells in each end of the reinforcement sheet to measure the forces in the reinforcement layers. In order to present tension force per meter, the measured loads were summed from the 2 load cells of each end as the width of the geosynthetic sheet was 1m. Of note, no tension forces were applied on the reinforcement layer at the early stage of connecting load cells, thus, load measurement in reinforcement layers can be attributed exclusively to the additional self-weight of the soil and external loads. Due to the limited number of load cells, tension forces could only be measured in two reinforcement layers. Measured tension forces were used to determine the tensile stress on the reinforcement layers as shown in Figure 3.14.

Figure 3.14. System of measuring tension in reinforcement layers.

The deformation in the lower reinforcement layer was measured at three points using three LVDTs which were connected to the bottom reinforcement layer from underneath of the testing tank as illustrated in Figure 3.10. Coin size aluminium plates were fastened on the reinforcement layers and connected by 3 mm diameter metal rode which was encased by a Perspex tube as shown in Figure 3.10. Also, in order to measure the settlement in the embankment surface, two LVDTs were mounted on top of the loading plate for measurement of the surface settlement of the loaded area. Two strong wood cross bars, which were attached to the box test by four clamps, were used to fix the LVDTs on the surface of loading area as shown in Figure 3.10. Several trials were performed to ensure that measurements taken were accurate records of the deformation of the bottom reinforcement layer and the settlement of loading area. LVDTs were slightly compressed at the beginning to ensure continuous measurement of movements. Despite the fact that loads were controlled and applied using an advanced Servo Hydraulic Actuator system installed by

ServoCon Ltd, an additional load cell was placed on top of the loading area to ascertain applied loads by independent precise measurements as shown in Figure 3.10. Finally, the recording and storage of the instrument readings was carried out using data acquisition system (Agilent 34970A) with software (Gilent BenchLink Data Logger 3 software). Due to the number of measuring devices and huge number of data points, two data acquisition systems were utilised in this investigation to record measurements every 0.5 seconds.

3.4.2.4 Load cells and LVDTs calibration

All load cells and LVDTs used in the main experimental test were calibrated prior to use. Seven compression load cells, eight tension load cells and five LVDTs were calibrated in this study.

Load cells calibration

Data acquisition system (Agilent 34901A 20) with Instron loading machine was used to calibrate the load cells as shown in Figure 3.15. The load cells were connected to the data logger which was adjusted to read voltage in mv unit due to the variation in compression or tension loads which were applied to the load cells by the Instron loading machine as shown in Figure 3.15. Then the relation between recorded voltages by the data acquisition system and the recorded loads by the loading machine were plotted in graphs as shown in Figures 3.16 and 3.17. It was clear that linear relationship between the recoded voltage and applied loads was generated for all load cells. These graphs then were used to determine the measured loads on piles, soft soil and reinforcement layers which were recorded by the data acquisition system in voltages (mv) to loads (kN). The accuracy of the load cells that were used for

measurement of loads on piles, soft soils and reinforcement layers, was found to be ± 1.80 % of the measured values whereas that for measurement of the externally applied cyclic loading was ± 1.0 % of the measured values.

Figure 3.15. Calibration of load cells (a) tension load cell (b) compression load cell.

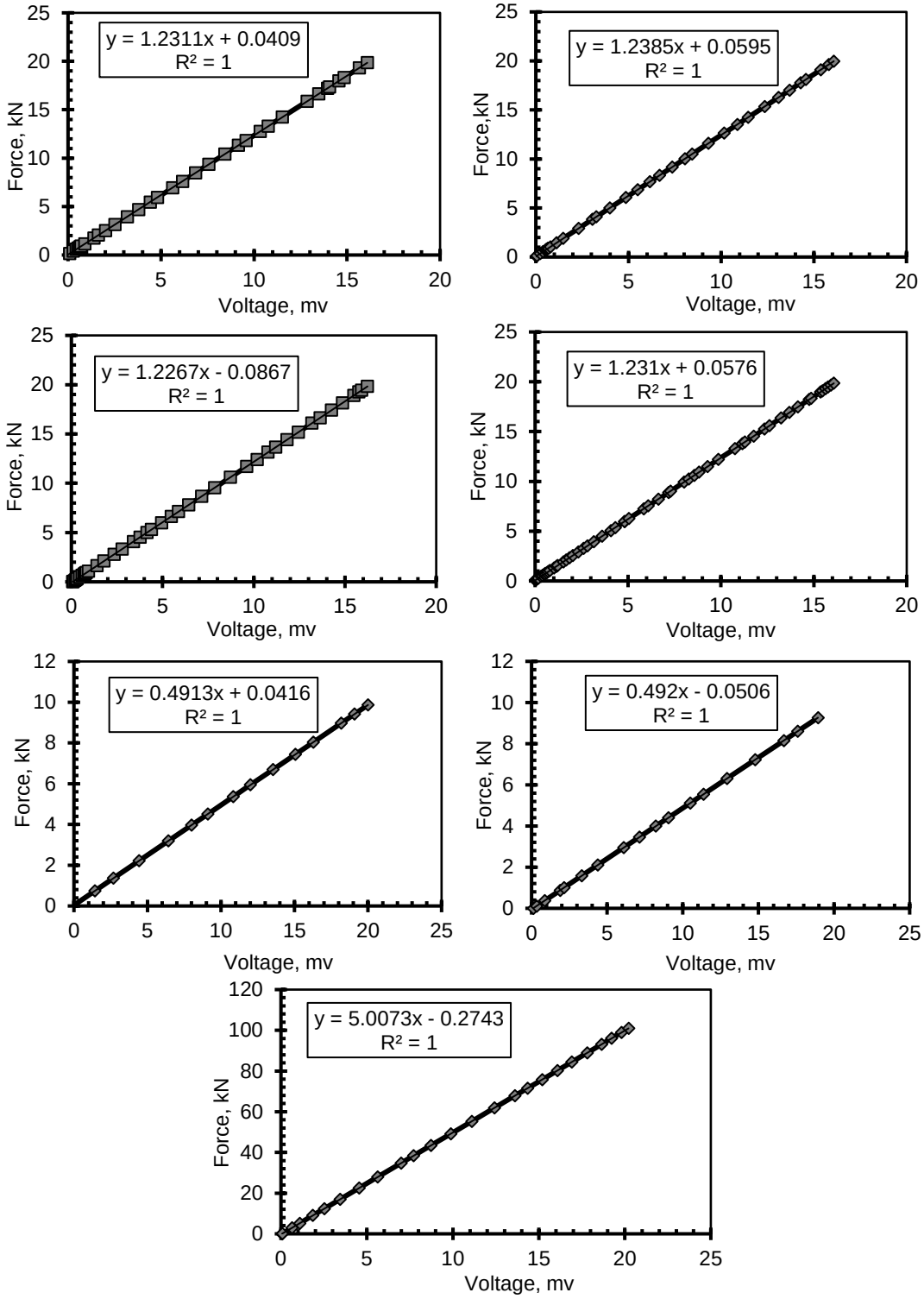

Figure 3.16. Calibration curves of compression load cells used in this study.

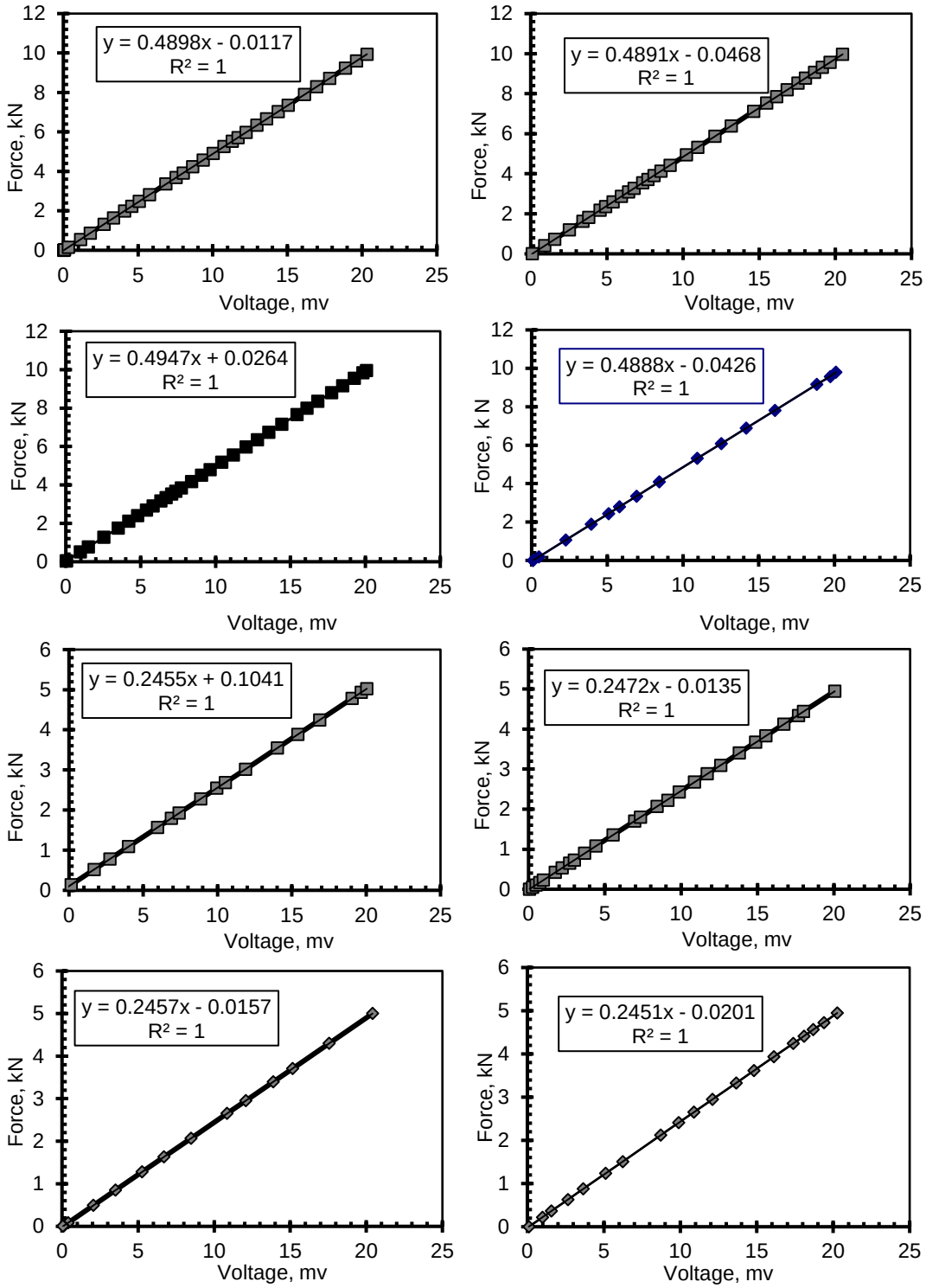

Figure 3.17. Calibration curves of tension load cells used in this study.

LVDTs calibration

In order to calibrate the LVDTs used in this study, data acquisition system (Agilent 34901A 20) and steel blocks with standard lengths were used as shown in Figure 3.18. The LVDTs were connected to the data acquisition system which was adjusted to read in voltage in (v) due to reflect the variation of LVDTs moved distance that can be read by using the standard blocks. The relation between the voltages (v) and LVDTs moving distance (mm) were then plotted in Figure 3.19. These graphs were then used to determine the measurements of deformations and settlements which were recorded by data acquisition system from voltages (v) to distance (mm) during the tests. Of note, Although, the range of LVDTs used in this study was between 0 mm to 100 mm, the calibration graphs ranged between10 mm and 100 mm. This was due to the relation curve between 0 mm and 10 mm was not linear. Therefore, to overcome this problem, it was initially compressed the LVDTs to a distance more than 10 mm before starting the tests. Figure 3.19 illustrates the calibration graphs of the five LVDTs used in this study. The LVDTs indicated that deformation measurements were taken with an accuracy of ± 2.0 % of the measured values.

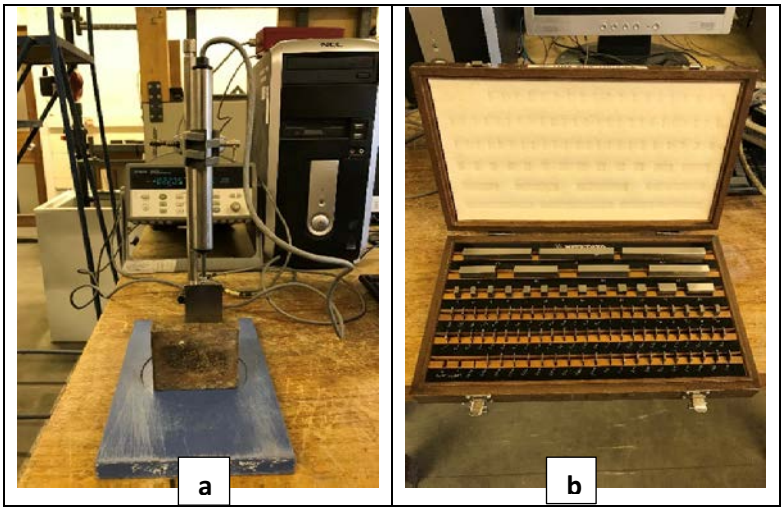

Figure 3.18. (a) LVDT calibration (b) standard steel blocks.

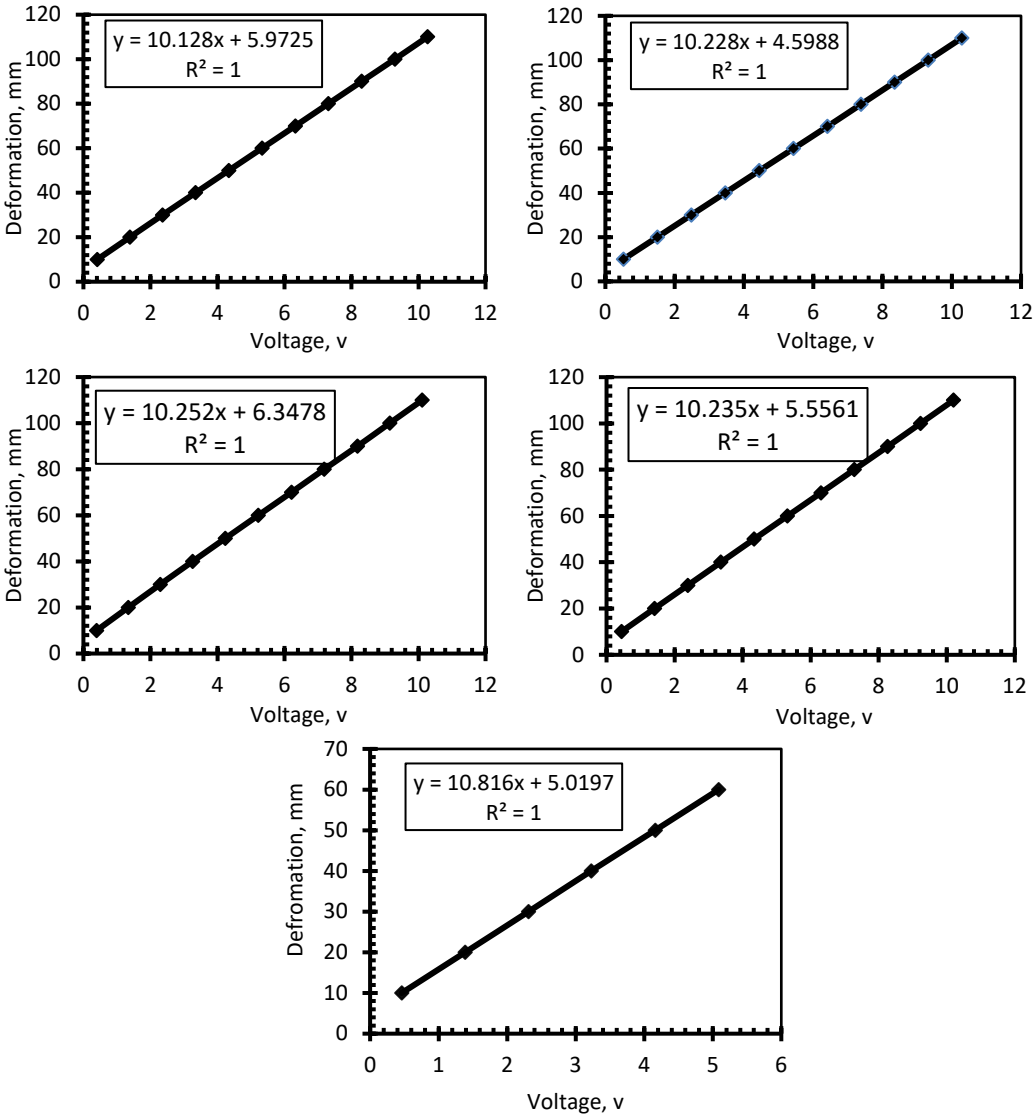

Figure 3.19. Calibration curves of LVDTs used in this study.

3.4.3 Material used

In this experimental study two different types of soil including soft soil and sands were utilised to develop sub-grade soft soil and embankments respectively whereas geotextile sheets were used to reinforce the embankment.

3.4.3.1 Sand fill

A typically available graded sand was used as the embankment fill material in this experimental study. The sand utilised had a range of particle sizes between 75 and 2360 µm as shown in Figure 3.20. The important index properties of the utilised sand are summarized in Table 3.9. According to British Standards Institution (2004), the sand soil was classified as even-graded coarse sand with silt and fine gravel. Also, the elastic modulus of this coarse sand which was determined by unconsolidated undrained triaxial test (UU) was 38 Mpa as shown in Figure 3.21.

Table 3.9. Properties of coarse sand soil used in this study.

Property	Measured value
d_{10}, µm	170
d_{30}, µm	350
d_{50}, µm	600
d_{60}, µm	850
Uniformity coefficient (C_u)	5
Coefficient of curvature (C_c)	0.85
Maximum dry unit weight, kN/m^3	17.96
Optimum water content, %	10.30
Specific gravity (G_s)	2.65
Angle of friction (ϕ), degree	38
Angle of friction between sand and reinforcement layer, degree	26
Elastic modulus (E_s), Mpa	38

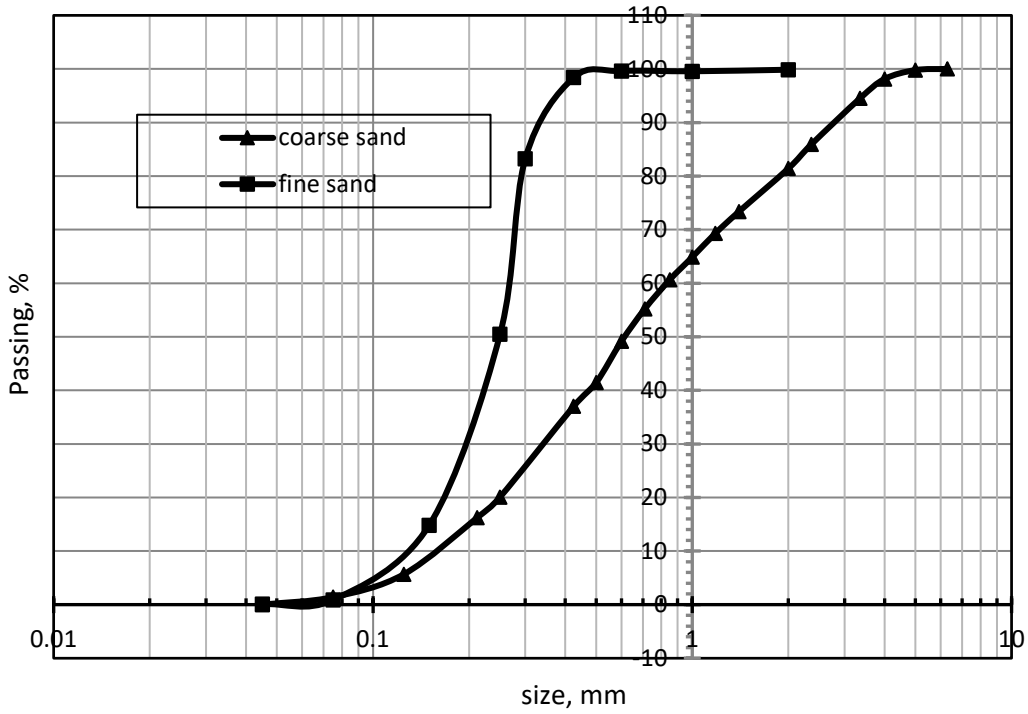

Figure 3.20. Sieve analysis curves of fine and coarse sand soils.

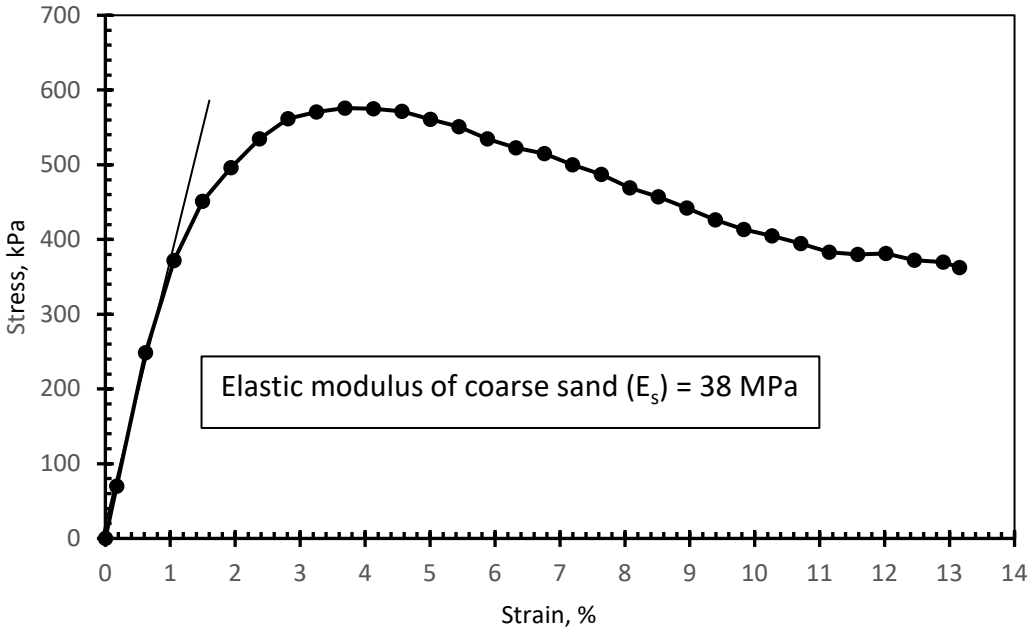

Figure 3.21. Stress – strain relationship for the used coarse sand.

3.4.3.2 Soft soil

In this study, a real soft soil was prepared and used as a sub-grade soil in all experiments. Three different types of soil namely coarse sand (CS), fine sand (FS) and pure clay powder (C) were utilised to create a soft soil. The three soils were mixed in different quantities as illustrated in Table 3.10 in order to select the mixture that produces weak sub-grade soil. It was planned to select the mixture that gives the lowest elastic modulus at maximum dry density. In order to accomplish the task, maximum dry density and moisture content were determined from standard Proctor tests for all three mixtures as shown in Figure 3.22.

Table 3.10. soft soil quantities.

Type	Mix % (CS: FS: C)
Soft soil 1	75% : 0% : 25%
Soft soil 2	50% : 25% : 25%
Soft soil 3	34% : 33% : 33%

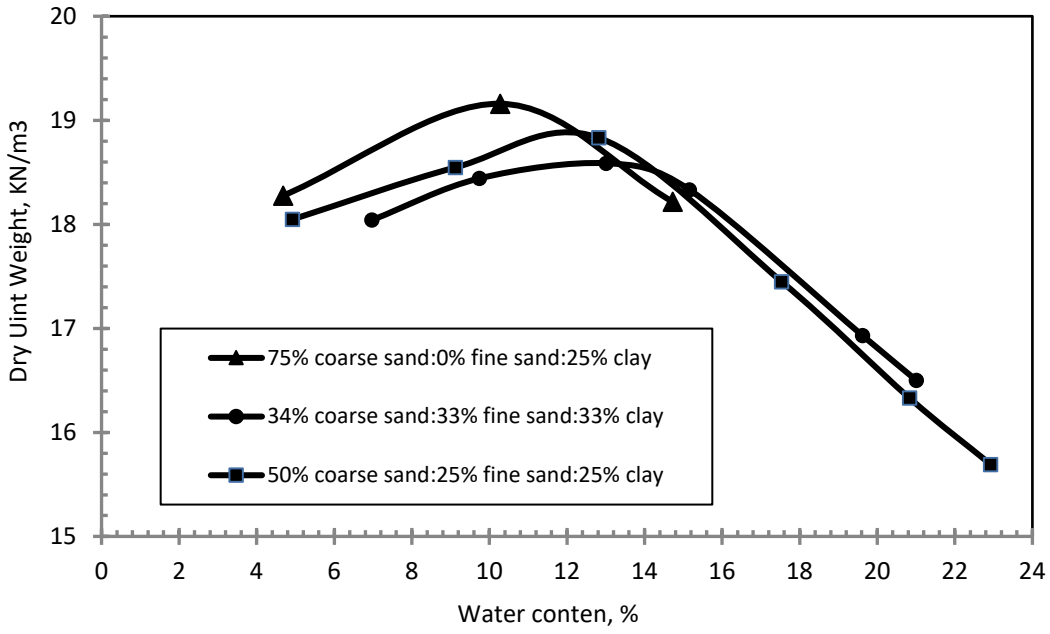

Figure 3.22. Compaction curve of different sub grade soils.

Specimens were then prepared at maximum dry densities and corresponding moisture content for measurement of the elastic modulus. Unconfined compression test was used to determine the elastic modulus of soft soil. However, it was surprising to find that there was not much difference in the maximum dry unit weight of the three mixtures and specimens 2 and 3 had an elastic modulus of less than that observed on specimen 1 as shown in Figure 3.23.

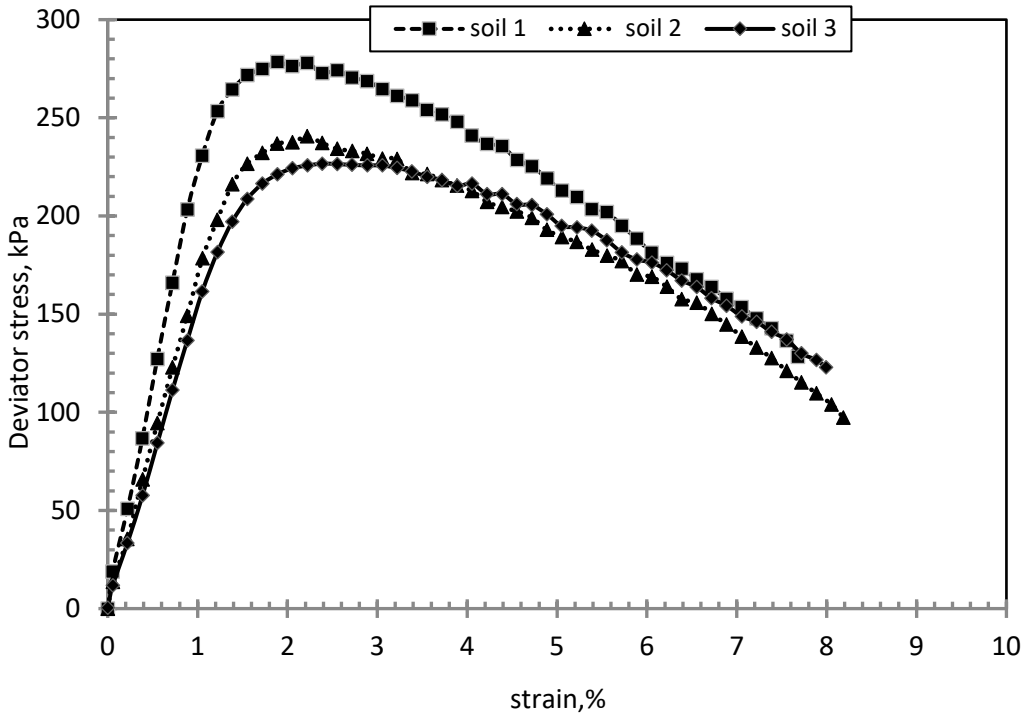

Figure 3.23. Stress – strain relationship for the three different mixtures of clay soil.

The elastic modulus of specimens 2 and 3 was nearly the same and equal to 16 MPa which was considered to be very high for the purpose of the tests. The second mixture that was prepared by addition of 50 % of CS, 25 % of FS, 25 % of C was then selected on the basis of practical consideration for mixing and compaction, materials availability and cost effectiveness. Figure 3.24

shows the compaction curve for the selected soft soil. In order to reduce the elastic modulus, specimens were prepared on the wet-side of the compaction curve by incremental increase in moisture content. These specimens were tested to determine the elastic modulus as shown in Figure 3.25. Moisture content increased up to 22 %. However, for the samples with high amount of water content unconsolidated undrained triaxial test (UU) were used due to difficulty of preparing formed samples. The elastic modulus of specimens that were compacted at dry unit weight of 15.95 kN/m^3 and moisture content of 22 % was found to be 0.425 MPa which was quite low to represent weak sub-grade soil as shown in Figure 3.26. The important index properties of the selected mixture are summarized in Table 3.11 according to British Standards Institution (1999) and (2002). The prepared soft soil was classified as clay soil with low plasticity. It should be noted that pore water pressure was not measured in this testing programme since the time required for consolidation is much longer than the time needed to apply all three stages of cyclic load.

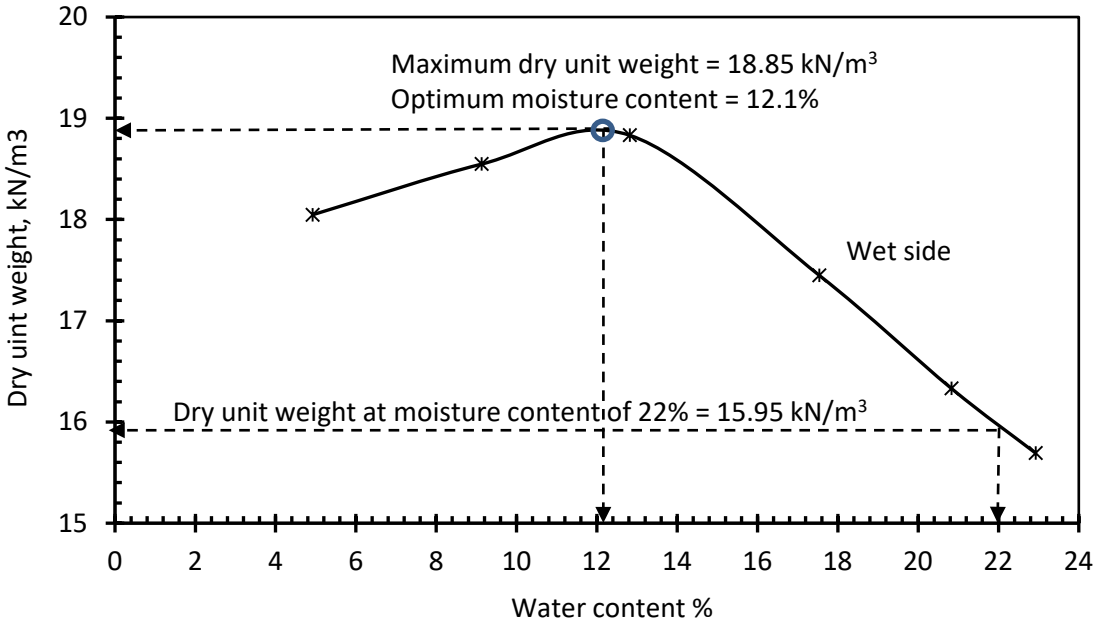

Figure 3.24. Compaction curve of sub grade soil.

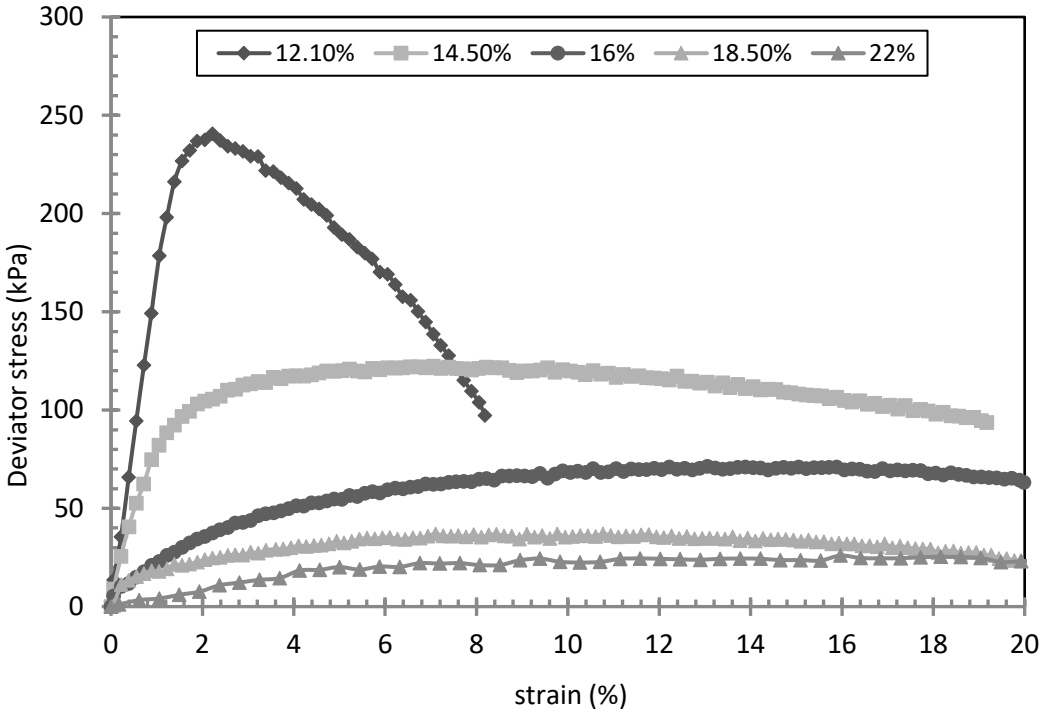

Figure 3.25. Stress – strain relationship for the used clay soil with different water content amount.

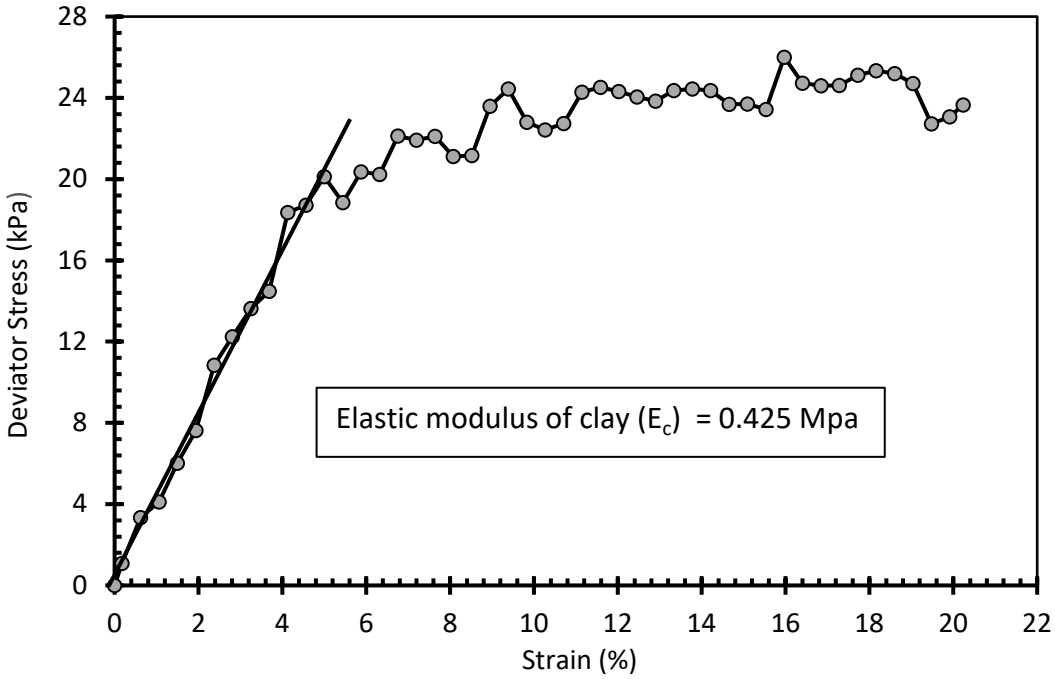

Figure 3.26. Stress – strain relationship for the used clay soil.

Table 3.11. Properties of soft soil used in this study.

Property	Measured value
Dry unit weight, kN/m^3	15.95
Moisture content, %	22.0
Liquid limit (LL), %	28.0
Plastic limit (PL), %	20.2
Undrained cohesion, kPa	13
Angle of friction, degree	0
Elastic modulus (E_c), kPa	425

3.4.3.3 Reinforcement

Careful consideration was given to the selection of reinforcement material so that a realistic behaviour for reinforced piled embankment can be simulated and assessed. As explained in section 3.4.1, the whole testing setup was scaled down by a factor of 4. As a result, a reinforcement material with a low tensile strength of 9 kN/m' was required for this study. Several reinforcement materials have been considered including geotextile and geogrid sheets. However, geogrids were excluded as available products have a much higher tensile strength than required and since the outcomes of Van Eekelen et al. (2012) suggested that there is no major difference in the interaction between geotextile and geogrid in piled embankment. Geotextile reinforcement materials were tested for use in this study. A wide-width tensile test was carried out the in the lab according to British Standards Institution (2015) on specimens of woven geotextile materials as shown in Figure 3.27. Figure 3.28 shows attained tensile stress against tensile strain results for the selected geotextile material. It can be seen that the maximum tensile strength of reinforcement materials was found to be 12.50 KN/m' which was recorded to occur at a strain of 11.0 %. The reinforcement material loses its strength post

peak value. However, at 5 % strain, the material exhibit a tensile strength of 5.8 kN/m' which is well below the value required by scaling down the whole testing rig. In addition, nearly elastic behaviour was noted in the first 2 % strain which is expected to occur in this kind of reinforcement material. Layers of woven geotextile with dimensions of 1400 mm in length and 1000 mm in width were used as reinforcement materials.

Figure 3.27. A wide-width tensile test for the used geotextile reinforcement material.

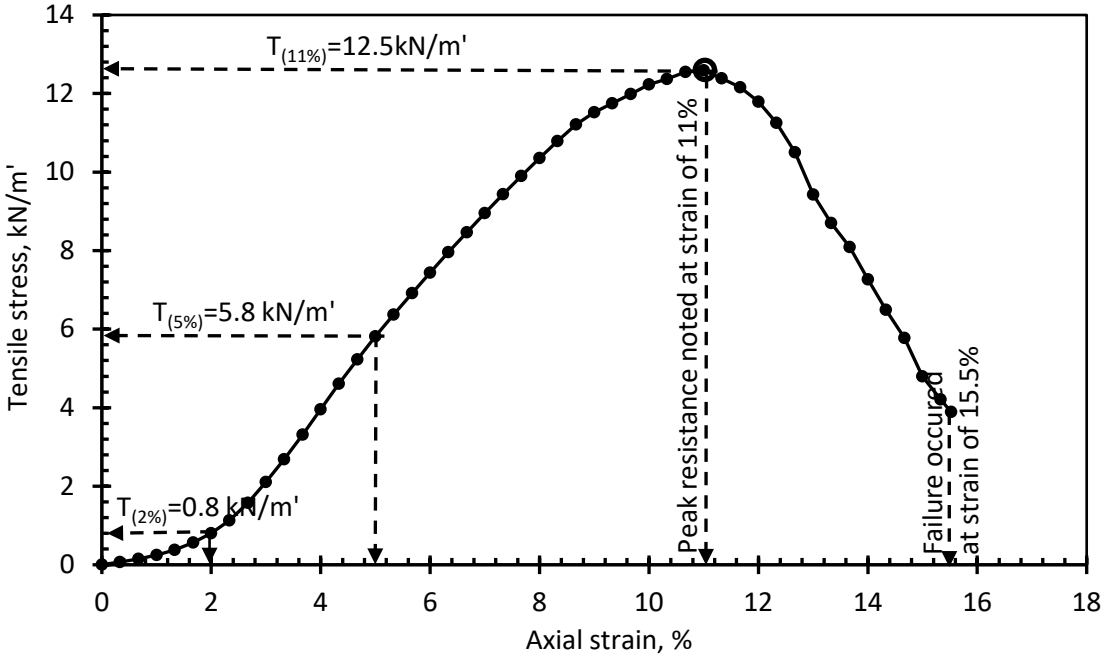

Figure 3.28. Tensile stress – strain relationship for the used geotextile reinforcement material.

3.4.4 Testing setup and procedure

Prior to the onset of the experimental programme, the testing tank was positioned in the central area of the loading frames so as to be centred with the actuator. Furthermore, the testing tank was also levelled to be precisely horizontal so that it was perpendicular to the vertical axis of the actuator.

The soft soil was prepared by mixing specific amounts of CS, FS and C and addition of predetermined quantity of water in a large mechanical mixture to ensure achieving uniform mixture. In total, around 400 kg of soft soil was prepared and stored for re-use in all tests. The soft soil was placed and compacted manually in layers of 50mm to fill in the space between the model piles. Once the soft soil was levelled off with the model piles, the surface of soft soil was covered by a dump proof sheet and surcharge pressure of 2.0 kPa was applied for 24 hours to ensure reaching; i. a uniform distribution of

water and ii. a pre-set dry unit weight which was determined based on the measurements taken by the load cells that were installed underneath the base of the soft soil. After the elapse of the 24 hrs period, the surcharge load and dump proof sheet were removed and any subsidence on the surface of soft soil was re-filled by the addition of same soft soil. Ultimately, the surface of soft soil was levelled off insuring that it coincided with the top level of piles. Readings from the load cells were taken to record the attained dry unit weight in each test. In addition, three specimens were collected for the determination of actual water content.

In order to prepare the embankment with the same dry unit weight, a sand raining technique was employed in this testing programme by which sand was poured through a perforated metal sheet that was placed at the top of the testing tank. A trial test was conducted in which 20 samples were collected from different heights and locations within the embankment for the determination of the dry unit weight. It was found that the average dry unit weight of the sand was 16.80 ± 0.05 kN/m^3. The achieved dry unit weight was almost 94% of the maximum dry unit weight determined from the standard Proctor test. According to Das (2010), the achievable dry density in engineering practice is required to be between 90% and 105%. Thus, the achieved dry unit weight of the embankment fill is considered to be acceptable. In this study three different heights of embankment (200, 400 and 600 mm) with and without reinforcement layers were investigated. When the height of the embankment was 200 mm around 520 kg of sand was poured into the bottom testing tank through the raining box. For unreinforced embankment, continuous raining of sand was maintained until reaching the required height.

Then the surface of the sand bed was levelled off to avoid any discrepancy in the initial overburden pressure and detrimental effects on the loading area. Whereas, in case of inclusion of reinforcement layers, sand raining was interrupted to allow the insertion of reinforcement layers at predetermined heights according to the testing programme. Bottom layer was always placed on top of a sand bed with a thickness of 25 mm to prevent damaging of reinforcement layer by the sharp edge of the model piles. Subsequently, the two ends of the reinforcement layer were fastened to the tension measurement mechanism and LVDTs were connected from underneath the testing tank. Then sand raining was continued to form the embankment until reaching the required level. In the case of inclusion of a layer or multiple layers of reinforcement, sand raining was temporarily ceased to enable the installation of reinforcement layers at particular levels. Then sand raining was resumed to complete the construction of the remaining part of the embankment. Of note, sand surface was levelled off prior to the placement of reinforcement layers which were inserted at a spacing of 50 mm. Also, in the case of increasing the height of the embankment, the upper part of the box was connected with the bottom part and the same process as the embankment with height of 200 mm was used for both unreinforced and reinforced soil. The amount of pouring soil into the connected test tank was approximately 1040 kg and 1560 kg of embankment with height of 400 and 600 mm respectively.

Figure 3.29. Reinforcement layer before filling the embankment soil into the box test.

Once the top level of the embankment was levelled off, this denotes the completion of Stage 0 and records of load cells were taken as shown in Figure 3.30. The loading plate was placed on the central area of the testing tank. Two LVDTs were securely mounted on top of the loading plate to measure settlement as shown in Figures 3.10 and 3.11. Then Servo Hydraulic Actuator was moved down slowly until it became in contact with the loading plate. Stage 1 of loading which is monotonic loading was initiated by gradually increasing the applied load up to 28 KN at a rate of 0.42 kN/sec. The load was maintained constant for 200 s. Then three stages of cyclic loading with different mean loads and amplitudes were performed with a constant frequency of 0.5 Hz. The cyclic loading in stages II, III and IV were (8-48 kN), (8-68 kN) and (8-88 kN) which are equivalent to the application of surface pressures of (8.9-53.3 kPa), (8.9-75.6 kPa) and (8.9-97.8 kPa) respectively. The amplitude of the applied load was increased with the stage to simulate, to a great extent, the

on-off nature of different cyclic loadings. Due to limitations with the data acquisition systems, data were recorded every 0.5 s so that four readings could be taken every load cycle. The number of cycles in all three stages of cyclic loading was kept at 1000 cycles. After the 3000 cycles was completed, the loading in stage V was reduced gradually at a rate of 0.42 kN/sec until complete unloading. Upon removal of the loading plate, the soil surface was scanned accurately to determine surface profile in particular areas of settlement and heave. Furthermore, the surface profile of the soft soil was accurately scanned after the removal of the embankment fill material. Finally, specimens of clay soil and sand soil were taken for determination of water content.

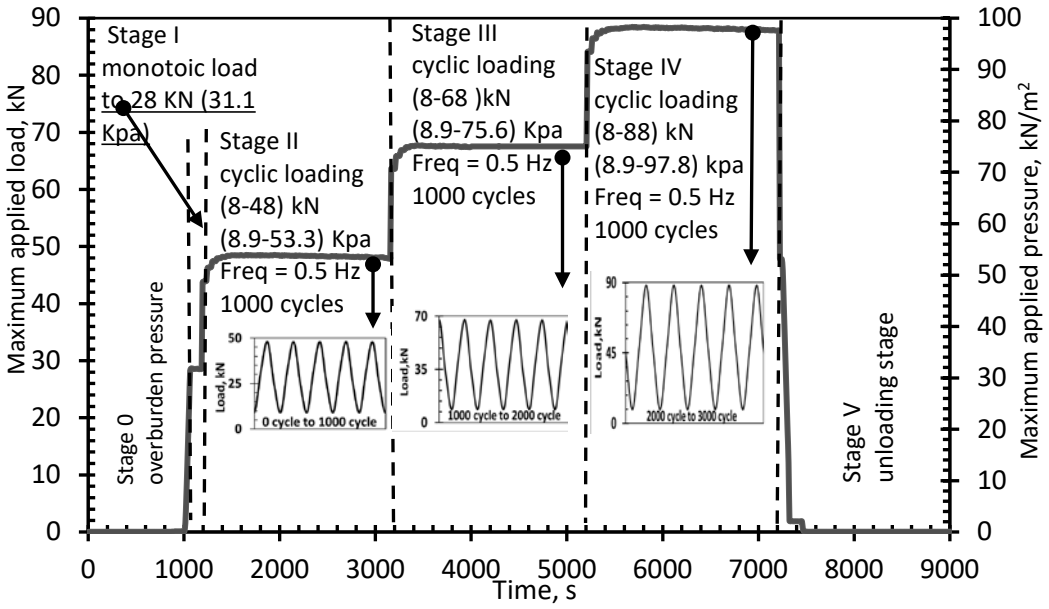

Figure 3.30. Different stages of maximum monotonic and cyclic loadings.

3.4.5 Testing programme

In this study, fifteen main experiments were performed in order for a deeper understanding of the behaviour of shallow unreinforced and reinforced piled embankment under cyclic loading conditions to be acquired. Three series of the tests with different height of embankment (200, 400 and 600 mm) were investigated on four samples with number of reinforcement layers varied from zero to three layers as shown in Table 3.12. Also, in order to compare the effect of loading via specific area and via full area, one reinforced 200 mm embankment test was carried out. All tests were undertaken whilst the thicknesses of the soft soil bed was kept at 200 mm.

Table 3.12. Summary of experimental programme.

Series	Number of tests	Variable parameters	Fixed parameters
I	3	Embankment height = 200 ,400, 600 mm	Soft soil thickness, pile width piles spacing and loading stages
II	4	Number of reinforcement layers = 0,1,2,3	Embankment height (200 mm), Soft soil thickness, pile width, piles spacing and loading stages
III	4	Number of reinforcement layers = 0,1,2,3	Embankment height (400 mm), Soft soil thickness, pile width, piles spacing and loading stages
IV	4	Number of reinforcement layers = 0,1,2,3	Embankment height (600 mm), Soft soil thickness, pile width, piles spacing and loading stages

3.5 Summary

In this chapter, the design and manufacture of the main experimental test and the two preliminary tests were presented. The dimensions of the main testing rig was determined in accordance with the scaling rules that were proposed and used in previous studies. Instrumentation system were designed and used to measure the pressure on the piles and soft soil, the tension in reinforcement layers the settlement in embankment surface and the deformation in lower reinforcement layer. Different stages of cyclic loading were applied by using an advanced Servo Hydraulic Actuator system by ServoCon Ltd via rigid plate which was positioned in the centre of the embankment surface. Two types of soil were used in this test, soft soil which were made in the laboratory by mixing three types of soil and coarse sand which used to build the embankment fill. Layers of woven geotextile were used as reinforcement.

California bearing Ratio (CBR) apparatus was used to apply repeated loads on unreinforced and reinforced samples of soil. Two types of soil, clay and medium coarse sand with layers of geotextile were tested in this experimental work. The compaction system used in this experiment was modified by increased the number of blows and reduced the height of hammer. A trapdoor apparatus was also designed and constructed to be able to apply repeated sequential active and passive arching. A load cell was attached to trapdoor to measure the pressure on it. Medium coarse sand soil was selected as fill materials. Raining box technique with constant height were used to keep a constant density during all tests. All the important properties of used materials were determined prior starting all the tests. Finally, all the load cells and LVDTs were calibrated before starting the tests.

CHAPTER FOUR

STRENGTH AND DEFORMATION OF REINFORCED SOILS SUBJECTED TO MONOTONIC AND REPEATED LOADS

4.1 Introduction

This chapter presents the attained results from California Bearing Ratio (CBR) and Repeated Load California Bearing Ratio (RL-CBR) tests (preliminary test 1) on reinforced and unreinforced samples. The effects of sand layer thickness and number of reinforcement layers on the behaviour of clay bed under static and repetitive loading cycles are examined and discussed hereafter.

4.2 Effect of monotonic and repeating loads on the strength of clay soil

Figure 4.1 presents the results of CBR and RL-CBR tests on a sample of clay soil (zero mm of sand layer). It can be clearly seen that the penetration load that caused a deformation of 2.50 mm was 95 N (CBR value). When the sample was released from this applied load, the deformation decreased to 2.38 mm. This difference in the deformation due to loading and unloading represents the elastic deformation and was found to be 0.12 mm and therefore the 2.38 mm penetration is taken as the plastic deformation. When the sample was reloaded repetitively to the CBR load of 95N the plastic deformation per cycle increased while elastic deformation decreased with further cycles of loading and unloading due to fatigue stress as shown in Figure 4.2. Careful inspection of Figure 4.2 reveals that the rate of increase in the value of plastic deformation decreased after the first few cycles. Furthermore, although the measured elastic deformation was relatively small, it decreased further with increasing number of cycles. The elastic deformation had nearly reached a

constant value after 15 cycles. From the results it can clearly be seen that repeated loading could increase the non- recoverable plastic deformation considerably which would result in permanent cracks and fissures within the subgrade soil. The plastic deformation was increased by 59 % from 2.38 mm at first cycle to 3.79 mm after 30 cycles of loading and unloading. On the other hand, the elastic deformation diminished with increasing number of cycles to 0.06 mm after 30 cycles as shown in Figure 4.2.

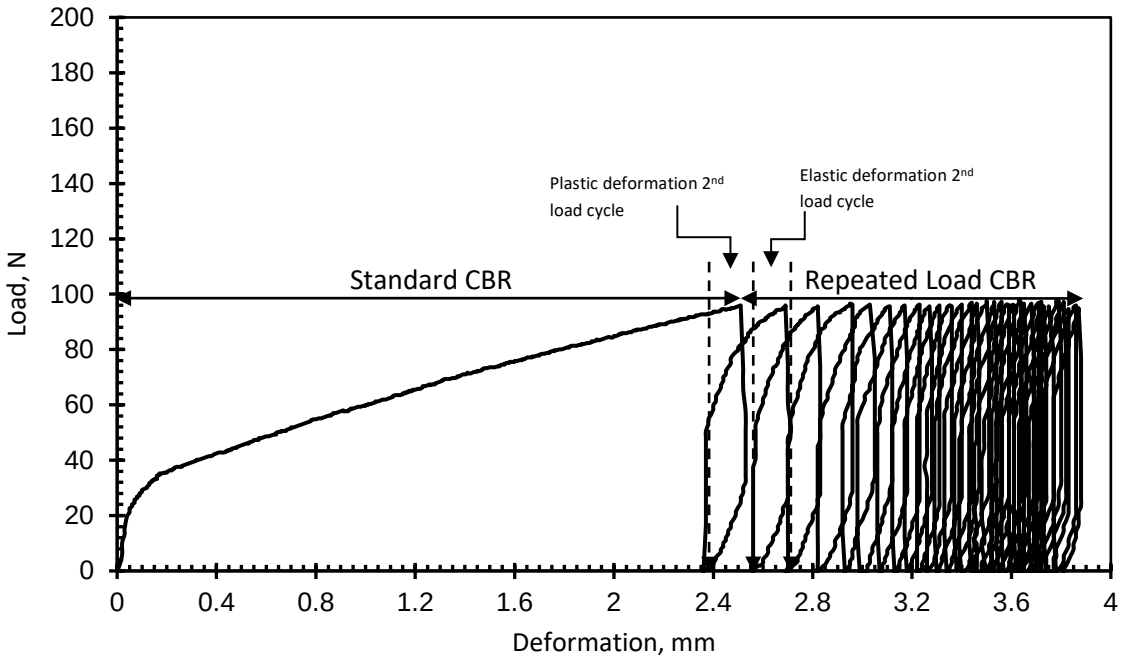

Figure 4.1. Load vs. deformation graph on clay sample under repeated loading condition.

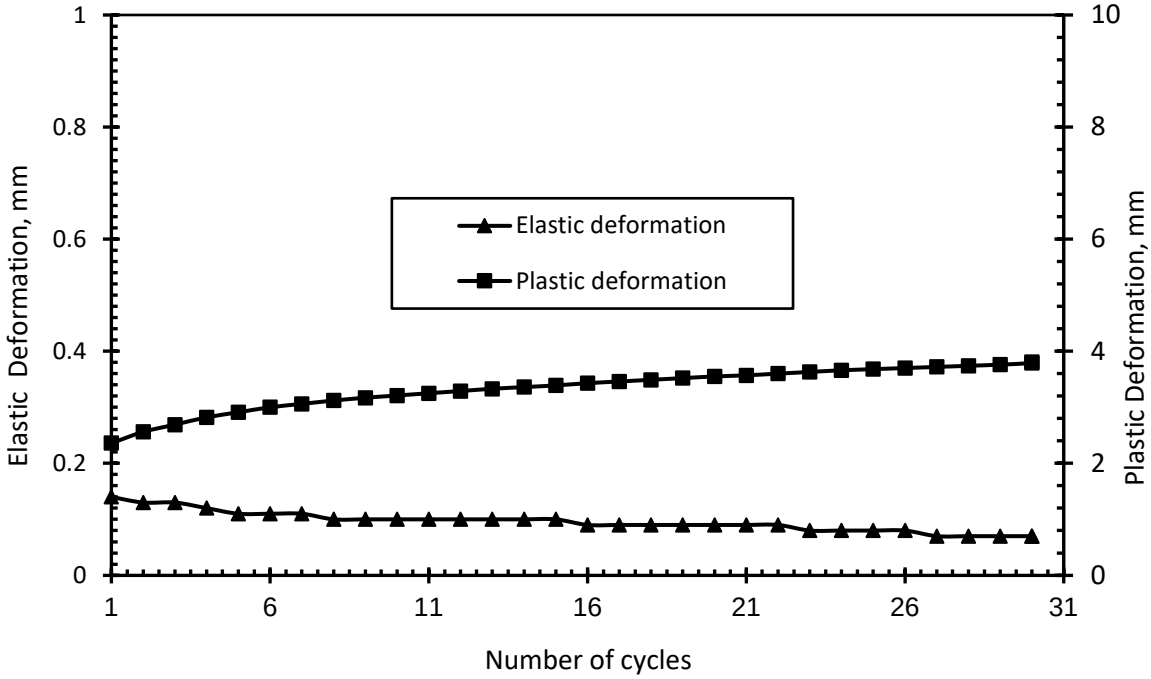

Figure 4.2. Elastic and plastic deformations of clay sample as a function of number of loading cycles.

4.3 Effect of thickness of sand layer

Figures 4.3, 4.4 and 4.5 present the results of CBR and RL-CBR tests on samples containing clay and sand where the sand layer was placed above the clay sample with various thicknesses. The sand layer was placed with thicknesses of 15, 25 and 40 mm, as shown in Figure 3.6. The results indicated that the applied load could be increased significantly with increasing thickness of sand layer. A remarkable improvement was noticeable when a thick sand layer of 40 mm was placed as shown in Figure 4.6. The load at a penetration of 2.50 mm on a sample which consisted of clay underneath a 15 mm thick layer of the sand was increased by about 30 % compared with that achieved on a sample of clay with a zero mm layer of sand. This load was further increased by 50 and 75 % when the thickness of sand layer was increased to 25 and 40 mm respectively. The thickness of sand layer is therefore found beneficial in increasing the load carrying capacity. The main reason for the

improvement was that granular materials have good strength properties compared with clay soil.

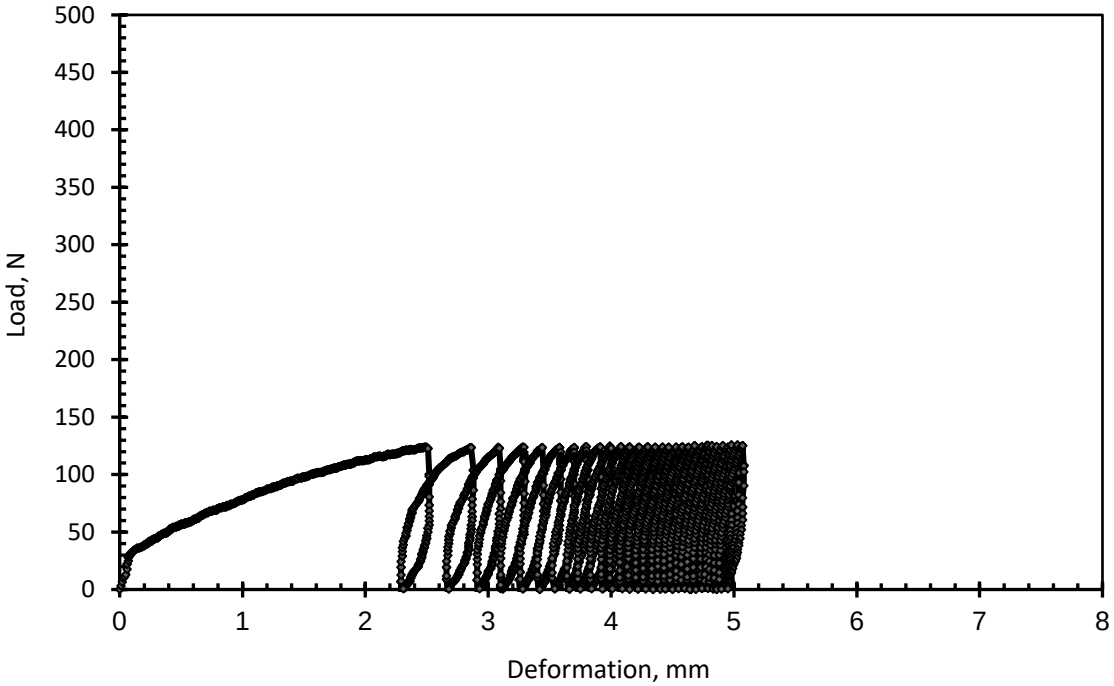

Figure 4.3. Load vs. penetration graph of clay + 15 mm of sand soil under repeating loading condition.

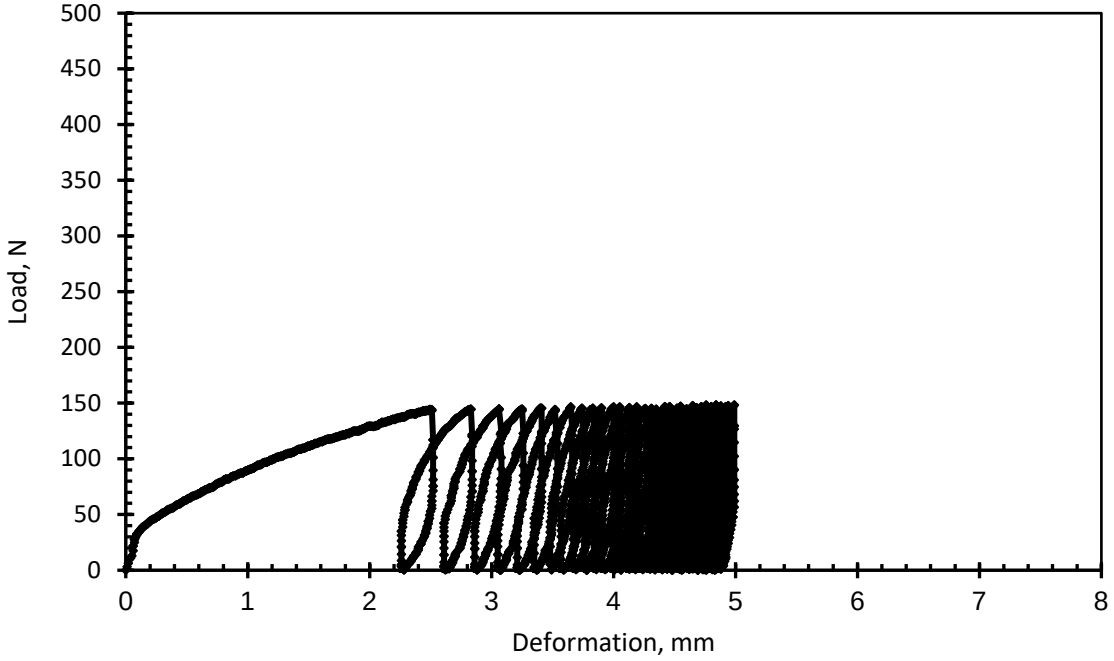

Figure 4.4. Load vs. penetration graph of clay + 25 mm of sand soil under repeating loading condition.

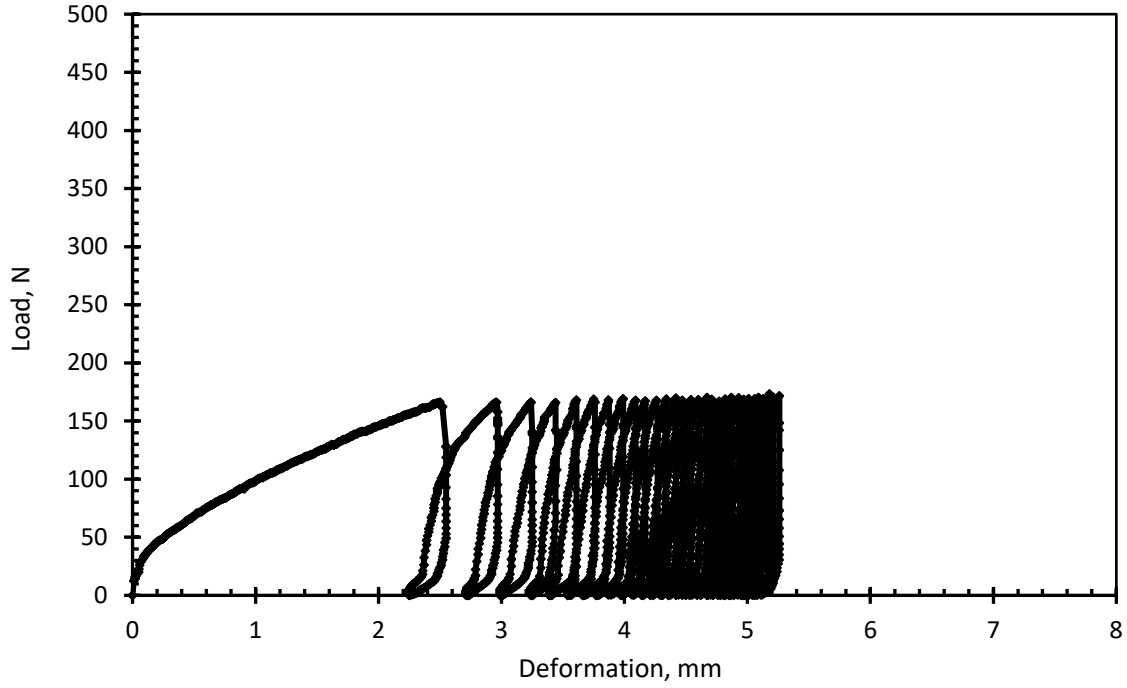

Figure 4.5. Load vs. penetration graph of clay + 40 mm of sand soil under repeating loading condition.

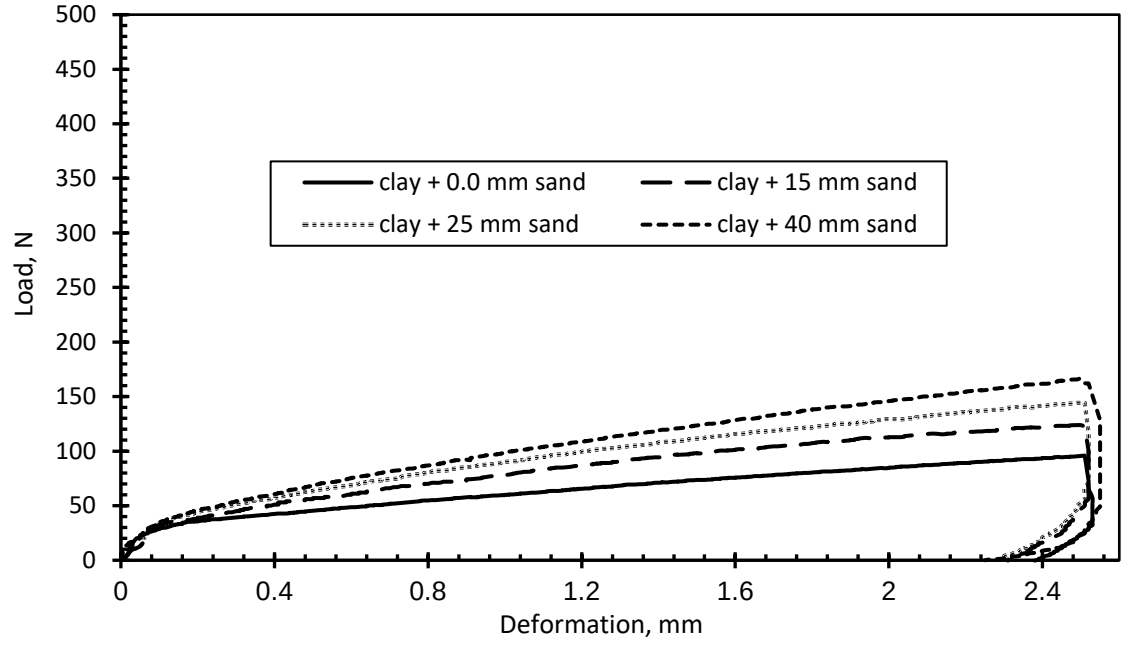

Figure 4.6. Load vs. Deformation graph of clay soil and clay with three different layers of coarse sand during first cycle.

Under repeated loading conditions the results show that the plastic deformation of the first loading cycle on clay samples overlaid with layers of

sand was slightly smaller than that obtained from a sample of clay only at their maximum load as shown in Figure 4.7 and Table 4.1. Performing cycles of loading and unloading on clay samples overlaid with layers of sand with different thicknesses yielded a higher plastic deformation than corresponding values of the clay sample as shown in Figure 4.7 and Table 4.1. Of note, the higher plastic deformation is due to the magnitude of load carrying capacity of these samples which was remarkably higher than the magnitude of load carrying capacity of the clay sample. However, if tests on samples of clay with different layers of sand were performed to the same maximum loading recorded for the clay sample, one would expect a substantial reduction in the anticipated value of plastic deformation compared with the clay sample as illustrated in Figure 4.7. This is due to the fact that the stiffness of the sand layer is higher leading to reduction in the overall deformation. Thus placing a layer of sand overlying clay subgrade would be effective in reducing long term plastic deformation provided that the same level of loading is maintained.

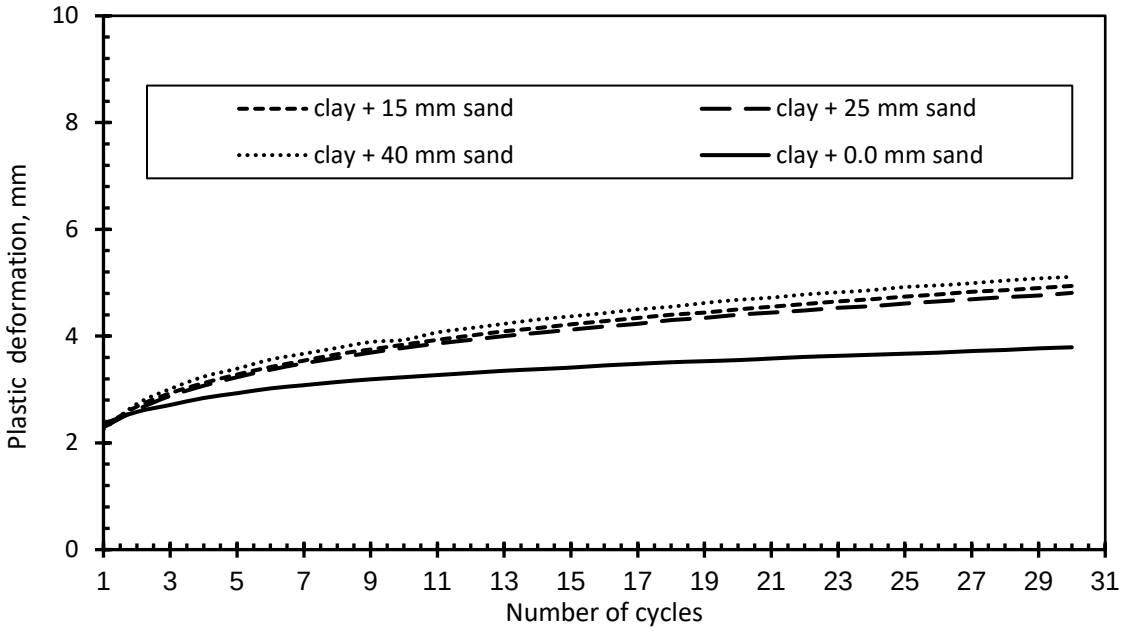

Figure 4.7. Plastic deformations of clay samples with different thickness of overlying sand versus number of cycles.

The elastic deformation during the first cycle of samples containing clay and a layer of sand with different thicknesses was observed to be higher than that attained on a sample of clay soil only as shown in Figure 4.8 and Table 4.1. The elastic deformation is directly related to the thickness of the sand layer which could be linked to the change in the characteristic properties of the material adjacent to the plunger. Figure 4.8 shows that the elastic deformation decreased with further cycles of loading and unloading. Data show that after 30 cycles of loading and unloading, the elastic deformation of clay samples with layers of sand reached almost the same level of deformation but it is still higher than that of the sample with clay only. The final value of the elastic deformation was not therefore significantly affected by the increase in the thickness of the sand layer.

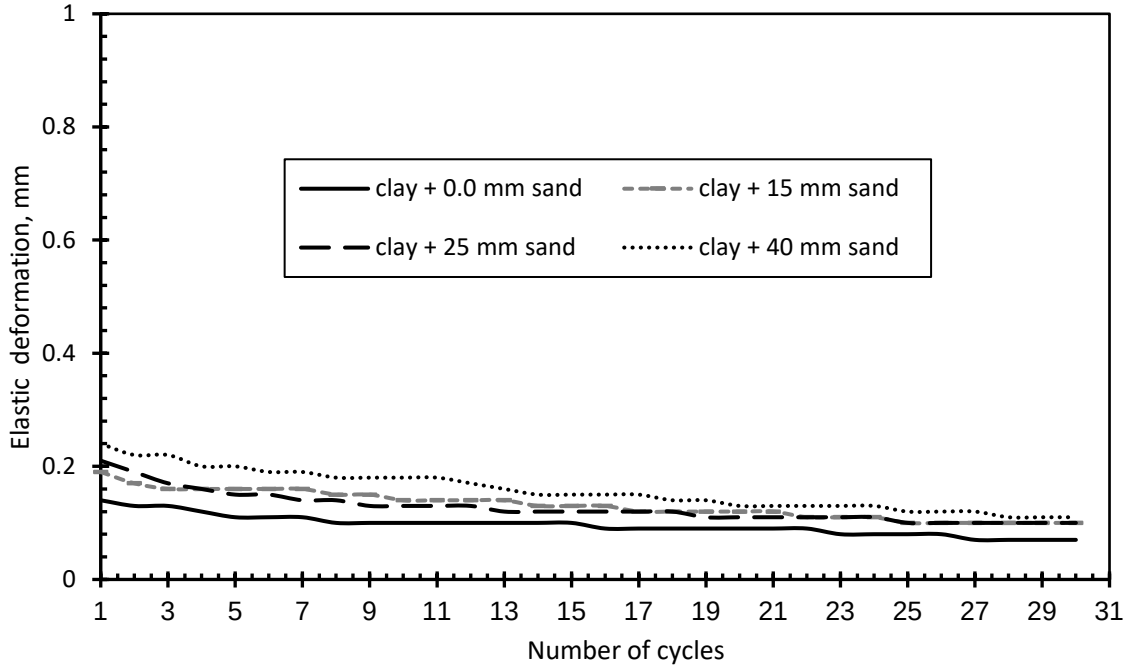

Figure 4.8. Elastic deformations of clay samples with different thickness of overlying sand versus number of cycles.

Table 4.1. Plastic and elastic deformation values of clay with different layers of sand under repeated loading conditions.

Sample	Load (N) at deformation of 2.50 mm	Elastic deformation (mm) after first cycle	Plastic deformation (mm) after first cycle	Elastic deformation (mm) after 30 cycles	Increasing in Plastic deformation (mm) in first 5 cycles per cycle (%)	Increasing in Plastic deformation (mm) in last 5 cycles per cycle (%)	Total Plastic deformation (mm) after 30 cycles
Clay + 0 mm of sand	95	0.14	2.36	0.07	4.90	0.50	3.81
clay + 15 mm of sand	125	0.18	2.32	0.10	8.30	0.80	4.94
clay + 25 mm of sand	145	0.21	2.29	0.10	8.30	0.70	4.87
clay + 40 mm of sand	166	0.24	2.26	0.11	9.80	0.90	5.11

4.4 Effect of position of single reinforcement layer

Figures 4.9 – 4.12 present the results of CBR and RL-CBR tests on samples containing clay overlaid with 40 mm of sand layer to examine the effect of changing the position of a single layer of reinforcement on the load carrying capacity and deformation characteristics under static and repeated loading conditions. The reinforcement layer was placed at the interface, 10, 20 and 30 mm above the interface as shown in Figure 3.6. From these results it is evident that reinforcing sand with one layer is beneficial in improving the load carrying capacity. Using a layer of geotextile reinforcement at the interface between clay and sand layers leads to a significant increase in the load carrying capacity by 60 % (from 166 N up to 265 N for unreinforced and reinforced samples respectively) as shown in Figure 4.13. The results also illustrate that changing the location of the reinforcement layer within the sand layer does not always provide the desired beneficial impact. For example, having the reinforcement layer at the mid-height of the sand layer yielded lower load carrying capacity in comparison with the case in which the reinforcement layer was placed at the interface between clay and sand as shown in Figure 4.13.

The highest degree of improvement was achieved when the reinforcement layer was placed within the sand layer at 10mm above the interface. This was marginally higher at 4 % over that recorded for a sample with reinforcement layer at the interface between clay and sand. This could be attributed to a slight increase in interface frictional resistance since the reinforcement layer is contained within the granular layer. However, when the reinforcement layer was placed at 20 or 30 mm above the interface, the attained load carrying capacity was lower than that achieved when the reinforcement layer was at or 10 mm above the interface. This would likely be due to the proximity of the reinforcement layer to the surface. The results attained in this study partly agree with previous results by Subaida et al., (2009) in which it was found that placing the reinforcement layer within the base course rather than at the interface always enhances the bearing capacity.

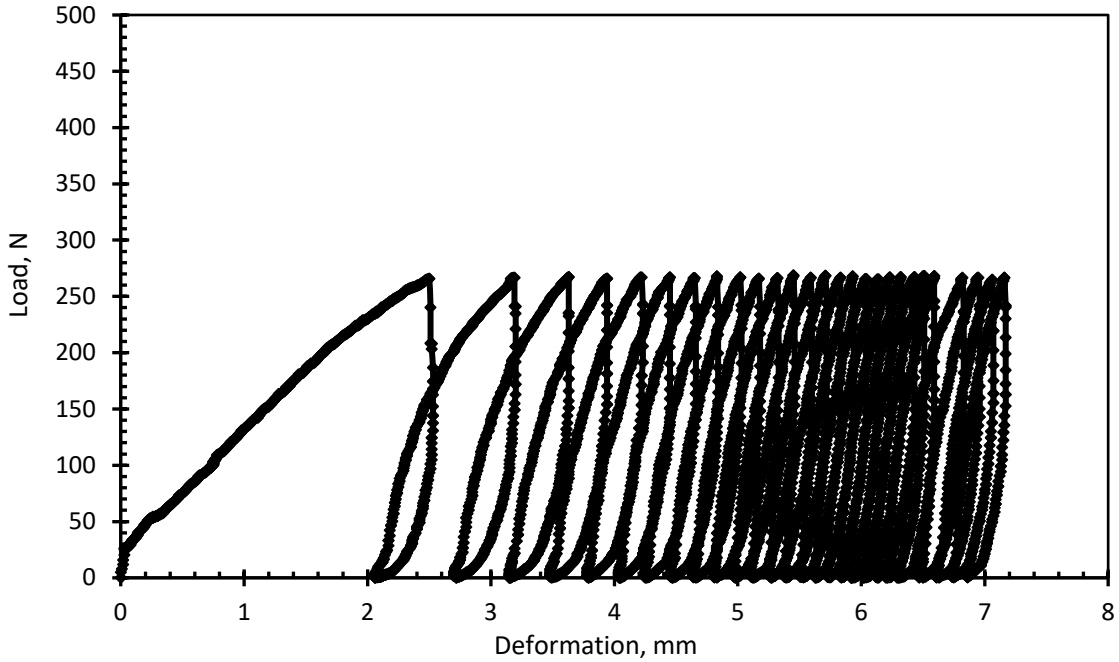

Figure 4.9. Load vs. penetration graph of clay + 40 mm of sand + layer of geotextile at the interface under repeating loading conditions (30 cycles).

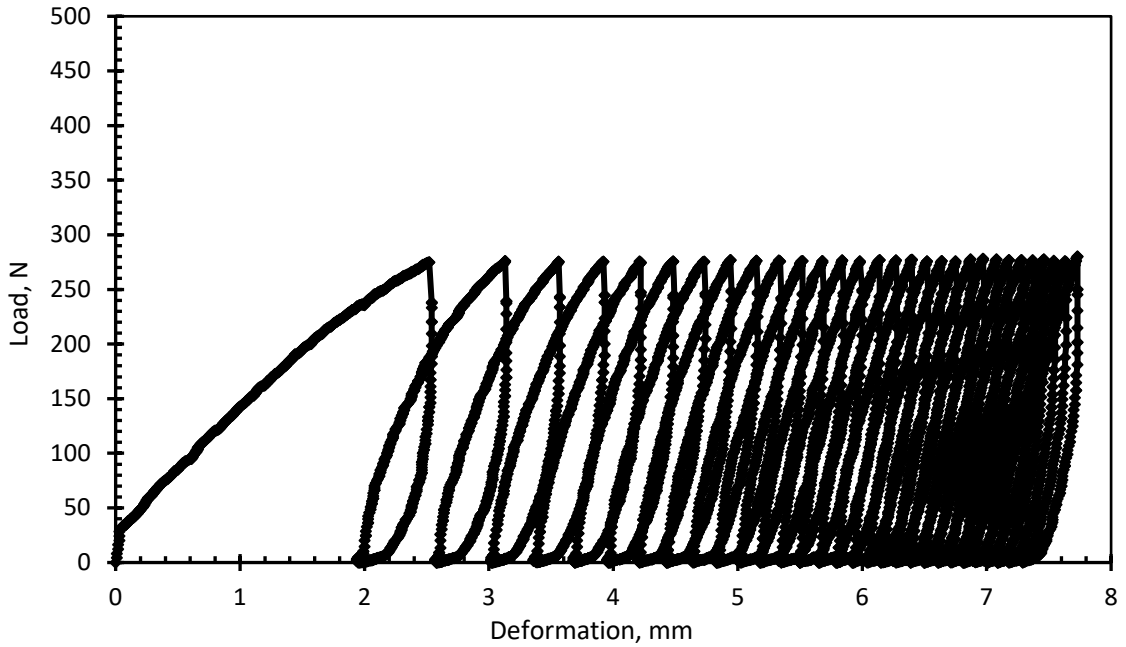

Figure 4.10. Load vs. penetration graph of clay + 40 mm of sand + layer of geotextile at 30 mm from the surface under repeating loading conditions (30 cycles).

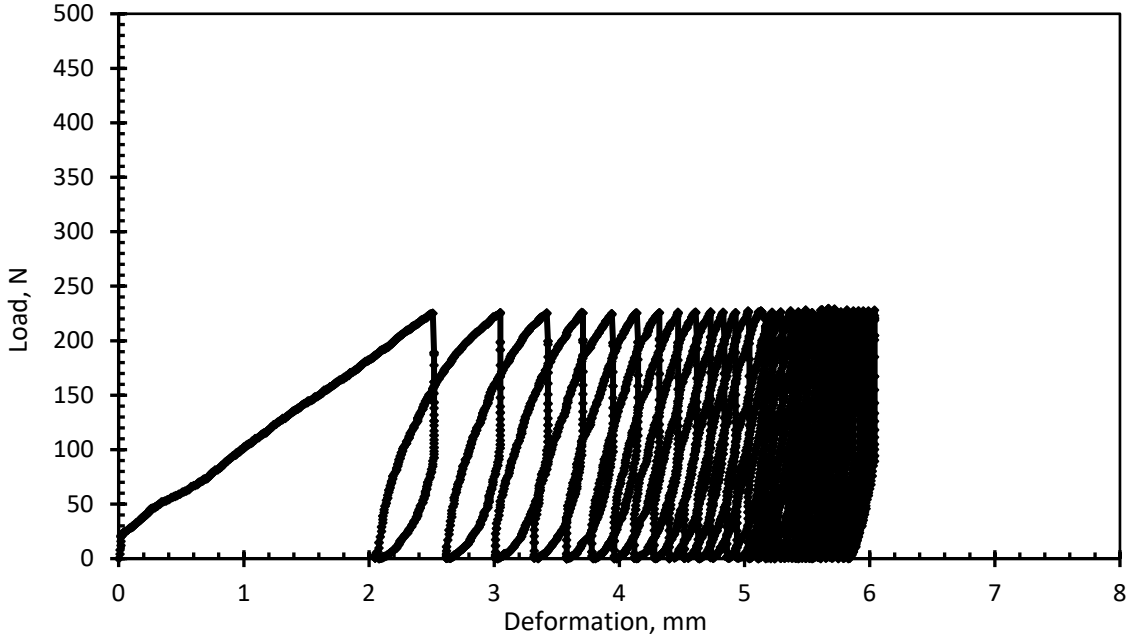

Figure 4.11. Load vs. penetration graph of clay + 40 mm of sand + layer of geotextile at 20 mm from the surface under repeating loading conditions (30 cycles).

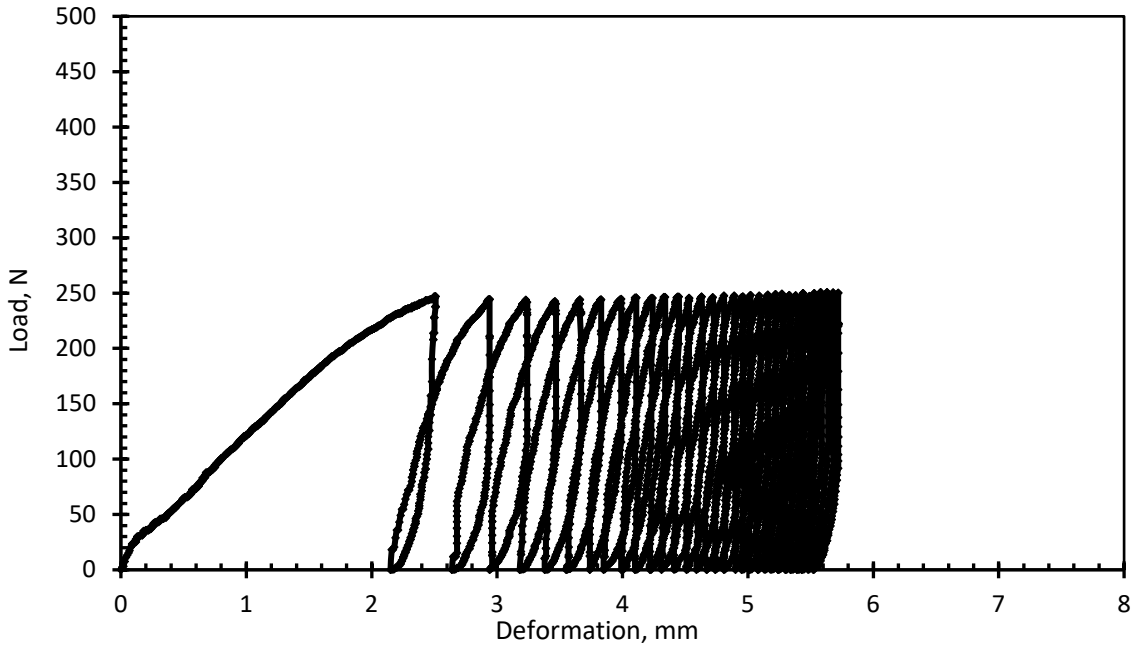

Figure 4.12. Load vs. penetration graph of clay + 40 mm of sand + layer of geotextile at 10 mm from the surface under repeating loading conditions (30 cycles).

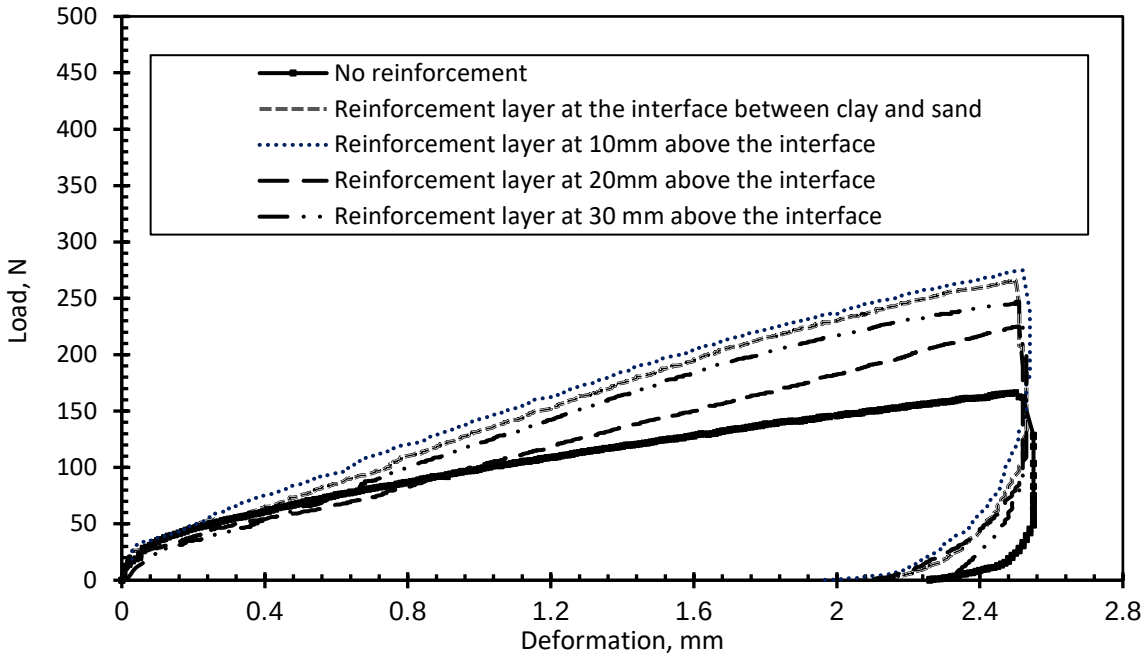

Figure 4.13. Load vs. deformation graph of clay with 40 mm sand and layer of geotextile at different positions during the first cycle of loading.

The results obtained under repeated loading condition show that plastic deformation of the first cycle decreased slightly compared with that of the

unreinforced sample irrespective of the location of the reinforcement layer as shown in Figure 4.14 and as illustrated by the values in Table 4.2. The plastic deformation of a sample of clay overlaid with a 40 mm layer of sand was 2.17 mm at the first cycle. When a layer of reinforcement was placed at the interface between clay and sand, the plastic deformation at first cycle was decreased by 8.4 % to about 2.06 mm. This reduction in the plastic deformation after the first cycle of loading and unloading was increased by about 13.30 % by decreasing the depth of the reinforcement layer to 30 mm (10 mm above interface). When the layer of geotextile was placed at a depth of 20 mm from the surface (20 mm above interface) and at a depth of 10 mm from the surface, the reduction in the plastic deformation was decreased to about 7.9 %. Furthermore, a reduction of 5 % in the plastic deformation was recorded from the experiment on a layer of geotextile that was placed at a depth of 10 mm from the surface. On the other hand, after 30 cycles, the plastic deformation recorded on a reinforced sand layer overlying clay subgrade increased more than those on unreinforced samples. The highest plastic deformation was recorded for the sample having a layer of geotextile at position of 10 mm above the interface. This is because the magnitude of load carried by reinforced samples was much higher than the load carried by unreinforced samples, with the sample with a layer of reinforcement at 10 mm above the interface resisting the highest load, as shown in Figure 4.14 and Table 4.2.

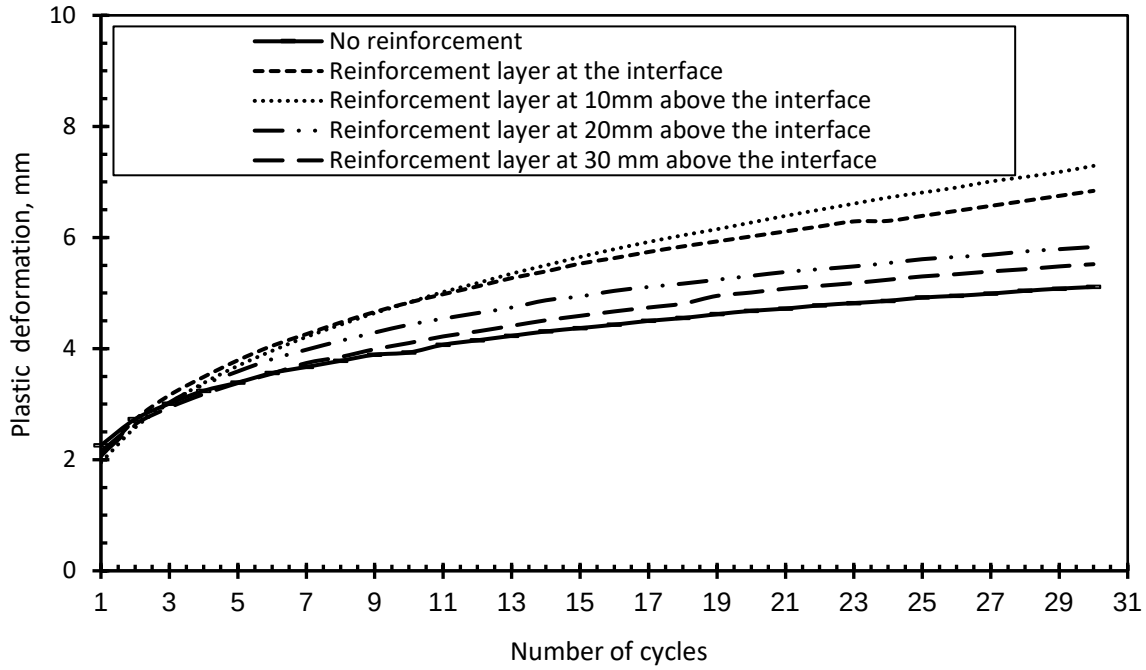

Figure 4.14. Plastic deformations of clay with 40 mm of sand and layer of geotextile at different positions versus number cycles of repeated loading.

Elastic deformation after completion of the first loading cycle on a sample of clay overlaid with a 40 mm layer of sand with a reinforcement layer at the interface was found to be 0.44 mm which is higher than that of the unreinforced clay and sand sample. When the reinforcement layer was placed at 10 mm above the interface, the elastic deformation increased by 25% to 0.55 mm. Inspection of Figure 4.15 illustrates that placing the reinforcement layer at 30 mm above the interface resulted in the smallest degree of elastic behaviour. In general, the elastic behaviour of all reinforced samples decreased with further cycles of loading and unloading. After 30 cycles of loading and unloading, the recorded elastic deformations were found to be 0.11, 0.30, 0.42, 0.20 and 0.19 mm for unreinforced samples, samples with reinforcement at the interface, 10 mm above interface, 20 mm above the interface and 30 mm above the interface respectively as shown in Figure 4.15 and Table 4.2. This is likely to be due to the variation of elastic strain of reinforcement layer to

reflect the change in its placement height and the axial stress applied on the reinforcement layer.

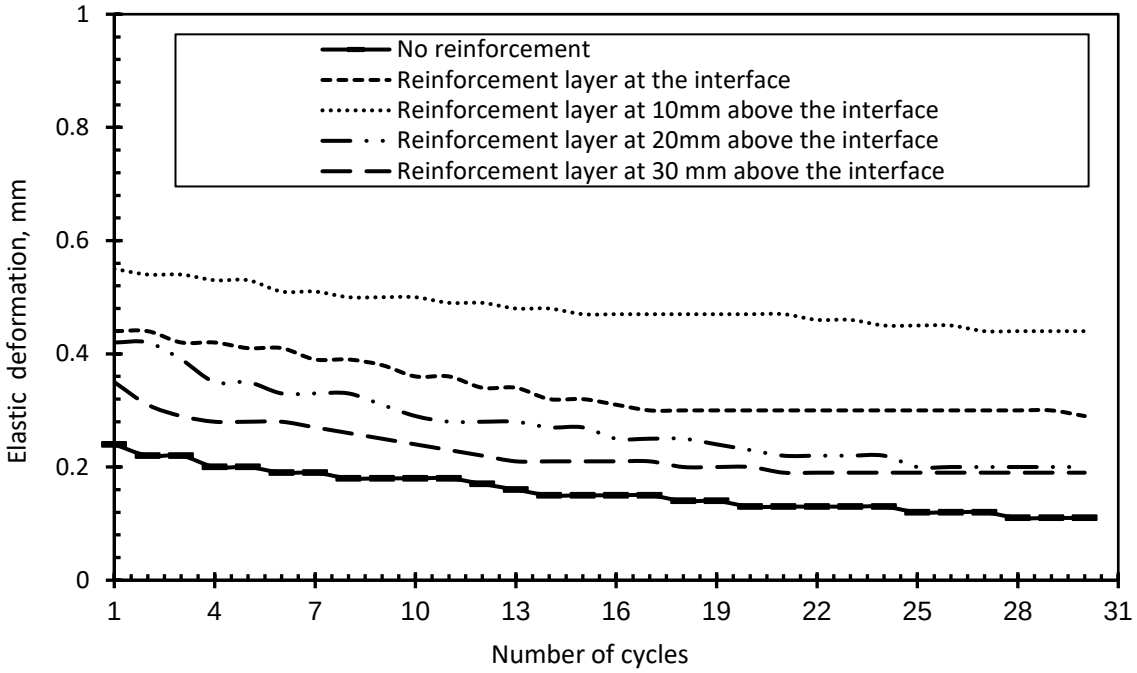

Figure 4.15. Elastic deformations of clay with 40 mm of sand and layer of geotextile at different positions versus number cycles of repeated loading.

Table 4.2. Plastic and elastic deformation values of clay with layer of sand and layer of geotextile at different positions under static and repeated loading conditions.

Sample	Load (N) at deformation of 2.50 mm	Elastic deformation (mm) after first cycle	Plastic deformation (mm) after first cycle	Elastic deformation (mm) after 30 cycles	Increasing in Plastic deformation (mm) in first 5 cycles per cycle (%)	Increasing in Plastic deformation (mm) in last 5 cycles per cycle (%)	Total Plastic deformation (mm) after 30 cycles
clay + 40 mm of sand	166	0.24	2.26	0.11	9.80	0.90	5.11
clay + 40 mm of sand + layer of geotextile at 40 mm from the interface	265	0.44	2.06	0.30	14.80	0.90	6.85
clay + 40 mm of sand + layer of geotextile at 30 mm from the interface	274	0.55	1.95	0.42	15.40	1.40	7.29
clay + 40 mm of sand + layer of geotextile at 20 mm from the interface	224	0.42	2.08	0.20	13.10	1.00	5.87
clay + 40 mm of sand + layer of geotextile at 10 mm from the interface	246	0.35	2.15	0.19	10.2	0.90	5.52

4.5 Effect of number of reinforcement layers on soil strength under repeated loading conditions

Figures 4.9, 4.16 and 4.17 show the results of the effect of number of reinforcement layers acquired on samples of clay overlaid with a 40 mm layer of sand. One, two and three reinforcement layers were placed at predetermined locations as presented in Table 3.3. Figure 4.18 compares the strength behaviour of samples prepared with an increasing number of reinforcement layers against a control test on unreinforced clay soil overlaid with a 40 mm layer of sand. It is evident that increasing the number of reinforcement layers is beneficial to enhance load carrying capacity. Data

showed that the measured load carrying capacity at a penetration of 2.50 mm of a sample which consisted of clay and 40 mm of sand with one layer of reinforcement at the interface was 265 N. This value was further increased by approximately 28.70 % by placing two reinforcement layers, one of which was located at the interface between clay and sand and the second layer was at 10 mm above the interface. Further enhancement was recorded by the addition of one more reinforcement layer at the mid height of the sand (a total of three reinforcement layers). In this case, the results show an increase of approximately 70 % in comparison with the unreinforced sample. This means that the strength of these samples increased significantly by increasing the number of reinforcement layers. This is because of the shear resistance and confinement effect leading to a substantial increase in the applied load carrying capacity.

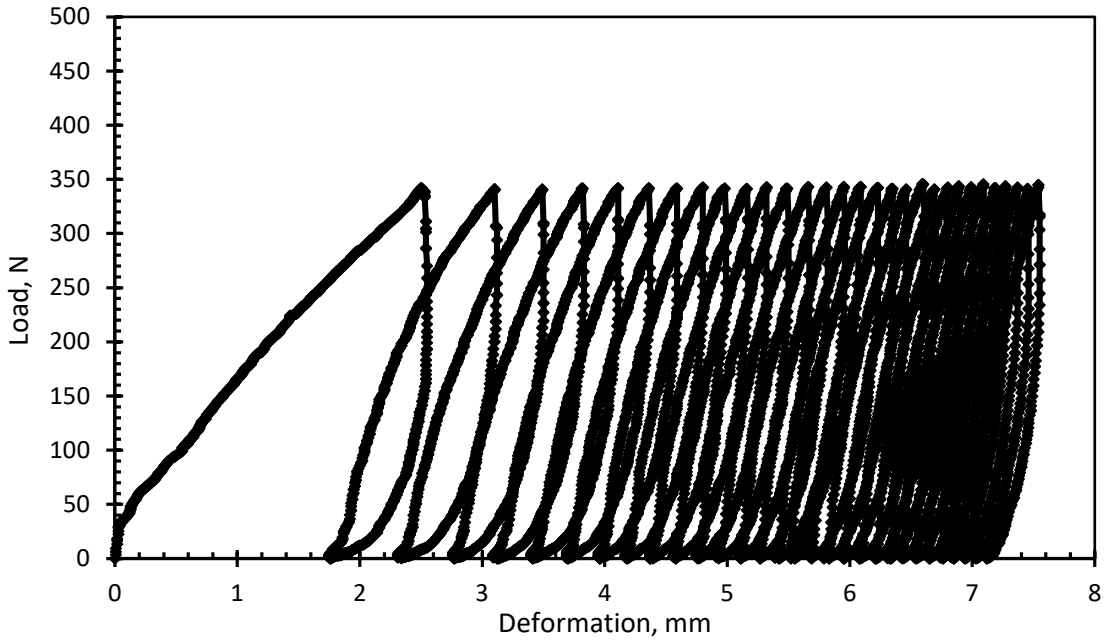

Figure 4.16. Load vs. penetration graph of clay + 40 mm of sand soil + two layers of geotextile under repeating loading condition.

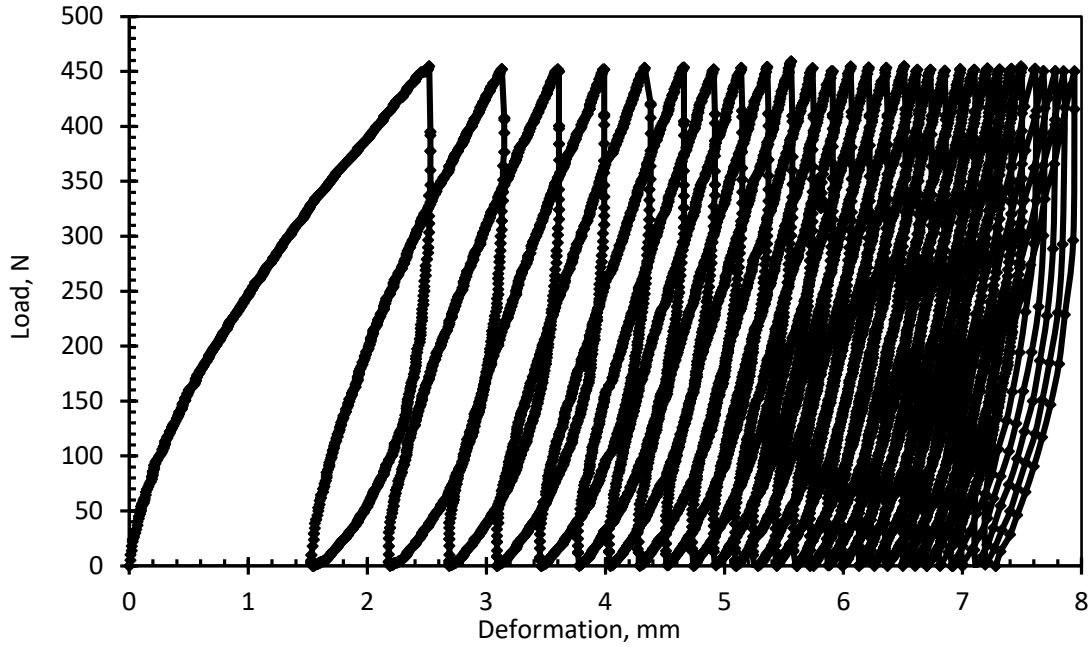

Figure 4.17. Load vs. penetration graph of clay + 40 mm of sand soil + three layers of geotextile under repeating loading condition.

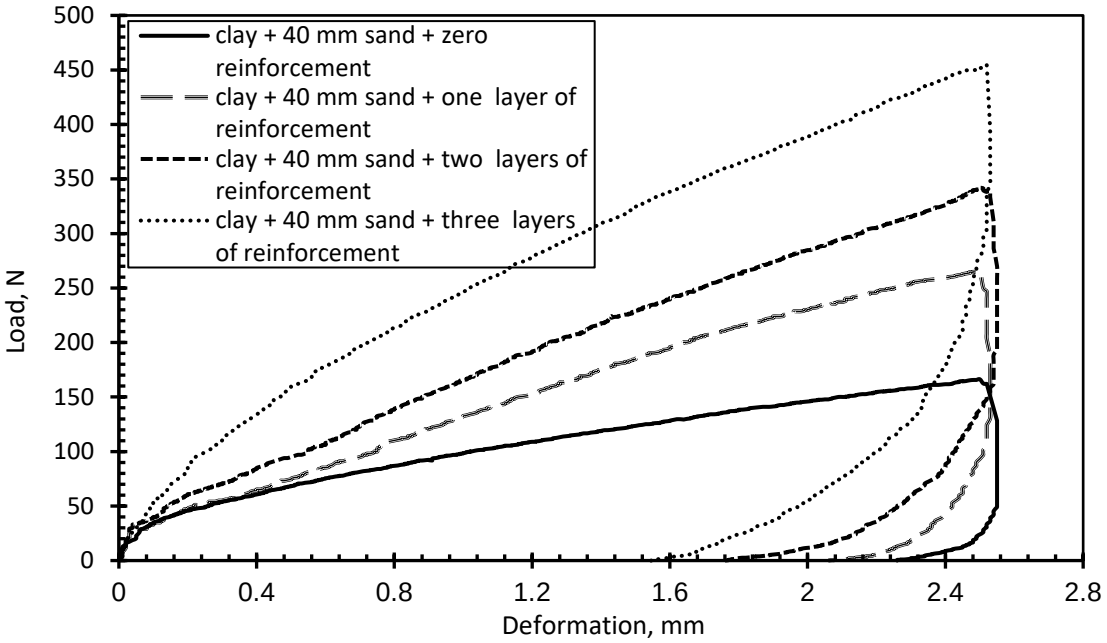

Figure 4.18. Load vs. deformation graph of clay with 40 mm sand and different number of reinforcement layers during first loading cycle.

The results also illustrate that the plastic deformation after the first cycle of loading on a sample of clay soil and 40 mm layer of sand with one reinforcement layer at the interface was 2.06 mm. The addition of more reinforcement layers was found to reduce the plastic deformation. The

determined plastic deformations were 1.76 and 1.54 mm for samples with two and three reinforcement layers respectively. Further cycles of loading and unloading were found to increase the plastic deformation in all samples due to the fatigue stress as shown in Figure 4.19. Thirty loading cycles resulted in plastic deformations of 6.85, 7.12 and 7.28 mm for samples with one, two and three layers of reinforcement respectively. Of note, the higher plastic deformation is due to the load cycles that were carried out at the maximum load carrying capacity for individual samples as illustrated in Figure 4.19 and Table 4.3.

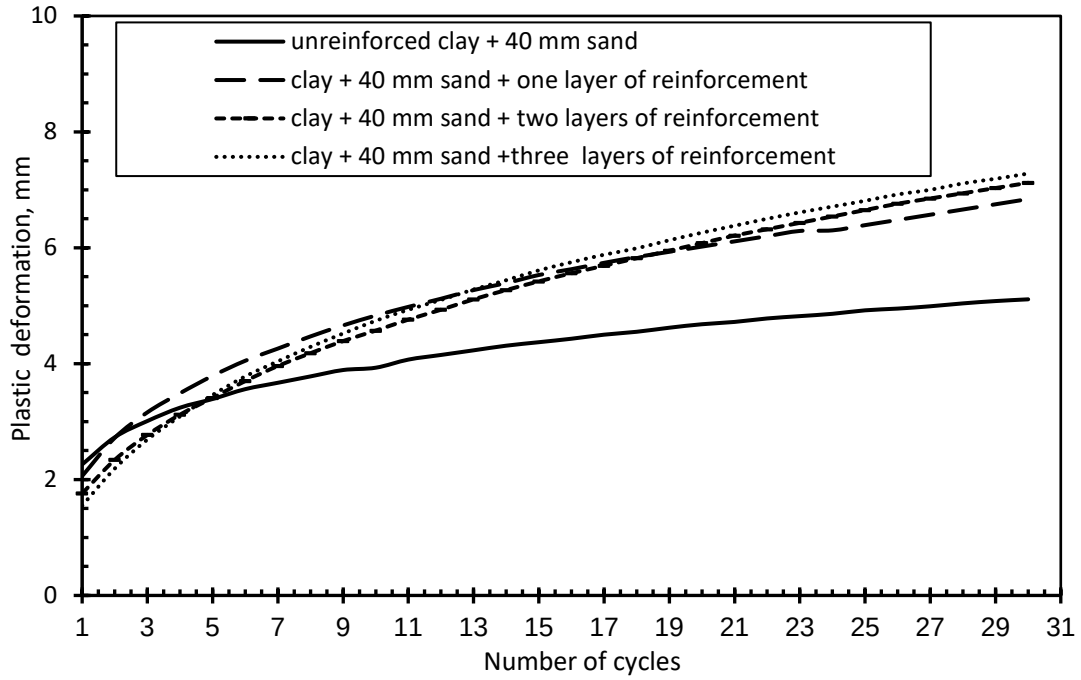

Figure 4.19. Plastic deformations of clay with 40 mm sand and different number of reinforcement layers.

Evaluation of the elastic deformation of the four samples illustrates that the elastic deformation after the first loading cycle increased with an increasing number of reinforcement layers as shown in Figure 4.20. This is due to the magnitude of load carried by reinforced samples being increased with increasing the number of reinforcement layers resulting in increasing the

elastic strain. However, performing more cycles of loading and unloading reduces the resilience of the samples to respond to load changes due to reduced elastic deformation caused by loading repetitions. Table 4.3 presents the elastic deformation values after the first and 30th cycles of loading.

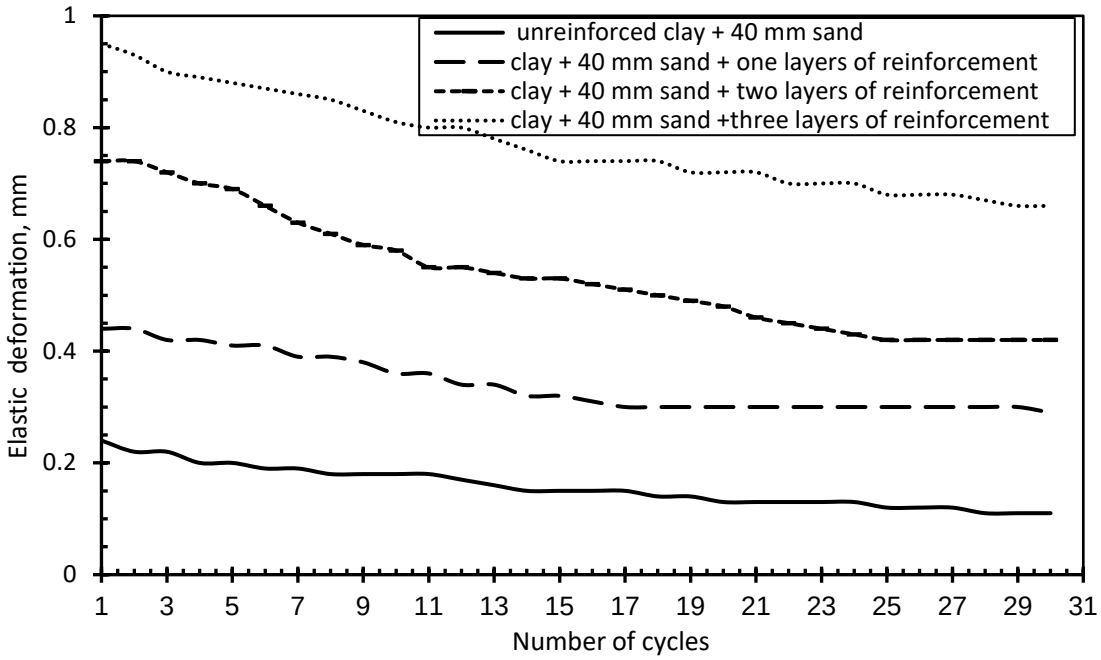

Figure 4.20. Elastic deformations of clay with 40 mm sand and different number of reinforcement layers.

Table 4.3. Plastic and elastic deformation values of clay with 40 mm sand and different number of reinforcement layers.

Sample	Load (N) at deformation of 2.50 mm	Elastic deformation (mm) after first cycle	Plastic deformation (mm) after first cycle	Elastic deformation (mm) after 30 cycles	Increasing in Plastic deformation (mm) in first 5 cycles per cycle (%)	Increasing in Plastic deformation (mm) in last 5 cycles per cycle (%)	Total Plastic deformation (mm) after 30 cycles
clay + 40 mm of sand	166	0.24	2.26	0.11	9.80	0.90	5.11
clay + 40 mm sand + one layer of geotextile	265	0.44	2.06	0.30	14.80	0.90	6.85
clay + 40 mm sand + two layers of geotextile	341	0.74	1.76	0.42	16.40	1.30	7.12
clay + 40 mm sand + three layers of geotextile	450	0.95	1.55	0.66	20.0	1.30	7.28

4.6 Deformation characteristics of samples tested to the same magnitude of load

The last series of experiments was undertaken to examine the effect of the magnitude of load as shown in Figure 3.3. and Table 3.3. RL - CBR tests were carried out on unreinforced and reinforced samples at the same load of 95 N which was achieved on a sample of clay soil. It was found that after the first loading cycle, the total deformation of the clay sample was 2.50 mm. This deformation was decreased to 1.37 mm by placing a 40 mm layer of sand on top of the clay soil as shown in Figure 4.21. This indicates that placing a layer of sand almost halves the total deformation. This could be attributed to the enhanced shear strength of the sand layer. Reinforcing the sand layer resulted in a substantial decrease in the total deformation to 0.95, 0.7 and 0.40 mm for 1, 2 and 3 layers of reinforcement respectively. Performing 30 cycles of loading and unloading on the clay sample resulted in increasing the total deformation to 3.87 mm. To reach the same total deformation on a sample of clay overlaid with a 40 mm layer sand, 45 loading cycles were carried out as shown in Figure 4.21.

When reinforcement layers were placed at the interface and within the sand layer, the number of loading cycles needed to reach a similar total deformation of 3.87 mm was deemed to be unrealistically high. The total deformation was found to stabilise well at a lower deformation, as shown by the shapes of the curves plotted in Figure 4.21 and for each of the reinforced samples, the deformation was less than 2 mm after 80 cycles. The highest reduction in the total deformation was recorded for a sample with three layers of geotextile. It can be noted that the largest portion of the total deformation occurs during the

first few loading cycles. The rate of increase in total deformation decreased with further cycles of repeated loading in particular with reinforced samples. This illustrates the effectiveness of addition of reinforcement layers in controlling total settlement as well as enhancing the load carrying capacity. This is because membrane action which is created between geotextile layers and soil would lead to a reduced deformation/settlement due to redistribution of stresses which is in agreement with previous studies (see for example, Asakereh et al. 2013; Tafreshi et al. 2014) who studied the effect of reinforcement layer on the behaviour of soil under cyclic loading conditions. They resulted that the number of cycles of load was increased significantly in reinforced samples compared with unreinforced sample. Also, they found that a large amount of the total settlement occurred during the initial cycles of loading and the rate of settlement decreased as the number of cycles of loading increased.

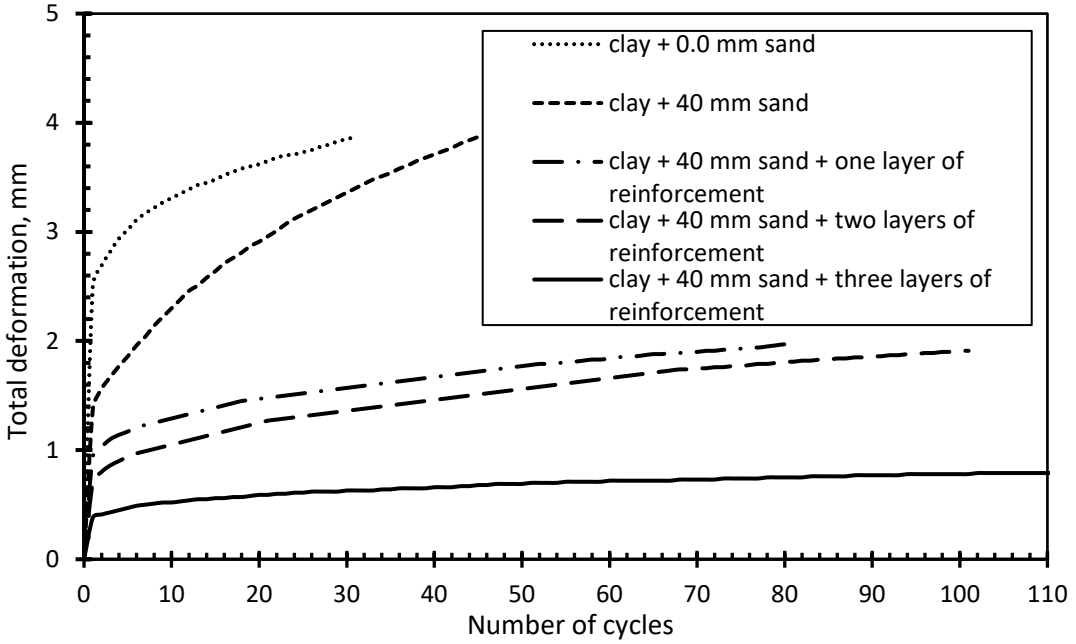

Figure 4.21. Total deformations of unreinforced and reinforced samples as a function of number of cycles at repeated load of 95 N.

4.7 Equivalent Elastic Modulus of Unreinforced an Reinforced Soil

Due to failure of roads, AASHTO recommended to use the resilient modulus to assess the stiffness of subgrade (National Cooperative Highway Research Program 2008). The resilient modulus is analogous to the elastic modulus and defined as the ratio of deviatoric stress to elastic strain under repeated loading conditions. Resilient modulus is best determined experimentally from Cyclic Triaxial Test. However, practically it is very expensive and not straight forward to be conducted in several developing countries. Thus, California Bearing Ratio (CBR) and Repeated Load California Bearing Ratio (RL-CBR) are deemed to be practical alternatives to gain insight of the behaviour of reinforced soil under repeated loading conditions. The equivalent modulus ($\mathrm{E_{equ}}$) which represents the overall stiffness of the sample as a bulk rather than the resilient modulus of materials can be used instead of resilient modulus. The equivalent modulus ($\mathbf{E_{equ}}$) is computed from the elastic deformation under repeated loading conditions (Molenaar et al. 2011; Araya et al. 2011; Araya et al. 2012) as given by equation (4.1).

$$\mathrm{E_{equ}} = \frac{1.513\mathrm{X}(1 - \mathrm{V}^{1.104})\mathrm{X}\,\sigma_{\mathrm{p}}\,\mathrm{X}\,\frac{\mathrm{D}}{2}}{\mathrm{u}^{1.012}} \qquad (4.1)$$

where; $\mathrm{E_{equ}}$ is equivalent modulus in (MPa), σ_{p} is stress under the plunger in (MPa), V is the Poisson's ratio (0.4), D is plunger dimeter (50 mm) , u is measured elastic deformation in (mm). When using this equation, the Poisson's ratio has to be estimated. This estimation is very easy when using only a single layer of material. However, estimation of the Poisson's ratio of a

sample contained more than one materials is not easy. In this study two types of soil and reinforcement were used, the Poisson's ratio was estimated to be 0.40, based on Araya et al. (2011) who used Poisson's ratio between 0.35 and 0.49.

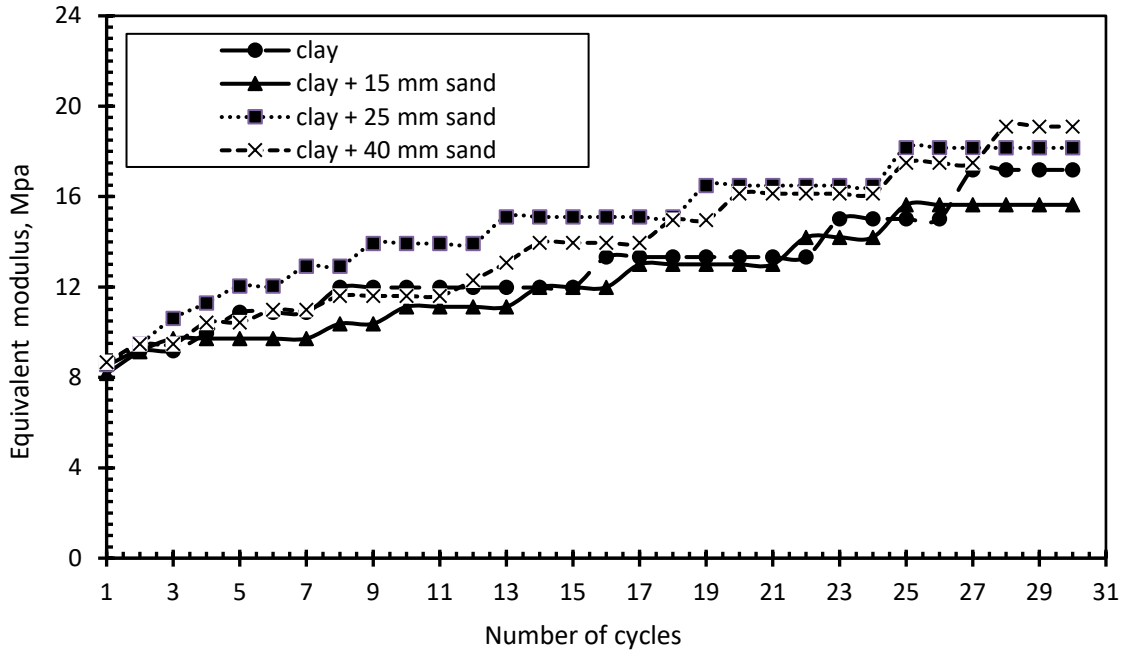

Figure 4.22. Equivalent modulus Vs number of loading cycles for (a) clay samples with different thickness of sand.

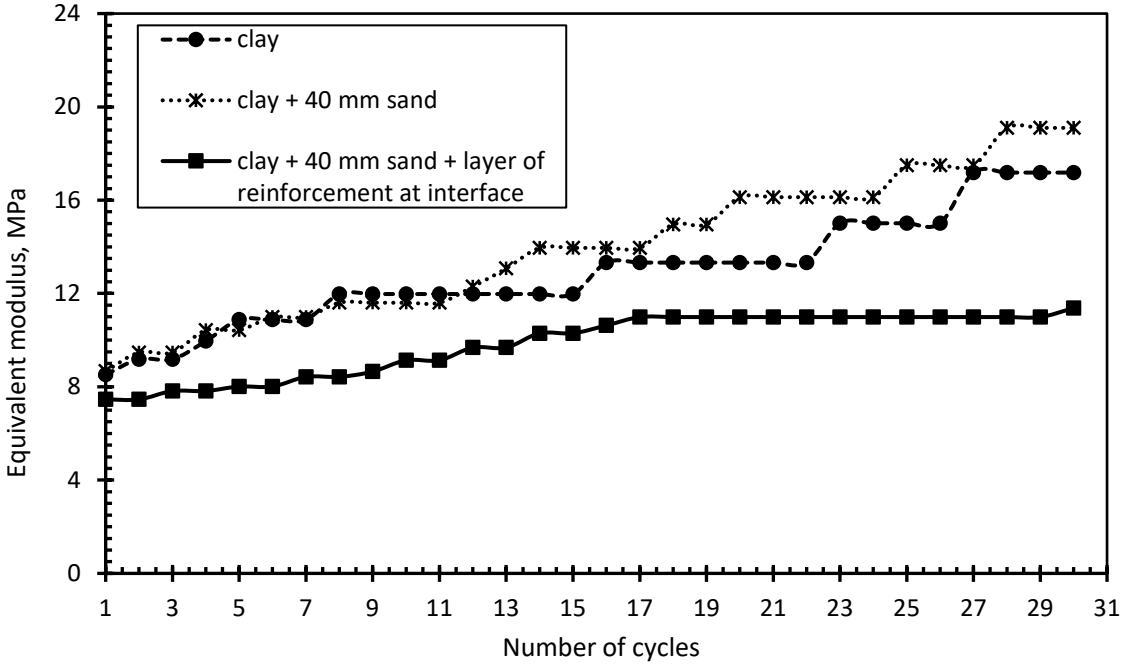

Figure 4.23. Equivalent modulus Vs number of loading cycles for unreinforced and reinforced samples with layers of reinforcement.

From Figure 4.22, it can be seen that the equivalent modulus at the first cycle of clay soil was about 8.50 MPa. This value was increased to about 17.20 MPa after 30 cycles. This means that the stiffness of soil increased with the number of cycles. This is due to the rearrangement of soil particles caused by load repetitions. When a layer of granular material was placed above the subgrade clay soil in different thicknesses, the equivalent modulus of all samples was increased with the number of load repetitions. However, the equivalent modulus of all samples was slightly higher than that in case of clay soil as shown in Figure 4.22. On the other hand, the equivalent modulus of reinforced samples was less than that unreinforced samples as shown in Figure 4.23. This is due to the higher elastic strains of reinforced samples compared with unreinforced ones. These results are in agreement with Kamel et al. (2004) and Asha and Latha (2012).

4.8 Secant modulus of unreinforced and reinforced soils

Secant modulus is defined as the slope of stress strain curve with respect to the origin and can be determined for each loading cycle. It is clear that the secant module decreases with the number of cycles. It was found that the secant modulus of clay samples at the first cycle of loading was about 2.44 MPa and decreased to about 1.58 MPa after 30 cycles as shown in Figure 4.24. This confirms that the elasticity of clay soil decreases with the number of cycles due to fatigue stress caused by load repetitions. The results suggest that when a layer of granular material with a thickness of 40 mm was placed above clay soil the secant modulus of the sample was increased by almost 70 % after the first cycle and about 30 % after 30 cycles as shown in Figure 4.24, reflecting the increase in load resistance and reduced deformation. Addition of

reinforcement layers was found beneficial to increase the value of secant modulus. When a layer of reinforcement was placed at the interface between clay soil and sand layer the secant modulus increased to about 175 % compared with that attained on a clay soil sample at the first cycle. Further, undertaking 30 cycles of loading, the secant modulus of reinforced sample was increased by 50 % in comparison with that of the clay soil. This is primarily due to the elastic modulus of reinforcement materials being higher compared with the soil materials as shown in Figure 4.24.

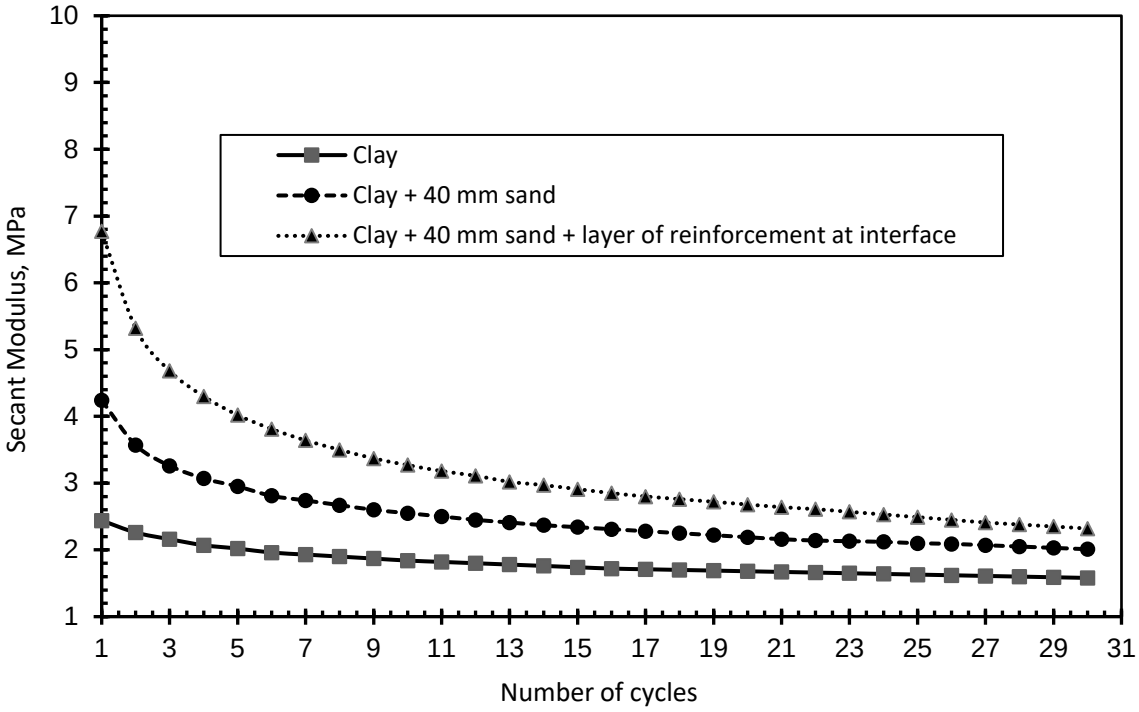

Figure 4.24. Secant modulus of unreinforced and reinforced samples versus number of cycles.

4.9 Summary

This chapter presented the laboratory tests that were performed to investigate the load-penetration behaviour of unreinforced and reinforced granular layer overlying soft subgrade soils under the effect of repeated loading conditions. The experimental results showed that coupled use of granular material and

reinforcement layers increases remarkably the load carrying capacity of soft subgrade soils. The highest degree of improvement was recorded when the reinforcement layer was located within the bottom third of the granular layer. Under repeated loading conditions, the plastic and total deformations of reinforced soils increased significantly whereas a decreased elastic deformation was recorded. At the same magnitude of repeated loading, the total deformation of reinforced samples was considerably small compared with unreinforced samples. Also, the results showed that with increasing the number of reinforcement layers huge number of loading and unloading cycles can be applied without increasing the deformation and loss the bearing resistance. Finally, addition of replacement sand layer with reinforcement layers results in a reduction in the determined equivalent modulus and enhancement of secant modulus.

CHAPTER FIVE

ANALYSIS OF SEQUENTIAL ACTIVE AND PASSIVE ARCHING IN GRANULAR MATERIAL

5.1 Introduction

In this chapter the results from the developed trap door test (preliminary test 2) are presented and analysed. The effect of repeated sequential active and passive arching on the distribution of stresses on the granular soil with different heights is examined and discussed. Data attained from the trapdoor experiments are presented as normalized load against normalized displacement. The normalized load on the trapdoor is determined by dividing the measured load on the trapdoor by its original value at zero displacement which is comparable to that in the free field. The normalized displacement is determined by dividing the trapdoor displacement by the width of the trapdoor. The normalisation of loads and displacements is adopted to enhance the presentation and comparison of data sets and to show clearly the percentage changes in load due to active and passive arching.

It is also important to note that the second and fourth series of testing underwent 10 cycles of movement of the trapdoor up to a displacement of 10 mm to simulate sequential active and passive arching. However, the third series of tests underwent 5 cycles of downward and upward movement up to displacements of 2 mm, 10 mm and 20 mm. All measurements were taken every 10 seconds. Hereafter, results are presented and discussed to clearly demonstrate the effects of underground inclusion displacement and height of

sand bed on the behaviour of arching of soil under sequential active and passive modes.

5.2 Effect of sequential active and passive arching

In this section, experiments were undertaken with a sand bed of 100 mm as illustrated in Table 3.6. Two experiments were conducted to ascertain the monotonic active and passive arching in granular soils. Load measurement on the trapdoor at rest conditions prior to the onset of displacement was found to be equivalent to the free field vertical stress times the area of the trapdoor. Figure 5.1 shows the normalised load against normalised deformation for monotonic active and passive arching. Data presented in Figure 5.1 show distinctive behaviour for granular soil during active and passive states. It is important to note that minimum load achieved during yielding of the underground inclusion (active arching) is 9.3 % of the original at rest load and was experienced after a settlement of 1 % of the inclusion width which is consistent with previous observations by Terzaghi (1943) and Igelsia et al. (2013). In contrast, the maximum load was found to be 217 % of the original at rest load and was observed at a normalised displacement of 2 %. It is also worth noting that the time of drop the load during active arching is almost double the time of increase the load during the passive arching to reach minimum and maximum load respectively. With further displacement, a relatively stable load is experienced during active and passive modes reaching a higher normalised load of 49 % and a lower normalised load of 163% during the active and passive modes respectively (as shown in Figure 5.1) beyond a normalised displacement of 5 %. This is due to the soil mass having reached the critical state and soil particles being re-organised along the slip planes.

The results, therefore, suggest that relying on maximum and minimum loads on the inclusion as a result of complete passive and active arching respectively seems to be unsustainable. Careful consideration would need to be taken during the design of underground inclusions, in particular when shallow granular soil cover that is equal to one width of the underground inclusion is used.

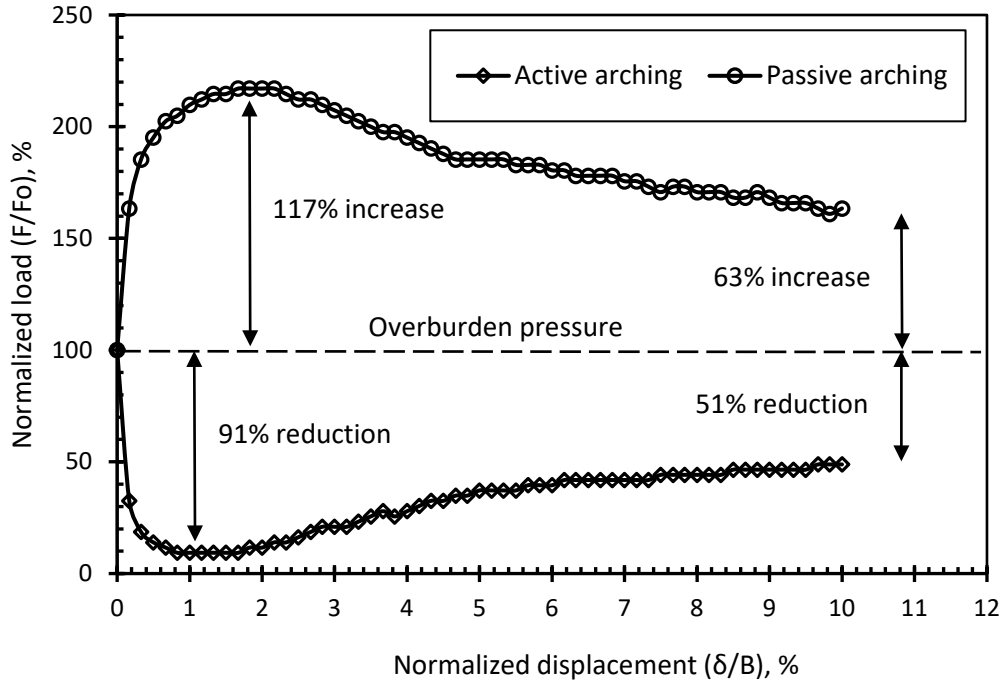

Figure 5.1. Normalised load versus normalised displacement during monotonic active and passive arching.

The next series of testing was conducted to investigate the effect of initial movement (yielding or rise of trapdoor) on subsequent behaviour of soil arching. Data captured for the load on the underground inclusion (trapdoor) during the initial release of pressure due to active arching or during initial compression of soil mass by passive arching are presented in Figures 5.2-a and b respectively. The monotonic active and passive relations presented in

Figure 5.2 show typical behaviour comparable to those presented in Figure 5.1. It was recorded that prior to the onset of tests, the soil mass seemed to be at rest and the recorded load on the trapdoor was directly related to overburden pressure. However, the relationships for subsequent cycles of active and passive modes are unique and different from those recorded for the monotonic relationships. This suggested a clear dependence of the behaviour of subsequent arching on the stress history.

As the underground inclusion (trapdoor) started to yield, a decreased pressure was observed due to the shear resistance in the soil illustrating the development of active arching (Figure 5.2a). Due to the initial dense packing of the sand bed with a unit weight of almost 100 % of that achieved from Standard Proctor Compaction test, the mass of soil above the trapdoor dilated vertically upon yielding of the inclusion which was recorded by the lower surface settlement rather than the trapdoor displacement. A similar interpretation was made by Villard et al. (2000) in which the rate of dilation was found to be higher than the trapdoor displacement causing the soil to fill the gap under the arching and thus increasing the arching effect. In contrast, the adjacent soil masses on both stationary regions (left and right sides of the inclusion) would dilate horizontally preventing the soil mass above the yielding inclusion from moving downwards which resulted in lowering the pressure on the inclusion (trapdoor). This has occurred entirely due to the internal friction and interlocking of sand particles and can be represented by the angle of friction and the angle of dilation. In contrary upon rise of inclusion from a 10 % yielding, passive arching started to form rapidly and gradually showed an

increased load on the inclusion reaching a maximum normalised load of 193 % after undergoing an upward normalised displacement of approximately 6 %.

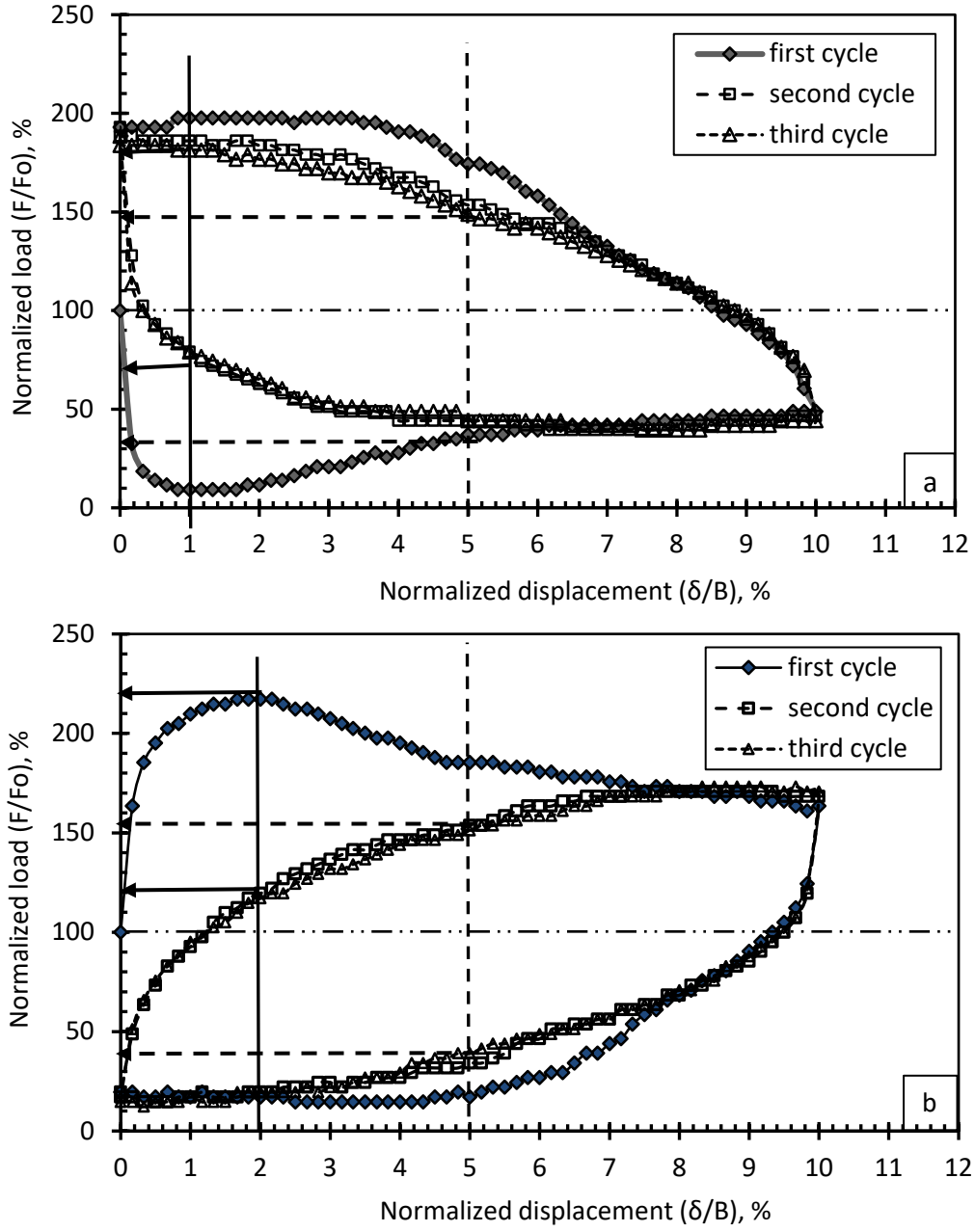

Figure 5.2. Normalised load versus normalised displacement during a. sequential active and passive arching and b. sequential passive and active arching.

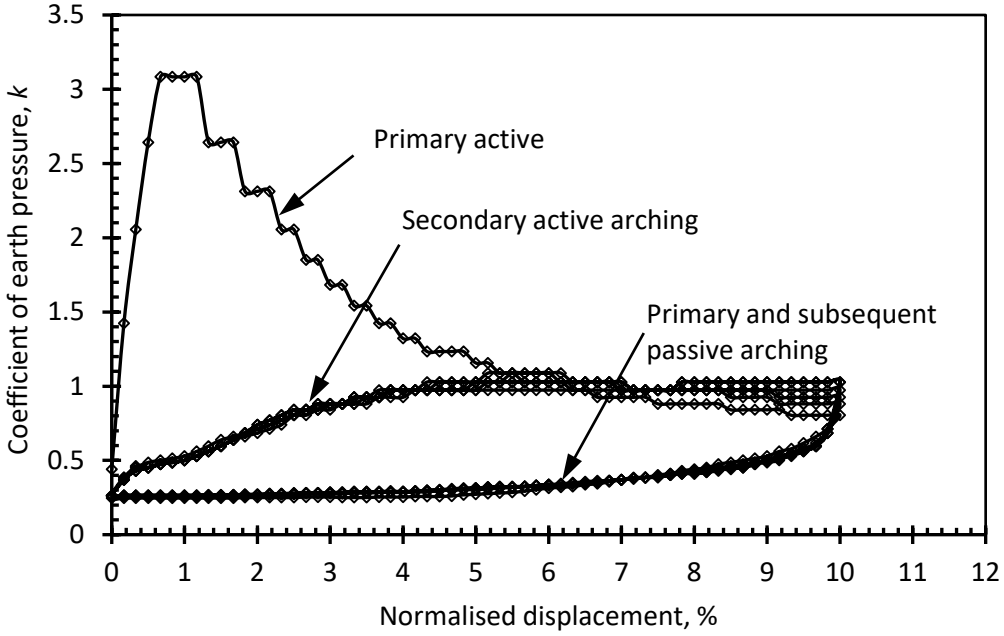

Figure 5.3. Coefficient of lateral earth pressure as a function of normalised displacement during sequential active and passive arching.

The second and subsequent relationships between normalised load and normalised displacement due to cycles of active and passive arching were similar resulting in intermediate but coinciding paths. During second and subsequent active modes, a minimum normalised load did not appear to occur, as evidenced by the data at a normalised displacement of 1 %, whereas the measured load at the critical state was similar. The normalized vertical load at a normalized displacement of 1 % during the second cycle was about four times greater than that which was observed at a normalized displacement of 1 % during the first cycle, as can be seen in Figure 5.2-a. Similarly, Figure 5.2-b illustrates that the normalised loads during the second and subsequent cycles of passive mode at a normalised displacement of 2 % no longer represented a peak value but were almost half of that measured during the monotonic passive resistance. Careful inspection of Figure 5.2 illustrates that the normalised load corresponding to 5 % normalised displacement is the

same during subsequent active and passive modes irrespective of the initial direction of displacement. This indicates that during alternating active and passive modes, the major and minor principal stresses change directions based on the direction of the inclusion's movement (trapdoor). To further explain the alteration of principal stresses during the redistribution of stresses, the lateral earth pressure coefficient was determined and plotted in Figure 5.3 as a function of inclusion's movement for various active and passive arching cycles. The value of coefficient of earth pressure was calculated by the ratio of the horizontal stress to the vertical stress which was determined from the measured load on the inclusion that is presented in Figure 5.2. Evans (1983) measured the horizontal stress during trapdoor tests and found that the horizontal stress remained fairly constant. It seemed therefore reasonable to assume a constant value of horizontal stress which is also consistent with earlier suggestion made by Terzaghi (1943) for the trapdoor test. The horizontal stress was then taken as the initial at rest. Of note, the initial lateral earth pressure coefficient was determined as k_o =1-sin (ϕ). As a result, a ko value of 0.46 is used in this investigation which is within the suggested range of 0.4-0.5 by Lambe and Whatman (1969) for sand beds that were created by vertical accumulation of sand particles under no significant lateral compression during sedimentation which is precisely similar to the preparation approach adopted in this investigation.

From Figure 5.3, it can be seen that the coefficient of earth pressure increased with increasing the downward displacement until reaching a maximum value of 3.0 at a normalized displacement of 0.67 %. The increase in the coefficient of lateral earth pressure led to a significant reduction in the vertical load on the

trapdoor (underground inclusion). At this stage the soil would behave as an elastic strain material mobilising the peak shear strength to provide maximum frictional resistance and hence the maximum active arching would be developed (Evans 1983).

Despite further yielding of the trapdoor, a fairly constant coefficient of lateral pressure was recorded which indicates that the rate of dilation continued but at a lower rate until reaching zero value at a normalised displacement of 5 %. Records of surface settlement along the centreline of the trapdoor illustrated that no surface settlement was recorded until reaching a yielding of 5 % as shown in Figure 5.4b. Costa et al. (2009) observed significant dilation in the soil region immediately above the trapdoor at failure. A reduced K value resulted in an increased vertical load on the yielding inclusion which can be attributed to a reduction in the angles of friction and dilation as a result of lowered shear strength of the soil. This indicates in turn a reduced arching effect. Due to the decrease in shear strength with increasing yielding of the inclusion, the soil would behave as a strain softening material (Evans 1983). With additional yielding of the inclusion beyond 5 %, the lateral coefficient of pressure reached a constant value of unity which was recommended by a number of researchers including Terzaghi (1943). Furthermore, a relatively constant load was measured on the trapdoor despite the value of normalised displacement indicating that the soil mass had reached the critical state. During this stage, most of inclusion yielding was transferred to the surface settlement as can be observed in Figure 5.4c.

Reversing the direction of movement at a normalised displacement of 10 % led to an increase in the measured load due to the formation of passive

arching. The major principle stress was then in the vertical direction leading to a value of lateral earth coefficient of 0.25 which is close to that determined by Rankine's theory. With further cycles of active and passive mode, the coefficient of lateral earth pressure stayed relatively stable at 1.0 and 0.25 for active and passive modes respectively excluding the first 4 % normalised displacement in each direction due to the instability in the soil mass as a result of dilation and contraction.

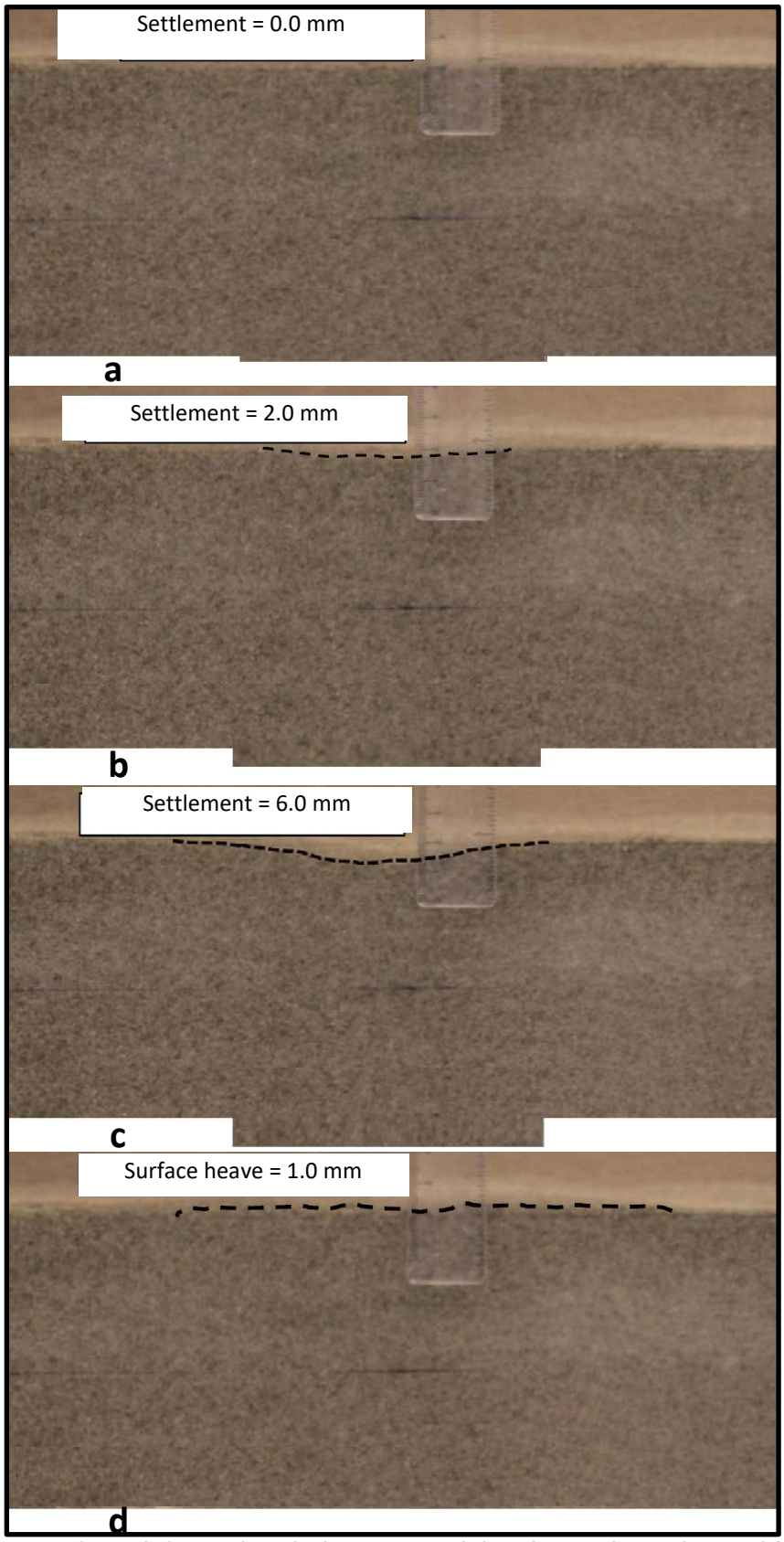

Figure 5.4. Surface deformation during sequential active and passive arching (first cycle) **a.** Active arching at normalised displacement of 2 %, **b.** Active arching at normalised displacement of 5 %, **c.** Active arching at normalised displacement 10%, **d.** Passive arching at normalised displacement of 10 %,

Figures 5.5a, 5.5b, 5.6a and 5.6b show pictures of the sand bed after cycles of active and passive modes. It can be seen that soil heave is recorded and observable after completion of the first cycle of active and passive mode. It may also be observed the occurrence of sand disturbance, in particular in the soil region immediately above the inclusion (trapdoor). This means that the volume of soil above the trapdoor was increased resulting in an imminent reduction in the sand density and shear strength. Despite conduction of further cycles of active and passive modes, surface settlement was comparative downward displacement indicating that no further significant change in the volume of the sand bed was evident which means that the shear strength of the sand remained relatively stable. This can be confirmed by the closure k values during active and passive arching as well as the improved steadiness of k values in Figure 5.3. The results, therefore, suggested that cycles of yielding and the rise of inclusion exacerbate the formation of active and passive arches causing significant changes to the load transfer on the inclusion in particular during the first cycle. This could be attributed to i. localisation of deformation along the same slip planes and causing shear bands as implied from the physical observations taken during the tests ii. shearing of the soil mass during the first cycle reducing the shear resistance along the slip planes and iii. permanent change in the vertical stress from the previous arching mode. The volume change of sand during shearing leads to dilation or contraction of the soil and hence change in density which affects the sand shear strength. Zhang et al. (2011) observed that dilation leads to significant volume change and consists of reversible and irreversible components. The later was found to gradually increase with continued

shearing whereas the reversible dilation depends upon the shearing direction. As a result, change in the angle of friction is imminent due to dilatancy of the soil mass which is influenced by the shearing direction.

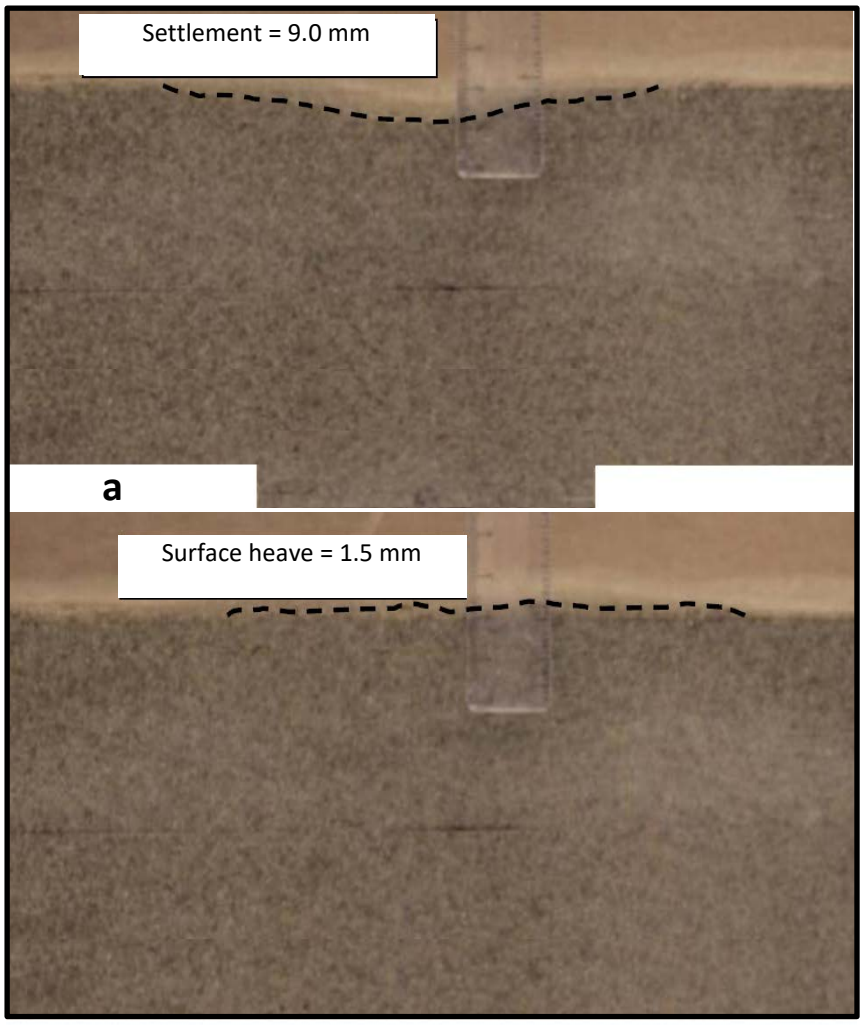

Figure 5.5. Surface deformation during sequential active and passive arching (second cycle) **a.** Second cycle of active arching at normalised displacement 10 %, b. Second cycle of passive arching at normalised displacement of 10 %.

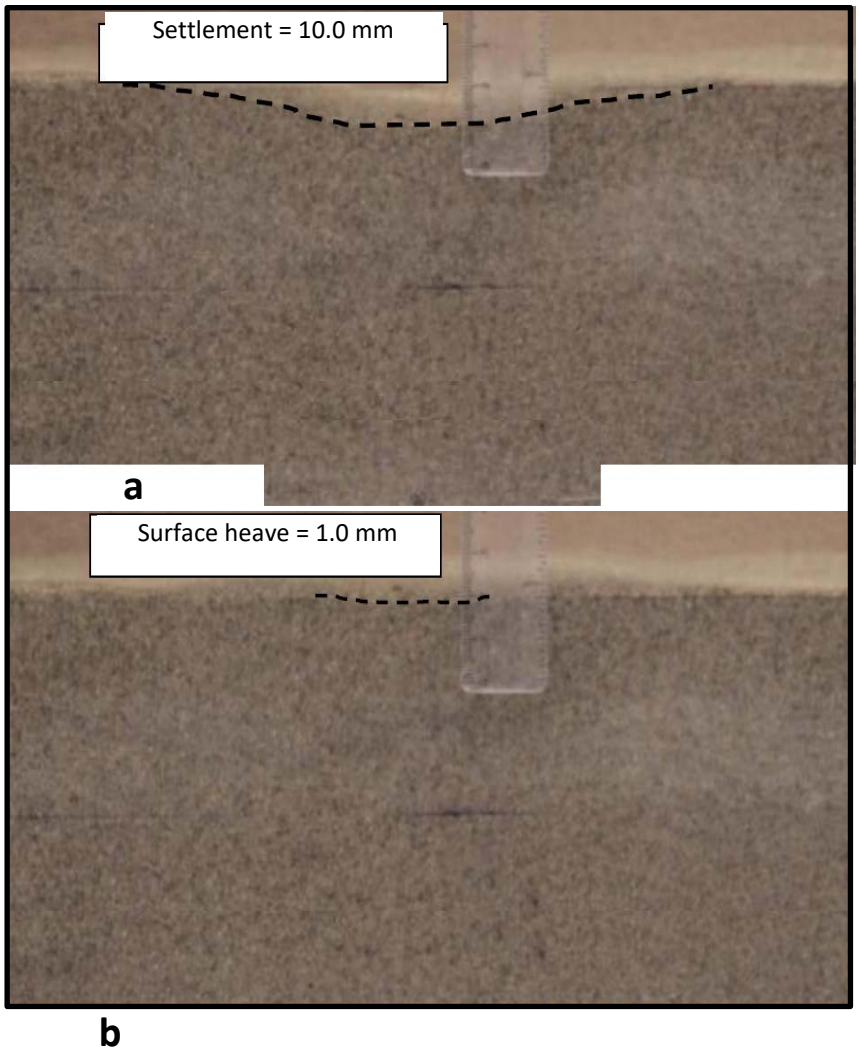

Figure 5.6. Surface deformation during sequential active and passive arching (Tenth cycle) **te**nth cycle of active arching at normalised displacement 10 % and **h.** tenth cycle of passive arching at normalised displacement of 10 %.

Figure 5.7 presents the results of sequential active and passive modes on a sample of dense sand with a height of 100 mm over different ranges of inclusion displacements of 2, 10 and 20 %. All three tests were started with yielding of the inclusion to a predetermined displacement to develop an initial active arching followed by reversing the movement so that the sand bed was in a passive mode. A number of cycles of active and passive mode were then performed over the predetermined displacement ranges. It can be seen that irrespective of the yielding displacement, the normalised load relations

followed the same load-deformation path for the monotonic active mode. The recorded normalised load on the inclusion is dependent on the magnitude of displacement prior to reaching the relatively stable load which was measured to be around 5 % normalised displacement. On reversing the displacement direction for the sand bed to be in the passive mode, different paths were followed up to reaching a maximum pressure on the inclusion of 180%. Subsequent cycles of active and passive arching followed the same paths as those for the second cycle which were consistent with previously discussed results in Figure 5.2. The data suggest that hysteresis in the relationship between normalised load and normalised displacement exists and is dependent on the displacement and route followed.

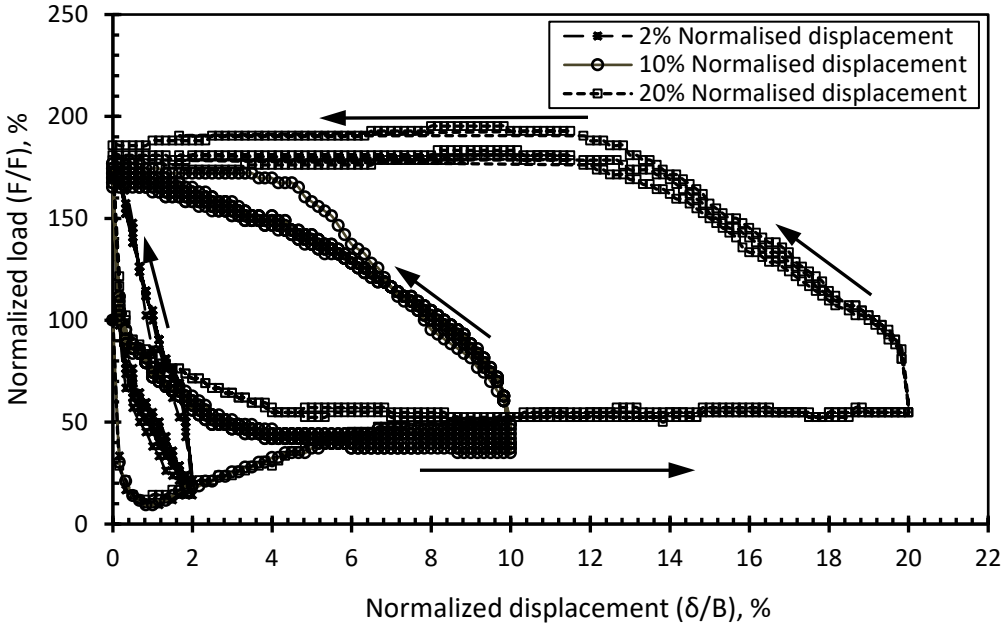

Figure 5.7. Relationships between normalised load and normalised displacement from cycles performed at different normalised displacement.

5.3 Effect of burial height

For the fourth series of experiments, samples of sand beds with different heights were examined to investigate the effect of sand height on sequential

active and passive arching. Results of tests with sand bed heights of 0.50, 1.0, 2.0, 3.0, 4.0 and 5.0 B where B is the width of the yielding inclusion (trapdoor) were presented in Figures 5.8, 5.9 and 5.10.

Figure 5.8 shows the normalised load during the initial yielding of the trapdoor. It is clear that increasing the height of the sand bed leads to a substantial reduction in the load on the inclusion because of the formation of a full and deep arch. The results are in agreement with those reported in previous studies (see for example, Terzaghi 1936; McNulty 1965; Ladanyi and Hoyaux 1969; Adachi et al. 1997; Iglesia et al. 2013). The data in Figure 5.8 also illustrate that with the increase in sand height, the relative change in normalised load with increasing yield displacement reduced greatly. This could be attributed to formation of a virtually stable arch which would be the case for deeply buried underground inclusions.

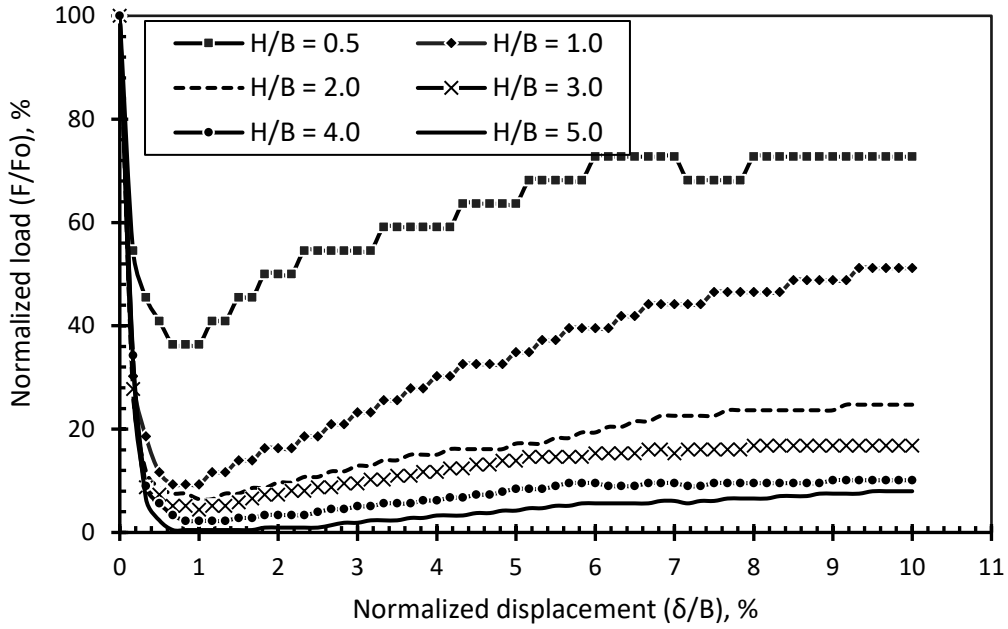

Figure 5.8. Normalised load versus normalised displacement during initial active arching as a function of bed height.

Results for full cycles of active and passive modes are presented in Figure 5.9 and 5.10. Data for the passive mode when the direction of movement was reversed to initiate passive mode showed different features as a function of sand bed height. For shallow heights up to H/B = 2.0, the normalised load responded quickly to the upward displacement leading to a rapid increase in the measured load. 100 % normalised load was observed to be reached within 1.5 % of normalised displacement as shown in Figure 5.9. However, with increasing the burial height, a large movement in the range of 4 % was required to reach 100 % normalised load. This could be attributed to the formation of a full arch in the case of high burial depths leading to significant dilation of the soil region immediately above the inclusion during the previous yielding and to the requirement for a large displacement to compress the soil under the arch prior to the transfer of load to the soil mass in the passive mode as shown in Figure 5.10.

In other words, small burial heights are only able to result in partial formation of active arching. Costa et al. (2009) noted that the behaviour of active arching of soil with shallow heights ((H/B) ≤2) is different from the behaviour of active arching of soil with deep heights ((H/B) ≥2) which is in agreement with the results presented above. The maximum normalised load on the passive mode is directly related to the burial depth. The data illustrate that despite the increase in the number of cycles, the normalized load was relatively constant regardless of the burial height of the soil as shown in Figure 5.9 and 5.10.

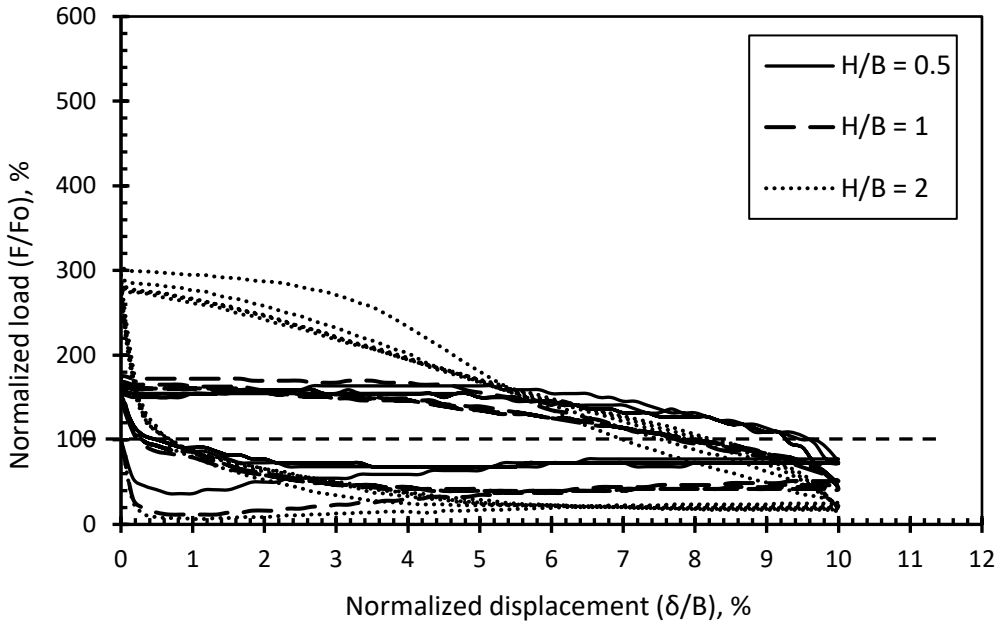

Figure 5.9. Normalised load versus normalised displacement during sequential active and passive arching.

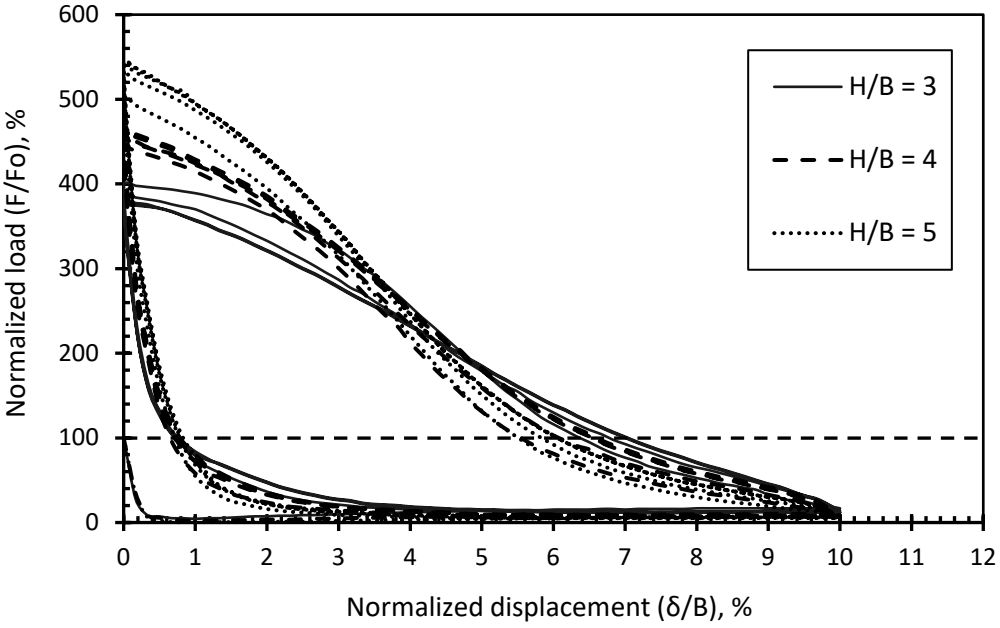

Figure 5.10. Normalised load versus normalised displacement during sequential active and passive arching.

5.4 Surface settlement

To enhance the discussion, surface settlement was plotted against the normalised soil height after the first and tenth cycles of sequential active and passive arching as demonstrated in Figure 5.11. A significant reduction in the measured settlement is experienced when the burial height increases beyond a normalised height of 2.50. Van Eekelen et al. (2003)'s study showed that shallow burial heights were not able to mobilize shear stress noticeably and the development of soil arching was incomplete. The data suggest that the critical height that is often considered to be the height at which the settlement is equal to zero, is between a normalised height of 2~3. Under repeated sequential active and passive arching cycles, surface settlement started to appear and increased with the number of cycles. No critical height could be confirmed after ten cycles of active and passive arching due to increased surface settlement as the surface settlement was recorded to be 4.0 mm after ten cycles. This means that the critical height was not only dependent on the burial height but also on the number of active and passive cycles, which is in line with the previous observation of a weakened arching mechanism under cyclic alterations of active and passive resistance.

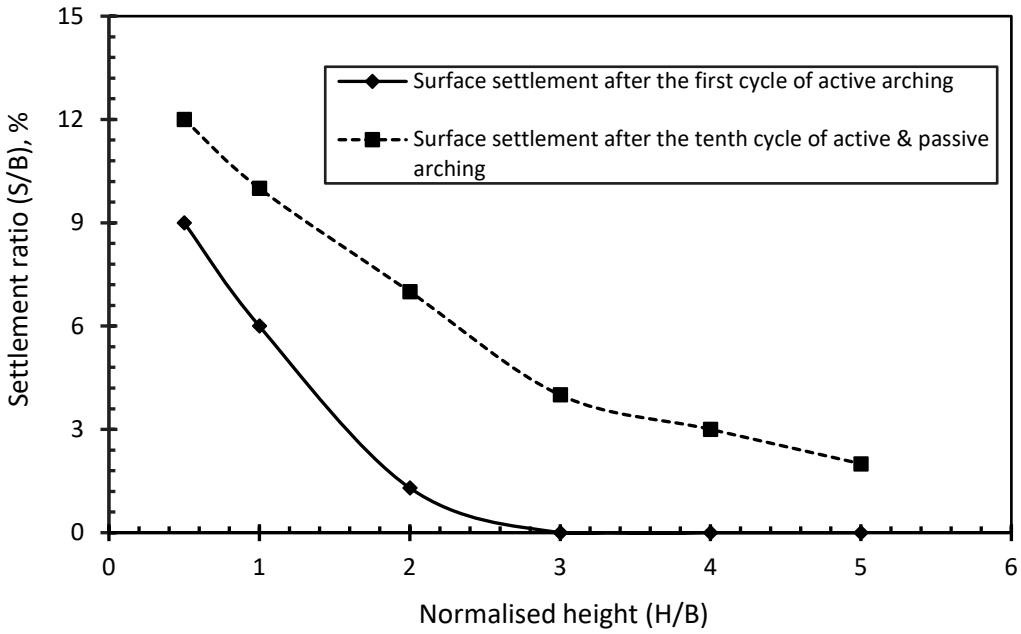

Figure 5.11. Surface settlement as a function of normalised height after first active arching and tenth cycle of active and passive arching.

5.5 Stress Reduction Ratio (SRR)

To aid the discussion for the effect of sequential active and passive arching on the behaviour of sand bed, stress reduction ratio (SRR) was also calculated. The stress reduction ratio (SRR) is determined by dividing the vertical pressure on the trapdoor by the initial at rest overburden pressure during the active mode under repeated sequential active and passive arching. If the SRR is equal to zero this means that all loads were transferred to the fixed sides (full arching). When SRR is equal to one this means that no arching is developed (Low et al. 1994). SRR provides a useful illustration of the effect of cycle number on the maximum arching of soil:

$$\mathrm{SRR} = \frac{\sigma_v}{\gamma H} \qquad (5.1)$$

where; σ_v is the vertical pressure on the trap door in(kN/m^2), γ is the soil unit weight in (kN/m^3) and H is the height of the soil bed in (m).

Figure 5.12 presents the results of the stress reduction ratio (SRR) with the number of cycles for different heights of soil under repeated sequential active and passive arching. It can be seen that most of stress increase occurs in the second cycle in comparison with loads measured during the first cycle. This means that arching in soil is substantially decreased during the first few active and passive cycles irrespective of the sand bed height. Increasing bed height has a minor influence on the stress reduction ratio. A slight effect was noted with further alteration of active and passive cycles due to weakened arches. Minor reliance was also observed on the burial height as shown in Figure 5.12.

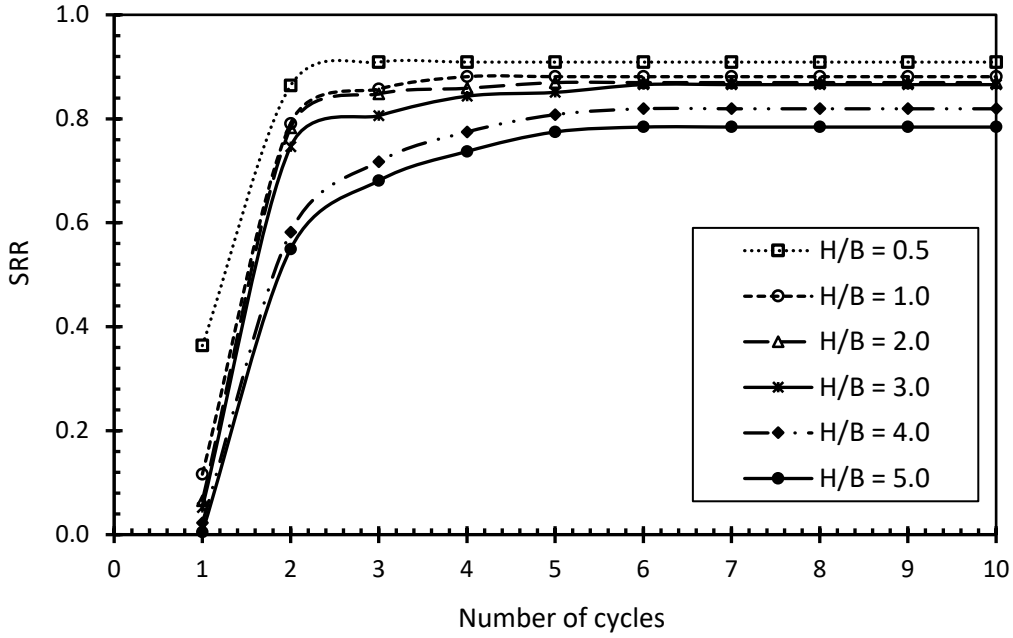

Figure 5.12. Stress reduction ratio versus cycle number of active and passive arching at 1% normalised displacement for various normalised heights.

5.6 Summary

In the present chapter, comprehensive investigation was carried out to examine the effect of repeated sequential active and passive arching on the

distribution of stresses within granular soil materials. The experimental results showed clearly that the magnitude of displacement of the yielding region significantly affects the formation of the arch and the degree of stress redistribution. Alternating the displacement of the underground inclusion exacerbated the formation of active and passive arching leading to a substantial reduction in shear resistance and stress redistribution. It is noted that the greatest loss in shear resistance occurs from the second cycle and remains virtually the same with further cycles. Sequentially alternating displacement of the underground inclusion is found to be detrimental to the formation of full active and passive arches irrespective of the burial height.

CHAPTER SIX

EXPERMENTAL ANANLYSIS OF UNREINFORCED AND REINFORCED SALLOW PILED EMBANKMENTS SUBJECT TO CYCLIC LOADING

6.1 Introduction

In this chapter, the results attained from reinforced piled embankment tests (main experimental work) for loads and deformations are presented and analysed. All experiments were conducted under 6 stages of loading namely; self-weight (stage 0), monotonic load (stage I), cyclic loading 1 (stage II), cyclic loading 2 (stage III), cyclic loading 3 (stage IV) and unloading stage (stage V) as shown in Figure 3.30. The effects of embankment height and number of reinforcement layers on the behaviour of soil arching, settlements and heaving are discussed and compared here after. Of note, i. all measured loads on piles and soft soil are converted into pressure for the sake of comparison and to aid the discussion, and ii, due to the huge number of data points, data points presented in figures represent the average of measured maximum values of 5 consecutive cycles. It should also be noted that some discrepancies were observed in the measured data. The pressure difference on the two piles did not exceed 6 % whist the discrepancy in the reinforcement tension force from the left- and right-hand side load cells was less than 7 %. The settlement surface difference between the two LVDTs was less than 4 %.

6.2 Analysis of unreinforced embankment

Figure 6.1 presents the variations of maximum pressure on piles and soft soil versus time during different stages of loading on 200, 400 and 600 mm high unreinforced embankments. Initially, during the stage where the loading was

from the self-weight of the soil bed (stage 0), it can be seen that the measured pressure on the piles was nearly the same as the pressure on the soft soil when the height of the embankment was 200 mm. These values are corresponding to the weight of embankment soil which indicated that no active arching was formed. When the height of the embankment was increased, the pressure on soft soil was increased slightly while the pressure on the piles was increased significantly. This indicated that the arching of soil was developed and increased with increasing the embankment height. The best improvement was recoded with embankment having height of 600 mm as shown in Figure 6.1. This was due to the increase of accumulation of shear resistance with increasing the embankment height enhanced the development of soil arching. (See for example, Han and Gabr 2002; Abusharar et al. 2009).

However, when monotonic load was initiated (Stage I) to the embankment, the pressure on the soft soil and piles started to increase irrespective of the embankment height. The rate of increase of pressure on the piles was significant compared with the pressure on the soft soil as shown in Figure 6.1. The results attained in this study agree with previous results by Girout et al. (2018) who found that the transfer of loads to the piles increased when surcharge loads was applied compared with the self-weight case. On the other hand, it was noted that the recorded pressure on the central piles was decreased significantly by increasing the embankment height while it was increased very slightly on the soft soil. For an applied surface pressure of 31.1 kN/m^2, the pressures on the piles were 68, 54 and 48 kN/m^2 for embankments of 200, 400 and 600 mm heights respectively. The recorded pressure on the

soft soil was 18, 19 and 21 kN/m^2 for 200, 400 and 600 mm high embankments respectively.

When the applied pressure on the soft soil and pile surfaces was only from the embankment self-weight, a uniform distribution of stresses would result at the whole ground of the embankment. On the other hand, when the external load was applied (monotonic load) and due to the surcharge load being applied to a specific area, the higher stresses would be concentrated in the centre of the testing rig which meant that the pressure on the central piles was higher than the on the outer piles. However, by increasing the embankment height, the distribution of stresses at the piles and soft soil level increased resulting in lower pressure on the central piles. The pressure on the soft soil was slightly affected due to i. the pressure on the soft soil being measured in the central panel ii. the summations of applied pressure (self-weight + monotonic load) on the soft soil and pile surfaces of the 200, 400 and 600 mm embankments being nearly the same and equal to 28.75, 28.26 and 28.82 kN/m^2 respectively.

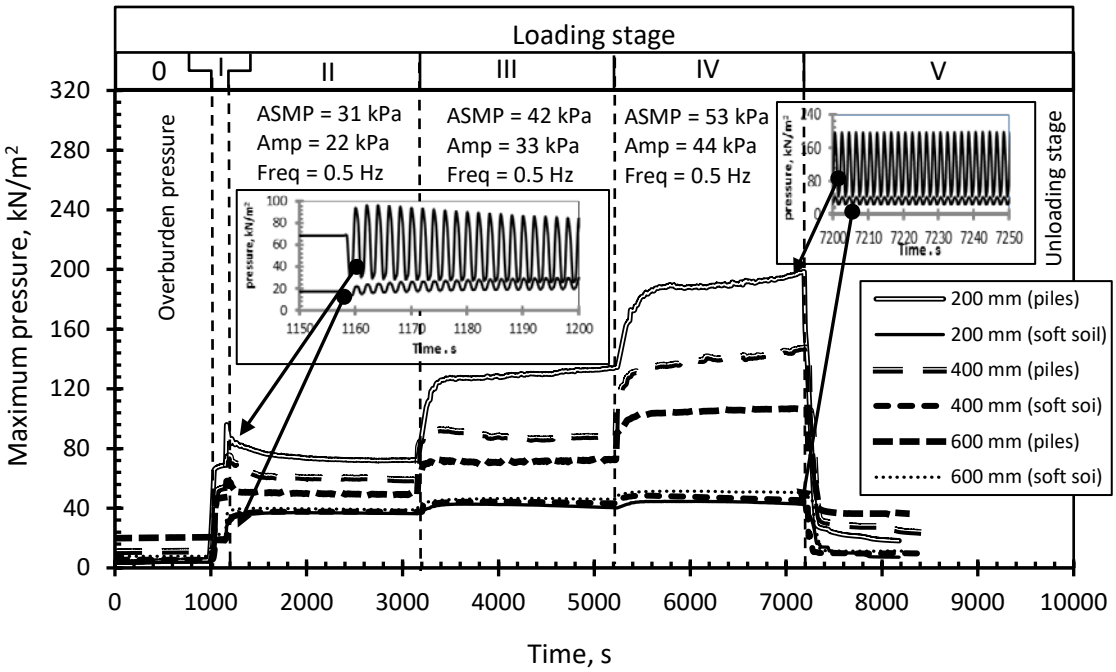

Figure 6.1. Maximum pressure on pile caps and soft soil for unreinforced embankments with different heights.

Where; ASMP = Applied Surface Mean Pressure, Amp = Amplitude and Freq = Frequency.

During Stage 2, cyclic load was applied with pressure between (8.90 and 53.20 kN/m^2). It can be seen from Figure 6.1 that remarkable drop in pressure on the pile caps was observed accompanied with a substantial pressure increase on the soft soil irrespective of the embankment height. This indicated the collapse of the formed arch in the embankment soil during the initial cycles of load. The pressure on the pile cap was decreased significantly over the first 20 cycles when the height of the embankment was 200 and 400 mm. It was decreased from 96 kN/m^2 to 82 kN/m^2 and from 86 kN/m^2 to 72 kN/m^2 for 200 and 400 mm unreinforced embankments respectively. Then it decreased gradually until reaching the stable pressure after 600 cycles for 200 mm embankment and after 280 cycles for the 400 mm embankment. The total reduction in the pressure on the piles was 25 % and 20 % of embankments of 200 and 400

mm in height respectively by the end of the first 1000 cycles. A stable pressure was reached for 600 mm high embankment after 80 cycles with a total reduction in the pressure on the piles of almost 14 %, from 59 kN/m^2 to 51 kN/m^2 and no further reduction in the pressure occurred on the piles during further cycles during this stage as shown in Figure 6.1. This is attributable to the loss in mobilised shear resistance along the vertical soil columns above pile caps by cyclic loads causing significant damage to the formed soil arching which is consistent with earlier findings by Heitz (2006), Heitz et al. (2008), Van Eekelen et al. (2010a) and Zhuang and Wang (2018). Also, it can be noted that the effect of cyclic loading on the arching of the soil decreased with increasing the embankment height which is in agreement with the results of Heitz (2006).

Despite the collapse of soil arching during the first stage of cyclic loading, entirely opposite behaviour was noted during subsequent stages of cyclic loads in which higher surface cyclic loading was applied. The results confirmed that most of the load was transferred to piles causing a significant increase in the pressure on pile caps alongside with a minor increase on soft soil. From Figure 6.1, one could notice that pressure on the piles was increased to 128, 92 and 72 kN/m^2 during the second stage of cyclic loading (for a surface cyclic pressure of 75.6 kN/m^2) and was increased to 184, 136 and 104 kN/m^2 during the third stage of cyclic loading (for a surface cyclic pressure of 97.8 kN/m^2) for 200, 400 and 600 mm high embankments respectively. Also, it can be seen that most of the increase in pressure on the piles occurred during the initial 100 cycles and then small increase in the pressure was recorded during the rest of the cycles during the second and third stages of cyclic loading as shown

in Figure 6.1. This could be attributed to the reinstatement of soil arching due to; i. increased dry unit weight of the embankment fill and ii. deformation of soft soil. Van Eekelen (2015) found that consolidation of soft soil improves the arching in embankment fill. In these experiments soft soil deformation was observed under the increased pressure by external cyclic loading. Improved shear strength of the embankment material was also imminent due to increased dry unit weight under the effect of load cycles. This could be due to densification of the embankment fill material by the act of dynamic compaction caused by the effect of cyclic loading. Consequently, the dry unit weight of embankment fill material might have increased. Data taken for deformation of the embankment surface and soft soil were used to estimate the change in volume of the embankment fill material. Since the weight of sand used to build the embankment was measured, the dry unit weight could then be estimated. Figure 6.2 shows the estimated dry unit weight of the embankment material during the three stages of cyclic loading for 200, 400 and 600 mm high embankments. The results show a degree of improvement in the dry unit weight of the embankment in particular during the early period of application of cyclic loading. As a result, some improvement in the shear strength of the embankment materials leading to recovery of the arching effect would be experienced leading to transfer of loads to piles in subsequent stages of load. However, the highest transfer of pressure on central piles was recorded with the embankment having a thickness of 200 mm and reduced with increasing the embankment height. This could be associated with increasing distribution of external load caused by increasing the embankment height. Also, the effect

of embankment height on the transfer of the loads was more obvious during the last stage of cyclic loading (stage IV).

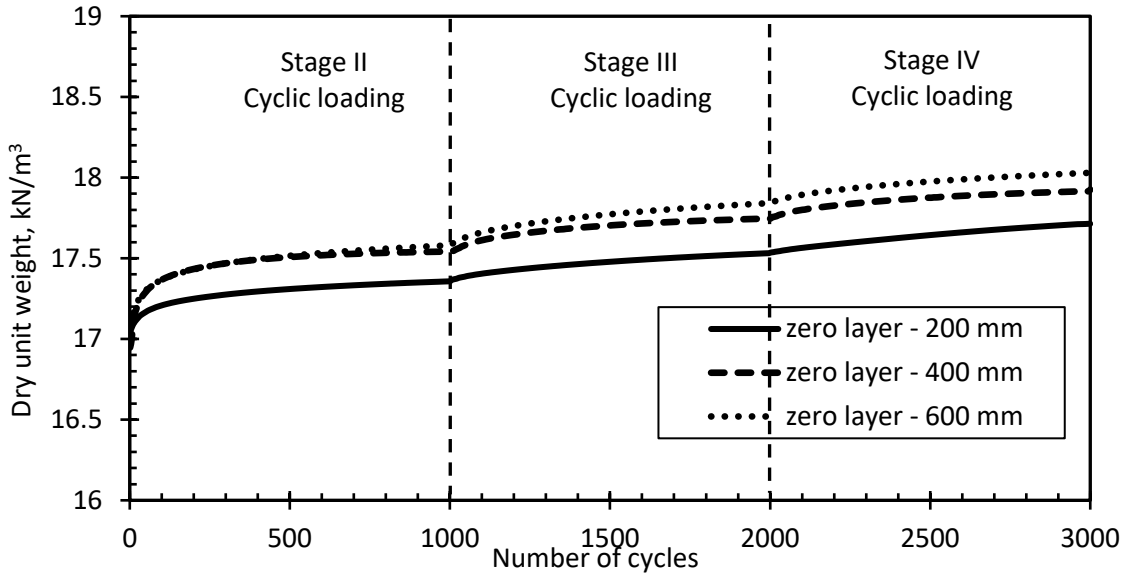

Figure 6.2. Estimated dry unit weights of unreinforced embankments for different heights during cyclic load.

In addition, Figure 6.3 shows that most of the cyclic load was taken by the piles and it significantly increased with increasing applied pressure and decreased with increasing embankment height. However, the pressure on the soft soil was quite small and slightly increased with increasing applied pressure and embankment height. It can be seen that during the first stage of cyclic loading (from cycle 515 to 530) the pressure on the central piles varied between a minimum pressure of 26, 28 and 32 kN/m^2 and a maximum pressure of 73, 62 and 49 kN/m^2 when the embankment heights were 200, 400 and 600 mm respectively. During the same stage the measured pressure on the soft soil ranged between a minimum pressure of 25, 31 and 34 kN/m^2 and a maximum pressure of 35, 39 and 41 kN/m^2 for 200, 400 and 600 mm high embankments respectively as shown in Figure 6.3. During the second and third stages of cyclic loading the rate of pressure on the central piles

increased compared with the first stage irrespective the height of the embankment. However, pressure on the soft soil was nearly unaffected by further increasing of external loading compared with the first stage of cyclic loading as shown in Figure 6.3. Finally, during the unloading stage (stage V) the pressure on the piles and soft soil was decreased significantly irrespective embankment height as shown in Figure 6.1. However, the pressure on the piles and soft soil was higher than that during the overburden stage (stage 0). This was due to the densification of fill materials and the consolidation of clay soil.

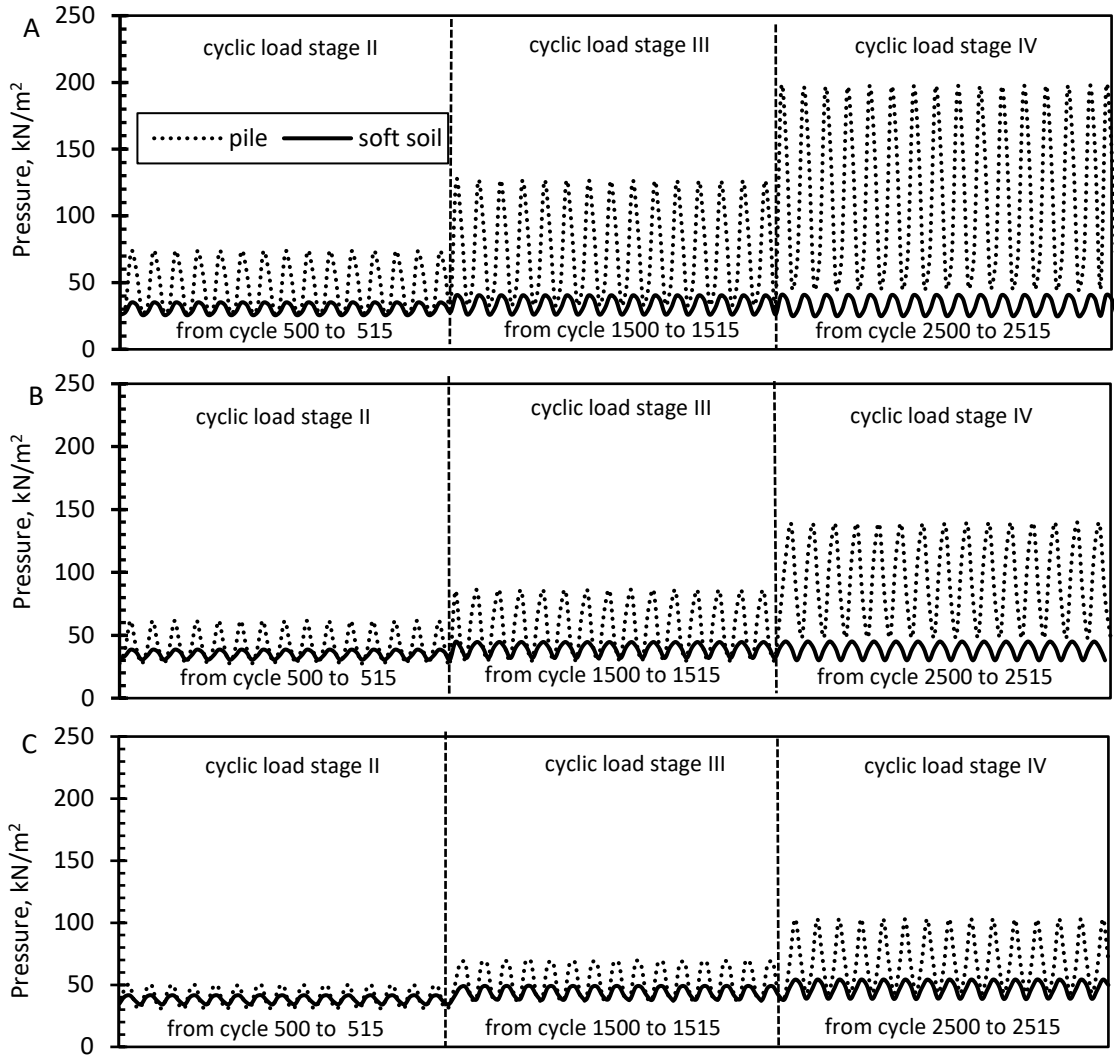

Figure 6.3. Variation of pressure on piles and soft soil of different embankment heights during cyclic stages (A) 200 mm (B) 400 mm(C) 600 mm.

6.3 Analysis of reinforced embankment

Inclusion of one, two and three reinforcement layers at predetermined locations was examined to evaluate the effects of reinforcement on the load transfer mechanisms within the embankment fill material with different heights, particularly to illustrate how the reinforced embankment system responds to external cyclic loads. Figures 6.4 - 6.7 show the effect of number of reinforcement layers on measured pressure on pile caps and soft soil during all stages of loading of 200 mm reinforced embankment. During stage 0 and I (overburden pressure and monotonic loading stages), it can be seen that increasing the number of reinforcement layers caused a slight increase on pressure measured at the pile caps accompanied with a slight reduction on the pressure on soft soil. With the inclusion of three layers of reinforcement, a 15 % pressure increase on the pile caps was recorded due to self-weight of the embankment. During the application of monotonic loading, a slight improvement to the load transfer mechanism was observed with the inclusion of two and three layers of reinforcement. The pressure on pile cap was measured to be 74 and 78 kN/m^2 for embankment reinforced with two and three layers of reinforcement giving a pressure increase of 9 and 15 % compared with unreinforced embankment. No effect was observed with the inclusion of one layer of reinforcement. This is due to the fact that the mobilised frictional resistance was not high enough to develop tension membrane effect. Nevertheless, a major benefit for the inclusion of reinforcement could be observed once cyclic load was applied after the monotonic load in stage II. Shortly after the onset of cyclic loading, the pressure on the pile caps was recorded to be 98, 120 and 136 kN/m^2 for embankments reinforced with one,

two and three layers of reinforcement for 200 mm embankment. This means that enhanced load transfer mechanisms within the embankment were experienced during cyclic loading with increasing the number of reinforcement layers leading to a higher pressure on the pile caps. With the inclusion of one reinforcement layer, it is likely that the tension membrane effect which is deformation dependant, is dominant causing increased transfer of loads to the pile caps. With the addition of more reinforcement layers, the reinforced embankment would behave as a heavily reinforced slab. Hence, an enhanced response to cyclic load was observed during various stages of loading on reinforced embankments. Inclusion of reinforcement layers lessened the immediate damage to the arch formed in the embankment material which was observed in Figures 6.5 – 6.7 and the subsequently gradual decline in transferred pile cap pressure in comparison with the unreinforced soil embankment. Consequently, the degree of deterioration of transferred load to pile caps which can be assessed by the loss of resistance over prolonged cycles, reduced with increasing the number of reinforcement layers. For the embankment with one layer of reinforcement, the measured pressure on the pile caps went down to 80 KN/m^2 at the end of Stage II after 1000 cycles as shown in Figure 6.5. Increasing the number of reinforcement layers increased the stability of the load transfer mechanisms. Comparing Figures 6.5 - 6.7 indicates that the drop in pressure on the pile caps over the 1000 cycles of Stage II of loading was reduced with increasing the number of reinforcement layers. When three layers of reinforcement were placed, the pressure on the pile caps decreased to 128 KN/m^2 at the end of Stage II of the cyclic loading.

Similar load transfer behaviour was observed with increasing the applied cyclic loading (stage III and IV) but even with an enhanced level of interaction and resistance. The results in Figures 6.4 - 6.7 illustrated that there was a minor increase in the pressure transferred on to the soft soil whereas most of the pressure increase was taken up by the piles over the first 50~60 cycles. Furthermore, the load transfer response was different to stage II, a gradual increase in pressure on pile caps was noticeable in most cases of inclusion of reinforcement layers and cyclic loads. This could be attributable to enhanced interaction between reinforcement layers and surrounding embankment material due to densification of embankment material and deformation of the underlying soft soil.

Careful inspection of pressure data on pile caps during stages III and IV in Figures 6.4 – 6.7 illustrate that maximum pressure on the central piles increased significantly with increasing number of reinforcement layers. Maximum measured pressure on the pile caps was 196, 220, 231 and 257 kN/m^2 from tests with zero, one, two and three layers of reinforcement. Since, the applied surface pressure was precisely similar in all experiments, the results therefore suggest that inclusion of the reinforcement layers enhanced the transfer of load to piles. The results also illustrated that under prolonged cycles, the pressure on the soft soil has experienced a very minor reduction rather than an increase which could be attributed to the effect of the soft soil deformation on load transfer mechanisms. It is clear that complex interactions occur on the shallow reinforced embankment subject to cyclic loading due to changes in dry unit weight of the embankment, deformation of the underlying soft soil and interactions between the reinforcement layer and adjacent soils.

The qualitative analysis of the data for dry unit weight implies that a good degree of densification to the embankment material occurs during the initial stage of cyclic load and reduces with further stages of loading and with the inclusion of reinforcement layers. Thus, the initially determined angle of friction for the embankment material and interface characteristics between the reinforcement material and adjacent soil may improve with prolonged cycles of external loading. The interface is characterised between reinforcement layers and adjacent soils and is a function of the normal stress which in the case of shallow embankments subject to traffic loads varies substantially along the perpendicular length of the reinforcement. Thus, variation in the friction resistance is imminent on the reinforcement layers. The relative contribution of different load transfer mechanisms is therefore dependant on fill material shear strength, frictional resistance and subsidence on underlying soft soil alongside with other factors e.g. pile spacing and thickness of embankment. However, the contribution of each mechanism cannot easily be identified and/or quantified.

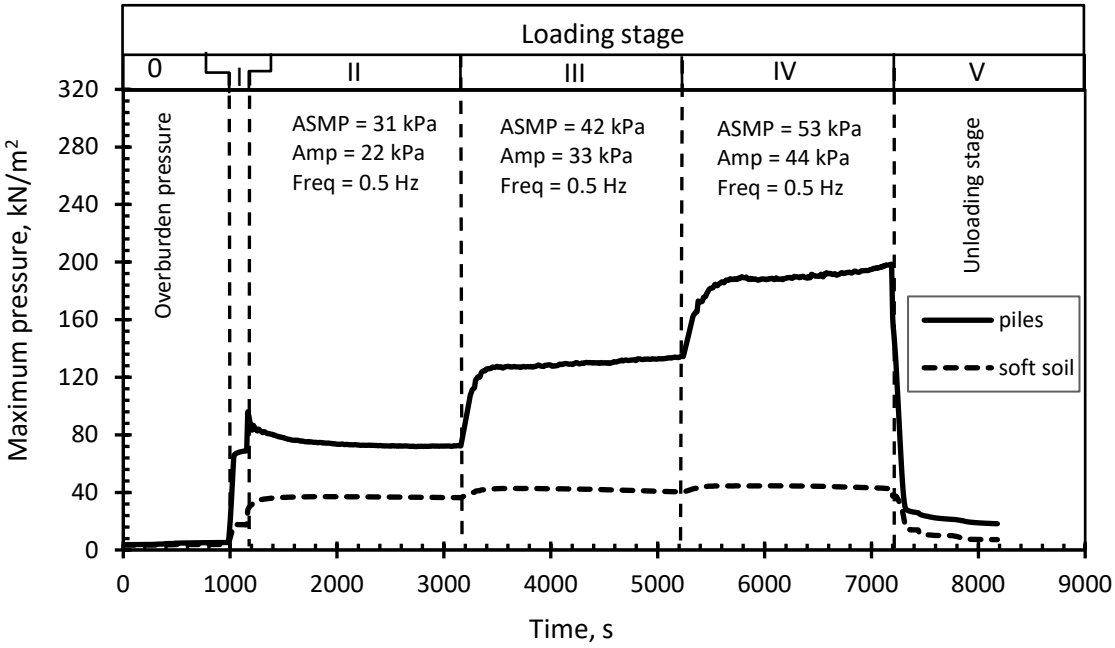

Figure 6.4. Maximum pressure on pile caps and soft soil for 200 mm unreinforced embankment.

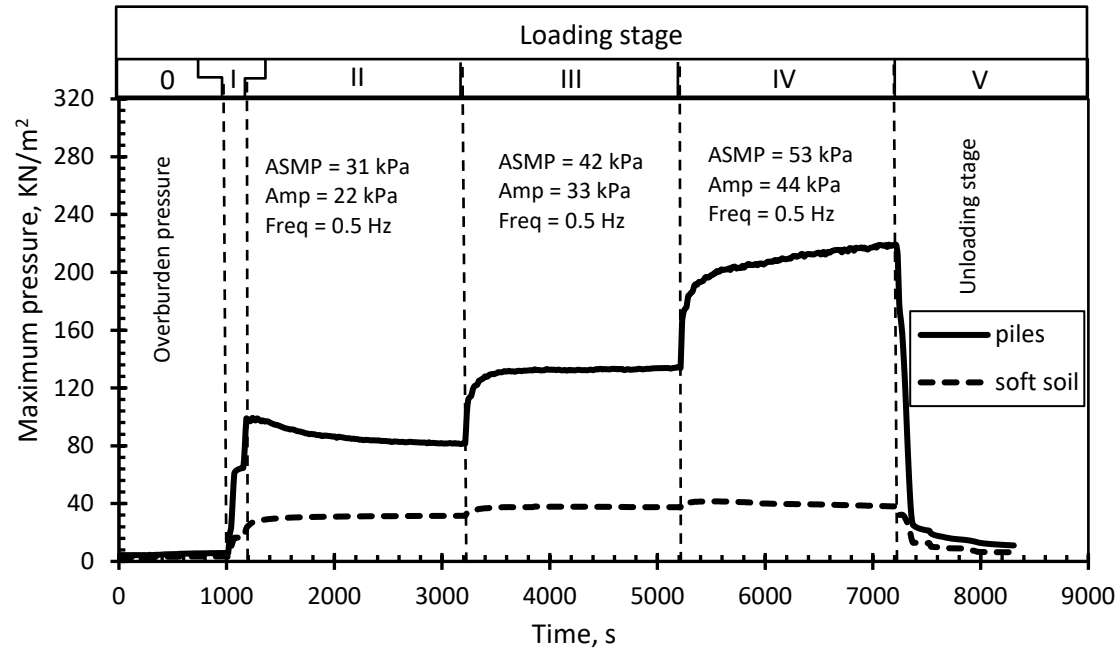

Figure 6.5. Maximum pressure on pile caps and soft soil for 200 mm one layer reinforced embankment.

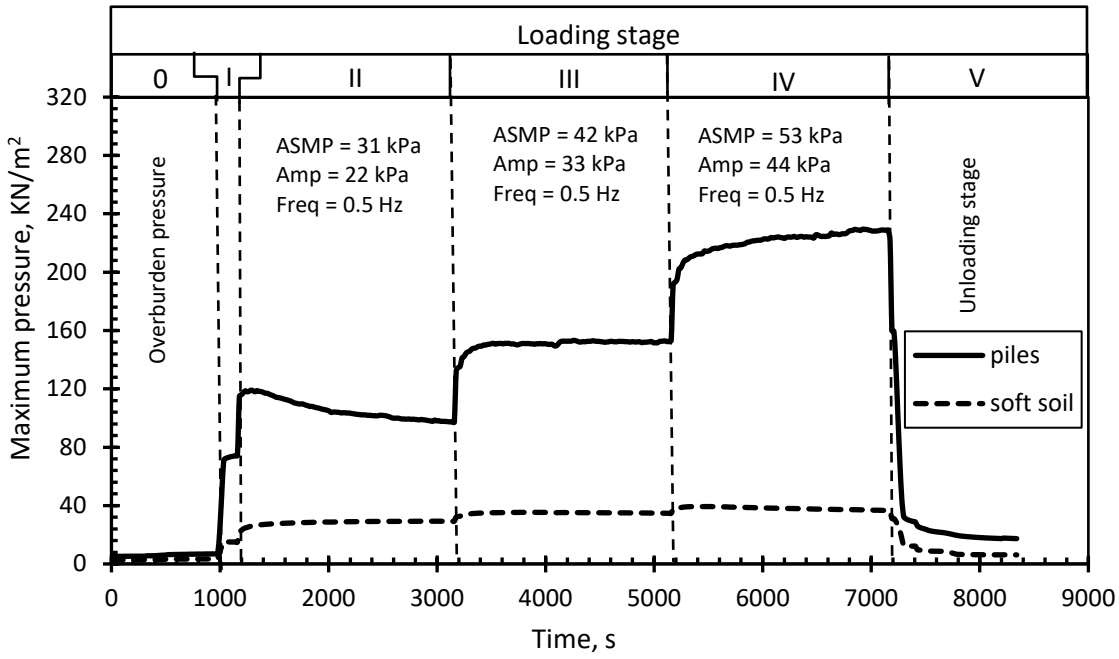

Figure 6.6. Maximum pressure on pile caps and soft soil for 200 mm two layers reinforced embankment.

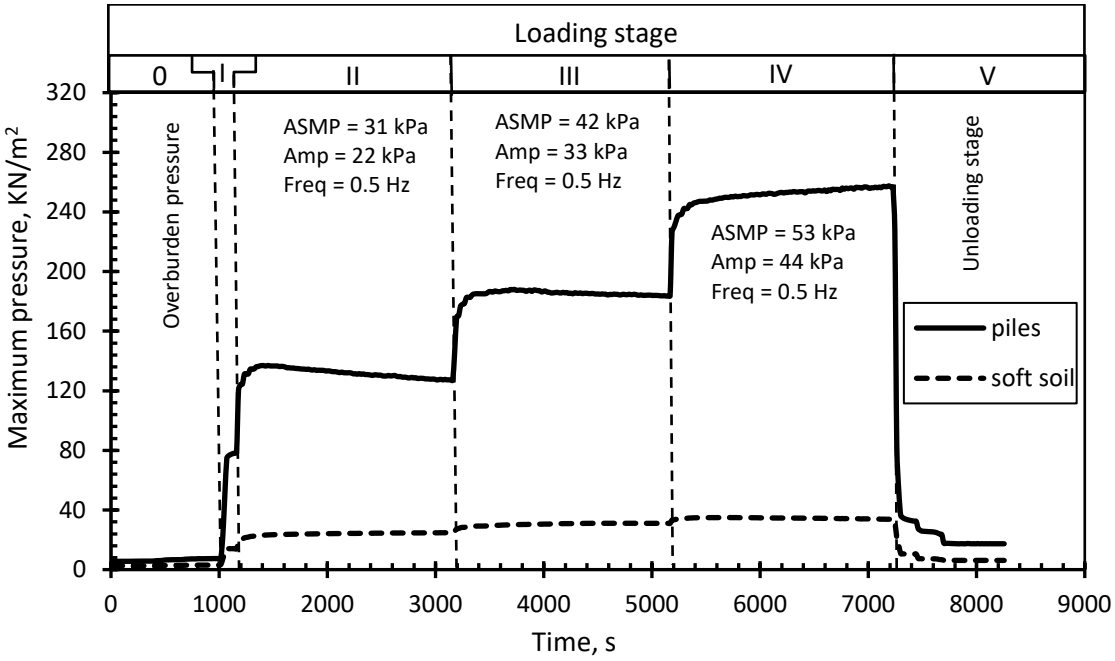

Figure 6.7. Maximum pressure on pile caps and soft soil for 200 mm three layers reinforced embankment.

Figures 6.8 – 6.15 show the effect of inclusion of reinforcement layers on the maximum pressure on the piles and soft soil for 400 and 600 mm high embankments. When the embankment height was increased to 400 and 600

mm, the same improvement as reinforced embankment with 200 mm height was recorded with placing a layer of reinforcement compared with the unreinforced embankment. However, the effect of increasing the number of reinforcement layers was decreased with increasing the height of the embankment. This means that including multiple layers of reinforcement within thicker embankments seems to slightly enhance the improvement of loading transfer mechanism compared with using one layer of reinforcement. This is due to the positions of the reinforcement layers not being changed irrespective of the embankment height. Therefore, the thickness of the infill materials above the reinforcement layers increased with increasing the embankment height resulting in the reinforced embankment behaving as a tensioned membrane as shown in Figures 6.8 - 6.15. When the applied cyclic loading increased, the pressure on the piles increased with a slight reduction in the pressure on the soft soil. However, the improvement was slightly less than that when the embankment height was 200 mm and it was decreased with increasing the embankment height due to the increase of the distribution of pressure at the base of the embankment as shown in Figures 6.8 - 6.15.

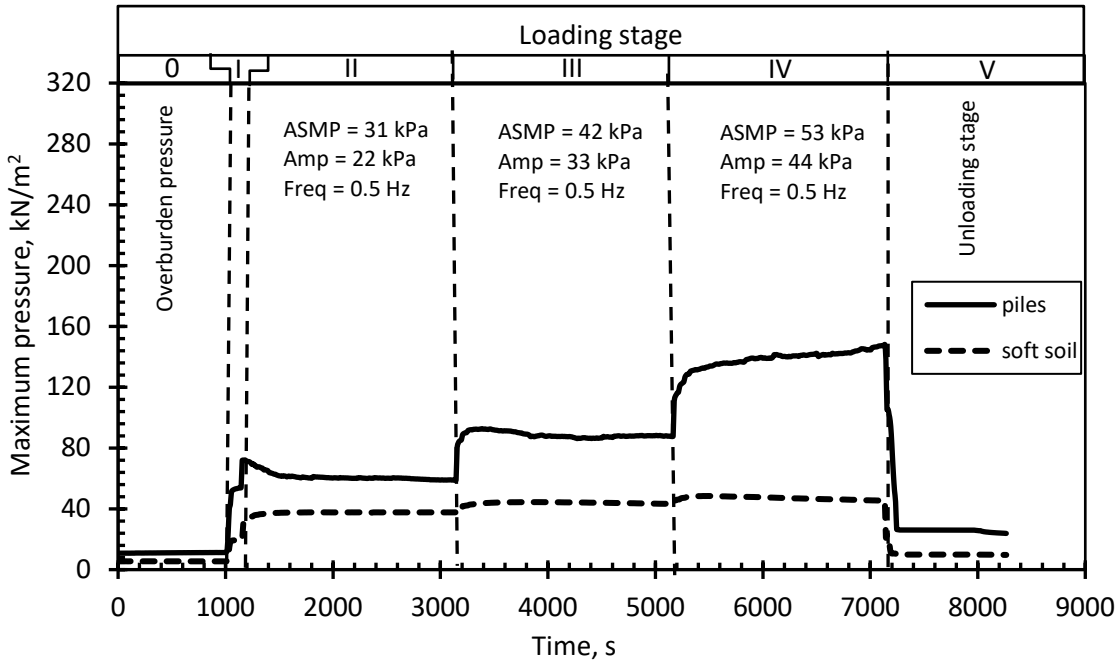

Figure 6.8. Maximum pressure on pile caps and soft soil for 400 mm unreinforced embankment.

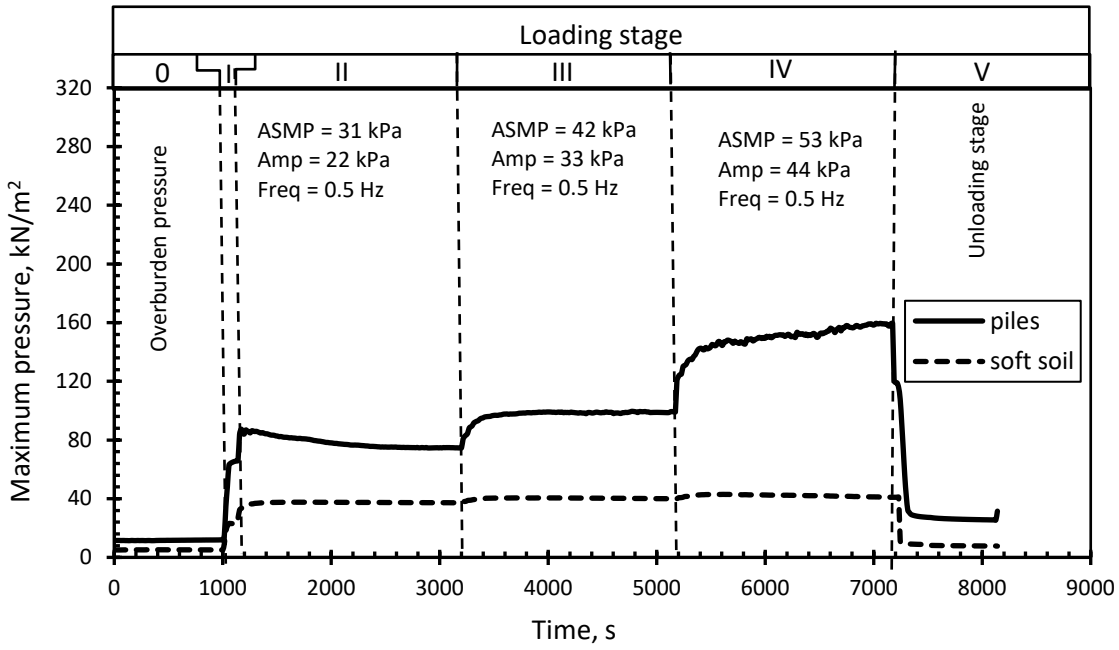

Figure 6.9. Maximum pressure on pile caps and soft soil for 400 mm one layer reinforced embankment.

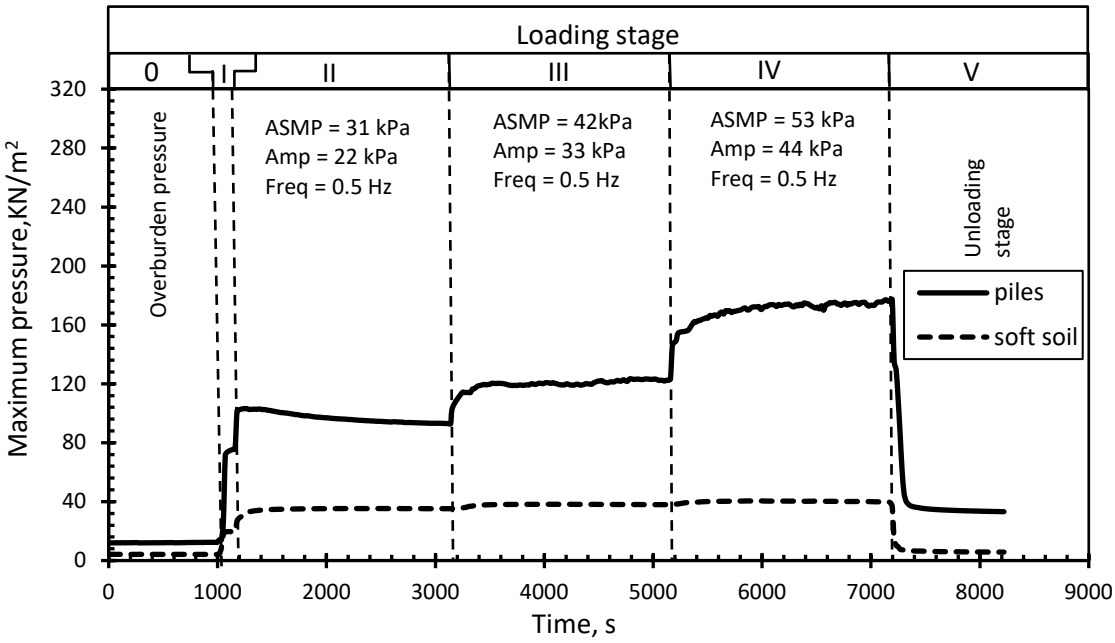

Figure 6.10. Maximum pressure on pile caps and soft soil for 400 mm two layers reinforced embankment.

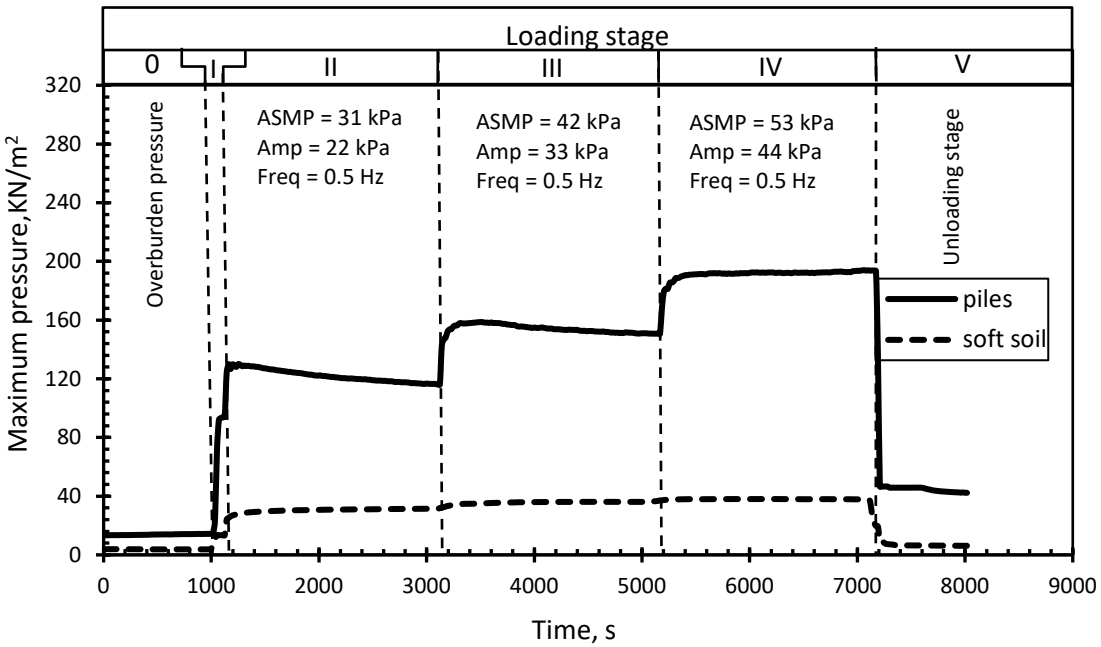

Figure 6.11. Maximum pressure on pile caps and soft soil for 400 mm three layers reinforced embankment.

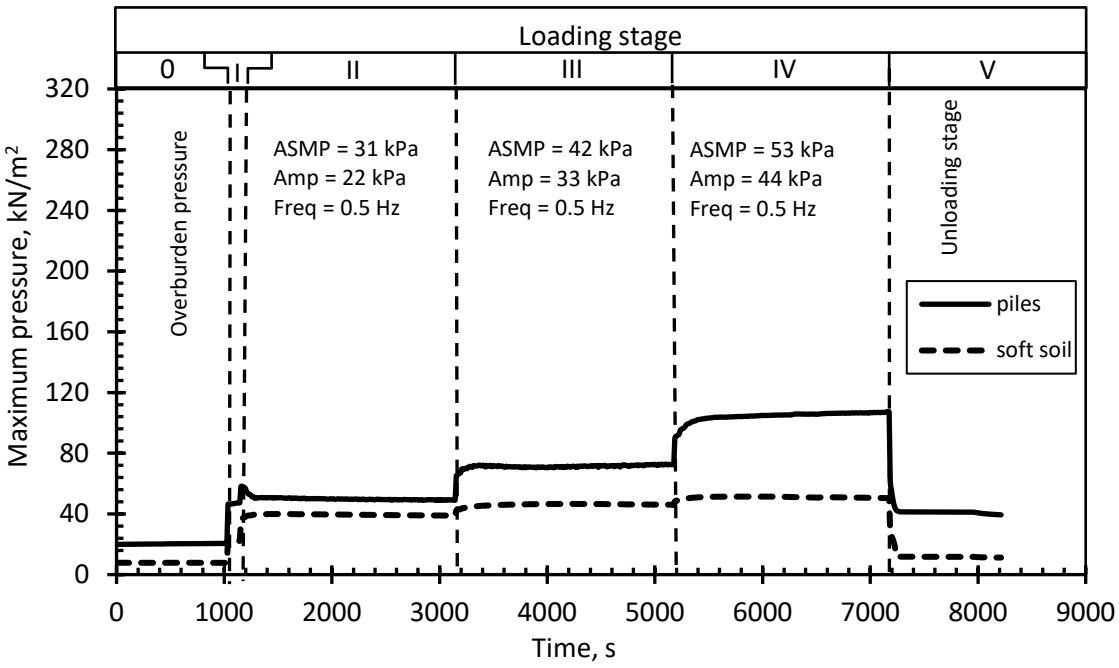

Figure 6.12. Maximum pressure on pile caps and soft soil for 600 mm unreinforced embankment.

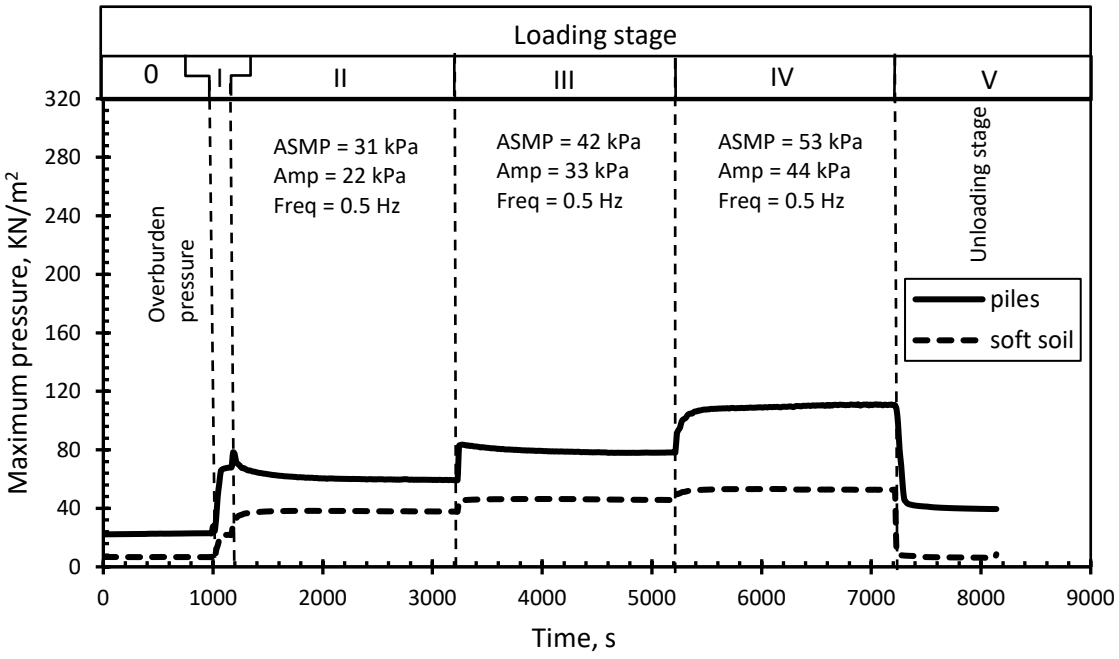

Figure 6.13. Maximum pressure on pile caps and soft soil for 600 mm one layer reinforced embankment.

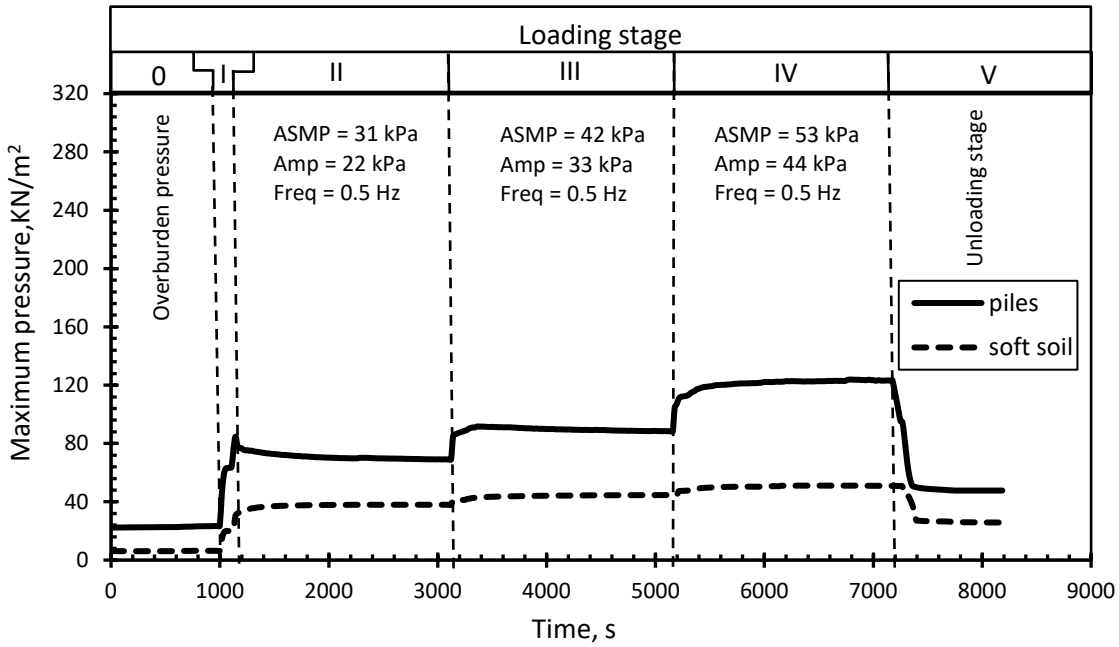

Figure 6.14. Maximum pressure on pile caps and soft soil for 600 mm two layers reinforced embankment.

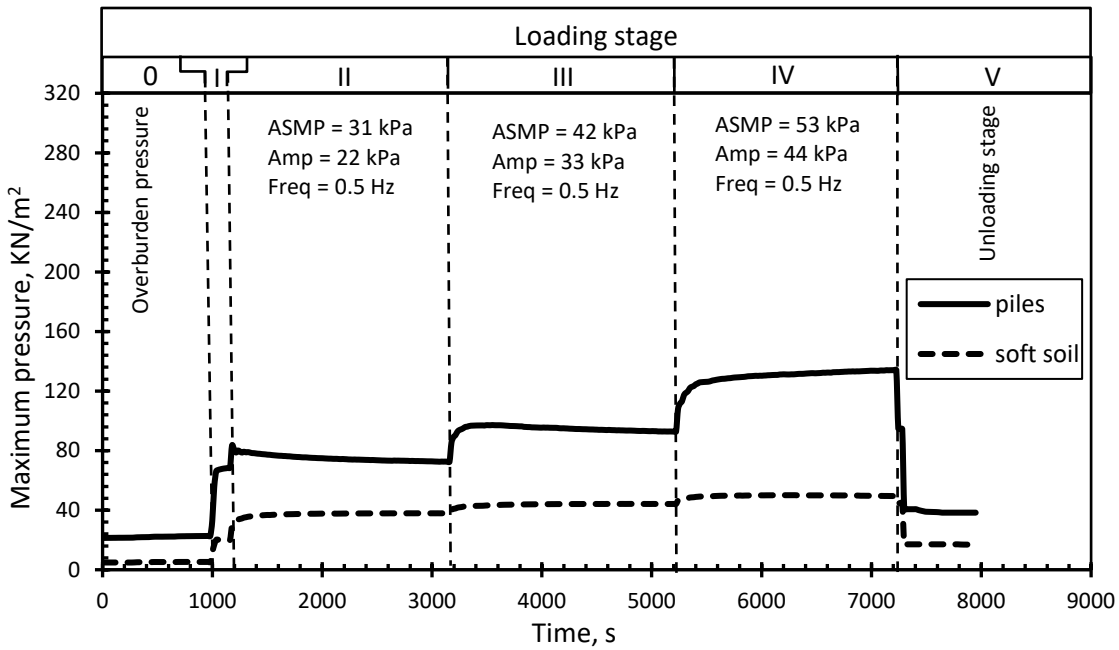

Figure 6.15. Maximum pressure on pile caps and soft soil for 600 mm three layers reinforced embankment.

6.4 Efficiency and stress concentration ratio

The efficiency of load transfer to the piles and stress concentration ratio were determined. Efficiency is defined as the ratio of the embankment load

transferred to pile to the total load of the embankment (Abusharar et al. 2009). However, this definition for the efficiency was proposed and developed for a uniformly distributed surcharge pressure over the whole surface area of the embankment. Calculations based on this definition are therefore no longer valid for assessing the efficiency of load transfer mechanisms due to the nature of applied loads e.g. traffic loads or train tracks for which the external load would be applied over a particular area of the embankment surface. Consequently, the pressure on pile caps would be different and directly related to the proximity of each pile cap to the loaded surface area. This issue is exacerbated where loads are applied on shallow embankments in which stresses would be very concentrated on a relatively small zone of the embankment that is beneath the loaded area. To overcome these difficulties with the calculation of efficiency, it was proposed to determine the efficiency based on measured data for transferred load to central piles and soft soils. These values would represent the minimum efficiency (worst case scenario). Figure 6.16 shows the measured variations on the efficiency (E) of load transfer to piles versus the number of cycles of unreinforced and reinforced embankments whereas Figure 6.17 illustrates the stress concentration ratio (SCR) between piles and soft soil in the central region underneath the loaded area.

$$\mathrm{E}\ (\%) = \frac{a\sigma_p}{a\sigma_p + s'\sigma_s} \tag{6.1}$$

$$\mathrm{SCR} = \frac{\sigma_p}{\sigma_s} \tag{6.2}$$

where, E is the pile efficiency in (%), a is the width of central piles in (m), σ_p is the measured pressure on piles in (kN/m^2), s' is the pile clear spacing in (m), σ_s is the measured pressure on soft soil in (kN/m^2), and SCR is the stress concentration ratio.

It can be seen that during the static load stage (overburden pressure) the efficiency and stress concentration ratio increased with increasing the embankment height and the number of reinforcement layers due to soil arching, tensioned membrane and stiffening effects. During the monotonic loading stage the efficiency and stress concentration ratio was increased significantly when the embankment height was 200 and slightly when the embankment height was 400 mm compared with the overburden pressure stage. However, when the embankment height was 600 mm a slight reduction in the efficiency and stress concentration ratio was recorded and compared with overburden pressure stage due to an increase the distribution of stresses. Incorporation layers of reinforcement improved the efficiency and stress concentration ratio irrespective of the embankment height as shown in Figures 6.16 and 6.17. However, the effect of increasing number of reinforcement layer was decreased with increasing embankment height. When cyclic loading was applied (stage II) the efficiency and stress concentration ratio were decreased with increasing the embankment height. When the embankment height was increased, the distribution of load at soft soil and piles level increased resulting in reduction in the stresses on the soft soil and piles. However, efficiency and stress concertation ratio were improved with incorporation of layers of reinforcement regardless of the embankment height. This improvement was decreased with increasing the embankment height as shown in Figures 6.16

and 6.17. In particular, inclusion of reinforcement layers reduced the expected loss of efficiency with prolonged cycles and under higher cyclic loading. It should be noted that the determined efficiency represents lower boundary values and other piles that are not in close proximity would be expected to retain higher efficiency. This is due to the nature of external load e.g. traffic load that was applied over a specific area of the embankment and the fact that the embankment had a shallow thickness. Although the stress concentration ratio was reasonably high as can be seen in Figure 6.17 this was not reflected on the determined pile efficiency in the central region due to; i. the characteristic of the experimented piled reinforced embankment, ii. the nature of applied dynamic load, iii. The effect of applying loads over a rigid plate and iv, the application of surcharge load over a particular area of the embankment.

In this study, experiments were conducted on piled reinforced embankment with a ratio between pile cap width to centre-to-centre pile spacing of 5 and a ratio of embankment height to pile spacing of 0.5, 1.0 and 1.5. This implies that the tested system for a shallow embankment on widely spaced piles which would result on concentration and less action of arching. Abusharar et al. (2009) found that the efficiency was decreased from 60 % to 40 % by increasing the pile width to centre to centre pile spacing from 1:2.5 to 1:4 whilst keeping the ratio of unreinforced embankment height to pile spacing 1.0. It is well documented that dynamic loads affect the strength of soil and cause fatigue to the reinforcement (see for example, Zanzinger et al. 2010). It can be seen from Figure 6.16 that starting cyclic loading caused a significant loss in the efficiency of unreinforced embankment. Inclusion of reinforcement layer mitigated the loss of efficiency regardless the embankment height. However,

addition of multi layers of reinforcement was more beneficial with the thinner embankment so that with 200 mm embankment and three of layers of reinforcement, efficiency was maintained nearly at the same level irrespective of the applied load. The results confirm addition of more than one layer of reinforcement enhances the performance of piled reinforced embankments subject to cyclic loads.

It is also noted that differences appear in the stress distribution below a load area based on the rigidity of the plate. In the case of rigid plate/footing above granular material as in this study, maximum pressure occurs beneath the centre of the loaded area (Azizi 2000). Thus, even with a load spread angle, the maximum pressure remains to occur in the central area of the embankment leading to pressure concentration on the central panel of the soft soil and piles and leading to lower efficiency.

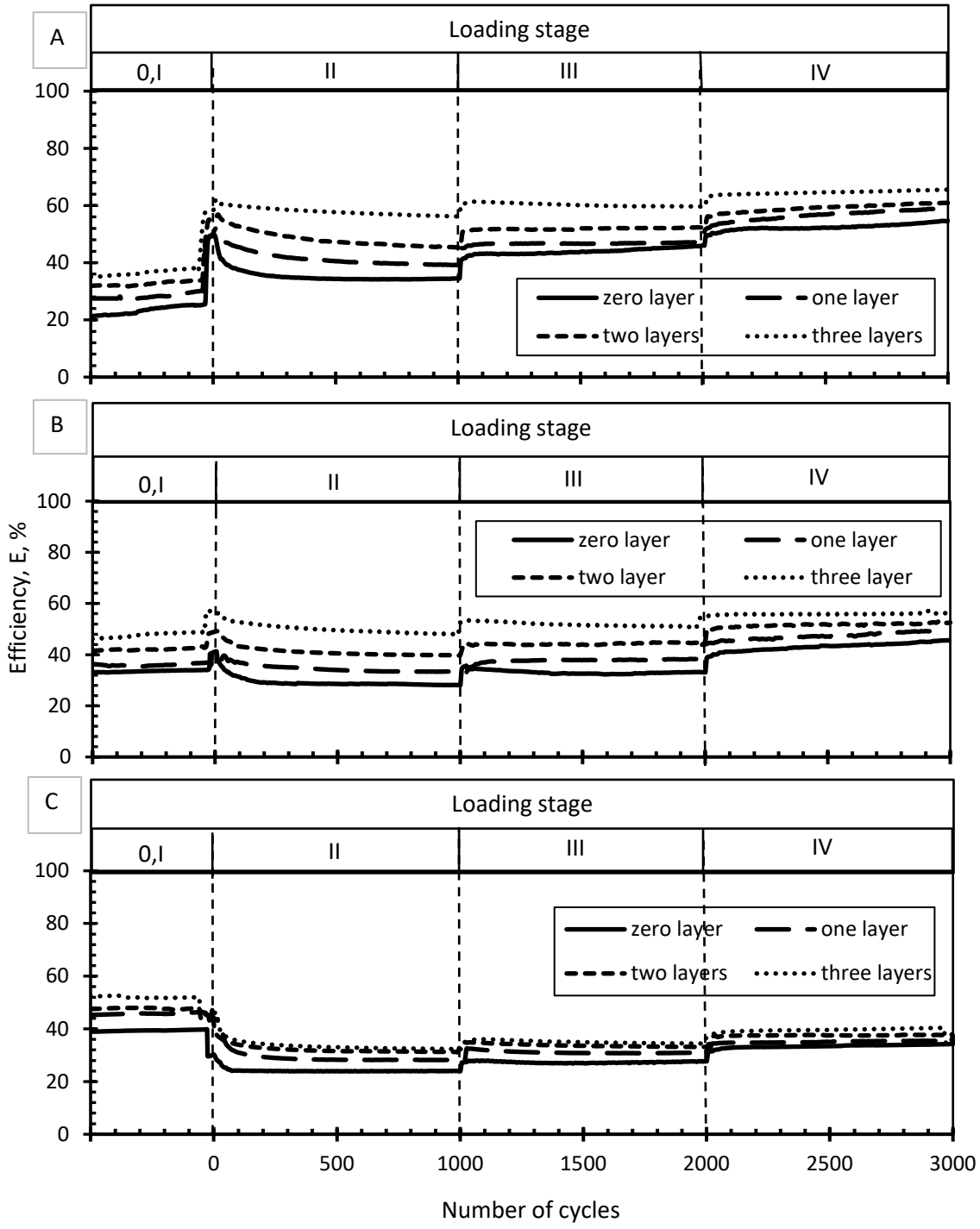

Figure 6.16. Efficiency of unreinforced and reinforced embankments for different embankment heights versus number of cycles (A) 200 mm (B) 400 mm(C) 600 mm.

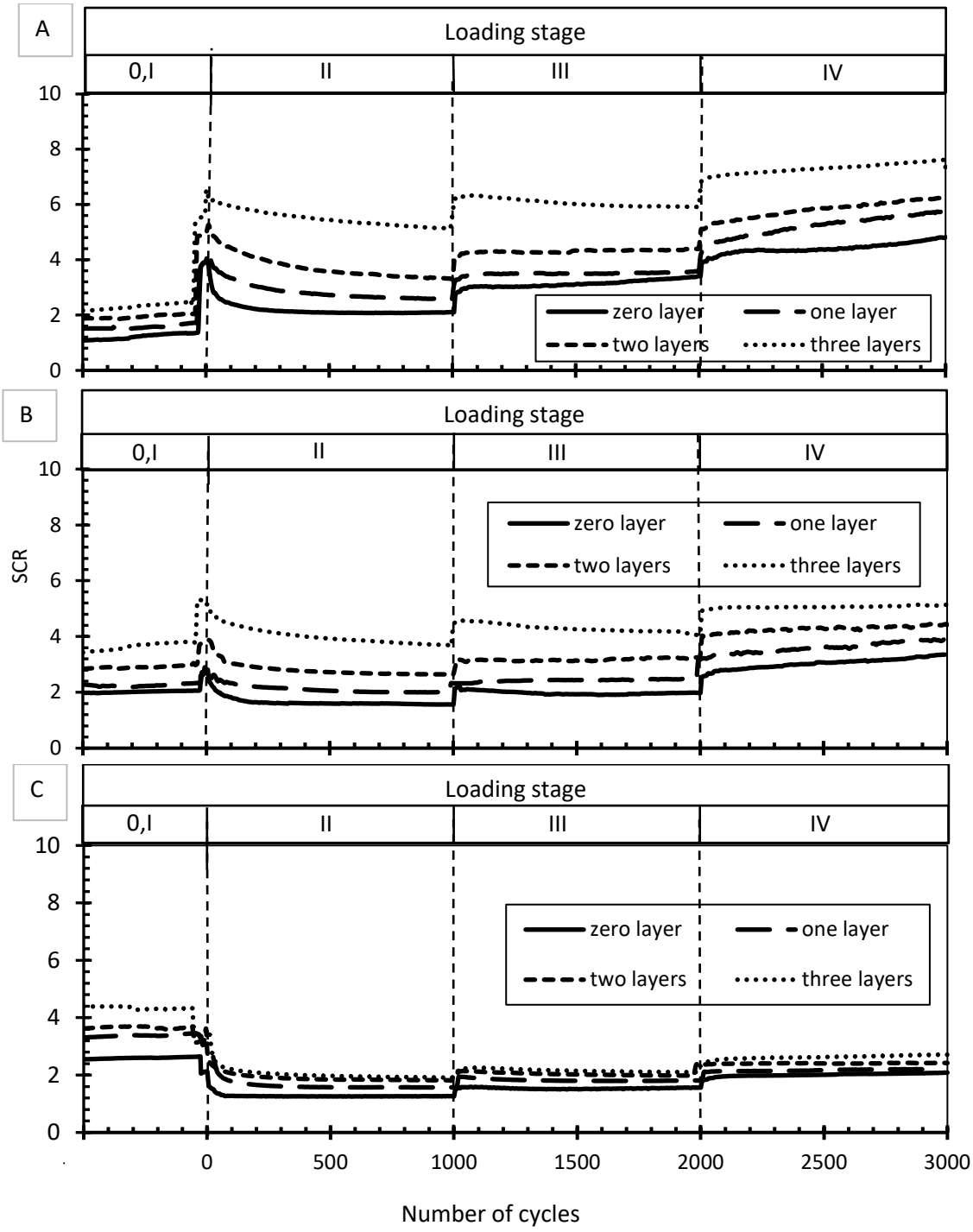

Figure 6.17. Stress concentration ratio of unreinforced and reinforced embankments for different embankment heights versus number of cycles (A) 200 mm (B) 400 mm(C) 600 mm.

6.5 Tension force in and deformation of reinforcement layers

Measurements of the forces generated on the reinforcement layers were taken by four load cells attached to both ends of each reinforcement layer. Of note, only the forces in two of the reinforcement layers could be measured due to the limited availability of load cells. In addition, it should be noted that the tension was measured at the ends of the reinforcement layers However, the maximum tension occurred in the area around the central piles adage (see for example, van Eekelen et al. 2015). Figures 6.18, 6.19 and 6.20 show the variation of tension forces during the three stages of cyclic loading (stages II, III and IV) on reinforced embankments of different heights. It can be seen that reinforcement layers responded instantaneously to cyclic loads with greatest tension force occurring in an embankment system with the inclusion of one reinforcement layer. Upon the application of cyclic loads, immediate increase in tension force was measured. The tension force in the reinforcement layers was directly related to the stage of the applied cyclic load. With increasing the number of reinforcement layers, a reduction in the tension force in reinforcement layers was noticeable. However, the results indicated that maximum tension forces always occur in the bottom layer. This is in agreement with Heitz et al. (2008) and Van Eekelen (2015) who found that highest strain was recorded in bottom layer which corresponds to higher tensile stresses.

When the height of the embankment was increased the tension force generated in the reinforcement layers increased compared with the tension forces in the 200 mm reinforced embankments as shown in Figures 6.19 and 6.20. This could be attributed to the fact that the distribution of pressure on the neighbouring panels was increased with increasing the embankment height

resulting in more pressure transferring to neighbouring panels and increased self-weight of the embankment. Also, it can be noted that the measured tension decreased slightly during the second and third stages of cyclic loading in particular for embankment with height of 200 and 400 mm which could be attributed to creep behaviour. Creep in reinforcement layers occurs when the reinforcement sheet is under applied loads for long period of time (see for example, Ariyarathne et al. 2013) or under cyclic loadings (see for example, Kongkitkul et al. 2004). Although in this study, the time of applying loads was not long, creep in the form of residual deformation may occur and reduce the tension in reinforcement layers due to the nature of cyclic loading as suggested by Kongkitkul et al. (2004).

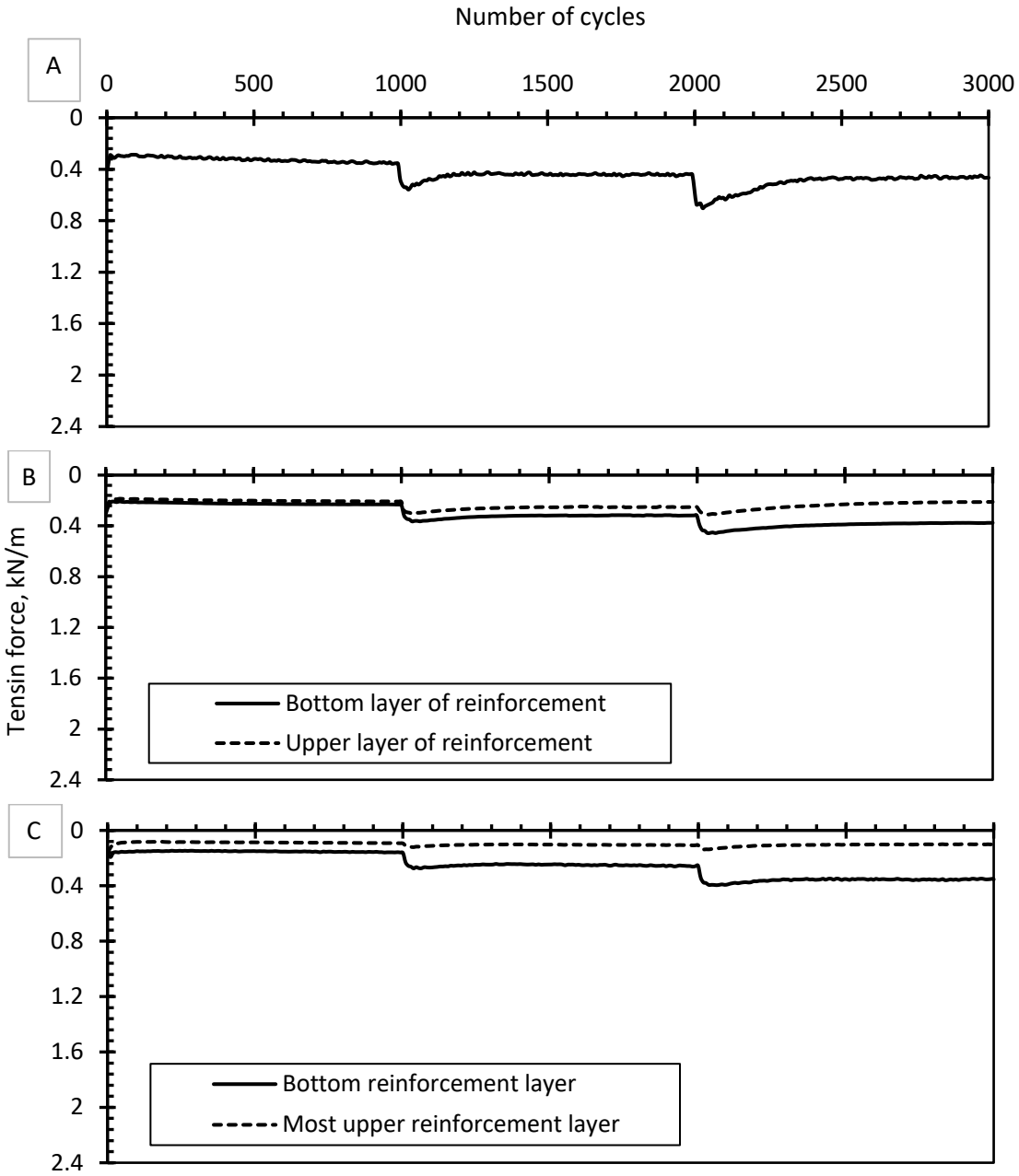

Figure 6.18. Tension force in reinforcement layers; A) one reinforcement layer, B) two reinforcement layers and C) three reinforcement layers of 200 mm reinforced embankment.

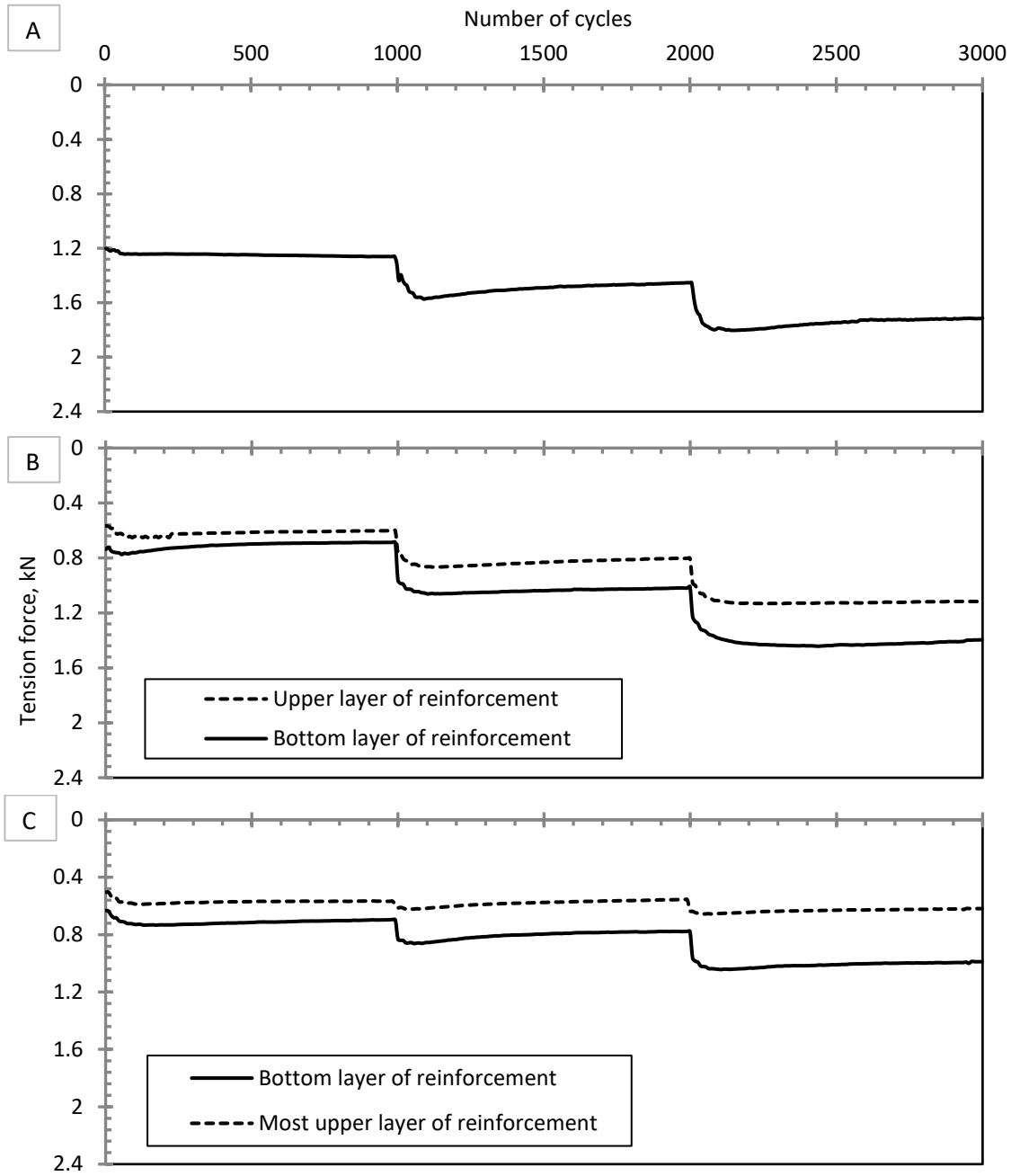

Figure 6.19. Tension force in reinforcement layers; A) one reinforcement layer, B) two reinforcement layers and C) three reinforcement layers of 400 mm reinforced embankment.

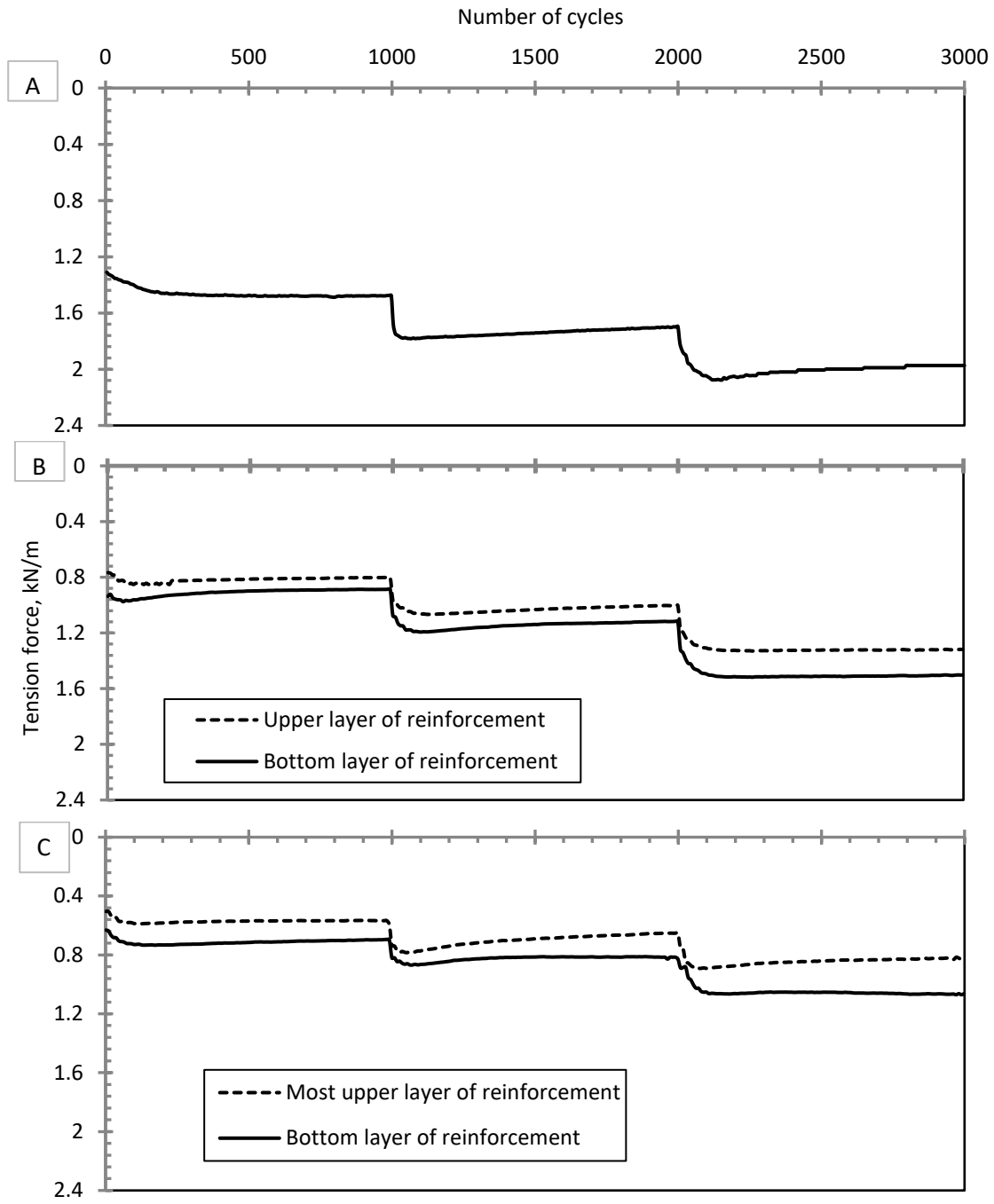

Figure 6.20. Tension force in reinforcement layers; A) one reinforcement layer, B) two reinforcement layers and C) three reinforcement layers of 600 mm reinforced embankment.

Figures 6.21, 6.22 and 6.23 present the deformation patterns at three points on the bottom layer of reinforcement layer of embankments with different heights. Points 1, 2 and 3 are located in the centre of the central panel, near the edge of the central panel and centre point of the adjacent panel as shown in Figure 3.10. It can be observed that a slight difference in the deformation of points 1 and 2 of less than 2mm existed which can be attributed to the effect of boundary conditions. The results show clearly that the deformation of the reinforcement layer is maximum in the central panel regardless of the embankment height which reflects higher pressure due to surface loads. However, the deformation was slightly increased with increasing the embankment height which could be attributed to increase in self-weight of the embankment. In addition, the deformation in outer panels was always less than the deformation in central panel which confirms that the pressure on the central panel is greater than the pressure on the two neighbouring panels. However, the deformation in the centre of the neighbouring panels (point 3) was increased with increasing the embankment height. This is due to the increase in the distribution of loads on the neighbouring panels leading to an increase in the pressure on the point 3 which resulted in an increase in the reinforcement layer deformation. The deformation during the first stage of cyclic loading was increased significantly by 220, 187 and 134 % in the middle of central panel (point 1) while it was increased by 200, 125 and 100 % in the middle of outer panel (point 3) of one layer reinforced embankment of 200, 400 and 600 mm heights respectively compared with static stages. About 50 % of the deformation during this stage was occurred during the initial 15 cycles at both points. The total deformation at the end of first stage of cyclic loading

was 16.0, 17.20 and 18.0 mm at point 1 while it was 6.0, 9.0 and 10.0 mm at point 3 for 200, 400 and 600 mm one layer reinforced embankments respectively. During the second and third stages of cyclic loading the rate of deformation was decreased gradually. The deformation in points 1 and 3 was increased by about 50 % at the end of stage three compared with the first cyclic loading stage as shown in Figures 6.21, 6.22 and 6.23.

Moreover, from Figures 6.21, 6.22 and 6.23 it can also be seen that with the inclusion of more reinforcement layers (two or three layers), substantial reduction in the deformation of the bottom layer can be achievable, not only in the central panel but also in the neighbouring panels regardless of the embankment height. By careful inspection of data in Figures 6.18 - 6.23, it is clear that the results of deformation and tension forces in the reinforcement layers are in agreement. In addition, the captured patterns for deformation and tension forces show similarities in the reaction towards the applied cyclic loads during the three stages of load increase. The results show that the deformation of Point 3 decreased with the increase in the number of reinforcement layers and was much less than that measured for Point 1. This confirms that less pressure was transferred to the two neighbouring soft soil panels with increasing the number of layers. In other words, stresses were intensified within the central region with increasing the number of reinforcement layers due to increased stiffness of the reinforced zone as it was evident from increased pressure on the central piles. This means that for a single layer of reinforcement, the tension membrane would be dominant in transferring the loads whilst with increasing the number of reinforcement layers, the reinforced zone works as a stiffened platform to transfer the loads to the piles. These

results are in good agreement with the outcomes of the numerical analysis by Ariyarathne and Liyanapathirana (2014) which found that the multi-layer reinforced system works as a stiffened platform while an embankment system with a single layer of reinforcement works as a tensioned membrane.

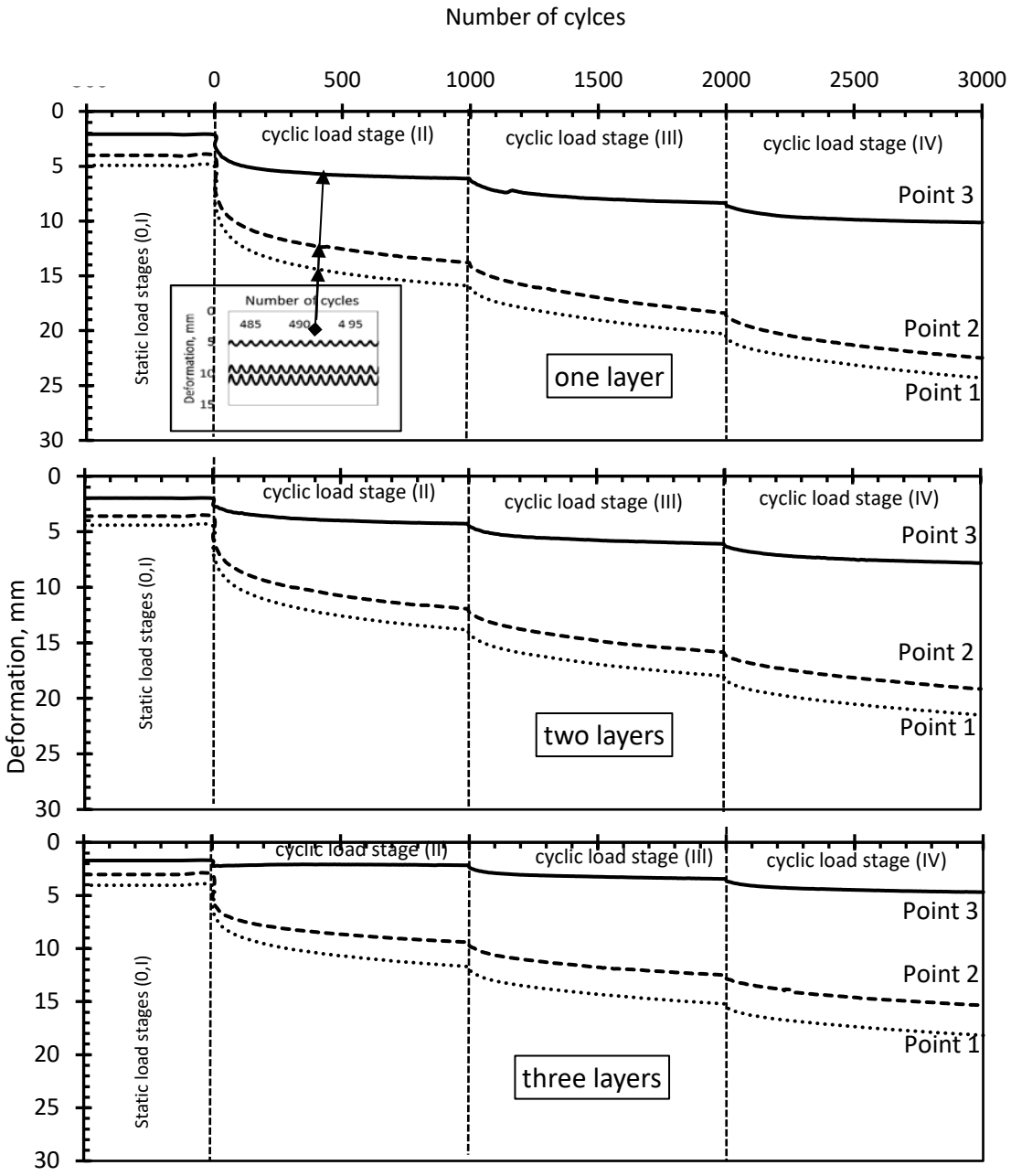

Figure 6.21. Deformations in the bottom reinforcement layer versus number of cycles of 200 mm reinforced embankment.

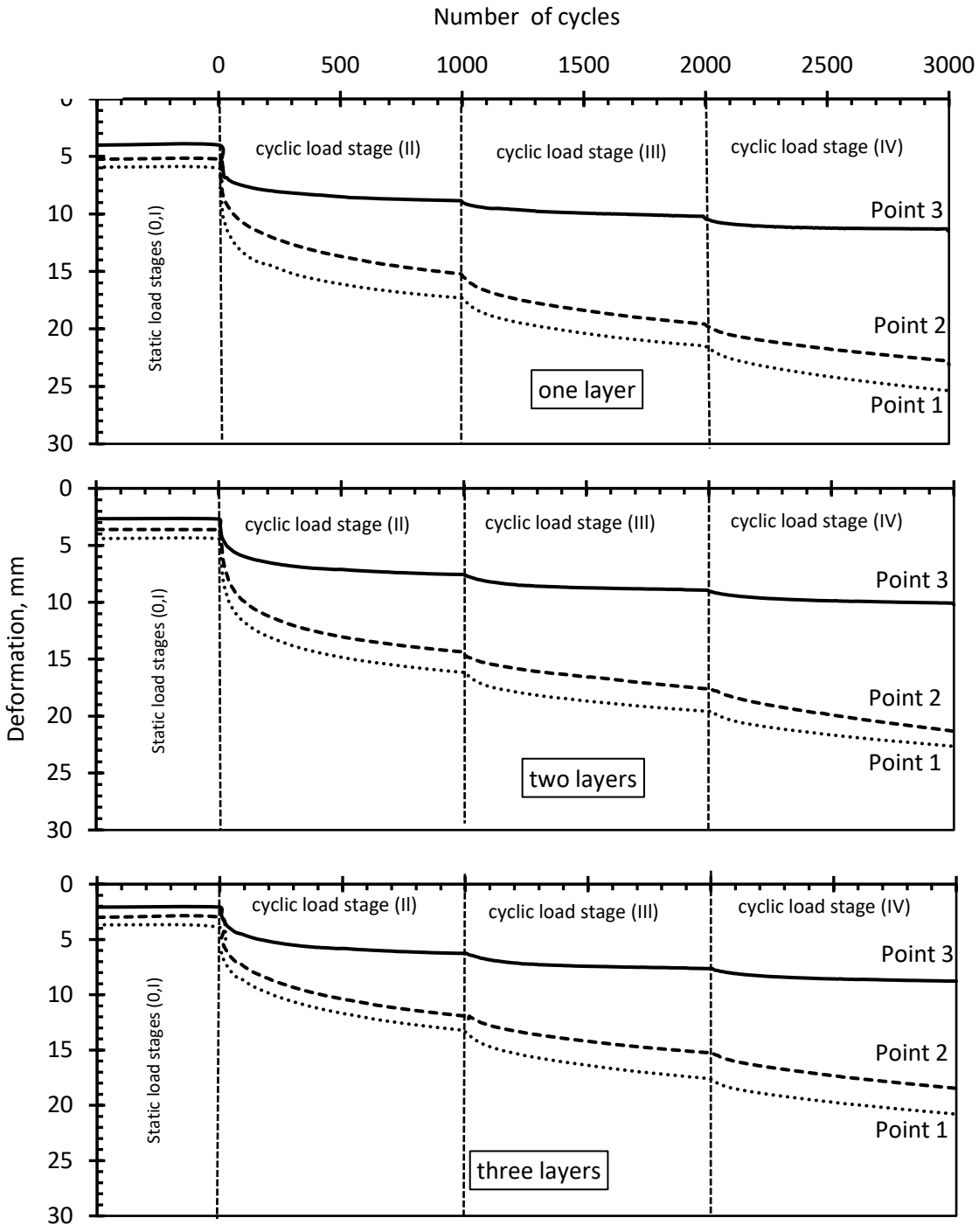

Figure 6.22. Deformations in the bottom reinforcement layer versus number of cycles of 400 mm reinforced embankment.

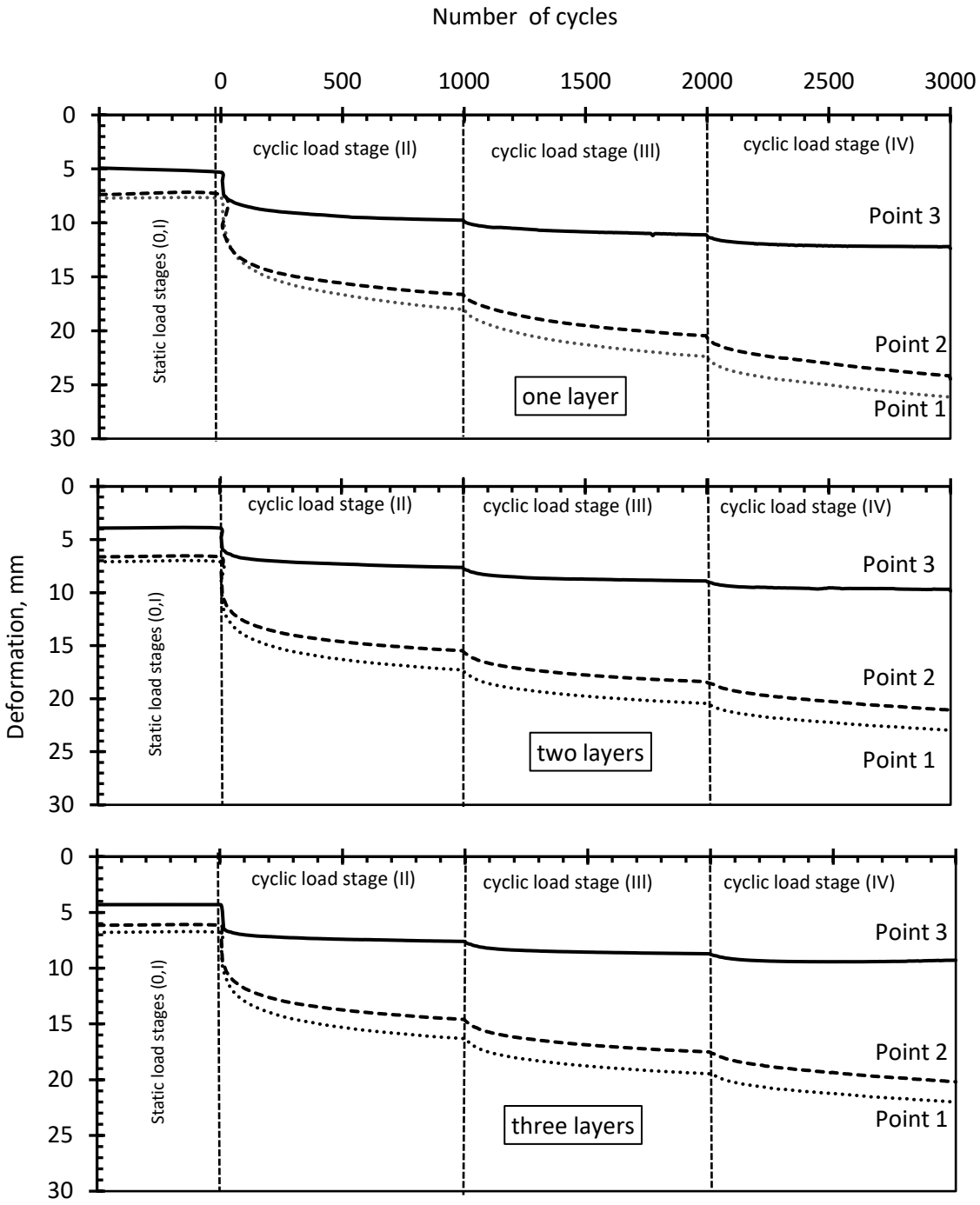

Figure 6.23. Deformations in the bottom reinforcement layer versus number of cycles of 600 mm reinforced embankment.

6.6 Settlements analysis

Figure 6.24 presents the measured maximum settlement of the loaded area from tests on unreinforced embankments of different heights versus the number of cycles. It can be seen that the measured settlement of the loaded

area increased with increasing the embankment height. Non-linear relationships for the measured surface settlement were very noticeable during the 1000 cycles of each stage of cyclic loading. It is clear that settlement decay occurred with further cycles. Increasing the pressure and amplitude resulted in increasing the settlement but at a lower rate.

Initially, the settlements were 3.50, 7.70 and 11.30 mm for 200, 400 and 600 mm unreinforced embankments respectively by the end of Stages 0 and I (static loads) as shown in Figure 6.24. However, During the first stage of cyclic loading (Stage II) the measured surface settlement started to increase significantly and then the rate of increase of the settlement decreased with further cycles. About 60 % 0f the settlement during this stage occurred during the first 100 cycle regardless of the embankment height. The settlements were about 17.50, 33.10 and 44.90 mm for 200, 400 and 600 mm high embankments respectively by the end of the first stage of cyclic loading (1000 cycles). When the applied load was increased the settlement was increased but with rate less than the first stage of cyclic loading. The settlements were 25.0, 43.40 and 59.70 mm at the end of Stage III and 32.50, 52.80 and 69.90 mm at the end of Stage IV for 200, 400 and 600 mm high unreinforced embankments respectively as shown in Figure 6.24.

It is clear the settlement increased with increasing the embankment height. This could be attributed to the increase in volume of soil of the embankment. Due to the unit weight of the fill being constant during all of the tests, the volume of voids was increased with increasing the embankment height resulting in an increase in the surface settlement. The reduction in the rate of settlement with further cycles could be attributed to the densification of the

embankment material. Inspection of the results indicated that approximately 54.0, 63.0 and 64.0 % of the total settlement of the 200, 400 and 600 mm unreinforced embankments respectively occurred by the end of first stage of cyclic loading (stage II) although the applied cyclic load during this stage was the lowest. This implied that significant rearrangement of soil particles occurred under the first stages of cyclic loading which in turn led to substantial densification of the embankment fill material as well as settlement of the underlying soft clay, consequently, increasing the interaction between the soil particles and reducing the surface settlement during the subsequent stages. Houda et al. (2016) concluded that about 50 % of the surface settlement of the unreinforced embankment occurred during the first 10 cycles of 50 cycles. In addition, the rate of reduction in void ratio of embankment material decreased with the number of cycles, which improved the arching effect.

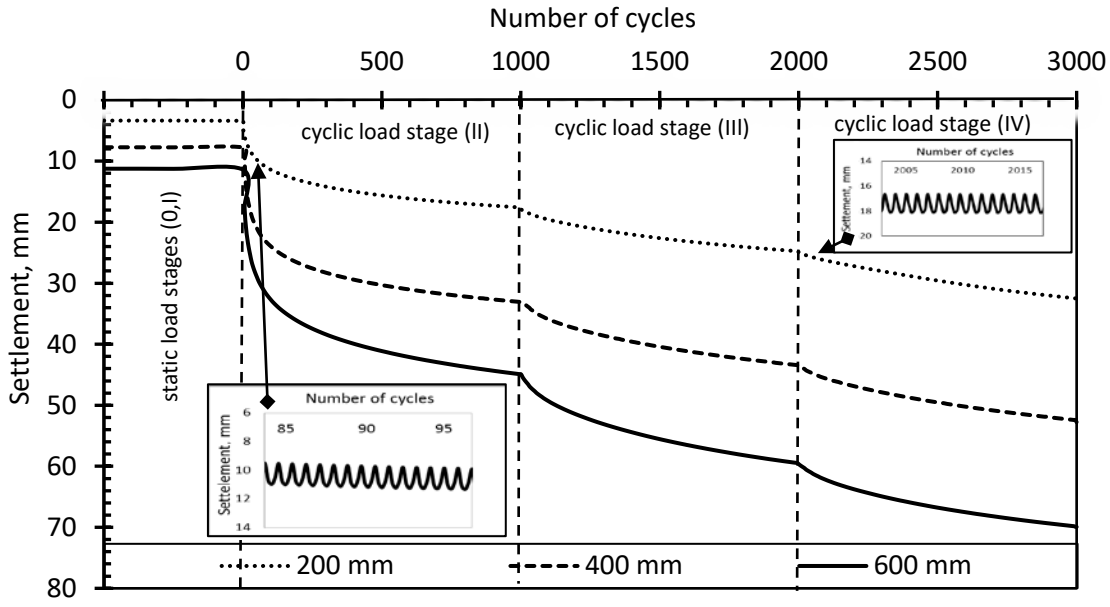

Figure 6.24. Settlements of loading plate versus number of cycles of different heights of embankment.

However, inclusion of reinforcement layers caused significant reduction to the observed surface settlement of the embankment as well as caused a further increase in the decay of settlement during Stages II-IV regardless the embankment height. Results of test on a 200 mm reinforced embankment with one layer showed a decreased settlement to 15.8, 21.8 and 26.8 mm at the end of stages II, III and IV respectively giving around 20 % reduction on the total settlement compared with unreinforced embankment as shown in Figure 6.25. When the embankment height increased to 400 and 600 mm, incorporation of one layer of reinforcement reduced the surface settlement at the end of first stage of cyclic loading to 27.8, 36 and 43.2 mm and 37.8, 52 and 62 mm respectively as shown in Figures 6.26 and 6.27. This is due to interaction between reinforcement layers and adjacent soils would improve which in turn contributes to the reduction in settlement in subsequent stages. When the number of reinforcement layers increased to two and three layers, the reduction in surface settlement was increased. However, the rate of settlement reduction was decreased with increasing the embankment height. Measured final settlements of 200, 400 and 600 mm reinforced embankments with one, two and three layers of reinforcement layers at the end of Stage IV were almost 26.8, 22.8 and 19.1 mm 43.6, 39.8 and 36 mm and 62, 60 and 58 mm respectively as shown in Figures 6.25, 6.26 and 6.27.

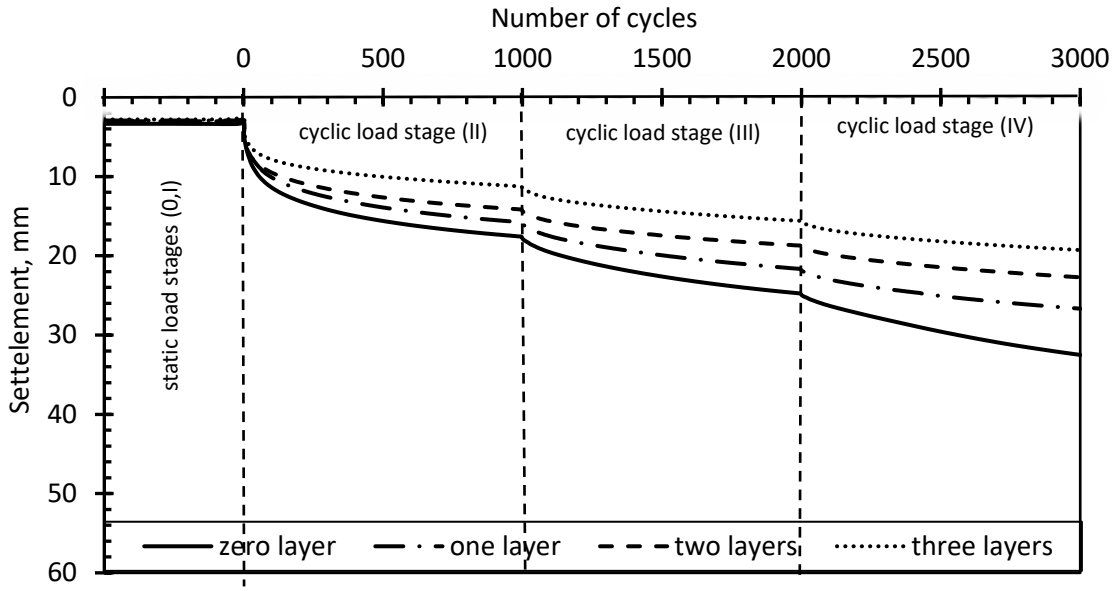

Figure 6.25. Settlements of loading plate versus number of cycles of 200 mm unreinforced and reinforced embankment.

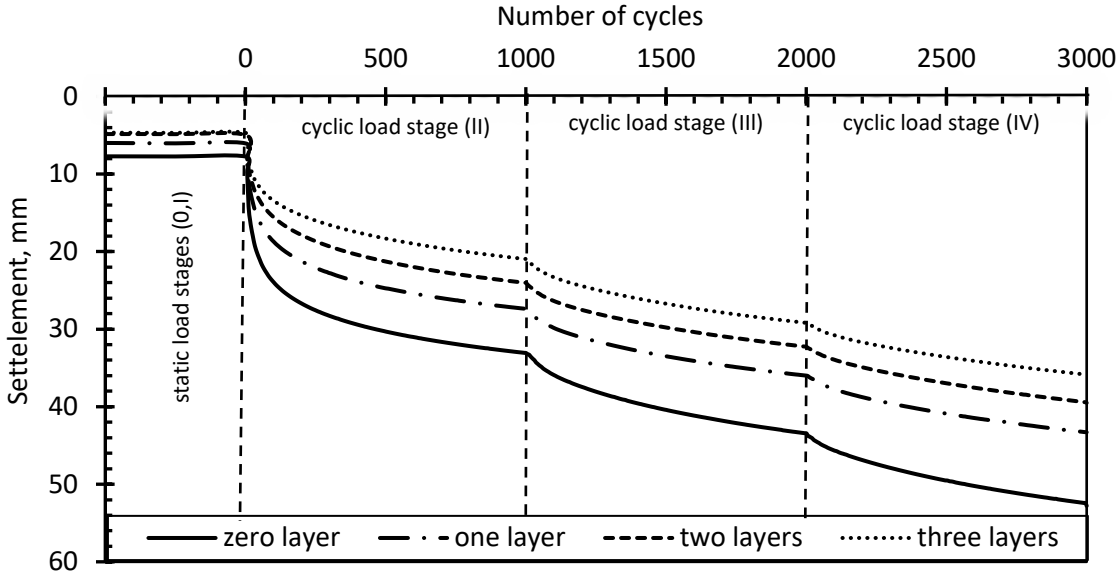

Figure 6.26. Settlements of loading plate versus number of cycles of 400 mm unreinforced and reinforced embankment.

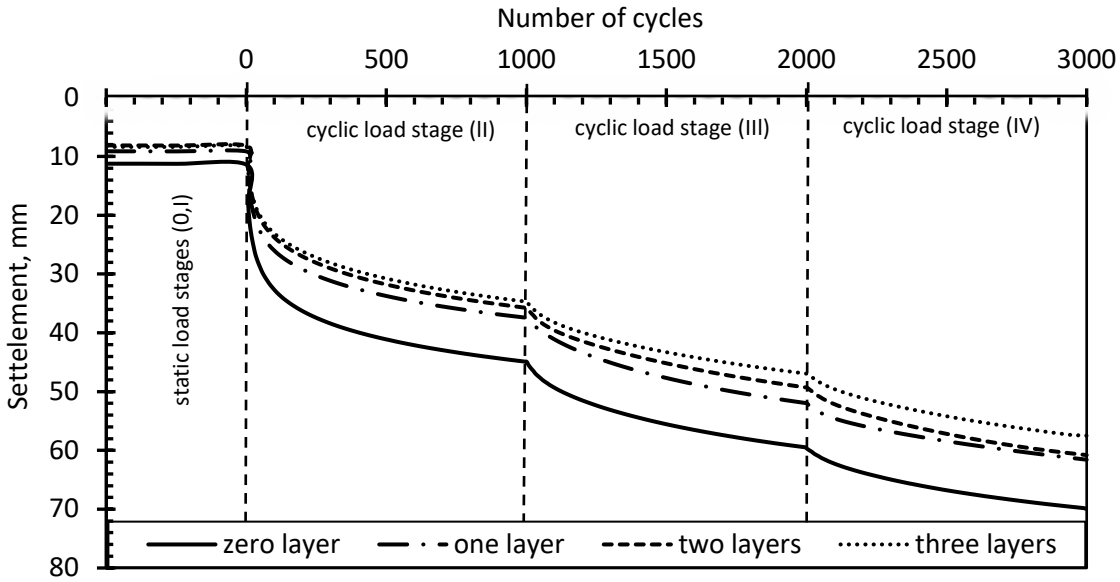

Figure 6.27. Settlements of loading plate versus number of cycles of 600 mm unreinforced and reinforced embankment.

Figure 6.28 shows the deformed shape of the embankment surface after the removal of the loading plate for 200, 400 and 600 mm unreinforced embankments. It was clearly seen that heaving the soil on both sides decreased with increasing the embankment height. The measured heave was reduced from 28.0 mm to 7.0 mm by increasing the embankment height from 200 mm to 400 mm as shown in Figure 6.28. When the height of the embankment was 600 mm, no heave was observed. This was attributed to the reduction of the unloaded areas by increasing the embankment height which resulted in decreasing the soft soil heave as well as the embankment surface heave.

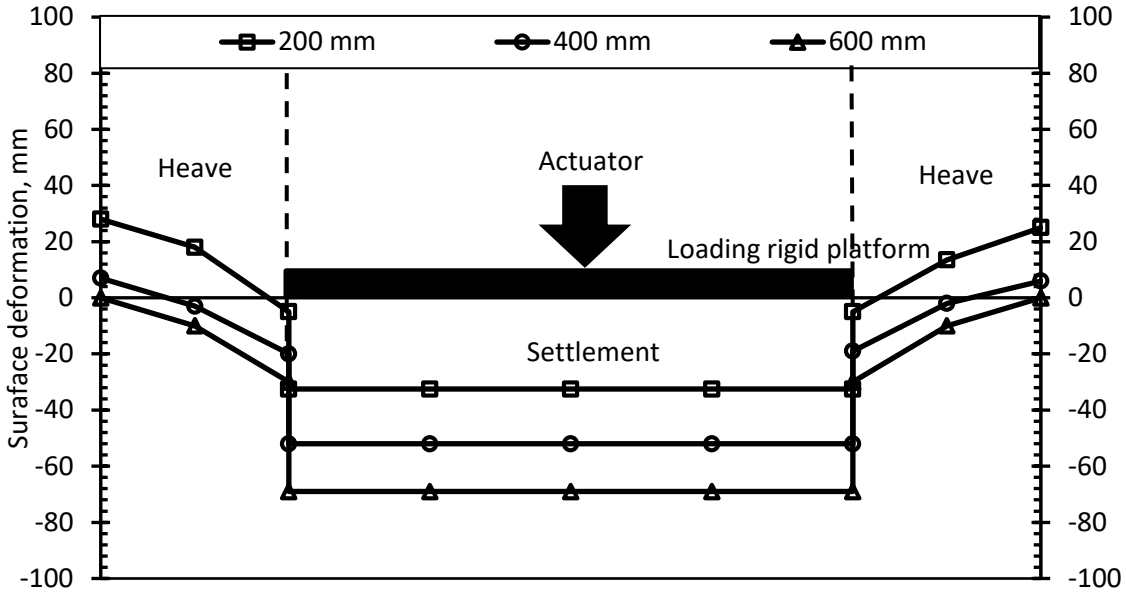

Figure 6.28. Soil surface settlement after removing the applied loads versus the box test distance of different heights of embankment.

Figure 6.29. Soil surface settlement after removing the applied loads of unreinforced embankment (A) 200 mm (B) 400 mm and (C) 600 mm.

Incorporating layers of reinforcement decreased the soil heave, especially for the embankment with a height of 200 mm a shown in Figure 6.30. Measured heave reduced from 28 mm to 1mm for unreinforced embankments and embankment reinforced with three layers of reinforcement respectively. However, nearly no heaving was observed in the embankments having heights of 400 mm and 600 mm as shown in Figures 6.31 and 6.32. The results therefore suggest that serious considerations need to be given to construction of unreinforced or lightly reinforced shallow embankments. Increasing the number of reinforcement layers clearly impacted positively on the experienced embankment soil heave due to the development of shear stresses along the reinforcement layers leading to increased confinement of the embankment material. Results of previous studies (see for example, Zhang et al. 2006; Latha and Murthy 2006) illustrated that inclusion of reinforcement layers on the soils leads to significant increase in the cohesion of reinforced soils which is deemed to be in the form of confinement. In addition, inclusion of reinforcement layers enhanced the load transfer mechanisms to pile caps and potentially reduced deformation of the underlying soft soil and embankment soil heave. The results of Rowe and Li (1999) suggested that increasing reinforcement stiffness caused a significant reduction in maximum vertical settlement and heave.

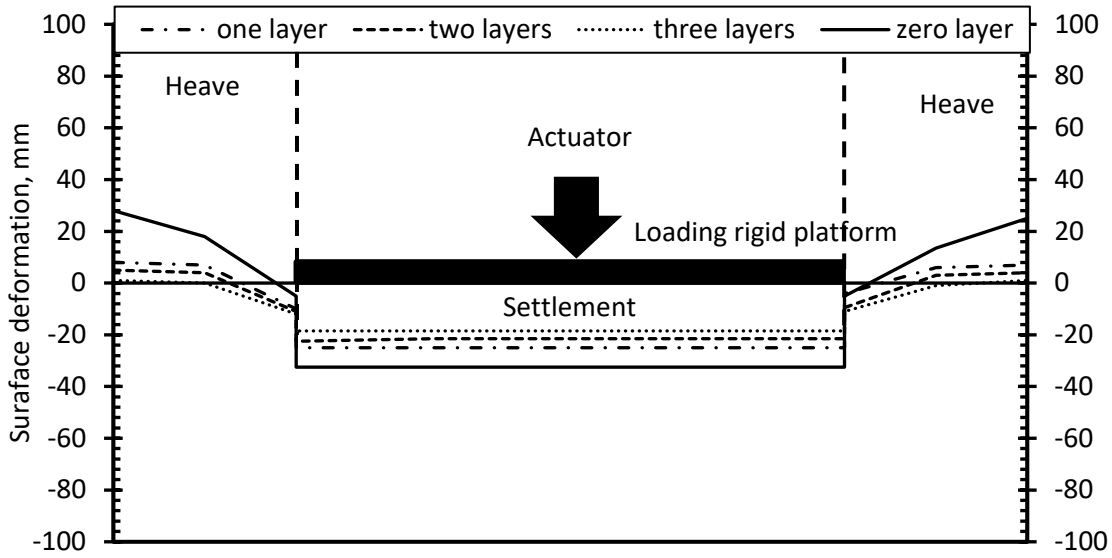

Figure 6.30. Soil surface settlement after removing the applied loads versus the box test distance of 200 mm embankment.

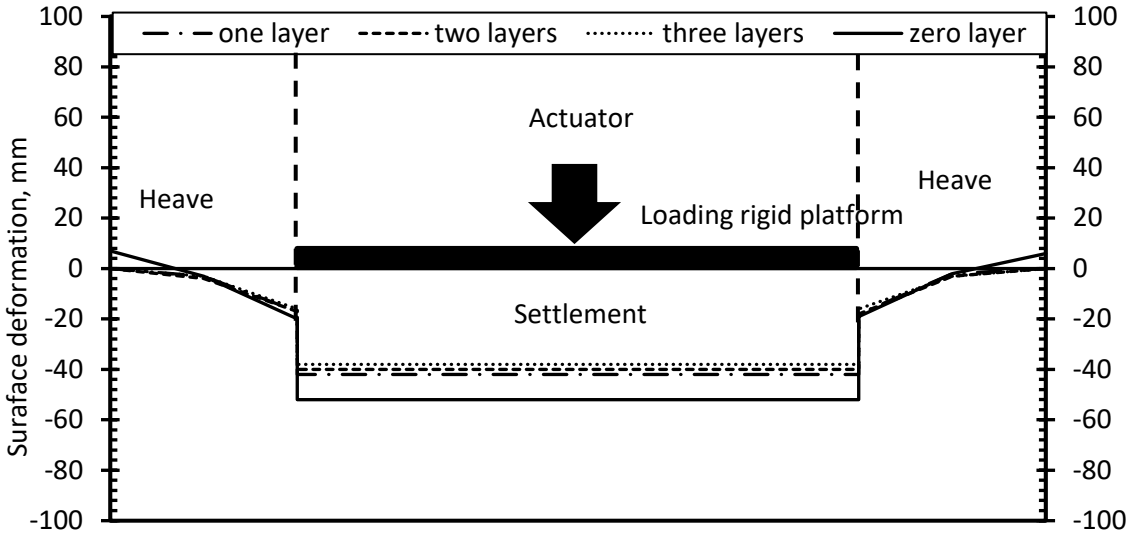

Figure 6.31. Soil surface settlement after removing the applied loads versus the box test distance of 400 mm embankment.

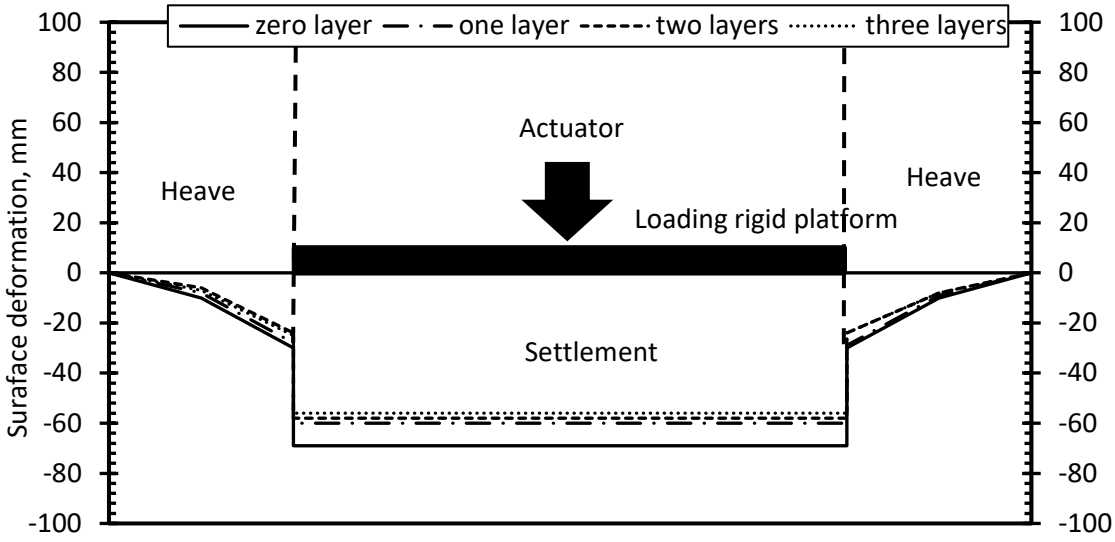

Figure 6.32. Soil surface settlement after removing the applied loads versus the box test distance of 600 mm embankment.

Figure 6.33. Soil surface settlement after removing the applied loads of three layers reinforced embankment (A) 200 mm (B)400 mm and (C) 600 mm.

Figure 6.34 shows the scanned deformation of the soft soil surface upon the completion of tests and removal of embankment materials of unreinforced embankment with different heights. It can be seen that distinct patterns of

deformation were formed in the central panel and the two neighbouring panels of soft soil. The central panel that was centred with the loading area showed a major compression and subsidence with maximum values recorded on the centreline. It can be noted that a slight reduction was observed in the central panel deformation when the height of the embankment was increased as shown in Figure 6.38. A significant difference in the soft soil deformation was observed in the two neighbouring panels of soft soil which showed a mix of subsidence and heave due to an increase in the non-uniform pressure caused by the external loading which resulted in increasing the lateral extent of the pressure. Major subsidence and heave were recorded with the thinner embankment and decreased with increasing the embankment height. This could be attributed to the increase the area of load distribution on the two neighbouring panels of soft soil which resulted in reduction in the pressure and therefore reduction in subsidence and heave of the soft soil as shown in Figure 6.34. However, although the increase of embankment height increases the spread of pressure on the two neighbouring panels, the pressure under the loading plate border was still higher than the pressure out the border of the loading plate which could be related to the high pressure applied by the external load. It was noticeable that heave on soft soil was always less than the subsidence.

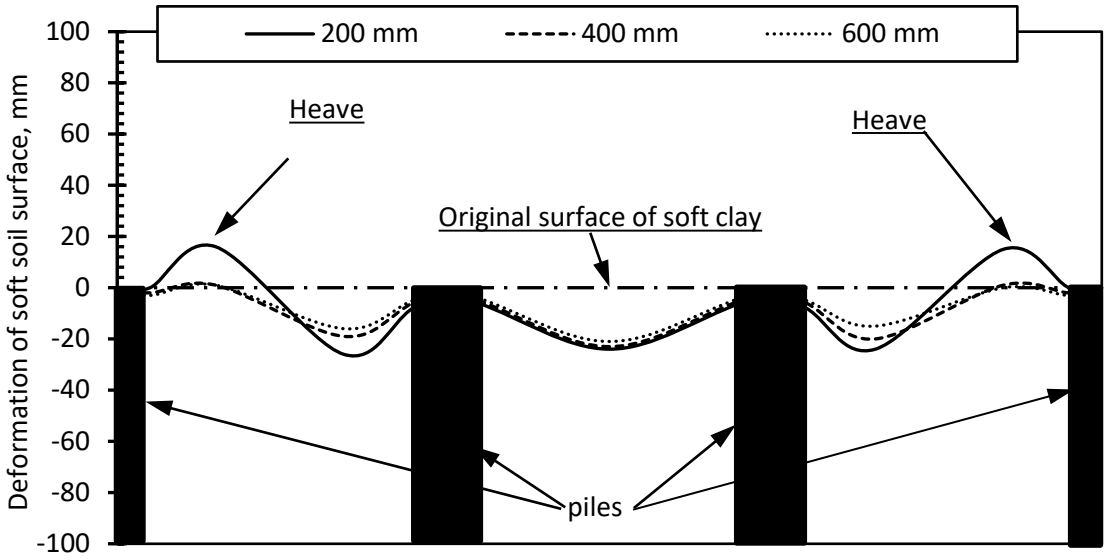

Figure 6.34. Measured deformations at the soft soil surface after completion of test of different heights of embankment.

Figure 6.35. Deformations at the soft soil surface after completion of test of 200 mm unreinforced embankment.

Also, the results showed a significant reduction on the subsidence of soft soil in the central panel as well as on the subsidence and heave in the two neighbouring soft soil panels with inclusion layers of reinforcement as can be seen in Figure 6.36. In addition, it can be seen that punching mechanism was occurred in the case of zero reinforcement layer at the boundary of middle piles. Also, it can be noted that, some degree of settlement at the boundary of

the pile in reinforced embankments was observed as shown in Figure 6.36 Of note, image analysis was performed in order to estimate the deformation at the piles boundary.

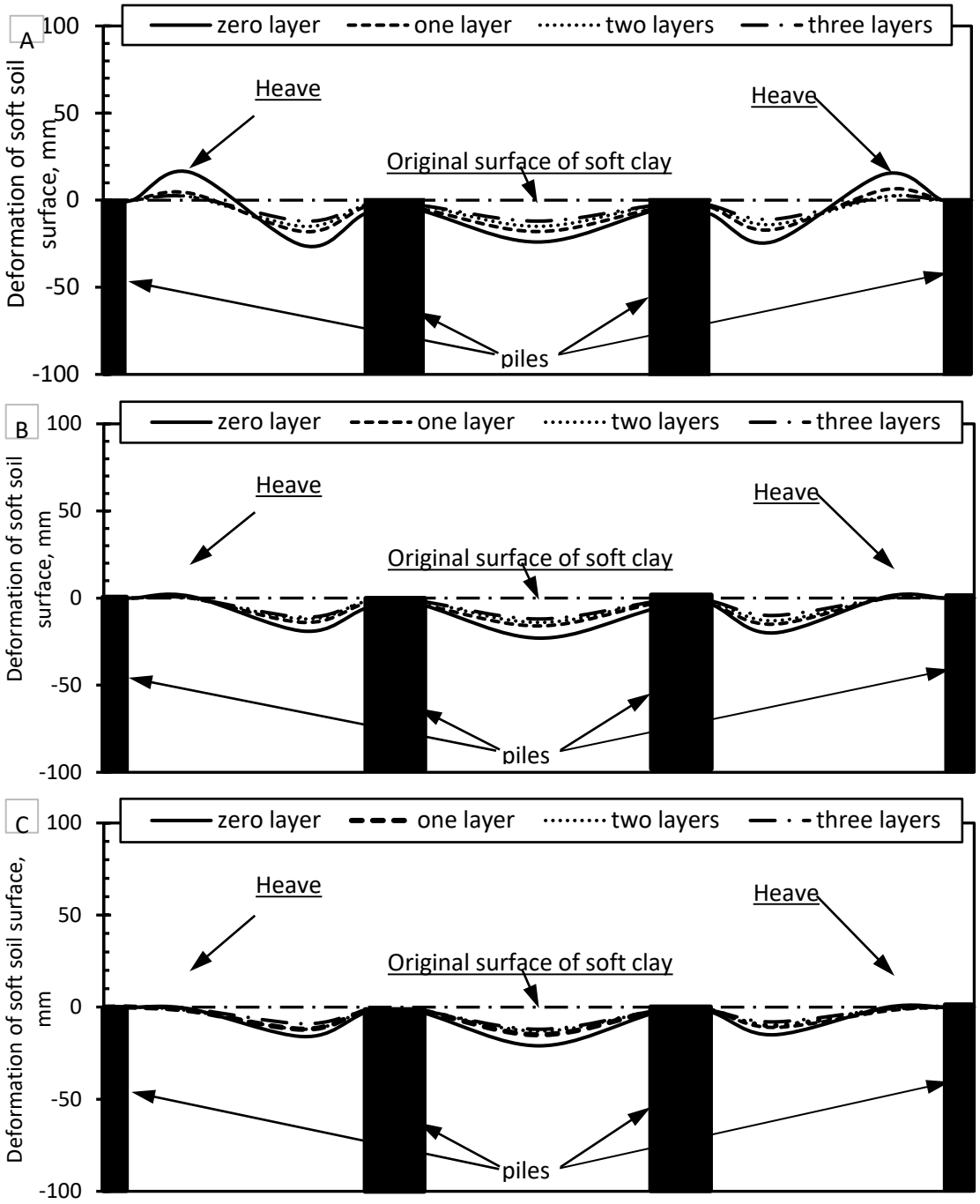

Figure 6.36. Measured deformations at the soft soil surface after completion of test of 200 mm embankment (A) 200 mm (B) 400 mm (C) 600 mm.

6.7 Comparison with the analytical methods

Experimental results are good sources for validation of analytical and numerical results. The test result in this study were compared with the analytical result which were calculated from Hewlett and Randolph (1988) equation which was presented as following:

.

$$\sigma_s = \left(\gamma H - \frac{\gamma s}{2}\right)\left(\frac{s-a}{s}\right)^{(k_p-1)} + \frac{\gamma(s-a)}{2} \qquad (6.3)$$

Hewlett and Randolph (1988) solution was used only for embankments without surcharges load. However, the pressure on the piles and soft soil was not only coming from self-weight and also due to the external loading, the equation 6.3 is amended to include the surcharges load as illustrated in equation 6.4 as following:

$$\sigma_s = \left(q + \gamma H - \frac{\gamma s}{2}\right)\left(\frac{s-a}{s}\right)^{(k_p-1)} + \frac{\gamma(s-a)}{2} \qquad (6.4)$$

Also, the test results were compared with Abusharar et al. (2009) analytical solution which was presented as following:

$$\sigma_s = \frac{\gamma\,(S-a)(k_p-1)}{2(k_p-2)} + \left(\frac{(S-a)}{s}\right)^{k_p-1}\left[q + \gamma H - \frac{\gamma S}{2}\left(1 + \frac{1}{k_p-2}\right)\right] \qquad (6.5)$$

where, σ_s is the stress on soft ground in (kN/m^2), K_P is the Rankine passive coefficient of earth pressure, γ is the unit weight of the embankment in (kN/m^3), H is height of embankment in (m), s is the centre to centre pile spacing in (m), a is the pile width in (m) and q is surcharge load in (kN/m^2).

Although, these equations have been developed for embankments under static loading conditions, the comparison with the test results can give better understanding of the effect of monotonic and cyclic loading on load transfer mechanism. As the measured surcharge loads during the cyclic loading stages varied between minimum value and maximum value, the maximum applied external load was only used to compare the experimental results and analytical results. Heitz et al. (2008) used the maximum applied surcharge load in order to calculate the stresses on the ground of the embankment by the analytical equation. Also, only the results of first stage of cyclic loading was used for the comparison due to the properties of the embankment and soft soil materials during the second and third stages of cyclic loading may be changed which may affect the calculation of the total applied load at the soft soil and piles level. In addition, the test result of 600 mm unreinforced embankment was only compared with the analytical result due to distribution of surcharge load at the soft subsoil and piles level was nearly the same.

Figures 6.37, 6.38 and 6.39 compare the loads on the soft soil and piles of 600 mm unreinforced embankment calculated from theses equations and the test results during the first, second and third stages. It can be seen that the load on soft soil and piles during the first stage of loading (overburden pressure) calculated from Abusharar et al. (2009), Hewlett and Randolph (1988)

equations and the test result were nearly the same shown in Figures 6.37 and 6.38. However, under the monotonic loading condition, the load calculated by analytical solutions on soft soil was gradually less than the test results while the load on piles calculated by the two methods was gradually higher than the measured load. The load on soft soil was 3.10, 3.08 and 4.46 kN while the load on piles was 3.90, 4.11 and 2.37 kN from Abusharar et al. (2009), Hewlett and Randolph (1988) and test results respectively as shown in Figures 6.37 and 6.38. This meant that there was a difference on measured load and calculated loads from the analytical methods. This difference might have occurred due to i. the speed rate of the monotonic load and ii. Applying external load via specific area leading to concentrate the pressure on area under the loading plate.

Under the cyclic loading conditions the measured load on soft soil and piles was significantly different from the results of the analytical solutions. The load on soft soil was 7.78, 4.5 and 4.39 kN while the load on piles was 2.46, 6.0 and 6.14 kN from the test results, Abusharar et al. (2009) and Hewlett and Randolph (1988) respectively as shown in Figures 6.37 and 6.38. This could be attributed to i. the reduction in the arching effect which occurred under the cyclic loads leading to increase the pressure on the soft soil and decrease the pressure on the piles, ii. concentration of loads in area under the loading plate in the middle of test rig as shown in Figures 6.37 and 6.38. In addition, in order to validate the experimental results, the total loads on the soft soil and piles measured in the experimental test were summed and then compared with the summation of loads on soft soil and piles calculated from the analytical solutions. The results from Figure 6.39 showed that the measured load and

calculated load was nearly the same which meant that the difference in the load on the soft soil or on the loads on the piles between the experimental and analytical results is related to the effect of cyclic loads and the loading area.

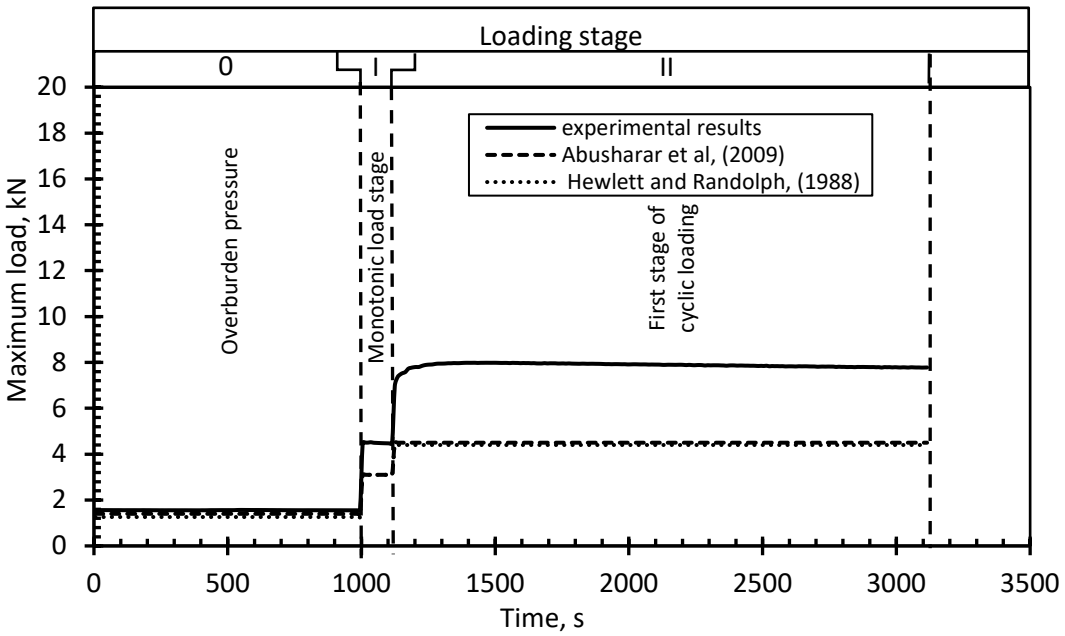

Figure 6.37. Comparison between test results and analytical results of 600 mm unreinforced embankment (maximum load on soft soil).

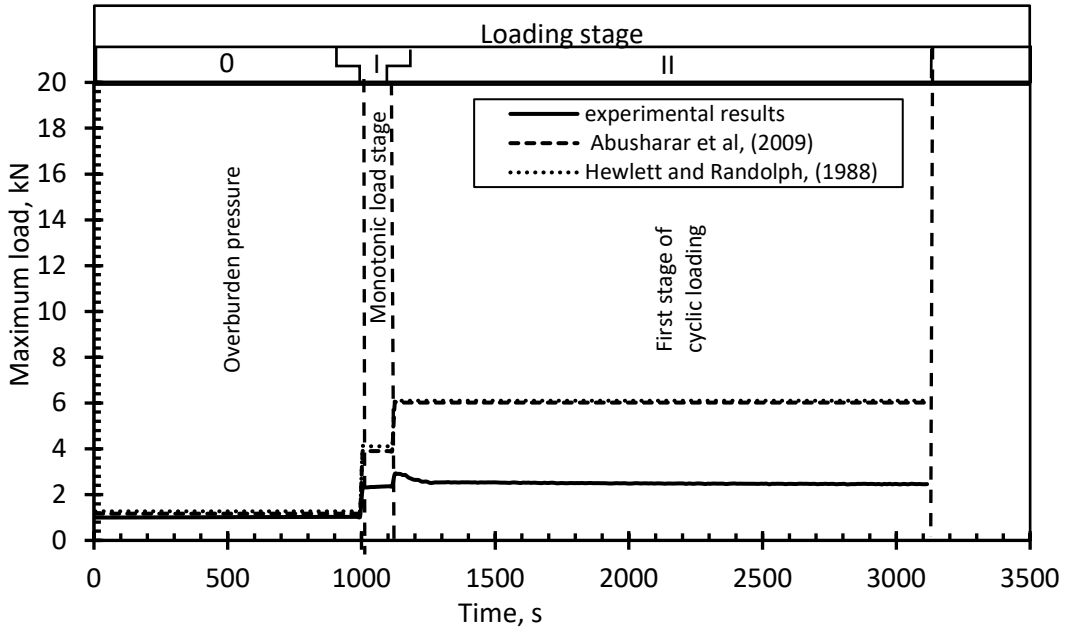

Figure 6.38. Comparison between test results and analytical results of 600 mm unreinforced embankment (maximum load on pile).

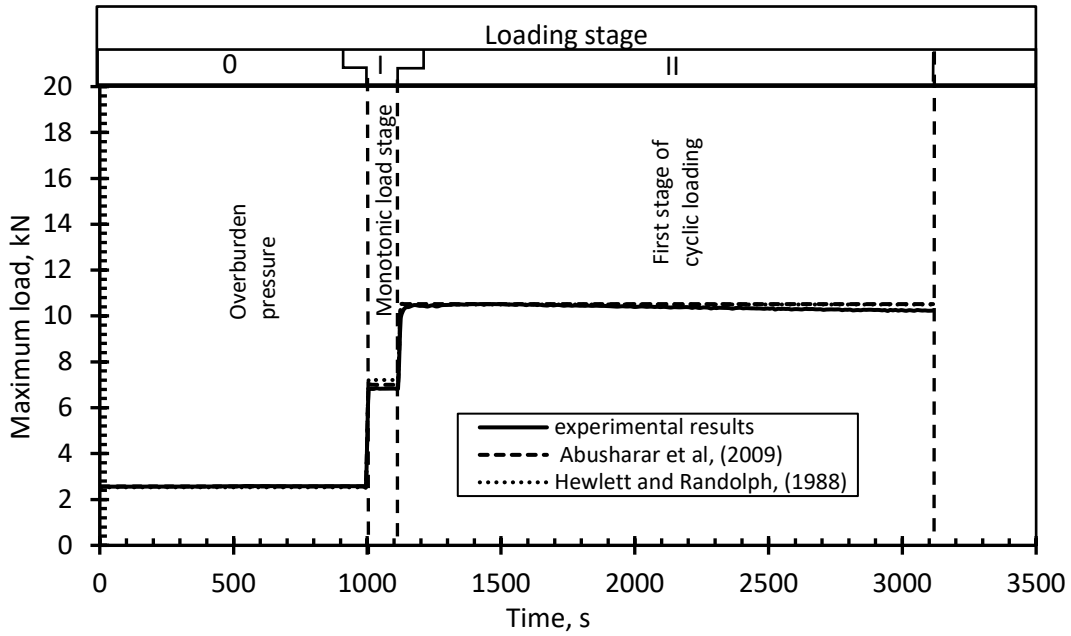

Figure 6.39. Comparison between test results and analytical results of 600 mm unreinforced embankment (maximum load on pile +soft soil).

6.8 Effect of loading area

Although applying external surcharge load over the whole area of the embankment increases the distribution of the pressure at level of soft soil and pile compared with applying the same external load on small zone of the embankment, it is beneficial to investigate the effect of the size of loading area on the load transfer mechanisms. This factor may be more important when the embankment weight is less than the applied external load. Figures 6.40, 6.41 and 6.42 compare the maximum pressure on piles and soft soil, the maximum surface settlement and the maximum deformation in reinforcement layer during different stages of loading on 200 mm reinforced embankment and the following notes can be drawn. i. There is a difference in the distribution of stresses within the embankment fill when the external load was applied via particular area, On other words, the maximum pressure was occurred in the central area of the embankment directly under the loading plate leading to

pressure concentration on the central panel of the soft soil and piles and leading to higher stresses in this region of the embankment as shown in Figure 6.40. ii. The surface settlement was small and constant over the whole embankment surface when the surcharge load was applied over the whole embankment area. However, applying the external load on specific area of the embankment caused large settlement under the loading area and small settlement or heave in the unloading areas as shown in Figure 6.41. iii. deformation in reinforcement layers was nearly equal in all panels under the equal external pressure on the embankment while there was a significant difference in the deformation between the panels under the loading area and the panels out of the loading area as shown in Figure 6.42.

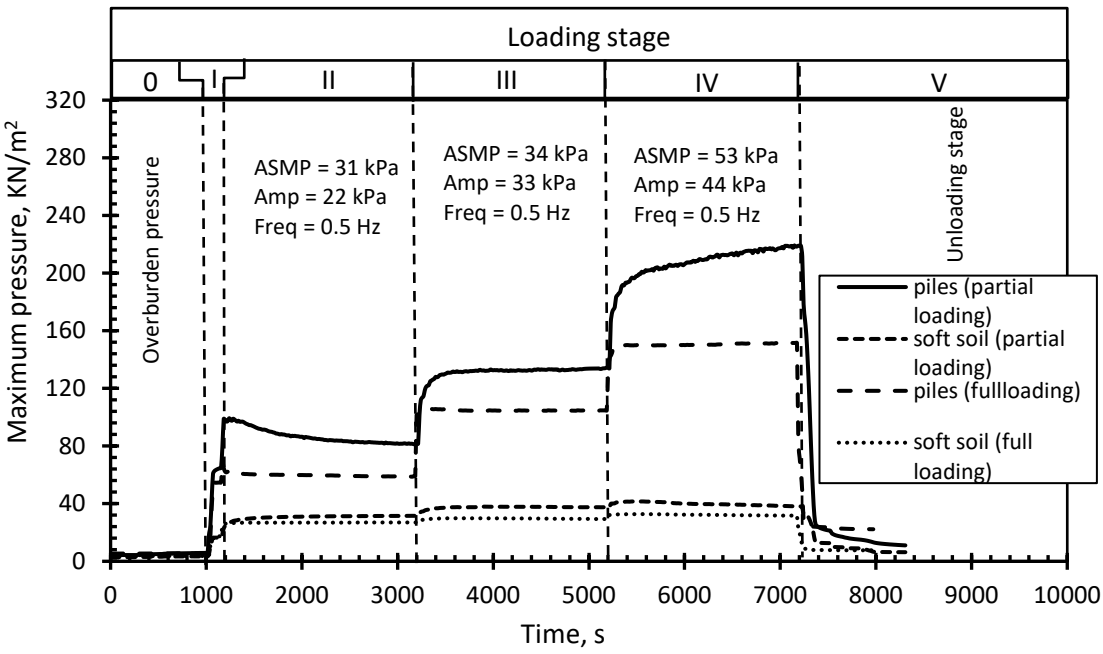

Figure 6.40. Maximum pressure on pile caps and soft soil for 200 mm one layer reinforced embankment.

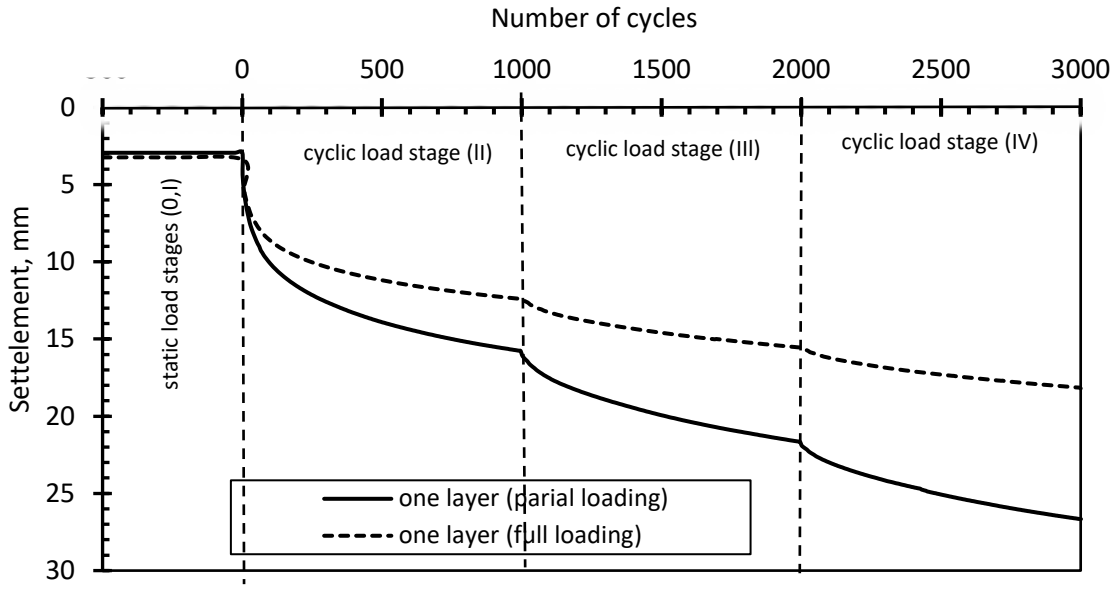

Figure 6.41. Settlements of loading plate versus number of cycles of 200 mm one layer reinforced embankment.

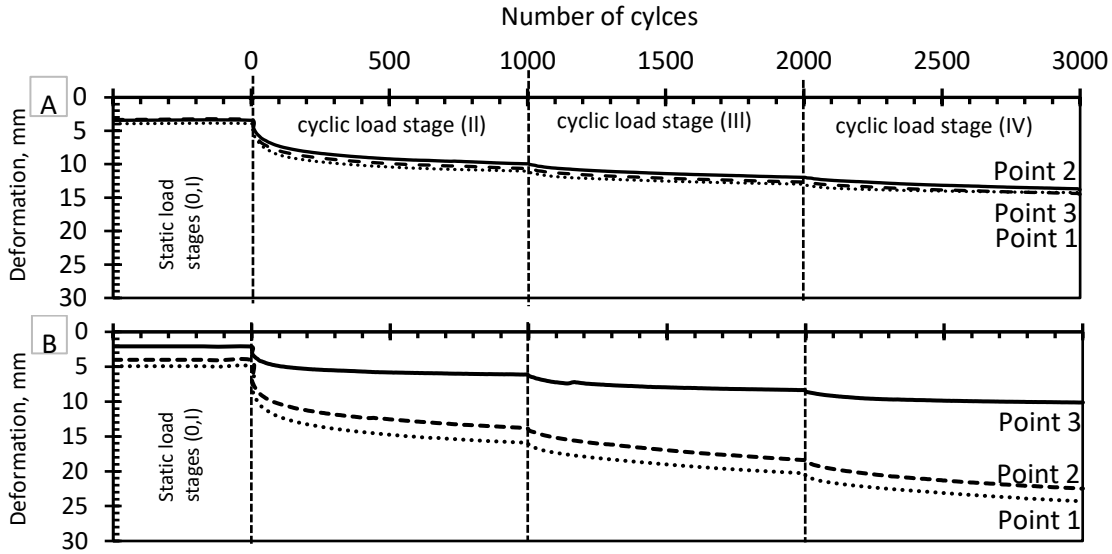

Figure 6.42. Deformations in the reinforcement layer versus number of cycles of 200 mm one-layer reinforced embankment (A) full loading (B) partial loading.

6.8 Summary

In this chapter the effect of three stages of cyclic loading applied on particular areas of unreinforced and reinforced shallow piled embankments of different heights was experimentally investigated and analysed. The experimental

results showed that the transfer of loads to the piles was increased during the monotonic loading stage but at a lower rate with increasing the embankment height. Under cyclic loading conditions the results showed clearly that collapse of soil arching is imminent and occurs during the first few cycles of load regardless of the embankment height. However, by increasing the number of cycles, arching of the soil started to improve again with the number of cycles due to densification of the embankment material and deformation of the subgrade soft soil. Including layers of reinforcement increased the magnitude of the loads transfer on piles cap. However, the improvement was more obvious for a thinner embankment. Also, the results clearly showed a significant reduction in surface settlement, soft soil settlement and heaving with increasing the number of reinforcement layers. Almost 50% of the surface settlement occurred during the first 100 cycles of cyclic loading. Increasing the embankment height increased the embankment settlement and reduced the heave. It is clear that the most crucial reinforcement layer appears to be the bottom one as it had the highest tension force and the tension in reinforcement layers increased with increasing the embankment height.

CHAPTER SEVEN

CONCLUSIONS AND RECOMMENDATIONS

7.1 Conclusions

In this study, a programme of experiments was carried out to acquire deep understating of the behaviour of unreinforced and reinforced shallow piled embankments under monotonic and cyclic loading conditions that applied via specific area. Two preliminary tests were also conducted to help undersigning and design of the main experimental tests. The results were presented and discussed in chapters 4,5 and 6. Summary and conclusion of the attained results are presented hereafter in this chapter.

A. Strength and deformation of reinforced soils subject to monotonic and repeated loads

Repeating Loading California Bearing Ratio (RL-CBR) experiments were carried out in order to assess the effects of i) placing layer of replacement granular materials with different thicknesses above soft subgrade soil, ii) location of reinforcement layer iii) number of reinforcement layers and iv) deformation characteristics of samples tested to the same level of loading. From the results of these experiments, the following conclusions could be drawn;

- Repeated cycles of loading and unloading increase the plastic deformation and total deformation of clay soil by 59 %. The rate of increase in plastic deformation is more prominent.
- Placing layers of sand above clay soil causes an increase in the load carrying capacity of clay soil. A remarkable increase of 75 % was

noticeable in the case of using a 40 mm thick layer of sand overlying a clay subbase.

- Placing a layer of reinforcement at the interface between clay and sand leads to further increase in the strength and load carrying capacity of reinforced samples as well as decreasing the deformation significantly.
- Position of reinforcement layer can significantly affect the strength of soil. The highest improvement was recorded when the location of the reinforcement layer was within the bottom third of the granular material.
- Using multiple layers of reinforcement leads to a significant increase in the strength of soil and a decrease in the settlement. It was found that the degree of improvement is directly related to the number of reinforcing layers.
- Attempts to find out the number of loading cycles required to reach the same deformation on reinforced samples was found to be unpractical. The total deformation is smaller and stays constant irrespective of the number of cycles, in particular for samples with three layers of reinforcement.
- Addition of replacement sand layer and reinforcement result in a reduction in the determined resilient modulus and enhancement of secant modulus.

B. Analysis of sequential active and passive arching in granular soils

A comprehensive laboratory investigation was conducted to explore the effects of sequential active and passive arching on the load transfer and re-

distribution of stresses using the well-known trapdoor test. The following conclusions can be drawn out of the presented results and discussion;

- Despite attainment of classical relationships for the normalised load during monotonic active and passive modes, significant change on the redistribution of loads occurs under sequential alteration of active and passive resistance. This highlights that relying on maximum resistance and minimum loads on the inclusion as a result of complete passive and active arching respectively seems not sustainable and requires special care.
- The results suggested that substantial weakening of soil arching occurs during the second cycle of active and passive arching onwards. This could be attributed to; localisation of deformation along the same slip planes causing shear bands ii. Shearing of the soil mass during the first cycle reducing the shear resistance along the slip planes and iii. Permanent change in the vertical stress from the previous arching mode whether active or passive.
- The lateral earth pressure coefficient is a good analogue reflecting changes of principal stress during active and passive modes. It is clear that the suggested value of K=1.0 by Terzaghi (1943) is still appropriate for sedimentary granular materials at large displacement. Likewise, a value of k=0.25 would appear to be reasonable for passive resistance during the passive mode.
- Increasing the displacement of the yielding inclusion showed limited effect of redistribution of loads and soil arching due to reaching the ultimate state.

- The load on the inclusion is dependent on the magnitude of displacement prior to reaching the relatively stable load. The data suggest that hysteresis in the relationship between normalised load and normalised displacement exists and is dependent on the displacement and route followed. Different paths are followed upto reaching maximum or minimum pressure on the inclusion.
- The critical height was affected significantly under repeated conditions of active and passive modes due to the collapse and/or reduction of soil arching.
- The results suggested that dilation of soil improves with increasing burial heights as a result of formation of full arching and leading to lowered loads on inclusion during yielding and improving capacity to absorb upward displacement during passive mode.

C. Analysis of shallow reinforced piled embankment with different heights subject to cyclic loads

An experimental programme was undertaken using a fully instrumented testing rig to assess the behaviour of unreinforced and reinforced shallow piled embankments with different heights under monotonic as well as cyclic loadings. Soft clay material was used as a subgrade soil whereas the embankment was built from a typical graded sand. Five loading stages were applied in each test. The following conclusions can be drawn out of the presented results and discussion.

- During stage 0 (self-weight of embankment), the pressure on piles increased with increasing the embankment height due to the arching

effect. Also, a slight increase on the pressure in pile caps was noted with increasing number of reinforcement layers. During the monotonic loading stage distinctive difference occurred in the pressure transferred to pile caps in which surface pressure was increased to 31kPa. This could be attributed to the pure arching effect in the case of unreinforced embankment and combination of load transfer mechanism in reinforced embankments. However, the rate of increase was decreased with increasing the embankment height.

- The results suggest that shallow unreinforced embankments perform poorly under the effect of cyclic loadings irrespective of the height of the embankment. Collapse of arching is imminent which could lead to significant transfer of surface loads to soft ground. However, the effect of cyclic loading was decreased with increasing embankment height. In addition, it was apparent that regain of strength due to densification of embankment material and deformation of soft subgrade soil would lead to partial or full recovery of arching effect with further stages of cyclic loadings. However, the rate of improvement was decreased with increasing the embankment height.
- Good degree of improvement in response and performance of piled embankment was noticeable with the inclusion of increased number of reinforcement layers, regardless of the embankment height. However, the rate of improvement was decreased with raising the embankment height. Also, including layers of reinforcement increased the stability of the soil arching and increased with increasing the number of reinforcement layers. However, increasing the embankment height

reduces the effect of multiple layer systems due to the increase of formation of soil arching.

- The tension force in reinforcement layers was measured to be at highest in the bottom reinforcement layer and reduced with increasing number of reinforcement layers. The tension in the reinforcement layers was increased with increasing the embankment height due to the pressure on the reinforcement layers on the neighbouring panels being increased with increasing the embankment height. Also, multiple layer systems work as stiffened platforms for thinner embankments. However, by increasing the embankment height, multi-layer systems seem to work as tensioned membranes. However, some reduction in the tension was observed during the second and third stages of cyclic loading due to creep effect. This effect was reduced with increasing embankment height.
- Increasing embankment height leads to increasing the surface settlement and decreasing the heaving of soil. Almost 50 % of the surface settlement occurred during the first 100 cycles of cyclic loading. Also, Increasing the number of reinforcement layers led to remarkable reduction on the measured surface settlement and deformation (e.g. settlement and heave) of soft soil regardless of the height of embankment.

7.2 Recommendations for future work

This work has given considerable insight into the effect of cyclic loads on the arching behaviour and tensioned membrane in reinforced piled embankment, and also considered the effects of repeating sequential active and passive

arching on the distribution of the stresses within granular soil. However, there is still some work which could be undertaken in the future:

- Further research has to be carried out to investigate the effect of different parameters under cyclic loading conditions such as soft soil thickness and consolidation time, reinforcement stiffness, pile width on the load transfer mechanism.
- In this study 2D experimental work was carried out under cyclic loading conditions. However, further experimental work in 3D has to be conducted.
- In this study the effect of multi layers of geosynthetics reinforcement was examined. However, studying the effect of increasing the stiffness of single geosynthetic reinforcement layer instead of using two or three layers of geosynthetic with low stiffness under cyclic loading condition is recommended.
- Applying loads via specific area on the embankment surface caused difference between the pressure on the middle piles and the pressure on the side piles as well as between the pressure on soft soil in middle panel and the pressure on soft soil in the neighbouring panels. However, more work is needed to measure the pressure on the sides of the piles and neighbouring panels.
- Applying cyclic loads on the embankment surface caused some densification in the embankment fill materials. The degree of densification is dependent on the degree of fill compaction prior to starting the tests. However, further studies should be carried out to

evaluate the effect of compaction degree on the load transfer mechanisms.

- It was noted that some amount of soft soil water content was raised up about 20 mm above the soft soil level, especially in the middle panel, due the consolidation under the applied cyclic loads. This amount of water was mixed with a layer of fill materials which is located directly above the soft soil level, as a result the properties of this part of fill soil and soft soil were changed. However, further studies should be conducted to study these effects.

REFERENCES

Abusharar, S. W., Zeng, J. J., Chen, B. G. and Yin, J. H. (2009) A simplified method for analysis of appiled embankment reinforced with geosynthetics. *Geotextiles and Geomembranes,* 27, 39-52.

Adachi, T., Kimura, M., Nishimura, T., Koya, N., and Kosaka, K. (1997) Trap door experiment under centrifugal conditions. Deformation and Progressive Failure in Geomechnics, *IS-Nagoya'97*, pp.725-730.

Ahmed Kamel, M., Chandra, S. and Kumar, P. (2004) Behaviour of subgrade soil reinforced with geogrid. *International Journal of Pavement Engineering,* 5, 201-209.

Almeida, M. S. S., Ehrlich, M., Spotti, A. P. and Marques, M. E. S. (2007) Embankment supported on piles with biaxial geogrids. P*roceedings of the Institution of Civil Engineers-Geotechnical Engineering,* 160(4), 185-192.

Araya, A. A., Huurman, M., Houben, L. J. and Molenaar, A. A. (2011) Characterizing mechanical behavior of unbound granular materials for pavements. *In Transportation Research Board 90th annual meeting.*1-17.

Araya A. A., Molenaar A. A. and Houben L.J. (2012) "Investigation of the resilient behavior of granular base materials with simple test apparatus", *Materials and structures*, Vol. 45(5), pp.695-705.

Ariyarathne, P., Liyanapathirana, D. S. and Leo, C. J. (2013) Effect of geosynthetic creep on reinforced pile-supported embankment systems. *Geosynthetics International,* Vol. 20(6), pp. 421-435.

Ariyarathne, P. U. (2014) *Numerical modelling of geosynthetic reinforced pile-supported embankments* (Doctoral dissertation, University of Western Sydney (Australia)).

Ariyarathne, P. and Liyanapathirana, D. S. (2014) Significance of geosynthetic reinforcement in embankment construction. *Australian Geomechanics Journal,* 49(3), pp.15-28.

Asakereh, A., Ghazavi, M. and Tafreshi, S. M. (2013) Cyclic response of footing on geogrid-reinforced sand with void. *Soils and Foundations,* 53, 363-374.

Ashs, M. N. and Latha, G. M. (2010) Modified CBR Tests on Geosynthetic Reinforced Soil-aggregate Systems, *Indian Geotechnical Conference,* December 16–18, 2010, Pages 297–300

Ashs M. N., and Latha G. M. (2011) Bearing resistance of reinforced soil–aggregate systems, *Proceedings of the Institution of Civil Engineers, Ground Improvement.* Volume 164 Issue GI2, 2011, Pages 83–95

Ashs, M. N. and Latha, G. M. (2012) Strength behaviour of reinforced soil – aggregate system under repeating and cyclic loading, *Geo Congress: State of the art and practice of geotechnical engineering*, *Oakland, California, USA, American society of civil engineering* (2012) 1513-1522

Azizi, F. (1999). *Applied analyses in geotechnics*. CRC Press.

Blanc, M., Thorel, L., Girout, R. and Almeida, M. (2014) Geosynthetic reinforcement of a granular load transfer platform above rigid inclusions: comparison between centrifuge testing and analytical modelling. *Geosynthetics International,* 21(1), pp.37-52.

Borges J. L. and Marques D. O. (2011) Geosynthetic-reinforced and jet grout column-supported embankments on soft soil: Numerical analysis and parametric study. *Geotextiles and Geomembranes,* 38, 883-896

British Standards Institution (1990) *BS 1377:1990. Methods of test for soils for civil engineering purposes-Part 2: Classification tests*. London: British Standards Institution.

British Standards Institution (1990) B*S 1377:1990. Methods of test for soils for civil engineering purposes-Part 4: Compaction-related testes* London: British Standards Institution.

British Standards Institution (1999) *BS 5930:1999 Code of practice for site investigations*

British Standards Institution (2002), *BS EN ISO 14688 - 1:2002 Geotechnical investigation testing Identification and classification of soil, Part 1: Identification and description*

British Standards Institution (2004) *BS EN ISO 14688 - 2:2004 Geotechnical investigation testing Identification and classification of soil, Part 2: Principles for a classification of soil.*

British Standards Institution (2015) B*S EN ISO 10319:2015 - Geosynthetics. Wide-width tensile test, British Standards Institution,* London, United Kingdom.

British Standard, BS8006 (1995). Code of practice for strengthened/reinforced soils and other fills. British Standards Institution, London

British Standard, BS8006-1: (2010). Code of practice for strengthened/reinforced soils and other fills. British Standards Institution, London.

Carlsson, B. (1987) Reinforced soil, principles for calculation, Terratema AB, Linköping (in Swedish).

Chegenizadeh, A. and Nikraz, H. (2012) CBR test on fibre reinforced silty sand. *International Journal of Civil and Structural Engineering*, 1(3), pp.1-5.

Chevalier, B., Combe, G. and Villard, P. (2007) Experimental and numerical studies of load transfers and arching effect in the trap-door problem. *Laboratoire Sols, Solides, Structures-Risques, Grenoble, France.*1-10

Chevalier, B., Combe, G. and Villard, P. (2008) Experimental and numerical studies of load transfers and arching effect. In Proc., 12th Int. Conf. of the *Int. Association for Computer and Advances in Geomechanics (IACMAG), Goa, India* (pp. 273-280). Tucson, AZ: Iacmag.

Chevalier, B., Combe, G. and Villard, P. (2009) Experimental and Numerical Study of the Response of Granular Layer in the Trap-door Problem. *In AIP Conference Proceedings* (Vol. 1145, No. 1, pp. 649-652).

Chevalier, B., Combe, G. and Villard, P.(2012) Experimental and discrete element modeling studies of the trapdoor problem: influence of the macro-mechanical frictional parameters. *Acta Geotechnica,* 7(1), pp.15-39.

Clark, C. M. (1971) Expansive-soil effect on buried pipe. *Journal-American Water Works Association.* 1971 Jul 1;63(7):424-7

Collin, J. G., Han, J., and Huang, J. (2005). Geosynthetic reinforced column support embankment design guidelines. *In Proceedings, the North America Geosynthetics Society Conference.*1-15.

Costa, Y. D., Zornberg, J. G., Bueno, B. S., and Costa, C. L. (2009) Failure mechanisms in sand over a deep active trapdoor. J*ournal of Geotechnical and Geoenvironmental Engineering.* 2009 Apr 27;135(11):1741-53.

Cui, Z. D., Yuan, Q. and Yang, J. Q. (2018) Laboratory model tests about the sand embankment supported by piles with a cap beam. G*eomechanics and Geoengineering,* 13(1), pp.64-76.

Dalvi, R. S. and Pise, P. J. (2012) Analysis of arching in soil-passive state. *Indian Geotechnical Journal,* 42(2), pp.106-112.

Das, B. M. (2010) *Geotechnical engineering handbook*. J. Ross Publishing.

Deb, K., Chandra, S. and Basudhar, P. K. (2008) Response of multilayer geosynthetic-reinforced bed resting on soft soil with stone columns. *Computers and Geotechnics*, 35(3), 323–330.

Deb, K. (2010) A mathematical model to study the soil arching effect in stone column-supported embankment resting on soft foundation soil. *Applied Mathematical Modelling,* 34(12), pp.3871-3883.

Deb, K. and Mohapatra, S. R. (2013) “Analysis of stone column-supported geosynthetic reinforced embankments.” *Appl. Math. Mode*l., 37(5), 2943–2960.

Dewoolkar, M.M., Santichaianant. K., and Ko, H.Y.(2007) Centrifuge modeling of granular soil response over active circular trapdoors. *Soils and foundations.* 2007;47(5):931-45.

Doris Asmani, M. Y., Hafez, M. A. and Shakri M, S. (2013) Comparison between Static and Dynamic Compaction for California Bearing Ratio (CBR), *EJGE*, 18,5857-5869

Duncan-Williams, E. and Attoh-Okine, N. O. (2008) Effect of geogrid in granular base strength–An experimental investigation. *Construction and building materials,* 22, 2180-2184.

EBGEO (2010) Emfehlungen für den Entwurf und die Berechnung von Erdkorpern mit Bewehrungen aus Geokunststoffen – EBGEO, 2. *German Geotechnical Society*, Auflage ISBN 978-3-433-02950-3.

Ellis, E. A., and Aslam, R. (2009). "Arching in piled embankments: comparison of centrifuge tests and predictive methods - part 1 of 2." *Ground Engineering,* 42(6), 34-38.

Ellis, E. A., and Aslam, R. (2009). "Arching in piled embankements: comparison of centrifuge tests and predictive methods - part 2 of 2." G*round Engineering*, 42(7), 28-31.

Elshakankery M. H., Almetwally A. A. and Tawfik K. A. (2013) Experimental Study of Bearing Capacity for Egyptian Soils Reinforced by Geotextiles, *Journal of Applied Sciences Research,* 9(3), 2013, 2378-2385.

Evans, C. H. (1983) "*An examination of arching in granular soils."* S.M. thesis, Dept. of Civil Engineering, MIT, Cambridge, MA.

Fagundes, D. D. F., Almeida, M. D. S. S. D., Girout, R., Blanc, M. and Thorel, L. (2015) Behaviour of piled embankment without reinforcement. *Proceedings of the Institution of Civil Engineers-Geotechnical Engineering,* 168(6), pp.514-525.

Fagundes, D. F., Almeida, M. S., Thorel, L. and Blanc, M. (2017) Load transfer mechanism an deformation of reinforced piled embankments. *Geotextiles and Geomembranes,* 45(2), pp.1-10.

Fattah, M.Y., Mohammed, H. A. and Hassan, H. A. (2016) Load transfer and arching analysis in reinforced embankment. P*roceedings of the Institution of Civil Engineers-Structures and Buildings,* 169(11), pp.797-808.

Fonseca, E. C. A., Palmeira, E. M., and Barrantes, M. V. (2018) Load and Deformation Mechanisms in Geosynthetic-Reinforced Piled Embankments. *International Journal of Geosynthetics and Ground Engineering*, 4(4),32,1-12.

Gangakhedkar, R. (2004) *Geosynthetic reinforced pile supported embankments* (Doctoral dissertation, University of Florida)

Gaoxiao, H., Quanmei, G. and Shunhua, Z. (2011) Mechanical analysis of soil arching under dynamic loads. *In Pan-Am CGS Geotechnical Conference.*1-7.

Gebreselassie, B., Lüking, J. and Kempfert, H.G. (2010) Influence factors on the performance of geosynthetic reinforced and pile supported embankments. *In 9th International Conference on Geosynthetics.* Brazil:[sn] (pp. 1935-1940).

Girout, R., Blanc, M., Thorel, L. and Dias, D. (2018). Geosynthetic reinforcement of pile-supported embankments. *Geosynthetics International,* 25(1) pp. 37-49.

Guido, V. A., Knueppel, J. D. and Sweeny, M. A. (1987) Plate loading tests on geogrid - reinforced earth slabs. *Proceedings Geosynthetics 87 Conference,* New Orleans, pp. 216-225.

Handy, R. L. (1985). The arch in soil arching. *Journal of Geotechnical Engineering,* 111(3), 302-318.

Han, J. and Gabr, M. A. (2002) Numerical analysis of geosynthetic-reinforced and pile-supported earth platforms over soft soil. *Journal of geotechnical and geoenvironmental engineering,* 128(1), 44-53.

Han, J. and Bhandari, A. (2009) Evaluation of geogrid-reinforced pile-supported embankments under cyclic loading using discrete element method. *In Advances in Ground Improvement: Research to Practice in the United States and China* (pp. 73-82).

Han, G. X., Gong, Q. M. and Zhou, S.H. (2015) Soil arching in a pile embankment under dynamic load. I*nternational Journal of Geomechanics*,15(6), pp.1-7.

Heitz, C. (2006) Bodengewölbe unter ruhender und nichtruhender Belastung bei Berücksichtigung von Bewehrungseinlagen aus Geogittern. Schriftenreihe Geotechnik, *University of Kassel*, Issue 19

Heitz, C., Luking, J. and Kempfert, H-G. (2008) Geosynthetic reinforced and pile supported embankments under static and cyclic Loading. I*n: Proceedings of the 4th European Geosynthetics. Conf Euro- Geo4, Edinburgh (UK)*, paper no 215,pp.1-8.

Hello B. L. and Villard. P. (2009) Embankments reinforced by piles and geosynthetics-Numerical and experimental studies dealing with the

transfer of load on the soil embankment. *Engineering Geology,* 106, 78-91.

Hewlett, W. J. and Randolph, M. F. (1988) Analysis of piled embankment. *Ground Engineering.* 21:12-18.

Horgan, G. J. and Sarsby, R. W. (2002) The arching effect of soils over voids and piles incorporating geosynthetic reinforcement. *Geosynthetics - 7th ICG - Delmas, Gourc and Girard (eds), Swets & Zeitlinger,* Lisse ISBN 90 5809 523 1, pp. 373-378.

Hossain M. A. , Adnan M. and Alam Md. M. (2015) Improvement of Granular Subgrade Soil by Using Geotextile and Jute Fiber, *International Journal of Science, Technology and Society*. Vol. 3, No. 5, 2015, pp. 260-265

Houda, M., Jenck, O. and Emeriault, F. (2016) Physical evidence of the effect of vertical cyclic loading on soil improvement by rigid piles: a small-scale laboratory experiment using Digital Image Correlation. *Acta Geotechnica*, 11(2), pp.325-346.

Huang J. and Han J. (2010) Two-dimensional parametric study of geosynthetic-reinforced column-supported embankments by coupled hydraulic and mechanical modelling, *Computers and Geotechnics,* Volume 37, Issue 5, July 2010, Pages 638–648.

Iglesia, G. R., Einstein, H. H. and Whitman, R. V. (1999) Determination of vertical loading on underground structures based on an arching evolution concept. *Proceedings 3rd National Conference on Geo-Engineering for Underground Facilities*, pp. 495-506.

Iglesia, G. R., Einstein, H. H. and Whitman, R. V. (2013) Investigation of soil arching with centrifuge tests. J*ournal of Geotechnical and Geoenvironmental engineering,* 140(2), p.04013005.

Jenck, O., Dias, D., and Kastner, R. (2007). Two-Dimensional Physical and Numerical Modeling of a Pile-Supported Earth Platform over Soft Soil. *Journal of Geotechnical and Geoenvironmental Engineering*,133(3), 295–305.

Jenck, O., Dias D. and Kastner, R. (2009) Three-dimensional numerical modeling of a piled embankment. *International Journal of Geomechanics,* 9(3), 102-112.

Jenck, O., Combe, G., Emeriault, F. and De Pasquale, A. (2014) Arching effect in a granular soil subjected to monotonic or cyclic loading: kinematic analysis. *In 8th international conference on physical modelling in geotechnics, Perth, Australia* (pp. 14-17).

Jones, C. J. F. P., Lawson, C. R. and Ayres, D. J. (1990) Geotextile reinforced piled embankments. In: *Proceedings of the Fourth International Conference on Geotextiles: Geomembranes and Related Products, Balkema,Rotterdam, The Netherlands*, pp.155–160.

Kempton, G., Russell, D., Pierpoint, N.D. and Jones, C.J.F.P. (1998) Two- and three-dimensional numerical analysis of the performance of piled embankments. *In Proceedings, 6th International Conference on Geosynthetics. Atlanta,GA,* (Vol. 2, pp. 767-772).

Kempfert, H. G., Zaeske, D. and Alexiew, D. (1999) Interactions in reinforced bearing layers over partial supported underground. *In: Geotechnical*

Engineering for Transportation Infrastructure, Balkema, Rotterdam, The Netherlands, 1527–1532.

Kempfert, H. G., Göbel, C., Alexiew, D. and Heitz, C. (2004) German recommendations for reinforced embankments on pile-similar elements. I*n: EuroGeo3-3rd European geosynthetics conference, Geotech Eng with Geosynthetics, Munich, Germany*,pp. 279–284.

Kongkitkul, W., Hirakawa, D., Tatsuoka, F. and Uchimura, T. (2004) Viscous deformation of geosynthetic reinforcement under cyclic loading conditions and its model simulation. *Geosynthetics International,* 11(2), pp.73-99.

Koutsabeloulis, N. C. and Griffiths, D. V. (1989) Numerical modelling of the trap door problem. *Geotechnique,* 39(1), pp.77-89.

Krynine, D. P. (1945) Discussion of “Stability and stiffness of cellular cofferdams,” by Karl Terzaghi, Transactions, *ASCE*, Vol. 110, pp. 1175-1178.

Kumar P. S. and Rajkumar R. (2012) "Effect of Geotextile on CBR Strength of Unpaved with Soft Subgrade" , *EJGE* ,Vol. 17,2012, 1355-1363.

Ladanyi, B. and Hoyaux, B. (1969) A study of the trap-door problem in a granular mass. *Canadian Geotechnical Journal,* 6(1), pp.1-14.

Lambe, T. W. and Whitman, R. V. (1969) *Soil Mechanics*, 553 pp. Jhon Wiley and Sons, N. York.

Latha, M. G. and Murthy, V. S. (2006) Investigations on sand reinforced with different geosynthetics. *Geotechnical Testing Journal,* 29(6), pp.474-481.

Lee, C. J., Wu, B. R., Chen, H. T. and Chiang, K. H. (2006) Tunnel stability and arching effects during tunneling in soft clayey soil. *Tunnelling and Underground Space Technology*, 21(2), pp.119-132.

Le Hello, B. and Villard, P. (2009) Embankments reinforced by piles and geosynthetics—Numerical and experimental studies dealing with the transfer of load on the soil embankment. *Engineering Geology,* 106(1-2), 78-91.

Lehn, J., Moormann, C. and Aschrafi, J. (2016) Numerical Investigations on the Load Distribution over the Geogrid of a Basal Reinforced Piled Embankment under Cyclic Loading. *Procedia engineering,* 143, pp.435-444.

Love, J. and Milligan, G. (2003) Design methods for basally reinforced pile-supported embankments over soft ground, *Ground Engineering,* 36(3).

Low, B. K., Tang, S. K. and Choa, V. (1994) Arching in piled embankments. J*ournal of Geotechnical Engineering*, 120(11):1917–1938.

Magnan, J-P. (1994) Methods to reduce the settlement of embankments on soft clay:Vertical and horizontal deformations of foundations and embankments. *ASCE*, 1(40):77–91.

McGuire, M. (2011). *Critical height and surface deformations of column-supported embankments*. Doctoral dissertation, Virginia Tech, Blacksburg.

McKelvey, J. A. (1994) The anatomy of soil arching. *Geotextiles and Geomembranes* 13, pp. 317-329.

McNulty, J. W. (1965) An experimental study of arching in sand (No. AEWES-TR-1-674). *Army engineer waterways experiment station Vicksburg MS.*

Meguid, M. A., Saada, O., Nunes, M. A. and Mattar, J. (2008) “Physical Modeling of Tunnels in Soft Ground: A Review,” *Tunn. Undergr. Sp. Tech,* Vol. 23, No. 2, pp. 185–198.

Mekkawy, M. M., White, D. J., Suleiman, M. T. and Jahren, C. T. (2011) Mechanically reinforced granular shoulders on soft subgrade: Laboratory and full scale studies. *Geotextiles and Geomembranes,* 29(2), 149-160.

Mitchell, J. K. (1981) State of the art—soil improvement. *In: Proceedings of the 10th ICSMFE. Stockholm,* vol. 4, pp. 509–65.

Molenaar A. A. A., Araya A. A. and Houben L. J. M. (2011) " Characterization of Unbound Base Materials for Roads Using a New Developed Repeated Load CBR Test", *Eighth International Conference on Managing Pavement As sets, Pontificia Universidad Catolica de Chile*, 2011.

Moradi, G., Bonab, M. H. and Abbasnejad, A. (2015) Experimental Modeling and Measuring Stresses and Strains during Arching Phenomenon. *Geosciences*, 5(2), pp.53-61.

Naeini, S. and Mirzakhanlari, M. (2008) The Effect of Geotextile and Grading on the Bearing Ratio of Granular Soils. *EJGE,* 13,1-10.

National Cooperative Highway Research Program (2008) *NCHRP Synthesis 382. Estimating Stiffness of Subgrade and Unbound Materials for*

Pavement Design. American Association of State Highway and Transportation Officials.

Naughton, P.J. (2007) The significance of critical height in the design of piled embankments. *In Soil Improvement* (pp. 1-10)

Nunez, M. A., Briançon, L. and Dias, D. (2013) Analyses of a pile-supported embankment over soft clay: Full-scale experiment, analytical and numerical approaches. *Engineering Geology*, 153, 53-67.

Oh, Y.I. and Shin, E.C. (2007) Reinforced and arching effect of geogrid-reinforced and pile-supported embankment on marine soft ground. Marine. *Georesources and Geotechnology*, 25, 97-118.

Okyay, U. S., and Dias, D. (2010) Use of lime and cement treated soils as pile supported load transfer platform. *Engineering Geology*, 114(1-2), 34–44.

Pardo, G. S. and Sáez, E. (2014) Experimental and numerical study of arching soil effect in coarse sand. *Computers and Geotechnics*, 57, pp.75-84.

Pham, H. V., Dias, D., and Dudchenko, A. (2018). 3D modeling of geosynthetic-reinforced pile-supported embankment under cyclic loading. *Geosynthetics International*, 1–52.

Pirapakaran, K. and Sivakugan, N. (2007a) “A laboratory model tostudy arching within a hydraulic fill stope.” *Geotech. Test. J.,* 30(6), 496–503.

Pirapakaran, K. and Sivakugan, N. (2007b) “Arching within hydraulic fill stopes.” *Geotech. Geologic. Eng.*, 25(1), 25–35.

Potts,V. J. and Zdravkovic, L. (2008) Finite element analysis of arching behaviour in soils. *The 12th International Conference of International Association for Computer Methods and Advances in Geomechanics (IACMAG), Goa, India*, October, 2008, pp. 3642-3649.

Potts, V. J, Zdravkovic, L. (2010) Finite-element study of arching behaviour in reinforced fills. Proc Inst Civil Eng Ground Improv 163(GI4): 217–229

Rowe, R. K. and Li, A. L. (1999) Reinforced embankments over soft foundations under undrained and partially drained conditions. G*eotextiles and Geomembranes,* 17(3), pp.129-146.

Roy, R. and Bhasi, A. (2018) Investigation of Arching Effect in Geosynthetic-Reinforced Piled Embankments. *Iranian Journal of Science and Technology*, Transactions of Civil Engineering, pp.1-14.

Russell, D. and Pierpoint, N. (1997) An assessment of design methods for piled embankments. *Ground Engineering,* 30 (11), 39–44.

Russell, D., Naughton, P.J. and Kempton, G. (2003) 'A new design procedure for pile embankments', *In: Proceedings of the 56th Canadian Geotechnical Conference and 2003 NAGS Conference, CGS Winnipeg, MB*. (Vol. 1, pp. 858-865).

Sas, W., Gluchowski, A. and Szymanski, A. (2012) Determination of the Resilient modulus MR for the lime stabilized clay obtained from the repeated loading CBR tests. *Annals of Warsaw University of Life Sciences-SGGW. Land Reclamation,* 44, 143-153.

Satibi, S., van der Meij, R. and Leoni, M. (2007) *Piled embankments: Literature review and required further research usung numerical*

analysis. Report No. 34, Institute for Geotechnical Engineering, University of Stuttgart.

Shen, S.L., Chai, J.C., Hong, Z.S. and Cai, F.X. (2005) Analysis of field performance of embankments on soft clay deposit with and without PVD-improvement. *Geotextiles and Geomembranes,* 23 (6), 463–485.

Stewart, M. E. and Filz, G. M. (2005) Influence of clay compressibility on geosynthetic loads in bridging layers for column-supported embankments. In Contemporary issues in foundation engineering. *ASCE* (pp. 1-14).

Stone, K. J. L. (1988) "*Modelling of rupture development in soils."* Ph.D. Dissertation, Wolfson College, Cambridge Univ., Cambridge, U.K

Stone, K. J. L. and Muir Wood, D. (1992) "Effects of dilatancy and particle size observed in model tests on sand." *Soils Found.,* 32(4),43–57.

Subaida, E., Chandrakaran, S. and Sankar, N. (2009) Laboratory performance of unpaved roads reinforced with woven coir geotextiles. *Geotextiles and geomembranes,* 27, 204-210.

Tafreshi, S. M., Khalaj, O. and Dawson, A. (2014) Repeated loading of soil containing granulated rubber and multiple geocell layers. *Geotextiles and Geomembranes,* 42**,** 25-38.

Terzaghi, K. (1936) 'Stress distribution in dry and in saturated sand above a yielding trapdoor', *Proceeding of the International Conference on Soil Mechanics and Foundation Engineering Bd.1. Cambrigde,* pp. 307-311.

Terzaghi, K. (1943). '*Theoretical Soil Mechanics'*, John Wiley and Sons, New York.

Truc, P. T. T. and Hino, T. (2018) Valuate the effect of embankment height and pile spacing to the behavior of the Geosynthetic-Reinforced Piled mmbankment using FEM. *Numerical Analysis in Geotechnics–NAG2018*, Ho Chi Minh City, Vietnam 1-9.

Van Eekelen, S. J. M., Bezuijen, A. and Alexiew, D. (2010a) The Kyoto Road Piled Embankment: 31/2 Years of Measurements. *In: Proc. of 9ICG, Brazil,* 1941-1944.

Van Eekelen, S. J. M. Nancey, A. and Bezuijen, A. (2012) Influence of fill material and type of geosynthetic reinforcement in a piled embankment, model experiments. *In: Proceedings of EuroGeo5, Valencia, Spain*. (Vol. 5, pp. 167-171)

Van Eekelen, S. J. M. (2015). *Basal Reinforced Piled Embankments. Experiments, field studies and the development and validation of a new analytical design model* (Doctoral dissertation, PhD thesis, Delft University of Technology).

Van Eekelen S. J. M. & Bezuijen A. (2012). Model experiments on geosynthetic reinforced piled embankments, 3D test series. *In 2nd European conference on physical modelling in geotechnics (Eurofuge-2012). Delft, The Netherlands*. (pp. 1-10).

Van Eekelen, S. J. M., Bezuijen, A., Lodder, H. J. and van Tol, A. F.(2012a). “Model experiments on piled embankments. Part I.” *Geotextiles and Geomembranes,* 32(3), 69–81.

Van Eekelen, S. J. M., Bezuijen, A., Lodder, H. J. and van Tol, A. F. (2012b) “Model experiments on piled embankments. Part II.” *Geotextiles and Geomembranes,* 32(3), 82–94

Van Eekelen, S. J. M., Bezuijen, A. and Van Tol, A. F. (2011) Analysis and modification of the British Standard BS8006 for the design of piled embankments.*Geotextiles and Geomembranes,*29, 345–359

Van Eekelen, S. J. M., Jansen, H. L., Van Duijnen, P. G., De Kant, M., Van Dalen, J. H., Brugman, M. H. A., van der Stoel, A. and Peters, M. G. J. M. (2010) The Dutch design guideline for piled embankments. *In 9th international conference on geosynthetics, geosynthetics for a challenging world*, Guaruja, Brasil. IGS, 23-27,

Van Eekelen, S.J.M., Bezuijen, A. and van Tol, A. F. (2013) An analytical model for arching in piled embankments. *Geotextiles and Geomembranes,* 39, pp.78-102

Van Eekelen, S. J. M. (2016) The 2016-update of the Dutch Design Guideline for Basal Reinforced Piled Embankments. *Procedia engineering,* 143, pp.582-589.

Van Eekelen, S. J., Bezuijen, A. and Oung, O. (2003) Arching in piled embankments; experiments and design calculations. *Proceedings of Foundations: Innovations, observations, design and practice*.885-94.

Vardoulakis, I., Graf, B. and Gudehus, G. (1981) Trap-door problem with dry sand: a statical approach based upon model test kinematics. *Int J Num Anal Methods Geomech* 5:57–78.

Villard, P. and Giraud, H. (1998) Three-dimensional modelling of the behaviour of geotextile sheets as membranes. *Textile Research Journal,* 68(11), pp.797-806.

Villard, P., Gourc, J. P. and Giraud, H. (2000) A geosynthetic reinforcement solution to prevent the formation of localized sinkholes. C*anadian Geotechnical Journal,* 37(5), 987-999.

Villard, P., Le Hello, B., Nancey, A., Chew, S. H. and Loke, K. H. (2004) March. Use of high strength geotextiles over piles results from a full-scale test'. *In Proceedings of the 3nd European Geosynthetics Conference, Munich, Germany (*Vol. 1, pp. 295-29)

Wang, L., Leshchinsky, B., Evans, T. M. and Xie, Y. (2017) Active and passive arching stresses in c′-ϕ′ soils: A sensitivity study using computational limit analysis. *Computers and Geotechnics,* 84, 47-57.

Wang, K. Y., Zhuang, Y., Liu, H. and Miao, Y. (2018) Soil arching in highway piled embankments subjected to moving shakedown limit loads. *European Journal of Environmental and Civil Engineering,* 1-15.

Yan, L., Yang, J.S. and Han, J. (2006) Parametric study on geosynthetic-reinforced pile-supported embankments. *In Advances in Earth Structures: Research to Practice* (pp. 255-261).

Yapage, N. N. S. and Liyanapathirana, D. S. (2014) A parametric study of geosynthetic-reinforced column-supported embankments. *Geosynthetics International*, 21(3), 213–232.

You-Chang, H., U., Song, Hai. and Zheng-Jun, Zhao. (2009) Expermental Study on Behavior of Geotextile - Reinforced Soil . *Critical Issues in Transportation Systems Planing , Development , and Management 2009.*

Yun-Min, C., Wei-Ping, C. and Ren-Peng, C. (2008} An experimental investigation of soil arching within basal reinforced and unreinforced

piled embankments. *Geotextiles and Geomembranes,* 26(2), pp.164-174.

Zaeske, D. (2001) Zur Wirkungsweise von unbewehrten und bewehrten mineralischenTragschichten über pfahlartigen Gründungselementen. Schriftenreihe Geotechnik, *Uni Kassel, Heft 10, February 2001* (in German).

Zanzinger, H., Hangen, H. and Alexiew, D. (2010). Fatigue behaviour of a PET-Geogrid under cyclic loading. *Geotextiles and Geomembranes,* 28(3), 251-261.

Zhang, M.X., Javadi, A.A. and & Min, X. (2006). Triaxial tests of sand reinforced with 3D inclusions. Geotextiles and Geomembranes, 24(4), pp.201-209.

Zhang, G., Wang, L. and Zhang, L. M. (2011) Dilatancy of the interface between a structure and gravelly soil. *Géotechnique* 61(1):75-84.

Zhao, L.S., Zhou, W. H. and Yuen, K. V. (2017) A simplified axisymmetric model for column supported embankment systems. *Computers and Geotechnics,* 92, pp.96-107.

Zhuang, Y. (2009) *Numerical modelling of arching in piled embankments including the effects of reinforcement and subsoil* (Doctoral dissertation, University of Nottingham).

Zhuang, Y., Wang, K. Y. and Liu, H. L. (2014) A simplified model to analyse the reinforced piled embankments, *Geotextiles and Geomembranes,* Volume 42, Issue 2, April 2014, 154-165

Zhuang, Y. and Li, S. (2015) Three-dimensional finite element analysis of arching in a piled embankment under traffic loading. *Arabian Journal of Geosciences,* 8(10), pp.7751-7762.

Zhuang, Y. and Wang, K. Y. (2018) Finite element analysis on the dynamic behaviour of soil arching effect in piled embankment. *Transportation Geotechnics,* 14, pp.8-21.